Recycling, regenerating and reusing reinforcement glass fibres

A thesis in fulfilment of the requirements for the degree of Doctor of Philosophy

By

Kyle Robert Pender

Department of Mechanical and Aerospace Engineering
University of Strathclyde
Glasgow
UK
2018

Declaration of Authenticity and Author's Rights

This thesis is the result of the author's original research. It has been composed by the author and has not been previously submitted for examination which has led to the award of a degree.

Signed:

Date: 10/09/2018

Acknowledgements

I would like to express my sincere gratitude to my supervisor Dr Liu Yang for his invaluable advice during the course of my studies. I appreciate the confidence he placed in me, giving me the opportunity to carry out this research with the freedom to tackle challenges independently. Without his guidance, this thesis would not have been possible. I would also like to thank my second supervisor Professor James Thomason, whose time and expertise were always given generously.

In addition, my sincere thanks go to all the present and past members of the Advanced Composites Group who I had the pleasure to work with. Their advice and assistance over the past few years was always given in full and it was a pleasure to work and socialise with everyone.

I appreciate the time and expertise donated by Dr Fiona Sillars and James Gillespie of the Advance Materials Research Laboratory who assisted with my laboratory work, as well as to all technicians in the Department of Mechanical and Aerospace Engineering, their support and hard work made this possible.

I also thank the Engineering and Physical Science Research Council and Nippon Electric Glass for their financial support.

I am especially grateful to my family who gave me everything I needed over the years, not least belief in myself.

Special admiration and gratitude is bestowed to Emma, who was there every day of my doctorate studies with love and support. Thank you.

Publications

Several results of this thesis have been published over the course of this PhD project in the following journal articles and conference contributions.

Pender K, Yang L. Investigation of catalysed thermal recycling for glass fibre reinforced epoxy using fluidised bed process. Polymer Composites. 2018 Under Review

Pender K, Yang L. Investigation of the potential for catalysed thermal recycling in glass fibre reinforced polymer composites by using metal oxides. Composites Part A: Applied Science and Manufacturing. 2017;100:285-93

Pender K, Yang L. Investigation into the use of metal oxides for catalysed epoxy resin decomposition. 20th International Conference on Composite Materials, Copenhagen: 2015.

Pender K, Yang L. Catalysed thermal decomposition of matrices for closed-loop recycling of fibre reinforced thermosets. 17th European Conference on Composite Materials, Munich: 2016

Abstract

Over the last decades, the use of glass fibre reinforced thermosets (GRT) has become widespread and commonly used in many sectors. Currently no commercial recycling process exists for GRT and the amount of waste generated has reached an unsustainable level. The value of recycled glass fibres (RGF) is reduced significantly due to loss in strength and surface functionality during recycling. Thermal recycling processes involve decomposing the polymer matrix at elevated temperatures to recover the reinforcement fibres. Exposing to such high temperatures degrades the strength of the fibres as well as removes the sizing on the fibre surface. The focus of this thesis is to investigate the potential for retaining and regenerating the strength and interface properties of thermally recycled glass fibres; in order to produce composites reinforced with RGF that could complete with those using virgin/pristine glass fibres.

In order to recycled GRT in-house, a lab scale thermal recycling system based on a fluidised bed reactor was initially designed and developed. To build on the already extensive research into this recycling process, this thesis aims to reduce the temperature required to recycle GRT within the fluidised bed by introducing a metal oxide catalyst to aid in the thermal decomposition of the thermosetting matrix. This novel line of research was selected due to the potential for reducing both the energy consumption of the recycling process and thermal damage sustained by the glass fibres during recycling. Using thermogravimetric analysis it was found that copper (II) oxide (CuO) was particularly active at catalysing the thermal decomposition of epoxy, reducing the decomposition temperature by up to 125 °C. When used within the fluidised bed recycling process, CuO facilitated recycling of glass fibre from glass fibre reinforced epoxy (GF-EP) at just 400 °C without compromising on fibre yield efficiency.

Another avenue of research in this thesis was assessing the potential of a variety of chemical treatments to regenerate the strength and surface functionality of thermally recycled glass fibres. It was found that soaking in hot NaOH solution could provide approximately a 130% increase in the strength of RGF; concluding that changes to surface morphology due to etching was the re-strengthening mechanism. The interfacial adhesion between RGF and 1) polypropylene (PP) and 2) epoxy were examined. It was found that the interfacial shear strength (IFSS) between RGF and

epoxy could be fully restored by first treating the RGF in NaOH solution. Regenerating the IFSS between RGF and PP proved more challenging despite the use of fibre sizing and PP matrix modification. GRP reinforced with RGF (with and without regeneration treatments) were prepare and mechanically characterised; however, the GRP exhibited significantly poorer mechanical properties than those prepared with virgin fibres. This drop in performance was typically attributed to a combination of 1) lower fibre strength, 2) poor fibre-polymer interfacial adhesion and 3) low fibre volume fraction within the GRP.

Contents

Declaration of Authenticity and Author's Rights i

Acknowledgements ii

Publications iii

Abstract iv

List of symbols xiv

List of figures xvi

List of tables xxix

1. Introduction 1

1.1 Background 1

1.2 Aims and Objectives 3

1.3 Outline of thesis 5

2. Recycling glass fibres with fluidised bed 6

2.1 Literature review 6

2.1.1 An overview of recycling technologies 6

2.1.1.1 Mechanical recycling 7

2.1.1.2 Chemical recycling 7

2.1.1.3 Thermal recycling 8

2.1.2 Effect of thermal recycling temperatures on glass fibre strength 11

2.1.2.1 Effect of thermal conditioning on glass fibre strength 12

2.1.2.2 Effect of thermal recycling on glass fibre strength 15

2.1.3 Effect of thermal recycling temperatures on the IFSS 18

2.1.3.1 Dehydroxylation of glass fibre surface 20

2.1.4 Conclusions of literature review 22

2.2 Fluidised bed recycling rig brief 22

2.3 Overview of the final fluidised bed rig design 23

2.3.1 Fluidised bed reactor design 25

2.3.2 Fluidising air supply 26

2.3.3 Air preheater 26
2.3.4 Recycled glass fibre separation system 26
2.4 Performance of fluidised bed recycling rig 27
2.4.1 Experiment 27
2.4.1.1 Materials 27
2.4.1.2 Preparing GF-EP recyclate 28
2.4.1.3 Single fibre tensile sample preparation and tensile test 28
2.4.1.4 Scanning electron microscopy for fibre surface analysis 30
2.4.2 Initial commissioning of fluidised bed rig 31
2.4.3 Characterisation of fluidised bed rig performance 32
2.4.3.1 Test strategy 32
2.4.3.2 Results and discussion 33
2.5 Conclusions 41
3. Catalysed thermal recycling of glass fibres 42
3.1 Literature review 42
3.1.1 Thermal decomposition of thermosetting polymers 43
3.1.1.1 Polymer thermal-oxidative decomposition mechanism 43
3.1.1.2 Epoxy thermal-oxidative decomposition 44
3.1.2 Metal oxide catalysts 47
3.1.2.1 Catalysis 47
3.1.2.2 Copper oxide 48
3.1.2.3 Cerium (IV) oxide 49
3.1.2.4 Cobalt (II,III) oxide 50
3.1.2.5 Metal oxide catalysts for polymer thermal decomposition 51
3.1.3 Conclusions of literature review 52
3.2 Experiment 52
3.2.1 Materials 52
3.2.2 Thermogravimetric analysis 53
3.2.2.1 Epoxy thermal decomposition analysis 53
3.2.2.2 Assessing reusability of metal oxide 55
3.2.2.3 Glass fibre sizing thermal decomposition 56

3.2.3 Differential scanning calorimetry for studying epoxy curing 57
3.2.4 Epoxy tensile sample preparation and tensile test 57
3.2.5 Thermally conditioning glass fibres within a furnace.....58
3.2.5.1 Thermally conditioning glass fibres in the presence of metal oxides .59
3.2.6 GF-EP processing.....60
3.2.6.1 Preparing GF-EP recyclate.....60
3.2.6.2 Thermal recycling GF-EP within a furnace.....60
3.2.6.3 Thermal recycling GF-EP with the fluidised bed process 61
3.3 Results and discussion.....62
3.3.1 Effect of integrated metal oxides on epoxy properties 62
3.3.1.1 Effect of integrated metal oxides on epoxy cure 62
3.3.1.2 Effect of integrated metal oxides on epoxy mechanical properties....63
3.3.2 Thermal analysis of epoxy thermal decomposition 64
3.3.2.1 Isothermal decomposition of epoxy 64
3.3.2.2 Non-isothermal decomposition of epoxy 71
3.3.2.3 Epoxy thermal decomposition kinetic study 78
3.3.3 GF-EP recycling within a furnace 88
3.3.3.1 Effect of metal oxides on GF-EP recycling using furnace 88
3.3.3.2 Effect of thermal conditioning temperature and time on glass fibre strength 92
3.3.3.3 Tensile strength of glass fibres recycled in a furnace 94
3.3.3.4 Temperature local to glass fibres during recycling 96
3.3.3.5 Effect of rapid thermal loading on the glass fibre strength 97
3.3.4 Glass fibres thermally conditioned in contact with metal oxides 98
3.3.4.1 Effect of metal oxides on glass fibre sizing decomposition 99
3.3.4.2 Strength of glass fibres thermally conditioned in contact with metal oxides 100
3.3.5 Catalysed fluidised bed.....101
3.3.5.1 Yield efficiency of recycled glass fibres 102
3.3.5.2 Strength of recycled glass fibres.....104
3.3.5.3 Reusability of CuO as an oxidation catalyst.....106
3.4 Conclusions.....108

4. Regenerating recycled glass fibres 110
4.1 Literature review 111
4.1.1 Regeneration of glass fibre strength 111
4.1.1.1 Applying sizing to increase glass fibre strength 111
4.1.1.2 Acid and basic treatments to increase glass fibre strength 112
4.1.1.3 Water treatments to increase glass fibre strength 117
4.1.2 Glass fibre interfacial adhesion 120
4.1.2.1 Sizing and silane coatings 120
4.1.2.2 Glass fibre – polypropylene interface and interfacial adhesion 122
4.1.2.3 Glass fibre – epoxy interface and interfacial adhesion 124
4.1.3 Regeneration of glass surface functionality 125
4.1.3.1 Effect of applying sizings on glass fibre – polymer interfacial adhesion 125
4.1.3.2 Methods for glass fibre surface rehydroxylation 126
4.1.4 Conclusions of literature review 127
4.2 Experimental 127
4.2.1 Materials 127
4.2.2 Glass fibre chemical treatments 128
4.2.2.1 NaOH treatment 129
4.2.2.2 Hot water treatment 130
4.2.2.3 Water vapour treatment 130
4.2.2.4 Hot APS treatment 130
4.2.2.5 RT APS treatment 131
4.2.2.6 Hydrochloric acid treatment 131
4.2.3 Fourier transform infrared spectroscopy 131
4.2.4 Microbond sample preparation and test 132
4.2.4.1 Preparation with polypropylene matrix 132
4.2.4.2 Preparation with epoxy matrix 133
4.2.4.3 Microbond test procedure 134
4.3 Results and discussion 137
4.3.1 Tensile strength of regenerated glass fibres 137
4.3.1.1 Effect of NaOH on glass fibres recycled from in-house recyclate 137

4.3.1.2 Effect of hot water on glass fibres recycled from in-house recyclate 155
4.3.1.3 Effect of water vapour on glass fibres recycled from in-house recyclate 161
4.3.1.4 Effect of hot APS on glass fibres recycled from in-house recyclate.163
4.3.1.5 Glass fibres recycled from wind turbine blade 165
4.3.1.6 Influence of gauge length on glass fibre strength.....168
4.3.2 Recycled glass fibre ─ polymer interface 169
4.3.2.1 IFSS between recycled glass fibre and polypropylene.....170
4.3.2.2 Investigation into glass fibre surface functionality after chemical treatments using FTIR.....173
4.3.2.3 IFSS between recycled glass fibre and epoxy 177
4.3.2.4 Effect of interface regeneration treatments on glass fibre strength .182
4.4 Conclusions.....184
5. Reusing recycled and regenerated glass fibres.....187
5.1 Literature review.....188
5.1.1 Reprocessing thermally recycled glass fibres.....188
5.1.2 Mechanical properties of GRP reinforced with thermally weakened glass fibres.....189
5.1.3 Mechanical properties of GRP reinforced with regenerated glass fibres192
5.1.4 Conclusions of literature review 196
5.2 Experiment.....196
5.2.1 Materials.....196
5.2.2 Glass fibre chemical treatments.....197
5.2.2.1 NaOH treatment 197
5.2.2.2 Hydrochloric acid treatment.....199
5.2.2.3 RT APS treatment 199
5.2.3 Preparation of GF-PP 200
5.2.3.1 Wet deposition process 200
5.2.3.2 Pre-consolidation and compression moulding 200
5.2.4 Preparation of GF-EP 202
5.2.5 Composite characterisation.....204

5.2.5.1 Tensile test....204
5.2.5.2 Three-point flexural test....204
5.2.5.3 Unnotched charpy impact test....205
5.2.5.4 Fibre content measurement....206
5.2.5.5 Fibre length measurement....206
5.3 Results and discussion....208
5.3.1 Mechanical properties of GF-PP....208
5.3.1.1 Kelly-Tyson model for estimating GF-PP tensile strength....208
5.3.1.2 Effect of MAPP content on GF-PP tensile strength....211
5.3.1.3 Effect of interface regeneration on GF-PP tensile properties....213
5.3.1.4 Effect of fibre strength and interface regeneration on GF-PP mechanical properties....219
5.3.1.5 Effect of NaOH concentration on GF-PP tensile strength....229
5.3.1.6 Effect of hot water treatment on GF-PP tensile strength....231
5.3.1.7 Effect of integrating new glass fibres on GF-PP tensile strength....231
5.3.2 Tensile properties of GF-EP prepared with recycled and regenerated glass fibres....233
5.4 Conclusions....237
6. Conclusions and Future work....240
6.1 Conclusions of the thesis....240
6.1.1 Thermal recycling glass fibres in fluidised bed....240
6.1.2 Catalysed thermal recycling of glass fibres....241
6.1.3 Regenerating recycled glass fibres....242
6.1.4 Reusing recycled and regenerated glass fibres....243
6.2 Future work....245
6.2.1 Thermal recycling glass fibres in fluidised bed....246
6.2.2 Catalysed thermal recycling of glass fibres....246
6.2.3 Regenerating recycled glass fibres....248
6.2.4 Reusing recycled and regenerated glass fibres....249
7. References....251

Appendix A. Fluidised bed recycling rig design A-1
A.1 Reactor A-1
A.1.1 Distributor plate A-1
A.1.2 Reactor height A-5
A.2 Cyclone separator A-6
A.2.1 Barth model for calculating fractional efficiency A-7
A.2.1.1 Barth model for calculating pressure drop A-8
A.2.1.2 Particle size A-9
A.2.1.3 Cyclone separator design assessment A-10
A.2.2 Final design A-14
Appendix B. Bundle vs. single fibre thermal conditioning B-1
B.1 Introduction B-1
B.2 Experiment B-2
B.2.1 Materials B-2
B.2.2 Single fibre thermal conditioning B-3
B.3 Results and discussion B-4
B.3.1 Phenomenological model of strength loss B-7
B.4 Conclusions B-10
Appendix C. Metal oxide as a catalyst for carbon fibre recycling C-1
C.1 Experimental C-1
C.1.1 Materials C-1
C.1.2 Thermal analysis C-1
C.1.2.1 Carbon fibre thermal decomposition C-1
C.1.2.2 CF-EP thermal decomposition C-1
C.1.3 Thermal conditioning carbon fibres C-2
C.2 Results and discussion C-2
C.2.1 Thermal analysis C-2
C.2.1.1 Carbon fibre decomposition C-2

C.2.1.2 CF-EP decomposition C-3
C.2.2 Strength of thermally conditioned carbon fibre C-4
C.2.2.1 Effect of thermal conditioning temperature C-4
C.2.2.2 Effect of contact with metal oxides C-5
C.3 Conclusions C-6
Appendix D. Fibre length degradation during processing D-1
Appendix E. Extended Kelly-Tyson model derivation E-1
E.1 Critical fibre length E-1
E.2 Extended Kelly-Tyson model E-1

List of symbols

APS	3-Aminopropyltriethoxysilane
c	Critical flaw length
CeO_2	Cerium (IV) oxide
CF	Carbon fibre
CF-EP	Carbon fibre reinforced epoxy
CRT	Carbon fibre reinforced thermoset
Co_3O_4	Cobalt (II,III) oxide
CuO	Copper (II) oxide
D	Fibre diameter
D_o	Original fibre diameter
DSC	Differential scanning calorimetry
Ea	Activation energy
F_{db}	Force at droplet de-bond
FDF	Forced draft fan
FRP	Fibre reinforced plastic
FRT	Fibre reinforced thermoset
FTIR	Fourier-transform infrared spectroscopy
GF	Glass fibre
GF-EP	Glass fibre reinforced epoxy
GF-polyester	Glass fibre reinforced polyester
GF-PP	Glass fibre reinforced polypropylene
GRP	Glass fibre reinforced plastic
GRT	Glass fibre reinforced thermoset
GMT	Glass mat thermoplastic
HCl	Hydrochloric acid
HF	Hydrofluoric acid

IFSS	Interfacial shear strength
K_{IC}	Mode I fracture toughness
l_d	Droplet embedded length
IDF	Induced draft fan
m	Mass
MAPP	Maleic anhydride grafted Polypropylene
NaOH	Sodium hydroxide
PP	Polypropylene
RGF	Recycled glass fibre
RT	Room temperature
SEM	Scanning electron microscope
TC	Thermally conditioned
TGA	Thermogravimetric analysis
UTS	Ultimate tensile strength
VOC	Volatile organic compounds
XPS	X-ray photoelectron spectroscopy
Y	Geometric stress concentration factor
η_o	Fibre orientation factor
$\sigma_{f,av}$	Average fibre strength

List of figures

Figure 1-1 Global composites materials by market segment for 2016, reproduced from [2] 1
Figure 1-2 Glass fibre global demand and availability for recycling, reproduced from [15] 3
Figure 2-1 Diagram of a typical pyrolysis process, reproduced from [7] 9
Figure 2-2 Schematic of fluidised bed thermal recycling process developed at the University of Nottingham, reproduced from [27] 11
Figure 2-3 Relative tensile strength of single glass fibre after thermal conditioning at a variety of temperatures and times, reproduced from [31] 12
Figure 2-4 Strength of thermally conditioned APS sized and unsized glass fibres at various temperatures, both treated as bundles and individually, reproduced from [32] 13
Figure 2-5 Tensile strength of glass fibres recycled using pyrolysis at various temperatures, reproduced from data in [38] 16
Figure 2-6 Comparison between tensile strength of glass fibres recycled using fluidised bed process and thermally conditioned glass fibres, reproduced from data in [16] and [25] respectively 18
Figure 2-7 Effect of thermal conditioning temperature and atmosphere on apparent IFSS between glass fibre and PP, reproduced from [55].....19
Figure 2-8 Schematic of in-house fluidised bed process designed in this thesis and used to recycle glass fibres throughout subsequent chapters 24
Figure 2-9 Images of the in-house developed fluidised bed recycling rig 25
Figure 2-10 Image of a single fibre tensile test sample in card template 28
Figure 2-11 Image of glass fibre under optical microscopy which was used to measure the fibre diameter with ImageJ 29
Figure 2-12 The fibre diameter distribution within the glass fibre mat (used throughout this thesis) highlights the need to measure the diameter of each single fibre tensile specimen individually.....30
Figure 2-13 Single fibre tensile test setup using Testometric M250-2.5CT.....30
Figure 2-14 Glass fibres recycled in fluidised bed (Vf=1.5 m/s) at a bed temperature of a) 400 °C, b) 450 °C, c) 500 °C, d) 550 °C and e) 500 °C + thermal cleaning at 550 °C for 60 min.....34

Figure 2-15 SEM images of glass fibres recycled in fluidised bed (Vf=1.5 m/s) at a bed temperature of a) 400 °C, b) 450 °C, c) 500 °C, d) 550 °C and e) 500 °C + thermal cleaning at 550 °C for 60 min. Polymer residue present on the surface of RGF is reduced by increasing fluidised bed temperature. 35
Figure 2-16 Tensile strength of glass fibres recycled at 500 °C at various fluidisation velocities. Fluidisation velocity does not appear to influence the strength of the RGF. 38
Figure 2-17 Tensile strength of glass fibres recycled at 1.5 m/s at various bed temperatures. Fluidised bed temperature does not appear to influence the strength of the RGF. 39
Figure 2-18 SEM images of the surface of glass fibres recycled from GF-epoxy recyclate in the fluidised bed at 500 °C. Damage to the RGF can be observed in the form of scratches on the fibre surface. 40
Figure 3-1 TGA thermograms of thermal-oxidative decomposition of epoxy showing 1) two distinct stages of decomposition and 2) influence of heating rate on the temperature required for decomposition, reproduced from [85] 46
Figure 3-2 SEM image showing CuO nanopowder evenly distributed in an epoxy specimen with particle size approximating that given by the supplier 53
Figure 3-3 Epoxy only TGA samples 54
Figure 3-4 Two sample arrangements used during TGA of epoxy thermal decomposition 55
Figure 3-5 TA instruments Q50 used for the TGA of epoxy thermal decomposition 55
Figure 3-6 Flow chart illustrating the method used to assess the reusability of CuO 56
Figure 3-7 NETSZCH STA 449 F1 Jupiter thermogravimetric analyser with beaker attachment, reproduced from [68] 57
Figure 3-8 Silicone mould with epoxy+CuO specimens prior to curing 58
Figure 3-9 Furnace arrangement for brief thermal loading of glass fibre bundle 59
Figure 3-10 Jig used for extended thermal conditioning of bundles with glass fibre bundle attached 59
Figure 3-11 Two sample arrangements used during GF-EP thermal recycling in the furnace 61
Figure 3-12 Tensile strength and modulus of epoxy with metal oxides integrated at 5% weight loading. The presence of the metal oxides does not appear to affect these mechanical properties of epoxy. 64

Figure 3-13 Mass as a function of time for metal oxides heated alone at 500 °C 65
Figure 3-14 Mass as a function of time with metal oxide beds at (a) 400 °C, (b) 450 °C, (c) 500 °C 66
Figure 3-15 Mass as a function of time at 500 °C in both CuO and epoxy with CuO in nitrogen between 0-30 min and in air between 30-50 min 67
Figure 3-16 Mass as a function of time with CuO bed, showing that epoxy can thermally decompose at just 375 °C in the presence of CuO 68
Figure 3-17 Mass as a function of time with 1.5% integrated metal oxide at (a) 400 °C, (b) 450 °C, (c) 500 °C. Time axis scale not consistent between plots.....69
Figure 3-18 Mass as a function of time with 5% integrated metal oxide at (a) 400 °C, (b) 450 °C, (c) 500 °C. Time axis scale not consistent between plots. 70
Figure 3-19 Mass as a function of temperature with metal oxide beds at (a) 2 °C/min (b) 10 °C/min. All metal oxides provide a reduction in thermal stability of epoxy under non-isothermal heating conditions, with CuO showing the greatest catalytic activity. 73
Figure 3-20 Average reduction in first and second stage onset and complete decomposition temperature with metal oxide beds. All the metal oxides tested successfully reduce the second stage onset and complete decomposition temperatures of the epoxy. 74
Figure 3-21 Mass as a function of temperature at a heating rate of 2 °C/min with (a) 1.5% and (b) 5% integrated metal oxide. All metal oxides provide a reduction in thermal stability of epoxy under non-isothermal heating conditions.....75
Figure 3-22 Average reduction in first and second stage onset and complete decomposition temperature with 1.5% integrated metal oxides. All the metal oxides tested successfully reduce the second stage onset and complete decomposition temperatures when integrated into epoxy at 1.5%. 76
Figure 3-23 Average reduction in first and second stage onset and complete decomposition temperature with 5% integrated metal oxides. All the metal oxides tested successfully reduce the second stage onset and complete decomposition temperatures. Increasing metal oxide content to 5% provides larger reduction in thermal stability compared to Figure 3-22 76
Figure 3-24 Effect of metal oxide content on second stage onset and complete decomposition temperatures.....77

Figure 3-25 Reduction in average complete decomposition temperature for the various sample arrangements. Integrating metal oxides in epoxy at 5% provides the lowest thermal decomposition temperature. 78
Figure 3-26 Thermograms of epoxy decomposition at various heating rates for a) epoxy only, b) 1.5% CuO and c) 5% CuO 81
Figure 3-27 Example of plot with straight lines of best fit used to find the Ea using K-A-S method at conversions up to 0.4 for a) epoxy only, 1.5% CuO and c) 5% CuO 82
Figure 3-28 Ea of epoxy decomposition at various values of conversion found using K-A-S method with integrated a) CuO, b) Co_3O_4 and c) CeO_2. CuO and CeO_2 provide a significant reduction in the Ea of the second stage of epoxy decomposition. 84
Figure 3-29 Average reduction in Ea with the use of the metal oxides across the conversion ranges. CuO integrated at 5% loading provides the overall largest reduction in Ea of second stage epoxy decomposition, within the conversions investigated. 85
Figure 3-30 Example of splitting the two stage epoxy decomposition process (example specimen is epoxy only at 1 °C/min)....86
Figure 3-31 Epoxy only decomposition Ea found using K-A-S method for each stage independently. Ea still not constant across conversion indicating the process cannot be described adequately by a single reaction model [91]. 87
Figure 3-32 Image of GF-EP after heating at 380 °C for 330min (a) without and (b) with CuO bed. Epoxy char residue is clearly decomposed more successfully with the use of CuO. 90
Figure 3-33 Tensile strength of glass fibre thermally conditioned for 25 and 60 min at various temperatures from 300 °C to 600 °C. As observed throughout the literature, both temperature and exposure time significantly weaken the glass fibres. 92
Figure 3-34 Strength loss of glass fibres after thermal conditioning in the range of recycling temperatures and times. For both conditioning temperatures, the plateau in the data clearly shows the steady state fibre strength when heating for extended periods....93
Figure 3-35 Tensile strength of glass fibres recycled from GF-EP composites with metal oxide bed 95
Figure 3-36 Tensile strength of glass fibres recycled from GF-EP composites with integrated metal oxides....96

Figure 3-37 Temperature measured directly on GF-EP composites surface during thermal recycling in furnace, showing substantial increase in temperature above furnace set point due to exothermic epoxy decomposition. 97
Figure 3-38 Tensile strength of glass fibres after heating at 600 °C, indicating that even short periods of heating can cause substantial weakening of glass fibres. 98
Figure 3-39 SEM of glass fibres recycled in the furnace; (a) without CuO (b) with integrated CuO, confirming that CuO is present on the surface of RGF 99
Figure 3-40 Mass loss of glass fibres assisted by metal oxides as a function of temperature 100
Figure 3-41 Tensile strength of glass fibres after direct thermal conditioning with metal oxides at different temperatures for 25 min. In all cases, fibre strength is lower when thermally conditioned in the presence of the metal oxides. 101
Figure 3-42 Comparison of composite recyclate (a) GF-EP (b) GF-EP+CuO.....102
Figure 3-43 Yield efficiency of glass fibres recycled from GF-EP in the fluidised bed at various temperatures. At all fluidised bed temperatures the fibre yield efficiency is improved with the use of CuO catalyst. 103
Figure 3-44 Char residue remaining on glass fibres remaining in fluidised bed reactor after recycling at 400 °C (a) without CuO (b) with integrated CuO. Visually, CuO provides significantly cleaner RGF. 104
Figure 3-45 Effect of thermal recycling temperature on glass fibre tensile strength. No significant difference in strength of RGF was observed with the use of CuO catalyst. 105
Figure 3-46 Epoxy thermal decomposition thermograms demonstrating the reusability of CuO as an aid for epoxy decomposition.....106
Figure 3-47 Plots used to calculate CuO thermal decomposition activation energy using the method of Kissinger (a) Epoxy only, (b) Epoxy+CuO(0), (c) Epoxy+CuO(1), (d) Epoxy+CuO(2) 107
Figure 4-1 Schematic representation of flaws and the effect of a surface treatment, reproduced from [130] 112
Figure 4-2 Strength increase of thermally conditioned (heat-treated) glass fibres as a function of fibre diameter reduction, showing that HF increases the strength of glass fibres through an etching mechanism, reproduced from [5].....113
Figure 4-3 Average strength of fibres thermally conditioned at 450 °C and treated in various concentrations of alkaline solutions for 10 min, reproduced from [34].....115

Figure 4-4 Influence of thermal conditioning temperature and chemical treatments on the average glass fibre strength, reproduced from [15]. Both NaOH and HF can substantially increase the strength of thermally conditioned glass fibres, however, the degree of regeneration is dependent on conditioning temperature. 116
Figure 4-5 Glass fibre diameter reduction as a result of treating in NaOH solution at various concentrations and durations, showing the etching effect NaOH has on the glass fibre surface, reproduced from [141] 117
Figure 4-6 Schematic of crack tip, comparing the geometry of uniform dissolution and dissolution with re-precipitation, reproduced from [51] 119
Figure 4-7 3-Aminopropyltriethoxysilane molecule 121
Figure 4-8 Hydrolysis of silane coupling agent, reproduced from [152] 121
Figure 4-9 Reaction of silane adhesion promoters on substrate, reproduced from [152] 122
Figure 4-10 Chemical structure of hydrolysed APS on glass fibre surface, reproduced from [154] 122
Figure 4-11 Chemical reaction between the amino group and the maleic anhydride molecule grafted on PP, reproduced from [158] 123
Figure 4-12 General reaction between amino-silane and epoxy resin, reproduced from [177] 125
Figure 4-13 End-of-life offshore wind turbine blade (a) as received before downsizing and (b) after downsizing before recycling 128
Figure 4-14 Sample preparation of microbond test 133
Figure 4-15 Temperature profile of vacuum oven used to prepare microbond samples, reproduced from [68] 133
Figure 4-16 Modified scalpel used to apply epoxy microbond droplets on glass fibres 134
Figure 4-17 Typical PP droplet on GF with dimensions measured for microbond test 135
Figure 4-18 Microbond test setup 135
Figure 4-19 Stereomicroscopy view of microbond of PP droplet, reproduced from [181] 136
Figure 4-20 Example of a typical load-extension plot output from Instron Bluehill 2 software 136
Figure 4-21 Tensile strength of glass fibres thermally conditioned in the furnace, recycled in the furnace and recycled in the fluidised bed then treated with NaOH at

1.5, 3 and 5 mol/L for 10 min. Only thermally conditioned glass fibres show any improvement in strength after the NaOH treatments. 139
Figure 4-22 Diameter of glass fibres thermally conditioned in the furnace, recycled in the furnace and recycled in the fluidised bed then treated with NaOH at 1.5, 3 and 5 mol/L for 10 min. Only thermally conditioned glass fibres exhibit a reduction in fibre diameter after the NaOH treatments. 140
Figure 4-23 Tensile strength and relative diameter of glass fibres recycled in the fluidised bed treated with NaOH at 5 mol/L for various treatment times. Increasing NaOH treatment time beyond 30 min provides regeneration of the RGF strength. 142
Figure 4-24 Tensile strength of glass fibres recycled in the fluidised bed then treated with NaOH at various concentrations and times. Under the conditions investigated, increasing both NaOH treatment concentration and time result in superior regeneration of RGF strength. 143
Figure 4-25 Tensile strength of glass fibres recycled in the fluidised as a function of NaOH concentration for 60, 120 and 180 min treatments 144
Figure 4-26 Glass fibre diameter after treating with NaOH at various concentrations and times, showing that higher NaOH concentrations more rapidly etch the RGF surface.....145
Figure 4-27 SEM image of fluidised bed recycled glass fibre treated with NaOH at 3 mol/L for 2 hour 147
Figure 4-28 SEM image of fluidised bed recycled glass fibre treated with NaOH at 5 mol/L for 2 hour 148
Figure 4-29 SEM image of fluidised bed recycled glass fibre treated with NaOH at 7 mol/L for 2 hour 148
Figure 4-30 SEM image of fluidised bed recycled glass fibre treated with NaOH at 10 mol/L for 2 hour.....149
Figure 4-31 SEM image of fluidised bed recycled glass fibre treated with NaOH at 5 mol/L for 2 hour, exhibiting a roughened surface which was not observed for untreated RGF. 150
Figure 4-32 Tensile strength of glass fibres as a function of diameter reduction after various NaOH treatment concentrations and times. Tensile strength of RGF treated in NaOH is not merely proportional to the quantity of surface material etched, illustrated by the plateau in strength observed when higher NaOH concentrations are used. 151

Figure 4-33 Tensile strength of glass fibres as a function of diameter reduction after various NaOH treatment concentrations and times 153
Figure 4-34 Relative mass reduction of NaOH treated fibres, calculated from change in diameters in Figure 4-26. As would be expected, glass fibre mass loss (as a result of etching in NaOH) depends on NaOH treatment time and concentration.....154
Figure 4-35 Tensile strength of fibres recycled in the fluidised bed followed by treatment in 90 °C water for 8, 16, 24 and 32, 72, 96, 192, 240 and 336 hour. Slight increase in RGF strength is observed in water treatments lasting 72 hour and greater. 155
Figure 4-36 Change in diameter of glass fibres recycled in the fluidised bed followed by treatment in 90 °C water for 96, 192 and 240 hour compared to that of silica rods, reproduced from [80] 157
Figure 4-37 SEM image of fluidised bed recycled glass fibre without water treatment 159
Figure 4-38 SEM image of fluidised bed recycled glass fibre treated with 90 °C water for 96 hour 160
Figure 4-39 SEM image of fluidised bed recycled glass fibre treated with 90 °C water for 240 hour 160
Figure 4-40 SEM image of fluidised bed recycled glass fibre treated with 90 °C water for 336 hour 161
Figure 4-41 Tensile strength of fibres recycled in the fluidised bed followed by treatment in 250 °C water vapour for 4, 8, 24 and 96 hour. No change in RGF tensile strength was observed as a result of exposure to water vapour under the conditions tested. 162
Figure 4-42 Reaction between APS and water to produce hydroxyl ion 164
Figure 4-43 Tensile strength of fibres recycled in the fluidised bed followed by treatment in 83 °C APS for 24, 120 and 240 hour. Hot APS provided no improvement in the strength of RGF under the conditions investigated. 164
Figure 4-44 Strength of RGF from both recyclate before and after various strength regeneration treatments at a gauge length of 5 mm. As was observed when using the in-house prepared recyclate, glass fibres recycled from the real world scrap also show an increase in strength after treating in NaOH and hot water. 166
Figure 4-45 Relative diameter for both recyclate after various strength regeneration treatments, showing that glass fibres recycled from the real world scrap exhibit higher surface etching rates. 167

Figure 4-46 Strength of fibres recycled from in-house prepared recyclate after NaOH and hot water treatment at 5 and 20 mm gauge length 169
Figure 4-47 IFSS between PP and glass fibres after the various treatments, Nagel data reproduced from [68].....171
Figure 4-48 IR spectra of RGF and RGF+HCl.....174
Figure 4-49 IR spectra of RGF+APS and RGF+HCl+APS 175
Figure 4-50 IR spectra of RGF+NaOH and RGF+NaOH+HCl.....176
Figure 4-51 IR spectra of RGF+NaOH+APS and RGF+NaOH+HCl+APS.....176
Figure 4-52 IFSS of various new and RGF with epoxy, measured using the microbond technique. The IFSS with epoxy is significantly reduced as a result of recycling in the fluidised bed; however, can be regenerated with both NaOH and APS treatments.....178
Figure 4-53 SEM image of glass fibre recycled from end-of-life wind turbine blade 180
Figure 4-54 SEM image of glass fibre recycled from end-of-life wind turbine blade treated in 7 mol/L NaOH solution for 2 hour showing significant surface pitting 180
Figure 4-55 Tensile strength of glass fibres is unaffected by treating in 1 vol% APS for 15 min 183
Figure 4-56 Tensile strength of glass fibres after treating with 10 mol/L HCl for 1 and 3 hour. RGF treated in NaOH show a slight reduction in strength after HCl treatment; however, given the error bars, it is unclear how significant this reduction is.....184
Figure 5-1 Tensile strength of GF-EP composites reinforced with thermally conditioned glass fibres treated in hydrofluoric acid (etching) and/or APS (silanisation), reproduced from [5].....193
Figure 5-2 Tensile strength of GF-PP composites with glass fibres receiving various regeneration treatments, reproduced from [15] 194
Figure 5-3 Effect of fibre APS coating and MAPP content on the tensile strength of injection moulded GF-PP, reproduced from [68] 195
Figure 5-4 Improving GF-PP dispersion with various rinses each lasting 90 s: a) 1x 37 vol% HCl, b) 2x 20 vol% HCl and c) 4x 10 vol% HCl.....199
Figure 5-5 Mould used to prepare GF-PP laminates 201
Figure 5-6 Various stages of GF-PP fabrication: a) dried GF-PP mat, b) preconsolidated layer, c) final compression moulded GF-PP laminate with tensile specimen geometry outlined 201

Figure 5-7 Randomly orientated discontinuous glass fibre mats used to prepare GF-EP with RGF.....202
Figure 5-8 Schematic of vacuum infusion layup used to prepare the GF-EP.....203
Figure 5-9 Image of vacuum infusion process set up used to prepare the GF-EP.203
Figure 5-10 Tensile test set up on Instron 5969 testing machine 204
Figure 5-11 Three-point flexural test set up on Instron 5969 testing machine 205
Figure 5-12 Unnotched impact test set up 205
Figure 5-13 IDM FASEP fibre length measurement system: a) FASEP software, b) scanner, c) dark field box, d) controller 207
Figure 5-14 Detection of crossing fibres by the FASEP software 208
Figure 5-15 Tensile strength of GF-PP estimated using K-T model at various fibre strengths and IFSS.....209
Figure 5-16 Calculated tensile of GF-PP produced with fluidised bed RGF, based on K-T model.....211
Figure 5-17 Ultimate tensile strength of GF-PP at various MAPP weight percentages, Nagel data reproduced from [68]. UTS plateaus at relatively high MAPP content, likely a result of incorporating as a powder within the wet deposition process.....212
Figure 5-18 UTS of GF-PP produced using fluidised bed RGF after various treatments.....214
Figure 5-19 Failure strain of GF-PP produced using fluidised bed RGF after various treatments. Matrix modification with MAPP significantly reduces the failure strain of the GF-PP.....216
Figure 5-20 Yield strain of GF-PP produced using fluidised bed RGF after various treatments.....217
Figure 5-21 Modulus of GF-PP produced using fluidised bed RGF after various treatments. GF-PP containing MAPP universally show a rise in the modulus which may be a higher of greater IFSS.....219
Figure 5-22 UTS of GF-PP produced using fluidised bed RGF after various treatments. Under most circumstances, using RGF treated in NaOH improves the UTS of GF-PP. 222
Figure 5-23 Failure strain of GF-PP produced using fluidised bed RGF after various treatments.....223
Figure 5-24 Stress-strain plots obtained during tensile testing of GF-PP prepared with RGF after various regeneration treatments and matrix modification 224

Figure 5-25 Modulus of GF-PP produced using fluidised bed RGF after various treatments. Preparing GF-PP with NaOH treated RGF does not appear to effect the composite modulus. 225
Figure 5-26 UFS of GF-PP produced using fluidised bed RGF after various treatments. In all cases, NaOH treatment increases the GF-PP UFS, with MAPP modification providing additional improvement to the strength. 227
Figure 5-27 Unnotched charpy impact energy of GF-PP prepared with fluidised bed RGF 228
Figure 5-28 Effect of NaOH concentration on GF-PP strength 230
Figure 5-29 UTS of GF-PP prepared with NaOH treated fibres as a function of fibre tensile strength 230
Figure 5-30 UTS of GF-PP prepared with both recycled and new glass fibres. There appears to be a near linear relation between UTS and ratio of new fibre content. . 233
Figure 5-31 UTS of GF-EP produced using fluidised bed RGF after various treatments. Reinforcing with RGF provides only a slight strength gain compared to epoxy only, most likely due to low fibre content. 235
Figure 5-32 Modulus of GF-EP produced using fluidised bed RGF after various treatments. In all cases, the modulus of the GF-EP is greatly increased with the addition of the RGF. 236
Figure 5-33 Failure strain of GF-EP produced using fluidised bed RGF after various treatments 237

Figure A-1 Pressure drops given as a function of porosity for a range of the bed depths and fluidisation velocities A-3
Figure A-2 Geometric pattern of orifices in perforated plat A-4
Figure A-3 Maximum distance between orifices as a function of porosity for various orifice diameters A-5
Figure A-4 CAD model of final perforated plate design A-5
Figure A-5 Investigation into the effect of fluidisation velocity, bed height and operating temperature on TDH A-7
Figure A-6 LHS) Geometry of cyclone separator as given in [245], RHS) Schematic of control surface CS given in [245] A-8
Figure A-7 Equivalent particle diameter as a function of fibre length, where D_f=15 µm A-11

Figure A-8 Pressure drop and inlet velocity for various cyclone diameters with a mass flow rate of 0.03 kg/s A-12
Figure A-9 Fractional separation efficiency as a function of particle size with a mass flow rate of 0.03 kg/s..... A-13
Figure A-10 The effect of varying the mass flow rate on pressure drop for a 0.15 m diameter cyclone..... A-13
Figure A-11 The effect of varying the mass flow rate on fractional efficiency for a 0.15 m diameter cyclone..... A-14
Figure A-12 The effect of varying the feed rate on pressure drop for a 0.15 m diameter cyclone with a mass flow rate of 0.03 kg/s A-15
Figure A-13 The effect of varying the feed rate on fractional efficiency for a 0.15 m diameter cyclone with a mass flow rate of 0.03 kg/s A-15
Figure A-14 Nomenclature for geometry of final cyclone design A-16
Figure B-1 Different procedures for single and bundle thermal conditioning..... B-1
Figure B-2 Tensile strengths of bare and APS-sized fibres after thermal condition, taken from [32]..... B-2
Figure B-3 Wire frame used for extended single fibre thermal conditioning with position of attached fibre drawn on B-3
Figure B-4 Wire frame used for brief single fibre thermal conditioning with position of attached fibre drawn on B-3
Figure B-5 Tensile strength of glass fibres thermally conditioned as fibre bundles B-4
Figure B-6 Tensile strength of glass fibres thermally conditioned as single fibres . B-5
Figure B-7 Tensile strength of fibres heated as bundles and single fibres for 60 min B-5
Figure B-8 Comparison between strength loss mechanism of thermally conditioned APS coated bundles (a) outline in [32] (b) outlined in this work..... B-7
Figure B-9 Phenomenological model based on measured strengths of glass fibres thermally conditioned as fibre bundles..... B-9
Figure B-10 Phenomenological model based on measured strengths of glass fibres thermally conditioned as single fibres B-9
Figure C-1 Carbon fibre thermal decomposition with the application of each of the metal oxides using TGA at 10 °C/min in air..... C-3
Figure C-2 CF-EP thermal decomposition with the application of each of the metal oxides using TGA at 3 °C/min in air C-4

Figure C-3 Tensile strength of carbon fibre thermally conditioned at 400, 500 and 550 °C for 60 min in air C-5
Figure C-4 Tensile strength of carbon fibres thermally conditioned in the presence of the metal oxides at 400 °C for 25 min C-6
Figure D-1 Average length of fluidised bed RGF during recycling and processing into GF-PP D-1
Figure D-2 Fibre length distribution produced by the FASEP software a) before recycling, b) after the fluidised bed, c) after wet deposition, d) after moulding..... D-2

List of tables

Table 2-1 Mass flow rate of air at the bed temperatures and fluidisation velocities investigated 32
Table 2-2 Effect of fluidised bed temperature and fluidisation velocity on glass fibre yield efficiency and cleanliness 37
Table 3-1 GF-EP dimensions for the various usages 60
Table 3-2 Operating conditions of the fluidised bed 62
Table 3-3 Enthalpy of epoxy cure and glass transition temperature found using DSC 63
Table 3-4 Full decomposition time for the various samples, arrangements and temperatures used during isothermal thermal analysis. Overall CuO shows the lowest decomposition times and therefore the greatest potential as a catalyst for use within a fluidised bed recycling process. 71
Table 3-5 Heating parameters and energy required for glass fibre liberation with metal oxide bed 88
Table 3-6 Heating parameters and energy required for glass fibre liberation with 5% integrated metal oxides 91
Table 3-7 Relative mass loss of glass fibres when thermally conditioned using TGA 99
Table 3-8 Activation energy of epoxy thermal decomposition when CuO is re-used up to three times 108
Table 4-1 Summary of the regeneration treatments, property targeted and technique used for characterisation 110
Table 4-2 Summary of various parameters used when preparing and carrying out each of the regeneration treatments 129
Table 4-3 Rinsing procedure after NaOH treatment for single fibre tensile test/microbond test specimens 130
Table 4-4 Range of microdroplet geometries used for microbond test with epoxy and PP 134
Table 4-5 Thermal history of glass fibres treated with NaOH at 1.5, 3 and 5 mol/L for 10 min 138
Table 4-6 Range of estimated flaw lengths on the surface of the various glass fibre samples and the relative reduction in diameter to remove the flaws 142

Table 4-7 Tensile strength of fibres recycled in the fluidised bed followed by treatment in 83 °C APS for 15 min 163
Table 4-8 Outline of the various regeneration treatments used on fibres recycled from wind turbine blade 165
Table 4-9 Summary of the matrix material, source of recycled fibre and regeneration treatment used to investigate the IFSS between polymer and RGF 170
Table 5-1 Summary of the GRP prepared and the source of RGF and regeneration treatment used 187
Table 5-2 Properties of GRP based on thermally conditioned glass fibres 190
Table 5-3 Properties of GRP based on thermally RGF 191
Table 5-4 Conditions used for large scale NaOH treatment 197
Table 5-5 rinsing procedure for RGF soaked in NaOH to ensure effective treatment residue removal prior to processing into GRP 198
Table 5-6 Conditions used for large scale HCl treatment 199
Table 5-7 Average fibre length and fibre tensile strength of fibres in GF-PP where NaOH treatment is at 7 mol/L for 2 hour 210
Table 5-8 Defining treatments and materials used in Figure 5-18 - Figure 5-27 213
Table 5-9 Tensile strength of GF-PP produced with 4 day water treatment at 90 °C 231
Table 5-10 Description of samples in Figure 5-30 232

Table A-1 Fluidised bed recycling system initial design parameters A-1
Table A-2 Dimensions of the cyclone separator A-16
Table B-1 Conditioning temperatures and durations used in the investigation B-4
Table B-2 Fitting parameters for phenomenological model at 300 °C B-10
Table C-1 Thermal decomposition onset temperature of carbon fibre with the application of the metal oxides C-3

1. Introduction

1.1 Background

Over the past several decades, composite materials have become commercialised on a large scale. The global composite market is expected to grow from $73 Billion to $115 Billion between 2016 and 2020, with a compounded annual growth rate of (CAGR) 8.1% [1]. Figure 1-1 shows the global composite material shipped in 2016 by market segment [2]. Fibre reinforced polymers (FRP) are often the material of choice for engineering application because of their good specific strength and stiffness. The CAGR of FRP material is estimated at 7.2% [3] with glass fibres and carbon fibres being the most common reinforcement materials used. The demand for reinforcement glass fibres and carbon fibres is estimated to grow at 6.4% and 14.2% respectively, between 2015 and 2020 [4]. Despite the higher projected growth rate, the demand for glass fibres still far exceeds that for carbon fibres. The annual global production of glass fibres and carbon fibres is expected to reach 7250 kton and 130 kton respectively, by the year 2020 [4]. Currently, glass fibre reinforced composites account for more than 90% of all the fibre-reinforced composites produced [5]. A consequence of this high demand in FRP is a large amount of composite production waste and end-of-life products. The disposal of this waste in an environmentally friendly and economically viable manner is one of the most important challenges currently facing the composites industry.

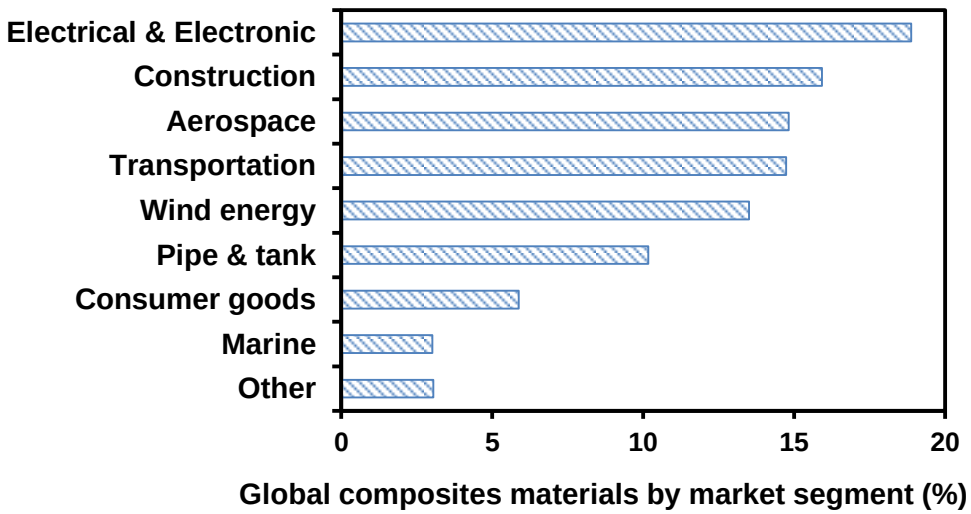

Figure 1-1 Global composites materials by market segment for 2016, reproduced from [2]

The majority of FRP utilise thermosets as their matrix material [6]. Thermosets cannot be remoulded and the constituent materials of thermoset-based composites cannot easily be separated due to polymer crosslinking. This makes fibre reinforced thermosets (FRT) inherently challenging to reuse/recycle [7]. Developments toward commercially recycling GRT lag those made in carbon fibre recycling [8, 9]. This is likely due to the significantly higher value that carbon fibre can retain after the recycling processes, as well as a substantially higher cost for new material. This thesis focuses on overcoming challenges facing recycling GRT, due to considerably high volume produced annually.

Historically, GRT waste streams were destined for landfill, which is a poor disposal strategy for materials requiring intensive energy input in their manufacture. It is currently illegal to landfill composite waste in numerous EU countries, due to the EU Directive on Landfill of Waste [10]. As of 2007, the End-of-life Vehicle Directive delegates responsibility of correct vehicle disposal to vehicle manufacturers; demanding 85% weight of such vehicles must be recycled or reused [11]. Landfilling GRT waste is being further discouraged in many countries by increased landfill taxes [8], incentivising the development of a commercially viable recycling solution.

As the fibres are potentially the most valuable part of the composite, the aim of many proposed recycling methods is to recover and reuse them as reinforcement in secondary composite components. Thermal recycling is an extensively researched method, which involves thermally degrading the composite in either an air or inert environment [6, 7, 12]. As the glass fibres are composed predominantly of silicon dioxide (melting point > 1700°C), they can be recovered and reused after the thermosetting plastics are decomposed. This thesis focuses on thermally recycling glass fibres however, alternative recycling methods that have been proposed are outlined in the following chapter, and the advantages and disadvantages of each are discussed. The typical temperature required for thermal decomposition of thermoset polymers is 450-550°C [7]. Exposure to such high temperatures significantly weakens the glass fibres [7, 13, 14], reducing their reinforcement potential and substantially devaluing them commercially.

Figure 1-2 shows that at present, up to 50% of the global demand for reinforcement glass fibres could be supplied by RGF. Developing composites reinforced with RGF that could compete with composites reinforced with new glass fibres would be a significant advancement toward reducing the quantity of landfilled waste. It has been

estimated that this could also reduce carbon dioxide emissions from glass fibre production by around 2 Mtonnes/annum [15].

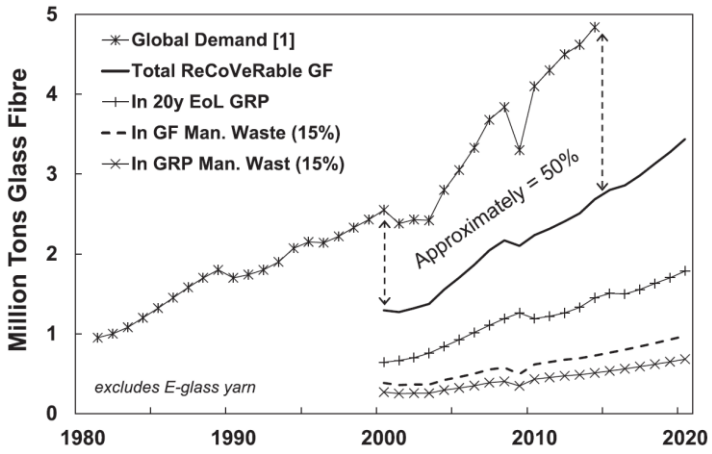

Figure 1-2 Glass fibre global demand and availability for recycling, reproduced from [15]

1.2 Aims and Objectives

As discussed above, strength loss during recycling significantly reduces the reinforcing capability of thermally RGF, which is a key impediment in the commercialisation of recycling GRT. The main aim of this thesis was to investigate the potential for retaining and/or regenerating the strength of thermally RGF; in order to produce composites reinforced with RGF that could complete with those using new glass fibres. To achieve this, four objectives are outlined:

1. **Develop an in-house process for thermally recycling GRT**

A thermal recycling rig was developed to better simulate the impact of such a process on RGF, in order to validate the subsequent work carried out using these glass fibres. The thermal recycling process that was developed in this work was based on a fluidised bed reactor. The thermoset matrix used throughout was epoxy due to its widespread commercial use.

2. **Investigate the use of a catalyst to aid epoxy thermal decomposition**

The potential for using a catalyst to aid epoxy decomposition was investigated as a means of overcoming obstacles associated with GRT thermal recycling. The ability of catalysts to lower the temperature and energy required for epoxy thermal

decomposition was studied. Furthermore, the effect of reducing recycling conditions on the strength retention of recycled glass fibres was also investigated.

3. **Investigate methods for regenerating the strength and interface properties of RGF**

The effect of post treating RGF was investigated as a means of regenerating strength lost during thermal recycling. Silane coupling agent and surface treatments were also studied to regenerate glass fibre surface functionality and improve adhesion with PP and epoxy matrices. These polymers were selected for the matrix materials in second life composites because of their widespread use and processability.

4. **Investigate the performance of composites reinforced with thermally recycled and regenerated glass fibres**

The performance of glass fibre reinforced polypropylene (GF-PP) and glass fibre reinforced epoxy (GF-EP) prepared with thermally recycled and regenerated glass fibres were investigated. The influence of matrix modification and a variety of other treatments, to improve interfacial adhesion between RGF and polymer matrices, were also studied in terms of GRP performance.

Much research has already been directed toward the development, optimisation and upscaling of the fluidised bed process for recycling waste FRT, with substantial advancements made over the last 20 years. Therefore, the novelty of this thesis does not necessarily lie in the design and development of the fluidised bed recycling rig, but rather in:

1) Investigating the use of a variety of catalysts to aid thermal recycling of GRT within the fluidised bed process
2) Examining the effectiveness of a range of chemical treatments at regenerating the strength and surface functionally of fluidised bed recycled glass fibres
3) Reintroducing the recycled and regenerated glass fibres within GRP as a reinforcement medium and characterising the mechanical properties of these “second life” GRP

1.3 Outline of thesis

Chapter 2 outlines the design of the thermal recycling rig and presents the results from the performance assessment of the rig.

Chapter 3 presents and discusses the work pertaining to the use of a catalyst as a means of aiding thermal recycling of GRT.

Chapter 4 gives the results of thermally RGF subject to various chemical treatments in order to improve their strength and interface properties with PP and epoxy.

Chapter 5 discusses the performance of GF-PP and GF-EP reinforced with recycled and regenerated glass fibres.

Chapter 8 summaries the conclusions of this thesis and gives suggestions for future work.

2. Recycling glass fibres with fluidised bed

In this chapter, the design and hardware used to construct the in-house fluidised bed recycling process is presented. The fluidised bed operating conditions, fluidisation velocity and bed temperature, are optimised in terms of glass fibre recovery efficiency and surface cleanliness. The strength of glass fibres recycled using the fluidised bed process are measured and the effect of fluidisation velocity and bed temperature on the strength are assessed.

2.1 Literature review

In this section an overview of proposed GRT recycling technologies is presented, with the benefits and drawback of the various methods discussed. The influence of exposing glass fibres to elevated temperatures, similar to that of a thermal recycling process, is explored in terms of fibre tensile strength and surface functionality.

2.1.1 An overview of recycling technologies

A multitude of technologies have been proposed and developed for recycling GRT materials. There are fundamentally three classifications of processes:

1) Mechanical pulverization/granulation techniques to reduce the size of the scrap GRT to produce recyclate
2) Thermal processing to break the scrap down into materials and energy
3) Chemical breakdown of the thermoset matrix into smaller weight molecules using a heated solvent

Prior to assessing the pros and cons of the various recycling techniques, the following question should be answered: what are the features that constitute a good GRT recycling process? To answer this, some such features are listed below:

- Capable of simultaneously processing dissimilar thermosetting polymers
- Tolerance to contaminates within the scrap GRT (e.g. metallic inserts)
- Capable of continuous operation
- Scalability to satisfy different geographic recycling requirement

- Maximize the value of resalable materials produced during the recycling process
- Low operating cost (relative to value of resalable materials produced during the recycling process)

Ultimately, the profitability of a recycling process will determine which technology(s) will be commercialised; however, the above list gives the characteristics that are likely to be met by such a process.

2.1.1.1 Mechanical recycling

Mechanical recycling involves size reduction of the GRP scrap, initially by low speed cutting/crushing to 50-100 mm. A high-speed mill or hammer mill is then used to further reduce the scrap size to 10 mm – 50 μm. Cyclones and sieves are then used to classify the scrap into fibre rich (coarse) and matrix/filler rich (fine) fractions [6, 12]. The finer fraction of recyclate can be used as filler (substituting calcium carbonate) in bulk moulding compound and sheet moulding compound. The mechanically RGF are generally weaker and shorter than virgin fibres and have poor interface with polymer matrices [6]. Using the coarse/fibrous fraction has therefore been shown to yield composites with reduced strength, even at low levels of loading [7]. ERCOM (Germany) [8] and Phoenix Fibreglass (Canada) [6] are two examples of companies which commercialised mechanical recycling of waste GRP, which later terminated business due to financial reasons. The crushing and milling process required for scrap size reduction can be energy intensive given the process yields short and weak fibres and filler material [6]. Despite this, mechanical recycling of GRP continues to be commercialised by Reprocover (Belgium), which produces non-structural components with ground GRP waste [9].

2.1.1.2 Chemical recycling

Chemical recycling processes use heated solvent/solvent mixture to break down the thermoset into smaller weight molecules [16]. Typical solvents used include sub/supercritical water [17, 18], glycols [19], acids and bases [6]. Chemical recycling can be performed at temperatures lower than that required for thermal recycling (<450 °C) while yielding clean fibres with no char residue [16]. Chemical recycling methods also have the potential for reclaiming materials from the depolymerised

resin, in the form of monomers or petrochemical feedstock [6]. While carbon fibres have retained 85-99% of their tensile strength during chemical recycling [20], studies using subcritical water to recycle glass fibre report a fibre strength retention of 30-60% [17, 18]. The solvents and catalysts used during chemical recycling have negative environmental and economic costs associated with disposal as well as potential health risks [16]. The chemical recycling process is highly dependent on matrix material; therefore, it would be difficult to recycle end-of-life composites, given that a mixture of polymers would likely be present in the waste stream [6].

2.1.1.3 Thermal recycling

Thermal recycling technologies can be further classified into combustion and pyrolysis processes.

Recycling using Pyrolysis

Pyrolysis involves heating the GRP to 300-1000 °C in the absence of air [6]. This causes depolymerisation of the plastic matrix into lower weight organic molecules such as oil, gas and solid char [7]. When applied to FRP, the pyrolysis process therefore allows for the recovery of the polymer matrix (in the form of smaller molecules) as well as the reinforcement fibres. The liquid and solid material can be recovered and used as feedstock for further chemical processes and the gas can be utilised in combustion processes. A diagram of a typical pyrolysis process is given in Figure 2-1.

The distribution of the pyrolysis products is dependent on the polymer type and treatment temperature [7]. The gas product accounts for 5-15% by weight, with the majority being CO_2 and CO, giving a relatively low calorific value of around 15-20 MJ/kg [6, 21, 22]. The liquid fraction accounts for 10-50% of the recovered material with a high calorific content of 30-40 MJ/kg, which is in the range of fuel oil [6, 7, 22]. The solid product typically accounts for 50-75% by weight, which comprises the reinforcement fibres, mineral filler and char residue [6, 7, 21, 22]. Cunliffe and Williams found that 16% of the solid residue was char (with the recycled fibres comprising the remaining constituent) which could be removed by combustion at 450 °C to obtain clean fibres [23]. Exposure to such high temperatures significantly

reduces the strength of RGF, which cannot replace new fibres without compromising the properties of the composites [6, 7].

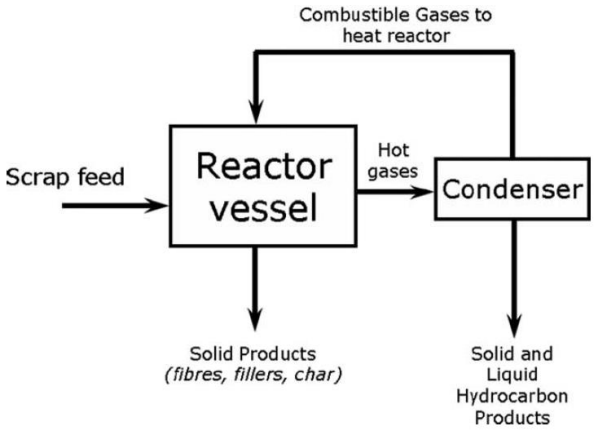

Figure 2-1 Diagram of a typical pyrolysis process, reproduced from [7]

A pyrolysis process was developed by ReFiber (Denmark) for the recycling of GRP wind turbine blades. After the size reduction, the material is fed into an oxygen-free rotating furnace at a temperature of 500 °C. Gas produced during the pyrolysis is used for electricity production as well as heating the furnace, and the fibres are cleaned in a secondary combustion processes. Due to strength loss, the RGF can only be used in non-structural applications such as thermal resistant materials. It remains cheaper to landfill end-of-life wind turbine blades, therefore, the process has not been successfully commercialised [24].

Recycling using Combustion

Combustion recycling processes involve heating the GRP in the presence of oxygen. This process can be used as an energy source, since combustion of typical polymer matrix materials is exothermic. Feeding ground GRP to cement kilns has been shown to be viable [25]. The combustion of the plastic provides energy (about 12 MJ/kg of waste) to the process and the solid residue (fibres and mineral filler) provide feedstock for the cement production [8]. The inclusion of the solids does not affect the ultimate strength of the cement [7, 25]. As with mechanical recycling, this method may be seen as a downcycling solution as it does not utilise the reinforcement potential of glass fibres. Zajon Logistik (Germany) used pulverized

GRP scrap as feedstock in cement kilns, however, the businesses terminated in 2014 due to financial difficulties [25].

The fluidised bed process has been demonstrated to successfully thermally recycle FRP [13, 14], while overcoming industrial challenges such as scalability, operation continuity, contaminant sensitivity, recovering clean fibres and processing dissimilar polymers [7, 26]. A fluidised bed is a phenomenon that can occur when a quantity of a solid particulate substance is placed under suitable conditions to cause a solid-fluid mixture to behave as a fluid. This is typically attained by introducing pressurised fluid through the particulate medium. This results in the medium then having properties and characteristics of regular fluids. The University of Nottingham pioneered this process for recycling glass fibre composite waste, a diagram of which can be seen in Figure 2-2 [27]. The recyclate undergoes size reduction processing to 10–25 mm using a shredder or hammer mill prior to recycling [13]. The fluidised bed reactor contains silica sand that is heated by a stream of pre-heated air. The matrix is rapidly combusted in the fluidised sand due to high heat transfer rates and mechanical abrasion. After liberation from the matrix, fibres and filler materials are carried by the stream of hot air and gas out of the reactor. The fibres and filler material are separated from the gas stream and the gas stream is subsequently introduced into a secondary combustion chamber. The gas is fully combusted at around 1000 °C, which can be used as an energy source and produces clean flue gas [13]. The typical temperature within the fluidised bed reactor is 450-550 °C [7], depending on the thermoset within the recyclate. Exposure to such high temperatures significantly weakens the glass fibres [14], reducing their reinforcement potential and substantially devaluing them commercially.

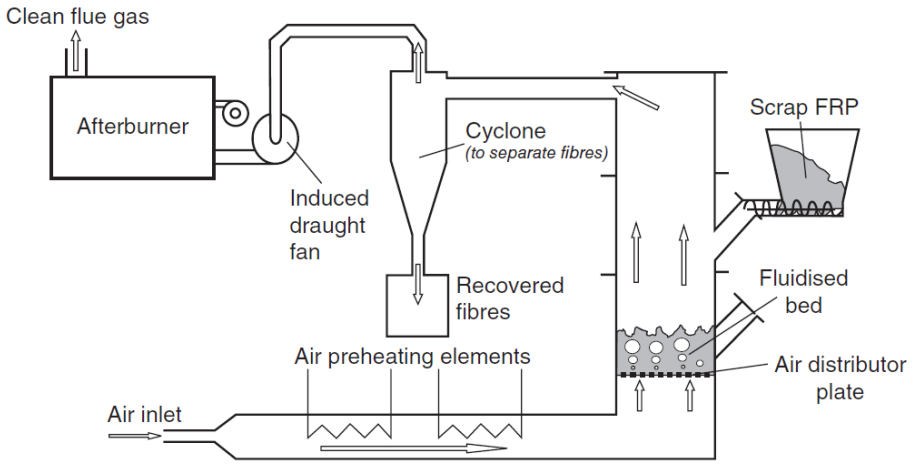

Figure 2-2 Schematic of fluidised bed thermal recycling process developed at the University of Nottingham, reproduced from [27]

A fluidised bed process for recycling GRT has not been commercialised however, a pilot scale system has been developed by the University of Nottingham, which is now used for recycling carbon fibre composite waste [28]. Pickering et al. conducted a study demonstrating a fluidised bed recycling process could financially break-even at a capacity of around 9000 ton of scrap GRT per annum [13]. The global production of glass fibre is expected to rise from 5000 kton in 2014 [29] to around 7250 kton in 2020 [4]. Over 1 Mtonnes of GRP were produced in Europe alone in 2013 [8]. Over 50% of GRP utilise thermoset matrices [6], hence the quantity of scrap GRT available will likely far exceed the minimum required for commercialisation.

2.1.2 Effect of thermal recycling temperatures on glass fibre strength

In this thesis, the terms “thermal conditioning” and “thermal recycling” will be used extensively; for clarity, these terms will now be defined. Thermal conditioning involves directly exposing fibres to an environment with an elevated temperature. In this case, the fibres are not within a matrix material when subjected to an elevated temperature. Thermal recycling involves exposing GRT to an environment with an elevated temperature in order to thermally decompose the polymer matrix and liberate the reinforcement fibres. In addition, the term “thermal cleaning” will also be used in this thesis. This refers to a process whereby fibres are thermally conditioned with the intention of thermally decomposing material present on the fibre surface,

such as sizings or residue present on the fibres after thermal recycling. Extensive research has been carried out to investigate the effect of elevated temperatures on glass fibre strength. It is concluded by numerous authors that thermal conditioning [5, 15, 30-35] and thermal recycling [13, 14, 22, 30, 36-38] processes can cause a significant reduction in glass fibre strength. It can therefore be stated that exposure to elevated temperatures leads to “thermal weakening” of glass fibres.

2.1.2.1 Effect of thermal conditioning on glass fibre strength

Both temperature and time of exposure influence the extent of fibre weakening. Glass fibre strength loss was found to increase with temperature when thermally conditioned and thermally recycled. It was observed that strength loss also increase with exposure time, until a constant minimum value is reached [31, 39]. An increase in conditioning temperature is associated with more rapid fibre weakening since this asymptotic minimum is attained faster at higher temperatures. Figure 2-3 shows the effect of both temperature and time on glass fibre residual strength [31].

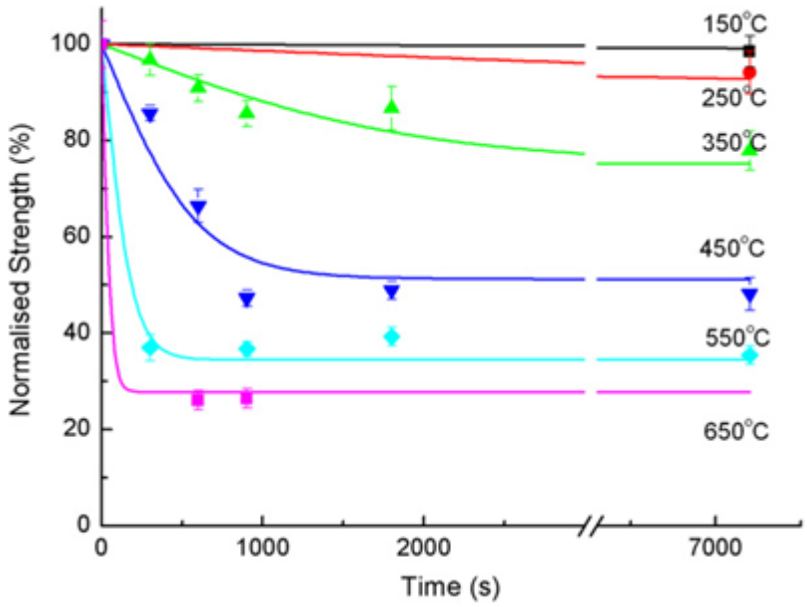

Figure 2-3 Relative tensile strength of single glass fibre after thermal conditioning at a variety of temperatures and times, reproduced from [31]

Jenkins et al. investigated the effect of sizing and its influence in reducing mechanical damage of thermally conditioned glass fibres [32]. Figure 2-4 shows that

3-aminopropyltriethoxysilane (APS) sized glass fibres are stronger than unsized fibres when exposed to less than 450 °C, if fibres tested are extracted from a thermally conditioned bundle. Figure 2-4 also shows that unsized glass fibres retain significantly more strength when treated as a single fibre, which was attributed to a less mechanical damage. Separating the unsized fibres from the bundle prior to thermal conditioning reduced damage sustained due to fibre-fibre interaction. This behaviour was not observed with APS sized fibres, which, when exposed to 300 °C or less, retained the same strength regardless of the order of individual fibre separation and heating. This is explained by the sizing protecting the fibres during handling; however, above 300 °C the sizing is thermally decomposed. As a result, fibres thermally conditioned as bundles at 450 °C or more exhibit the same strength loss regardless if they are sized initially. Finally, Figure 2-4 shows the strength of all four conditions converge after exposure to 600 °C. This demonstrates that mechanical damage does influence the measured strength; however, there is still another underlying mechanism which is responsible for strength loss in thermally conditioned glass fibres.

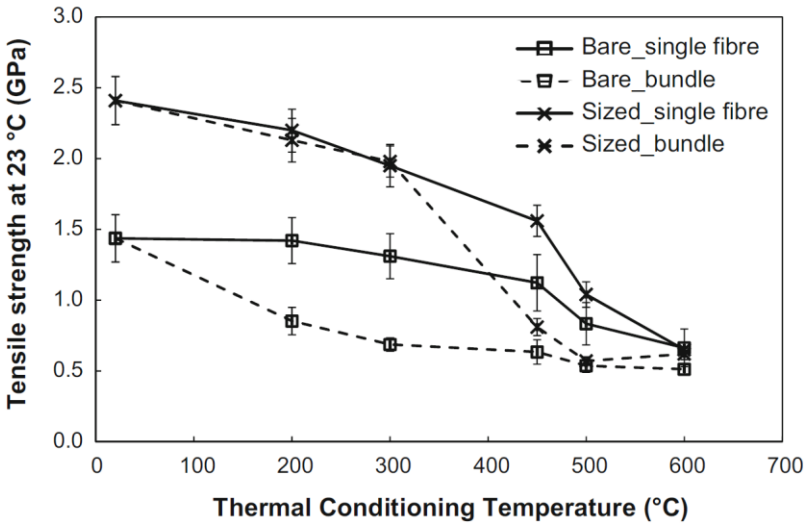

Figure 2-4 Strength of thermally conditioned APS sized and unsized glass fibres at various temperatures, both treated as bundles and individually, reproduced from [32]

The mechanism of thermal weakening of glass fibres is still under discussion in the literature, and there is no consensus on the physical change(s) that occur in glass fibre that can account for the strength loss [40]. The proposed mechanisms can typically be split into two categories, bulk or surface phenomenon.

Otto suggested that thermal conditioning affects the bulk structure of the glass fibres [41]. It was observed that glass fibres heated above 400 °C exhibited length contraction and could return the fibre modulus to that of annealed glass. Thermal conditioning at 500 °C for 24 hour resulted in a length contraction of approximately 0.23%. Similarly, Yang and Thomason also observed changes in glass fibre modulus and length while heating using thermo-mechanical analysis [42]. In both cases, it was observed that length contraction and fibre modulus increased with conditioning temperature [41, 42]. Aslanova et al. measured changes in glass fibre internal friction and shear modulus at various temperatures using a low frequency torsion pendulum under vacuum [43]. It was observed that above 300 °C the relative shear modulus began to increase which was attributed to glass fibre compaction. It was proposed that this could be due to enthalpy relaxation of deformations within the glass structure that were created by the drawing process used to form the fibres. The concept of enthalpy relaxation is given further weight by the work carried out by Ya et al. who used differential scanning calorimetry (DSC) to measure energy flow when heating glass fibres over a range of temperatures [44]. An exothermic peak was observed between 300 °C and 700 °C, which was attributed to the release of excess enthalpy within the glass network. Yue shows that enthalpy relaxation is a consequence of quenching the glass fibres during production [45]. A “frozen-in isotropic network” is formed with excess enthalpy present within the glass fibre structure. It is therefore suggested that structure rearrangement occurs in glass fibres above 300 °C [40], where the energy state of the glass network is lowered.

It is proposed that anisotropic relaxation is another structural change that occurs during thermal conditioning of the glass fibres. It is suggested that straining during fibre drawing process results in axial anisotropy [42]. Ya et al. suggests that exposure to elevated temperatures induces anisotropic relaxation of the glass structure [44]. Ya et al. heated glass fibres to various temperatures and observed the birefringence using optical microscopy. The birefringence was found to reduce around 250-300 °C; no birefringence was observed after heating for 10 and 3 hour at 400 °C and 550 °C respectively [44]. Lund and Yue also reported reduction in anisotropy of glass fibre when thermally conditioned [46]. It was theorised that drawing melt during fibre production causes axial alignment of defects; subsequent heating of the glass fibres causes them to lose alignment, inducing fibre strength loss.

Rather than bulk structure change, Feih et al. proposed that the strength loss of glass fibre is due to an increase in flaw severity on the surface of thermally conditioned fibres [47]. Indeed, the strength of glass fibre is typically considered to be controlled by surface flaws [40, 48]. Feih et al. introduced an "artificial" surface flaw on the surface of a silane sized glass fibre using an ion beam [47]. It was found that the strength of these fibres were similar to thermally conditioned glass fibres. Furthermore, fracture surface analysis and fracture toughness modelling showed that the properties of the bulk structure were unchanged following exposure to elevated temperatures. It was concluded that the surface flaws only needed to grow between 180 and 400 nm (depending on flaw geometry) during thermal conditioning. Feih et al. suggest that flaw growth occurs during thermal recycling by water molecules (from sizing or atmosphere) diffusing into the glass fibre structure and reacting with stressed siloxane bonds at the crack tip [47]. The surface flaw theory is bolstered by work carried out by Sakka [49] and Yang et al. [5]. They demonstrate that thermally conditioned fibres can be partially re-strengthened after reducing their diameter by etching with hydrofluoric acid (HF). This is discussed further in Chapter 4.

Despite the indirect evidence, Feih et al. did not present direct observation of a non-artificially induced flaw on the surface of thermally conditioned fibre. Scanning electron microscopy was sufficient to image the artificial flaws. If the thermally induced flaws have a similar geometry, they too should be observable with this technique [47]. Furthermore, it is not entirely clear how water promotes the surface crack growth during thermal conditioning. It is understood that water is damaging to glass fibre, however, much of the investigations in this area are on freshly drawn and flaw free glass fibres [40]. Mould [50], Ito and Tomozawa [51] and Li and Tomozawa [52] in fact demonstrated that the strength of abraded bulk glass increases after storing in water or water vapour. This phenomenon is further discussed in Chapter 4.

2.1.2.2 Effect of thermal recycling on glass fibre strength

The strength loss of glass fibres thermally recycled using pyrolysis [22, 37, 38] and fluidised bed [13, 14] processes have been reported. Williams et al. observed a 45% drop in tensile strength after recycling glass fibre using pyrolysis at 450 °C [22]. Cunliffe et al. also used pyrolysis for glass fibre recycling and the effect of recycling

temperature was investigated [38], as shown in Figure 2-5. After liberating with pyrolysis, the glass fibres were cleaned of char residue by heating in air at the same temperature as was used for pyrolysis. Contrary to what is found when thermally conditioning glass fibres [5, 15, 30-35], no clear correlation between the pyrolysis temperature and the tensile strength was found between 400 °C and 650 °C. No treatment time was given by Cunliffe et al. for the final thermal cleaning stage in air. The strength of thermally conditioned fibres is dependent on both temperature and time [31], hence inconsistent thermal cleaning time could explain the lack in correlation. Figure 2-5 shows that increasing the pyrolysis temperature to 800 °C significantly reduced fibre strength.

Åkesson et al. used microwave pyrolysis to recycle glass fibres from GRT [37]. Fibre bundles from a roving were infused with polyester and the strength of the bundle after thermal recycling was compared to that of the virgin roving. Åkesson et al. reported recycling glass fibres bundles with strength loss of just 25% using microwave pyrolysis at 360 °C and 440 °C, again, no relation between pyrolysis temperature and fibre strength was observed. Since the change in bundle strength is given (opposed to single fibre) this data cannot be directly compared to [22, 38], however, relative strength loss is typically higher when testing bundles after thermal weakening due to fibre-fibre abrasion during tensile testing [31].

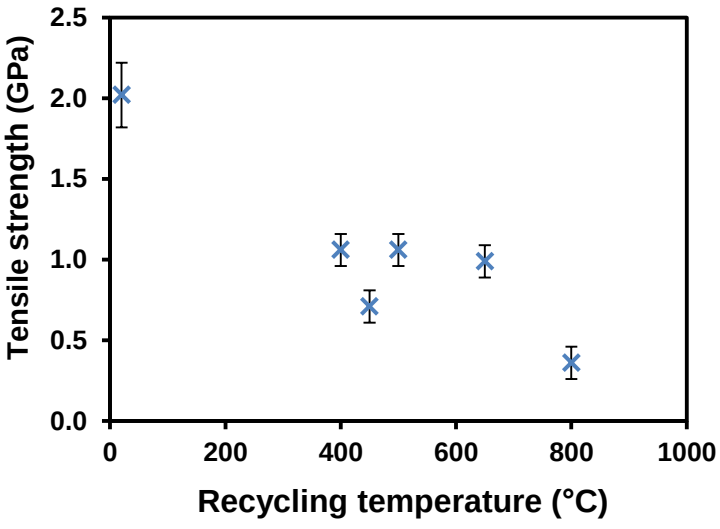

Figure 2-5 Tensile strength of glass fibres recycled using pyrolysis at various temperatures, reproduced from data in [38]

Kennerley et al. measure the strength of thermally recycled glass fibre using the fluidised bed process [14]. Both recycling temperature and fluidisation velocity were varied and the reported strength can be seen in Figure 2-6. In agreement with [5, 15, 30-35], fibres exposed to higher temperatures exhibit more strength loss. Pickering et al. observed similar strength loss when recycling using the fluidised bed process under the same conditions [13]. Kennerley et al. reported envisaging a reduction in RGF strength with fluidisation velocity, due to the additional agitation in the fluidised bed. No such relation was observed and the strength of RGF was not influenced by the fluidisation velocity [14].

The steady state strength of glass fibres thermally conditioned in [31] (Figure 2-3) have also been included in Figure 2-6. The strength of recycled and conditioned fibres is comparable after exposure to 450 °C. However, fibres recycled in the fluidised bed at 550 °C and 650 °C are weaker than found in [31] at the same treatment temperature. Since the steady state strength of conditioned fibres is given in Figure 2-6, the dissimilarity between recycled and conditioned fibres cannot be attributed to differences in exposure time. Although it is not fully understood what causes the additional damage, it could be speculated that it is either a result of thermal decomposition of the polymer matrix (in order to liberate the fibres), or mechanical damage induced by processing in the fluidised bed. Thomason et al. showed that glass fibres do not sustain any additional damage when recycled from GRT in a furnace, compared to thermally conditioning at the same temperature [15]. This suggests that the fibres are likely mechanically damaged during processing within the fluidised bed recycling system. Whether this damage is sustained within the fluidised bed itself, or upstream during fibre separation is still unclear.

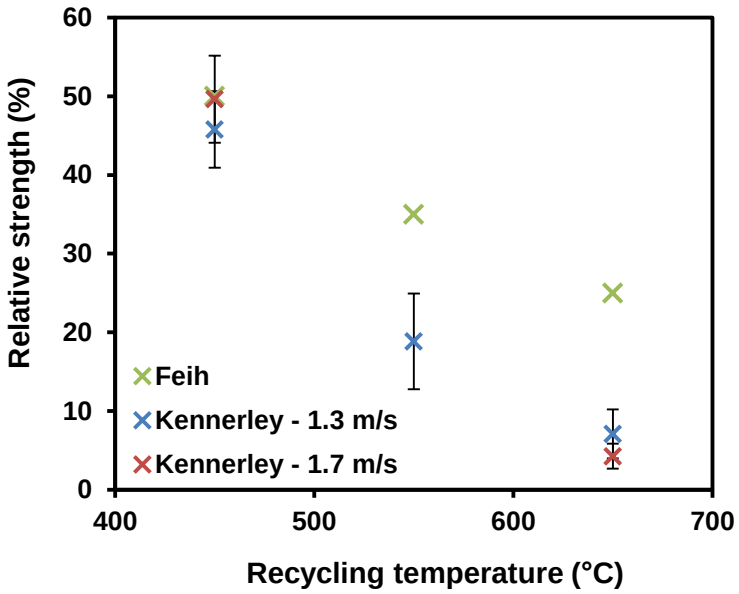

Figure 2-6 Comparison between tensile strength of glass fibres recycled using fluidised bed process and thermally conditioned glass fibres, reproduced from data in [16] and [25] respectively

2.1.3 Effect of thermal recycling temperatures on the IFSS

Using thermally recycled or thermally conditioned glass fibres as reinforcement produces composites with diminished mechanical performance, due to the poor fibre strength and interfacial adhesion between the glass fibres and polymer matrix [5, 15, 37, 53, 54]. Several authors have used micromechanical techniques to measure the IFSS between thermally conditioned glass fibre and a PP matrix [5, 15, 55, 56]. Yang et al. [5] and Thomason et al. [15] thermally conditioned glass fibres at 500 °C for 25 min in air. Using the microbond test, Yang et al. reported a drop in apparent IFSS from 16 MPa to 8 MPa after thermal conditioning [5]. In agreement, Thomason et al. observed a reduction in apparent IFSS from 14.7 MPa to 9.2 MPa [15]. Nagel et al. also used the microbond test to investigate the effect of thermal conditioning temperature and atmosphere on apparent IFSS between glass fibre and PP [55]. The results for the study are reproduced in Figure 2-7. The temperature at which the apparent IFSS reduced significantly (250 °C in air) correlated with thermogravimetric analysis (TGA) data that indicated most of the sizing begin to decompose between 200 °C and 250 °C [55]. It was concluded that thermal decomposition of the sizing resulted in reduced adhesion with PP, lowering the measured IFSS. Roux et al. used the fragmentation test on GF-PP however only the critical fibre length was reported [56]. It was observed that the critical fibre length of composites made with

pyrolysed fibres was lower than in new composites. If the fibre diameter and fibre strength were equal in both composites, this would suggest the IFSS increased due to the thermal conditioning. Although the fibre strength was not measured in [56], the fibre was likely weakened as a result of the pyrolysis process [22, 37, 38]. It is therefore difficult to make any conclusions regarding the IFSS values in [56]. In addition to micromechanical techniques, Bikiaris et al. [57] and Åkesson et al. [37] used fracture surface analysis to conclude that the interfacial adhesion is diminished after thermally conditioning glass fibres.

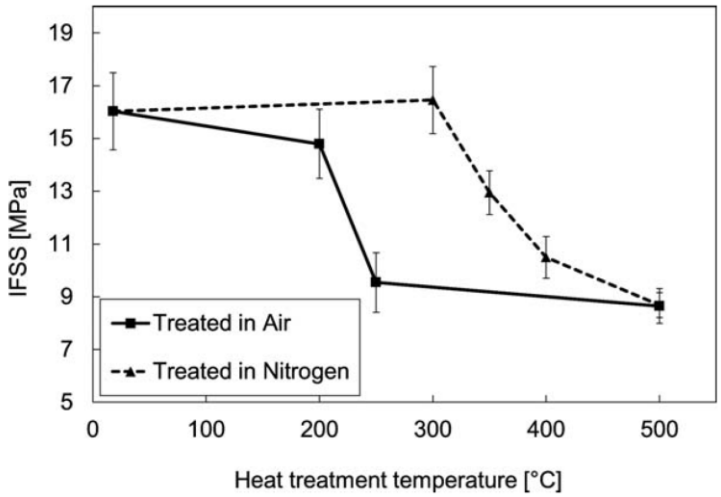

Figure 2-7 Effect of thermal conditioning temperature and atmosphere on apparent IFSS between glass fibre and PP, reproduced from [55]

Although the exact composition of sizings are typically confidential and vary depending on the polymer matrix material, most contain an organic film former and an organofunctional silane coupling agent [58]. Several authors have studied the thermal behaviour of sizings [55, 59, 60] and organosilanes [32, 61] using TGA. Nagel et al. performed TGA on PP compatible commercially sized glass fibres in air and found that most of the sizing is degraded below 300 °C [55]. Both Nagel et al. [55] and Feih et al. [31] observed a reduction in sizing thermal stability when heated in air opposed to nitrogen. Gao and Su thermally degraded two different commercial sizings using non-isothermal TGA at a heating rate of 20 °C/min. It was observed that both sizings degraded at around 320 °C in air [60]. Rudzinsk et al. performed TGA on APS in combination with several commonly used film formers which were prepared in-house [59]. It was found that all the sizings fully degraded

by a temperature of 550 °C when pyrolysed at 10 °C/min. Peak rates of decomposition occurred at around 350 °C. Jenkins et al. studied the thermal behaviour of an APS film using simultaneous TGA and DSC under air. It was observed that the APS decomposition completed at 650 °C, with the main organics starting to degrade around 300 °C [32]. Pham and Chern studied the thermal decomposition of four other organosilanes in addition to APS. Although they showed different thermal behaviour, all silanes decomposed between 300 °C and 650 °C [61], similar to the observations of Jenkins et al. [32]. The peak rates of mass loss occurred between 400 °C and 550 °C [61]. Based on the thermal analysis data [32, 55, 59-61] it is clear that exposure to typical thermal recycling temperatures results in the removal of the sizing.

2.1.3.1 Dehydroxylation of glass fibre surface

Silane coupling agents used in the production of GRP bond to the glass via interaction with the surface hydroxyl groups. Low hydroxyl density on the surface of glass fibres may therefore lead to a weaker interfacial adhesion between the glass and polymer matrix, ultimately compromising the mechanical properties of GRP based on thermally RGF. Several authors have observed a reduction in hydroxyl group concentration on the surface of glass fibre [62, 63] and silica [64-66] after exposure to elevated temperatures. It is suggested that the dehydroxylation is the result of surface silanol groups condensing to form siloxane bonds as shown in Equation 2-1.

Equation 2-1 Mechanism of silanol condensation on the surface of glass fibres [64]

$$[\equiv Si - OH] + [HO - Si \equiv] \rightarrow [\equiv Si - O - Si \equiv] + H_2O$$

Zhuravlev used a deuterium exchange method to measure the hydroxyl density on the surface of amorphous silica after thermally conditioning in vacuum in the temperature range 200-1100 °C [64, 65]. It was found that on a completely hydroxylated silica surface, the average number of silanol groups is 4.9 OH nm^{-2}. This value includes both free silanol groups as well as neighbouring hydrogen bonded hydroxyl groups. After conditioning at 500-600 °C, around 60-70% of the hydroxyl groups are lost. The hydroxyl density reduces further to less than 0.15 OH nm^{-2} when conditioning at 1100 °C. Using contact angle goniometry, Liu et al.

measured the hydroxyl density on E-glass fibre to be 2.29 OH nm^{-2} [62]. This value is likely lower than pure silica due to the various other constituents in E-glass. After conditioning in a nitrogen atmosphere at 600 °C, the hydroxyl concentration reduced to 1.71 OH nm^{-2}. From the contact angle of water at point of zero charge, Carre et al. reported a hydroxyl concentration of 2.5 OH nm^{-2} on glass slide, which were pyrolysed at an undisclosed temperature [67]. No value for hydroxyl concentration was given for the un-pyrolysed glass slides; however, the reported value is comparable to that measure on silica that was conditioned at 500 °C by Zhuravlev [64].

All the above studies conditioned the glass fibres/silica in an inert atmosphere, opposed to air, which would better simulate thermal recycling of glass fibres using combustion. It is therefore unclear whether condensation and dehydroxylation will occur on the surface of thermally RGF. Using the microbond technique, several authors have measured the IFSS of glass fibres thermally conditioned at typical recycling temperatures [5, 15, 68]. In all cases, the re-application of APS regenerated the IFSS with PP back to that observed when using new fibres. Since the APS apparently bonded to the fibre, it may be concluded that dehydroxylation of the fibre surface did not occur (to a degree that would effect the IFSS) when conditioning the glass fibres.

The literature is lacking insight into the resulting surface of glass fibres thermally recycled from GRP. It is therefore unclear what effect the matrix thermal decomposition will have on the surface of RGF, in terms of hydroxyl concentration. Kennerley et al. observed that resizing (γ-methacryloxypropyltrimethoxysilane) fluidised bed RGF then processing into polyester based dough mould compound (DMC) did not lead to an increase in strength of the composites, when compared to using unsized RGF [14]. The recycling temperature was high enough to assume that the original sizing was at least partially removed during the recycling process [32, 55, 59-61]. The ineffectiveness of the sizing at increasing the composite strength may therefore be caused by low hydroxyl concentration on the RGF, resulting in low interfacial adhesion.

2.1.4 Conclusions of literature review

A fundamental challenge facing the recycling of glass fibre reinforced thermoset materials is the lack in value of the recycled materials, making commercialisation economically problematic. Mechanical recycling techniques have been commercialised; however, the RGF lose their reinforcement potential so can only be downcycled and used as filler material. Methods involving thermally decomposing the matrix material can successfully recover clean fibres without the use of chemicals. Pyrolysis processes for recycling carbon fibre have been commercialised, however no industrial scale process has been developed for thermal recycling of glass fibres. Thermally recycling glass fibres has two major obstacles to overcome: the severe loss in glass fibre strength and the lack of interfacial adhesion between RGF and polymer matrices. The cause for thermal weakening of glass fibres is still debated in the literature; however, most theories involve structure changes within the fibre or the propagation of surface flaws. It is clear that poor interfacial adhesion arises due to the removal of the organic sizing, which decomposes at typical thermal recycling temperatures. To increase the reinforcement potential and commercial competitiveness with new fibres, the strength and/or interfacial adhesion of thermally RGF must be regenerated.

2.2 Fluidised bed recycling rig brief

A fluidised bed reactor and fibre separation system was developed as a means of thermally recycling FRT. This method for recycling fibre was previously established in [13, 14, 36] and has been demonstrated to successfully continuously recycle fibres at high rate of recovery. Fluidisation is a process where by a particulate material is converted from a static state to a dynamic fluid-like state. This is achieved by passing a fluid up through the particulate material and allows for high heat and mass transfer rates [69]. For FRT recycling, pre-heated air is used as the fluidising fluid, which can facilitate rapid thermal oxidative decomposition of the thermoset matrix, thus releasing the fibres that are then recovered and reused.

A lab scale prototype of such a recycling process was commissioned in-house as part of this work. The aim was to recycle glass fibres in a manner similar to that of an industrial process, to better simulate the impact of such a process on the fibres in

terms of both mechanical properties and re-processability. The prototype rig should be able to:

1. Operate at a high enough temperature to thermally decompose thermoset matrices
2. Yield glass fibres that are relatively clean and free from excessive entrained sand
3. Successfully separate glass fibres from the combustion gas stream
4. Allow for a high enough rate of fibre recovery

2.3 Overview of the final fluidised bed rig design

This section describes the fluidised bed recycling rig, designed for the thermal decomposition of composite waste and subsequent collection of RGF. The hardware used to construct the system was selected based on the outcomes and requirements established during the design phase described in Appendix A. Figure 2-8 shows a schematic of the in-house fluidised bed recycling process.

The fluidising air is supplied via a centrifugal forced draft fan (FDF), which is pre-heated using an electric air heater. The air passes through a 90° piping before diffusing across an expansion cone and entering the sand bed that sits on the distributor plate. The air fluidises the sand, in turn heating the sand to the desired operating temperature. Combustion gases and entrained fibres, produced during polymer thermal decomposition, enter the freeboard and pass through the cyclone with the aid of an induced draft fan (IDF). The cyclone separates the fibres from the combustion gases and feeds the fibres into a collection box.

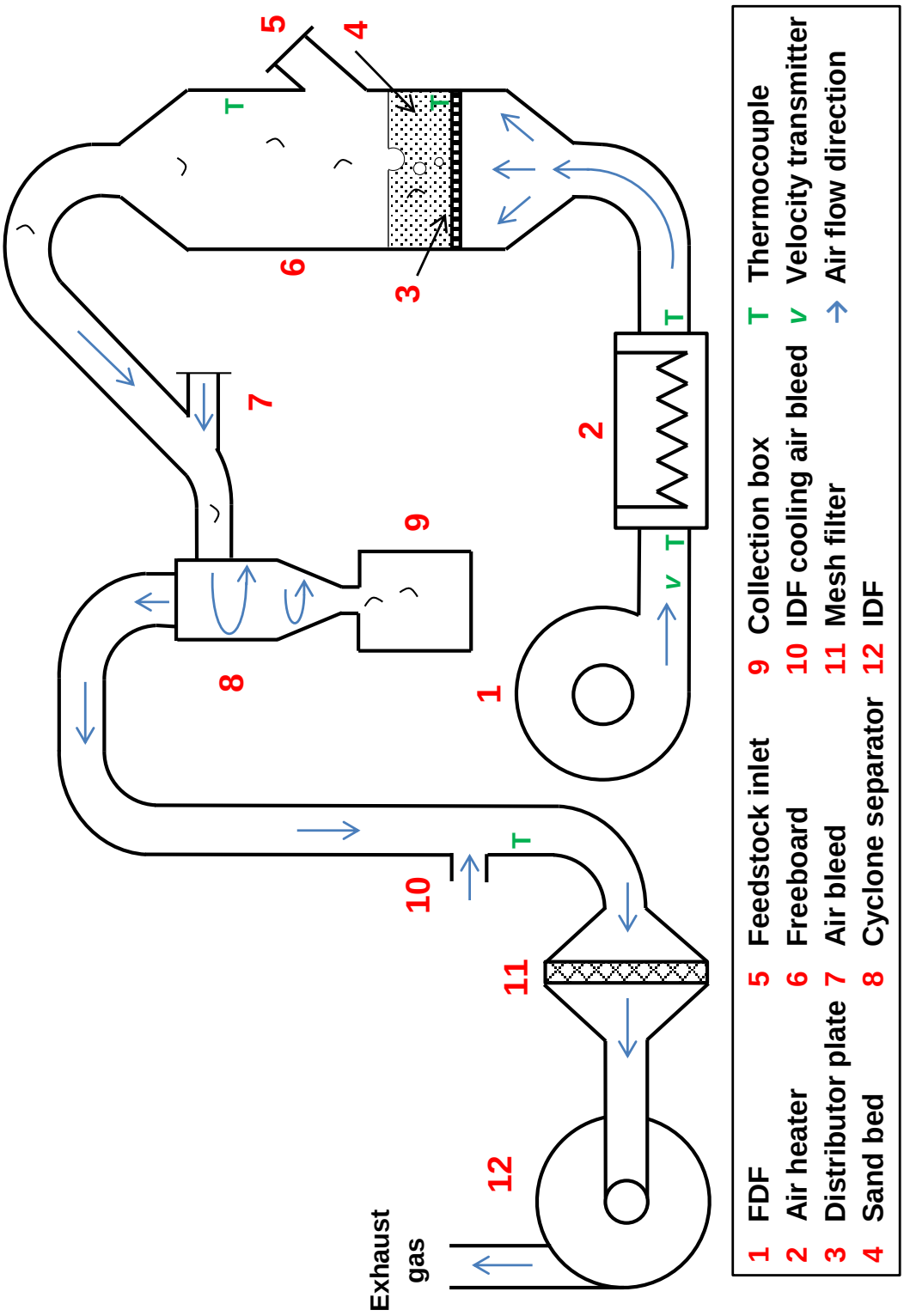

Figure 2-8 Schematic of in-house fluidised bed process designed in this thesis and used to recycle glass fibres throughout subsequent chapters

Figure 2-9 shows two images of the in-house developed fluidised bed recycling rig with thermal insulation applied to the reactor.

Figure 2-9 Images of the in-house developed fluidised bed recycling rig

2.3.1 Fluidised bed reactor design

The polymer matrix is thermally decomposed within the fluidised bed reactor, which is fabricated from a 316 stainless steel pipe with a diameter of 211 mm. The height of the reactor freeboard is approximately 1.3 m to encourage disengagement of the fluidised sand within the reactor, avoiding excessive sand entrainment into the separation section of the process. Silica sand with nominal particle size 0.5-1.0 mm is used as the bed medium, which sits on a distributor plate with a porosity of around 9%. The distributor plate is comprised of two perforated stainless steel plates sandwiching a 0.4 mm aperture mesh to contain the sand. The composite recyclate

is fed manually into the reactor through an access pipe, located just above the expanded bed. The reactor is kept under a slight negative pressure with an IDF located downstream of the separation system. This prevents volatilised polymer escaping the system and allows the reactor to be opened during operation to feed recyclate.

2.3.2 Fluidising air supply

The fluidising air is supplied to the reactor via a centrifugal fan supplied by Fans & Blowers Ltd. The FDF allows the flow rate to be varied with a relatively constant pressure rise of 8.7 kPa. The fan pressure rise required for the system was established from the pressure drop across the air preheater, the pressure drop across the distributor plate and sand bed. The fluidisation velocity is regulated by controlling the fan speed with a Parker AC10 inverter and the flow rate is measured with an Omega FMA 1000 velocity transmitter.

2.3.3 Air preheater

Before entering the reactor, the air is preheated using a Sylvania SureHeat® Max with a maximum rating and outlet temperature of 30 kW and 750 °C respectively. The pressure drop across the heater is relatively low at 3.0-3.5 kPa. The recycling temperature of the bed is regulated via PID control using a West MAXVU16, with a thermocouple located within the expanded sand bed. To avoid overheating, RS ESM-7720 limit controllers are used to monitor the heater inlet and outlet temperatures.

2.3.4 Recycled glass fibre separation system

A cyclone with the geometry outlined in Appendix A was fabricated from 316 stainless steel. A centrifugal fan supplied by Fans & Blowers Ltd was used as an IDF; drawing the fibres and polymer volatiles from the freeboard and keeping the reactor under a negative pressure. The fan speed is regulated with a Parker AC10 inverter. Room temperature air bleeds are located upstream of the IDF to avoid overheating. A mesh based filter is located between the cyclone separator and IDF

to catch any fibres which pass through the cyclone without separating from gas stream.

As part of initially commissioning the rig, it was discovered that the cyclone was performing at poor separation efficiency. It would frequently become blocked with stagnated bundles of RGF. It was identified that the optimal air flow rate for fluidisation and fibre entrainment in the reactor was too low for the cyclone to operate efficiently. To overcome this, an air bleed was added to the cyclone inlet, see Figure 2-8. By operating the IDF at a higher airflow rate than the FDF, the airflow entering the cyclone could be increased without increasing the fluidisation in the reactor. After installing the addition it was then found that the vortex created within the cyclone was entering the collection box and unsettling the RGF. To decouple the vortex, four guide vanes were attached parallel to the vertical outlet of the cyclone. These two additions greatly improved the separating performance of the cyclone.

2.4 Performance of fluidised bed recycling rig

This section assesses the performance of the prototype fluidised bed recycling rig. The rig was subject to an initial commissioning phase in order to ensure it could meet the basic requirements of operation outlined in 2.2. In addition, the operating conditions were optimised to improve fibre yield efficiency, cleanliness and tensile strength.

2.4.1 Experiment

2.4.1.1 Materials

E-glass fibres used in this work were from a tri-axial (0 °/ -45 °/+45 °) 3-ply continuous mat supplied by Hexcel Reinforcements UK Ltd. The preform was used to manufacture GF-EP recyclate in-house for the fluidised bed recycling rig. PRIME 27 Resin (epoxy phenol novolac based) and PRIME 20LV extra slow hardener (cycloaliphatic and aliphatic amine based) were supplied by Gurit. This was used as the matrix for the recyclate for the fluidised bed recycling rig.

2.4.1.2 Preparing GF-EP recyclate

The GF-EP used throughout the work was manufactured in-house. The epoxy resin and hardener were mixed at a weight ratio of 100:28 according to recommendation of the supplier. The 3-ply mat was then infused with the epoxy at a weight ratio of 60% glass fibre. The fibre weight fraction was established by doing a burn off test of a section of the composite. The epoxy was cured at RT for 24 hour followed by a post cure heat treatment at 65 °C for 7 hour, following supplier's instructions. The cured GF-EP laminates were cut into various sizes depending on the requirements of the RGF. For example, recyclate was cut into 60x15 mm pieces when the strength of RGF was measured, since the RGF had to be long enough to prepare single fibre tensile specimens at a gauge length of 20 mm.

2.4.1.3 Single fibre tensile sample preparation and tensile test

All single fibre tensile testing was performed following ASTM C1557-03. Card tabs were cut out of 250 g/m^2 grade paper. Double-sided tape was placed on the paper tab approximately 1 mm away from the cut out window. The glass fibres were placed on top of the double-sided tape and Loctite Gel Superglue was applied to the fibres at the upper and lower edge of the window, as seen in Figure 2-10. Tensile strength of at least 30 single fibres from each test was characterised at 20 mm gauge length.

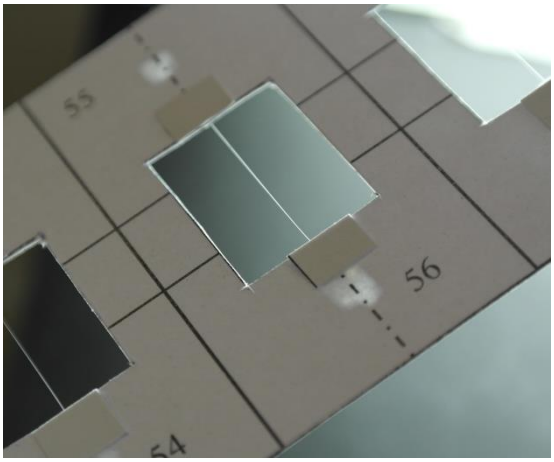

Figure 2-10 Image of a single fibre tensile test sample in card template

Fibre diameter measurement

Prior to tensile testing, the diameter of each single fibre specimens was measured to ensure the fibre strength could be calculated accurately. The cross sectional area of each fibre was assumed circular and found by capturing an image of the fibre using an Olympus GX51 optical microscope under x500 magnification. From the captured image, the diameter was then measured using ImageJ software as seen in Figure 2-11.

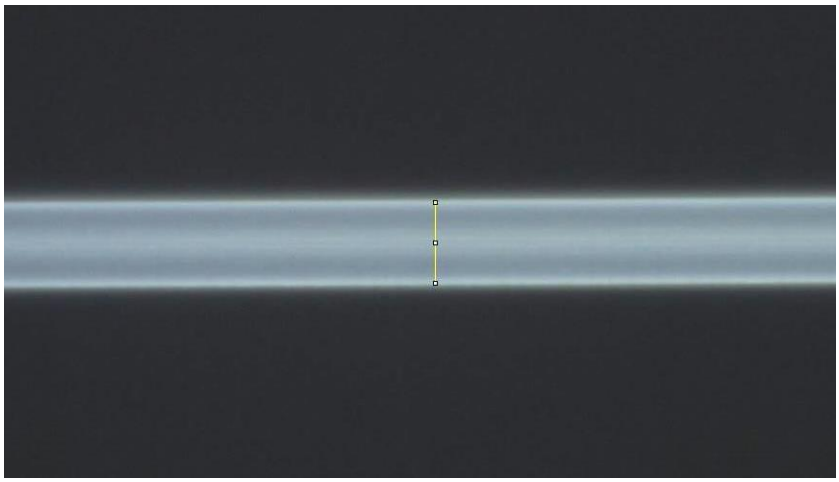

Figure 2-11 Image of glass fibre under optical microscopy which was used to measure the fibre diameter with ImageJ

Figure 2-12 gives the fibre diameter distribution within the continuous glass fibre mat supplied by Hexcel Reinforcements UK Ltd, which was used throughout this thesis. The distribution comprises the diameters of 425 individual glass fibres within the mat and highlights the need to measure the diameter of each single fibre tensile specimen individually, opposed to using a mean value during stress calculations.

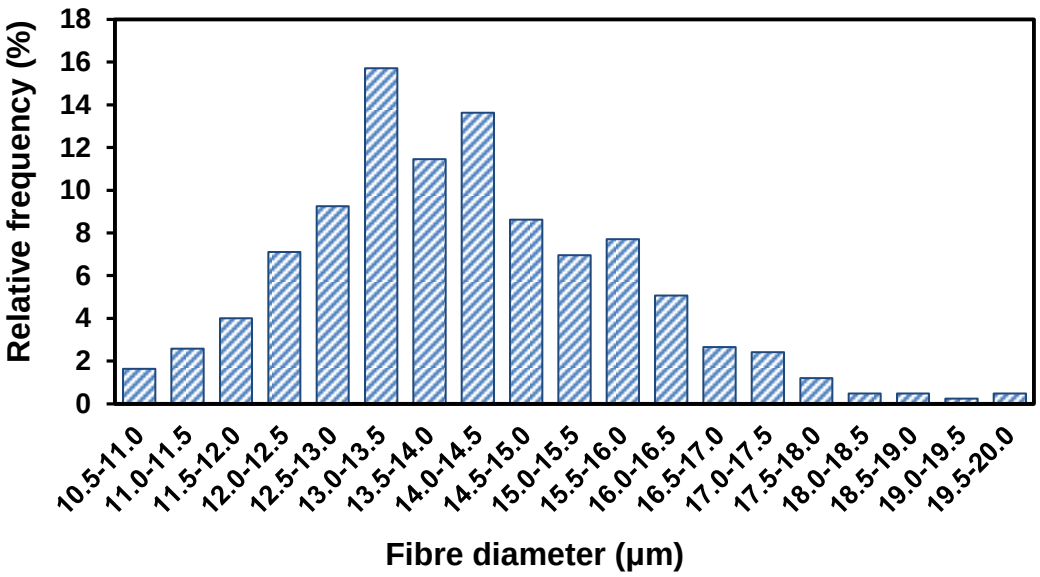

Figure 2-12 The fibre diameter distribution within the glass fibre mat (used throughout this thesis) highlights the need to measure the diameter of each single fibre tensile specimen individually

Tensile testing of the fibres was performed using a Testometric M250-2.5CT with a 5 N load cell at a strain rate of 1.5 %/min at ambient conditions. The single fibre tensile test set up is shown in Figure 2-13.

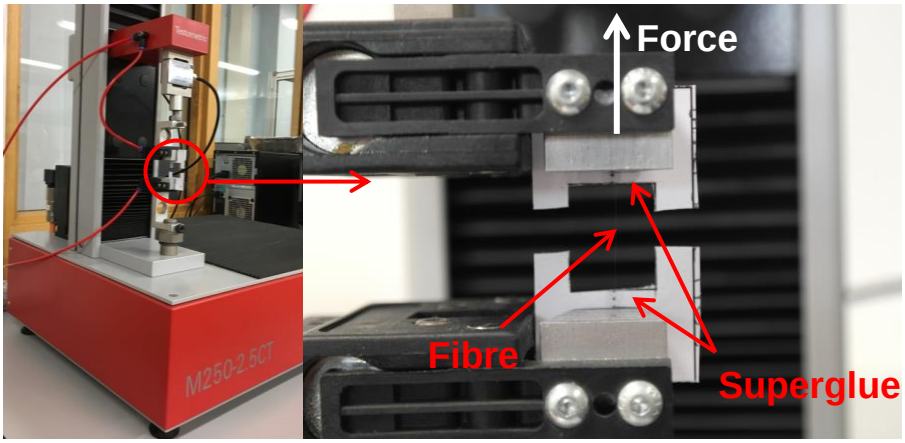

Figure 2-13 Single fibre tensile test setup using Testometric M250-2.5CT

2.4.1.4 Scanning electron microscopy for fibre surface analysis

A Hitachi SU6600 scanning electron microscope (SEM) was used to analyse the surface of fluidised bed RGF. Carbon adhesive tape was used to glue the

specimens on aluminium stubs. The samples were gold coated to prevent charging when they were analysed under SEM.

2.4.2 Initial commissioning of fluidised bed rig

During commissioning of the rig it was discovered that pre-heating the sand bed to the maximum anticipated operating temperature of 550 °C was relatively fast (< 60 min), when running the heater at maximum outlet temperature of 750 °C. The control system implemented could also maintain a constant bed set point temperature throughout recycling. Throughout initial testing of recycling GF-EP, a bed temperature of 500 °C, recyclate size of 10 x10 mm and static bed height of 150 mm were used. It was found that the thermoset matrix could in fact be thermally decomposed within the fluidised bed reactor at this temperature. Liberated glass fibres were able to exit the sand bed, following the airflow through the freeboard and into separation system. With the alterations to the cyclone inlet (as discussed in 2.3.4) the cyclone separator functioned adequately; the yield efficiency of the rig is further discussed in 2.4.3.2.

The RGF appeared visually clean after recycling at 500 °C, with little residue present on the fibre surface. Again, the recycled fibre cleanliness and factors affecting it are further investigated in 2.4.3.2. Sand entrainment and contamination with RGF was severe and unacceptably high at fluidisation velocities above 1.7 m/s. Moving forward, 1.7 m/s was set as an upper limit for the fluidisation velocity.

Finally, the rate of fibre recovery (i.e. composite feed rate) was assessed. It was quickly discovered that feeding the composites greater than 3 g/min (60% weight glass fibre) caused blockages at the cyclone inlet. This is the narrowest pipe section and the dimensions are based on the cyclone design given in Appendix A. According to the design assessment, increasing this (in turn increasing cyclone diameter) would reduce the pressure drop across the cyclone and lower the separation efficiency. For this work, this cyclone was kept and a maximum feed rate of 3 g/min used. Although this limited that rate of fibre recovery, the total RGF required for this work is relatively low. The micromechanical characterisation techniques used required very small quantities of glass fibre. Work associated with re-processing RGF into composites demands a much larger quantity of fibres. Chiefly, the prototype recycling rig was developed to better simulate the impact of

such a process on the RGF to further validate the subsequent work carried out on these fibres. Although the rate of fibre recovery is low from a processing perspective, it is thought that the conditions within an industrial scale recycling process can still be adequately replicated.

2.4.3 Characterisation of fluidised bed rig performance

2.4.3.1 Test strategy

This section gives the method used to characterise the fluidised bed rig and optimise the operating conditions. Two key operating conditions 1) fluidisation velocity and 2) bed temperature were initially identified as parameters likely to significantly affect the RGF. The fluidisation velocity is an independent controllable variable however, it is a function of both air density (determined predominantly by the bed temperature) and mass flow rate. Table 2-1 outlines the bed temperatures and fluidisation velocities investigated; in addition, the corresponding mass flow rates the FDF was required to produce are also given. For a given fluidisation velocity, the mass flow rate had to be reduced when increasing the reactor temperature due to the reduction in air density.

Table 2-1 Mass flow rate of air at the bed temperatures and fluidisation velocities investigated

Bed temperature (°C)	Mass flow rate (kg/s)		
	1.2 m/s	1.5 m/s	1.7 m/s
400	0.0220	0.0275	0.0312
450	0.0205	0.0256	0.0291
500	0.0192	0.0240	0.0272
550	0.0180	0.0225	0.0255

The feed rate and static bed height remained constant throughout testing at 3 g/min and 150 mm respectively. Recyclate was fed into the fluidised bed at the stated feed rate for 45 min, after which the system was ran for a further 15 minutes without inputting any more recyclate. Since the fibre weight fraction of the recyclate was 60%, Equation 2-2 was used to evaluate the yield efficiency for each test condition.

Equation 2-2 Yield efficiency of prototype fluidised bed recycling rig

$$Yield\ efficiency\ (\%) = \frac{Mass\ of\ recycled\ GF}{Mass\ of\ composite\ input \times 0.6} \times 100$$

The cleanliness of RGF was established by subjecting the RGF to a thermal cleaning process. Thermal cleaning was carried out in order to remove any non-decomposed epoxy residue present on the recycled fibre surface. This was performed by thermally conditioning the RGF in a Carbolite CSF 1200 furnace at 550 °C for 120 min, which was previously determined to be sufficient to remove residual epoxy. The mass of glass fibres was measured before and after thermal cleaning and the yield efficiency calculated using Equation 2-3.

Equation 2-3 Yield efficiency after cleaning RGF

$$Yield\ efficiency\ (\%) = \frac{Mass\ of\ fibres\ after\ cleaning}{Initial\ mass\ of\ recycled\ fibres} \times 100$$

2.4.3.2 Results and discussion

Figure 2-14 shows the state of fibres recycled in the fluidised bed rig (with fluidisation velocity of 1.5 m/s) at various bed temperatures as well as after thermal cleaning in the furnace. There is clearly a correlation between the visible cleanliness of the RGF and the bed temperature, where a reduction in recycling temperature below 500 °C yields significantly darker fibres. After thermal cleaning, this is removed and the fibres are like new in appearance. Non-decomposed epoxy residue is therefore the probable cause for this darkening; more specifically char, given the black colour and temperature resistance.

Figure 2-14 Glass fibres recycled in fluidised bed (Vf=1.5 m/s) at a bed temperature of a) 400 °C, b) 450 °C, c) 500 °C, d) 550 °C and e) 500 °C + thermal cleaning at 550 °C for 60 min

Figure 2-15 shows SEM images of individual RGF taken from the bundles in Figure 2-14. SEM images were taken of multiple fibres from each recycling schedule and the images shown in Figure 2-15 are typical of those found. In agreement with Figure 2-14, the degree of residue present on the fibres is typically higher for those recycled at lower temperatures. A significant portion of the surface of fibres recycled at 400 °C and 450 °C are covered with residue. Recycling at 500 °C and 550 °C yields relatively clean fibres with only slightly greater contamination than the thermally cleaned fibres.

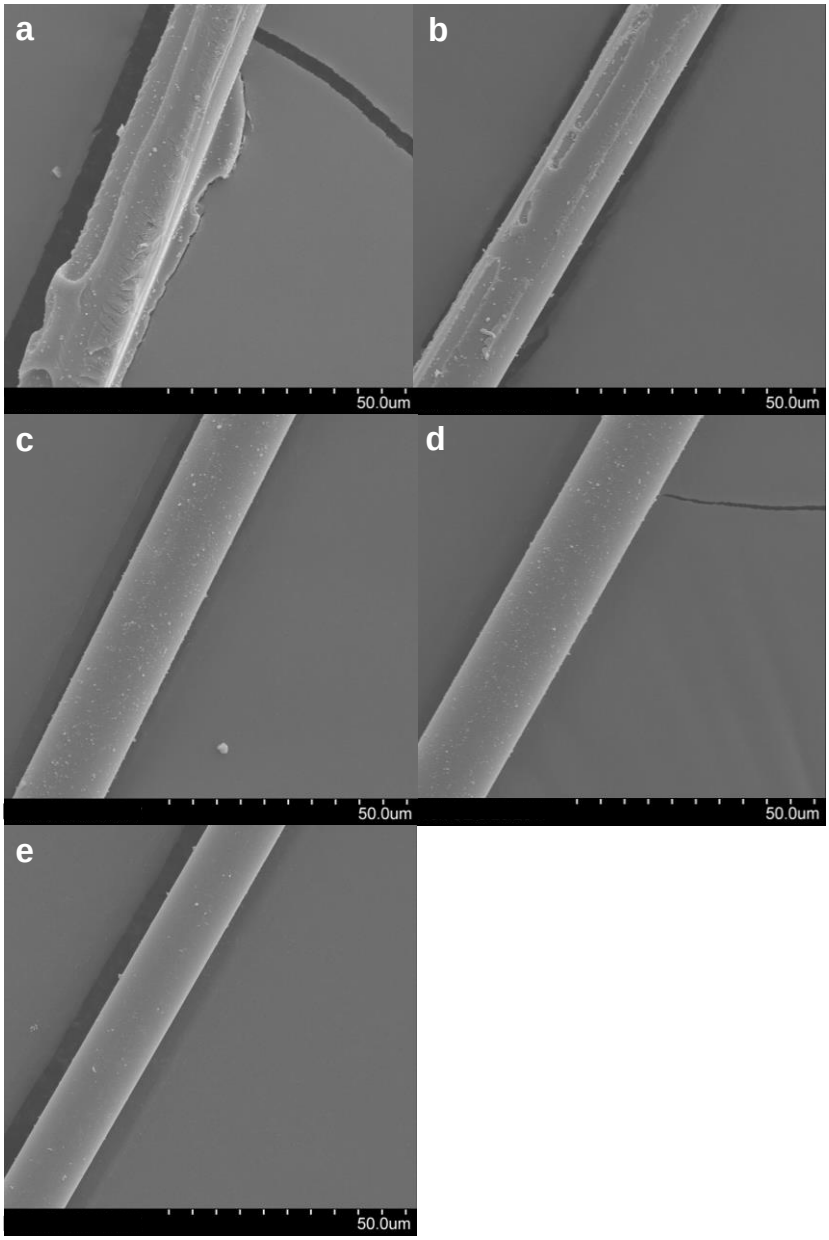

Figure 2-15 SEM images of glass fibres recycled in fluidised bed (Vf=1.5 m/s) at a bed temperature of a) 400 °C, b) 450 °C, c) 500 °C, d) 550 °C and e) 500 °C + thermal cleaning at 550 °C for 60 min. Polymer residue present on the surface of RGF is reduced by increasing fluidised bed temperature.

Table 2-2 gives the fibre yield efficiency and cleanliness after recycling in the fluidised bed at various temperatures and fluidisation velocities. In the temperature range investigated, the yield efficiency of the rig is improved greatly as the bed temperature increases. The exception to this is between 500 °C and 550 °C, which provide similar yield values. Increasing the bed temperature presumably allows for faster rates of epoxy decomposition, more rapid fibre release from matrix and higher

rates of fibre recovery. After recycling at 400 °C it was found that almost all un-recovered fibres remained in the bed, with little present in the filter upstream of the cyclone. Conversely, very little fibre remained in the bed after recycling at 500 °C and 550 °C, with nearly all un-recovered fibres found in the filter. There are therefore two explanations for fibres not being successfully collected as a result reducing the yield efficiency; 1) they were unable to exit the reactor and 2) inefficiency in the cyclone separator. The former is likely a result of fibres not becoming liberated from the matrix. This is due to the epoxy matrix not decomposing sufficiency because the required temperature was not achieved or inadequate time given before ending testing.

There is also a trend between bed temperature and relative mass loss after thermal cleaning, however the amount of non-decomposed residue present constitutes a relatively small portion of the recovered fibre mass in all cases. The effect of bed temperature on residue has been demonstrated quantitatively in Table 2-2; although, the difference appears more distinct visually in Figure 2-14 and Figure 2-15. As with overall yield efficiency, this trend is not observed between recycling temperatures of 500 °C and 550 °C. In general, it appears that increasing the bed temperature promotes char thermal decomposition on the fibre surface allowing cleaner fibres to be recovered.

Table 2-2 shows that there is no clear relation between fluidisation velocity and yield efficiency or fibre cleanliness, however, visually there appeared to be additional sand particles within the RGF when fluidising at 1.7 m/s. The higher fluidisation velocity appears to have caused an increase in sand entrainment, which is undesirable. The mass of sand present was not quantified as it proved difficult to effectively separate the sand and fibre phases. The key variable in increasing fibre yield efficiency is clearly the bed temperature. Based on this, as well as the recycled fibre cleanliness, it can be concluded that the operating bed temperature should be at least 500 °C. For the range of values tested, the fluidisation velocity does not appear to influence the yield efficiency of the rig.

Table 2-2 Effect of fluidised bed temperature and fluidisation velocity on glass fibre yield efficiency and cleanliness

Temperature (°C)	Fluidisation velocity (m/s)	Yield (%)		Mass loss after thermal cleaning (%)
		After fluidised bed	After thermal cleaning	
400	1.2	5.47	5.37	1.68
	1.5	5.90	5.81	1.57
	1.7	5.93	5.82	1.81
450	1.2	41.0	40.5	1.22
	1.5	42.4	41.8	1.32
	1.7	43.7	43.1	1.36
500	1.2	62.5	61.9	0.98
	1.5	63.2	62.5	1.00
	1.7	63.5	62.7	1.15
550	1.2	60.6	60.0	1.00
	1.5	63.5	62.9	0.98
	1.7	60.9	60.1	1.18

The tensile strength is an important mechanical property in determining the reusability and value of the RGF. As such, retaining the fibre strength during the recycling process by selecting appropriate operating conditions should be promoted. Thus, the effect of fluidisation velocity and bed temperature on the tensile strength of RGF was investigated.

Influence of fluidisation velocity on recycled glass fibre strength

Glass fibres were recycled at a fluidisation velocity of 1.2 m/s, 1.5 m/s and 1.7 m/s with a constant bed temperature of 500 °C. The results from the single fibre tensile tests are given in Figure 2-16. In all cases, the fibres sustained significant strength loss during the recycling process. The data indicates that the fluidisation velocity

does not influence the strength of RGF; around 75% reduction in tensile strength was observed for all cases tested. The degree of strength loss is in close agreement with Pickering et al. who reported an 80% reduction in tensile strength when recycling using a fluidised bed process at 550 °C [13]. An increase in strength loss with fluidisation velocity may be expected due to additional mechanical damage within the bed, however, this was not observed.

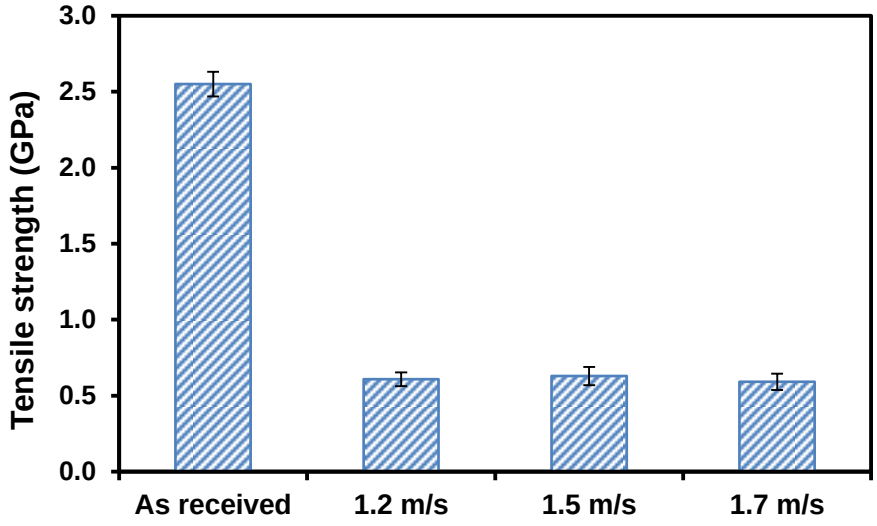

Figure 2-16 Tensile strength of glass fibres recycled at 500 °C at various fluidisation velocities. Fluidisation velocity does not appear to influence the strength of the RGF.

Influence of fluidised bed temperature on recycled glass fibre strength

Glass fibres were recycled at a bed temperature of 400, 450, 500 and 550 °C with a constant fluidisation velocity of 1.5 m/s. The results from the single fibre tensile tests are given in Figure 2-17. As with Figure 2-16, the strength of RGF drops by around 75% for all bed temperatures, suggesting the bed temperature does not affect the fibre strength. The relationship between glass fibre strength and thermal conditioning temperature is well established in the literature [5, 31, 32, 35, 40]. Pickering et al. indeed reported an increase in fibre strength loss with bed temperature; recycling at 450, 550 and 650 °C yielded fibres with strength loss of 50%, 80% and 90% respectively [13]. Despite the similarities in the recycling process outline in [13] and the one used in this work, the methods for fibre separation and recovery are entirely different. Pickering et al. use a rotating sieve to separate the fibres, which might reduce fibre abrasion and weakening. The cyclone

separation method used in this work may cause additional damage to the already thermally weakened RGF. There may in fact be a relation between the strength retention of fibres entering the freeboard and bed temperature as in [13], however, excessive mechanical damage during separation could obfuscate this. Irrespective of the cause, there is no observed relation between strength loss and bed temperature for the rig used in this work. This means reducing the bed temperature has no discernible benefits in terms of recycled glass fibre strength.

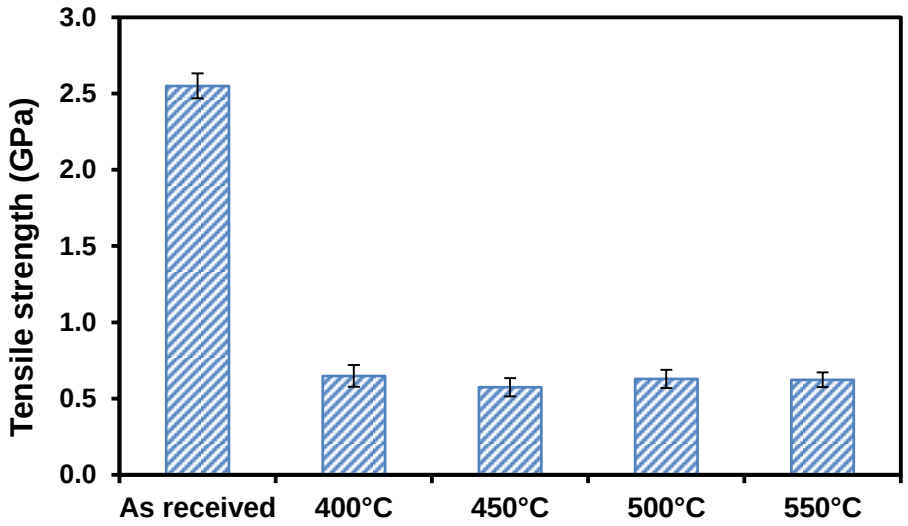

Figure 2-17 Tensile strength of glass fibres recycled at 1.5 m/s at various bed temperatures. Fluidised bed temperature does not appear to influence the strength of the RGF.

The surface of fibres recycled in the fluidised bed was further studied under high magnification SEM, as seen in Figure 2-18. The presence of apparent damage was ubiquitous on the surface of recycled fibres in the form of scratches and depressions. It is unclear whether the damage is induced thermally or mechanically during recycling. Given the high hardness of silica sand, abrasion from this sand in the fluidised bed may be a likely cause. No such features were observed on the surface of glass fibres simply thermally conditioned within a furnace at the same temperature, suggesting the damage is a result of mechanical attrition during recycling. Pickering et al. [13], Fenwick [36] and Kennerley [14, 70] reported the properties of glass fibres recycled using a fluidised bed, however, no such features were discussed. The depth of the damage cannot be determined using SEM, however the topography of the fibre surface could be further explored using atomic force microscopy. Although it is well understood that the measured strength of glass

fibres is controlled by surface flaws (extrinsic strength) [48], to the best of the authors knowledge, direct observation of such features on glass fibres have not been reported. Indeed, the lack of observed flaws on the surface of glass fibres may be the strongest argument against the thermal weakening mechanism proposed by Feih et al. and others [47, 68]. It is unclear whether the detectable damage is strength limiting or to what extent (if any) it contributes to the weakening of the glass fibres. These recycled fibres are considerably weaker than is reported in the literature when thermally conditioning at the same temperature, suggesting this damage may in fact influence the fibre strength.

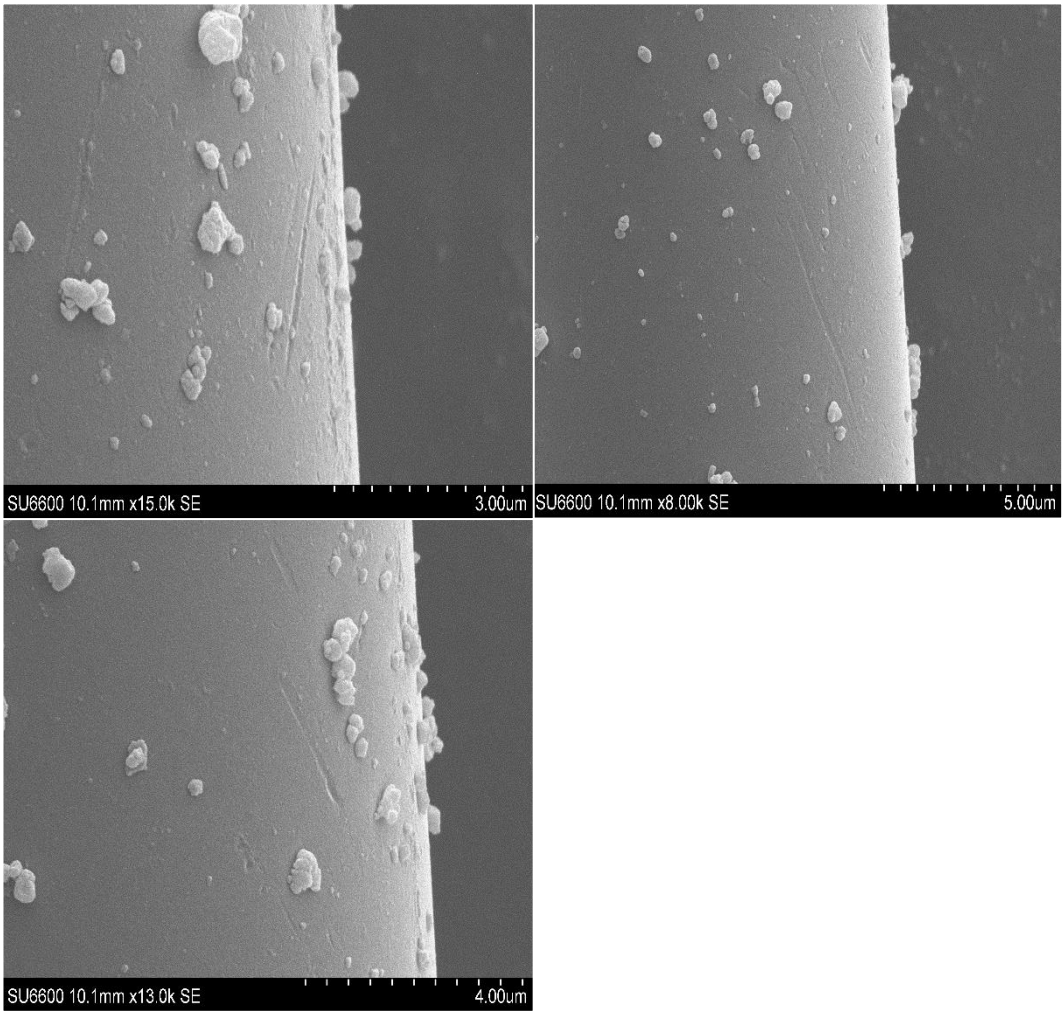

Figure 2-18 SEM images of the surface of glass fibres recycled from GF-epoxy recyclate in the fluidised bed at 500 °C. Damage to the RGF can be observed in the form of scratches on the fibre surface.

2.5 Conclusions

In this chapter, the final design of the fluidised bed rig was outlined as well as hardware used to construct, operate and control the process. During initial commissioning, it was found that the rig could meet the basic requirements of operation. In-house prepared GF-EP could be thermally decomposed within the fluidised bed and fibres subsequently recovered using the cyclone separator. Limitations of the recycling rig were established during this phase, with the maximum composite feed rate limited to 3 g/min for the following work.

The effects of fluidisation velocity and bed temperature were investigated in terms of fibre recovery efficiency and cleanliness. It was found that the bed temperature is critical for increasing the yield efficiency of RGF. A clear relation between the bed temperature and degree of non-decomposed contamination on the RGF was also established. The fluidisation velocity did not appear to influence the yield efficiency of the rig; however, additional sand contaminants did appear to increase when fluidising at 1.7 m/s.

The influence of fluidisation velocity and bed temperature on recycled glass fibre tensile strength was investigated. It was found that neither fluidisation velocity nor bed temperature affects the strength of RGF, with a strength loss of around 75% observed for all conditions tested. Given the well-established relation between thermal conditioning temperature and glass fibre strength loss, the lack in a clear relation may suggest the fibres sustain significant additional mechanical damage during the recycling process, such as in the reactor or cyclone separator.

3. Catalysed thermal recycling of glass fibres

In this chapter the effect of three commercially available metal oxide nanopowders, copper (II) oxide (CuO), cobalt (II,III) oxide (Co_3O_4) and cerium (IV) oxide (CeO_2) on facilitating composites thermal recycling is assessed. Initially the influence of the metal oxides on epoxy cure is explored using DSC. The effect of integrating metal oxides on the mechanical properties of epoxy is further investigated through tensile testing. TGA is used to investigate to effect of the metal oxides on the thermal decomposition of epoxy. Isothermal and non-isothermal heating schemes are used to assess the effect of the metal oxides on the temperature and time required to thermally decompose epoxy.

The effect of thermal conditioning on the tensile strength of glass fibres is investigated as a means of estimating strength loss of thermally RGF. The metal oxides are used in the thermal recycling of GF-EP within a furnace. The effect of these metal oxides on reducing the recycling conditions within the furnace, reducing energy consumption during recycling and promoting fibre strength retention is presented.

CuO is used within the fluidised bed rig and its ability to reduce the recycling conditions assessed in terms of the yield efficiency and RGF strength. Finally, the effect of re-using CuO to assist epoxy decomposition is investigated.

3.1 Literature review

In this section the mechanisms behind polymer thermal-oxidative decomposition are outlined. A summary of the literature related to thermal-oxidative decomposition of epoxy, through a variety of analytical techniques, is given. An overview of the uses of CuO, Co_3O_4 and CeO_2 as oxidation catalysts is provided and research into the use of metal oxides as catalysts for the thermal decomposition of polymers is reviewed.

3.1.1 Thermal decomposition of thermosetting polymers

3.1.1.1 Polymer thermal-oxidative decomposition mechanism

For clarity in this work, a distinction between thermal decomposition and thermal degradation will be made. Thermal decomposition can be defined as a “process whereby the action of heat or elevated temperature on an item causes changes to the chemical composition” [71]. Thermal degradation is defined as a “process whereby the action of heat or elevated temperature on a material, product, or assembly causes an adverse change in one or more properties” [71]. In terms of thermal recycling of thermoset-based composite material, thermal decomposition is the relevant change in material. Since this work is concentrated on thermally recycling composites through combustion within a fluidised bed process, thermal-oxidative decomposition of polymer materials will be the focus of this review. The mechanism for thermal-oxidative decomposition of generic polymeric materials is auto-oxidation; a process that involves the major steps of initiation, propagation, branching, and termination [72]. Polymer thermal decomposition is typically initiated by either hydrogen abstraction or chain scission, which in turn generate highly reactive polymer free radical (R·).

Equation 3-1 Polymer free radical generated via hydrogen abstraction

$$polymer \rightarrow R\cdot + H$$

Equation 3-2 Polymer free radical generated via chain scission

$$polymer \rightarrow R\cdot + R\cdot$$

The propagation of thermal decomposition through auto-oxidation involves polymer free radicals reacting with molecular oxygen to produce peroxyl radicals (ROO·). Through hydrogen abstraction of another polymer chain, peroxyl radicals can form hydroperoxides (ROOH) and another polymer radical.

Equation 3-3 Peroxyl radical generated via auto-oxidation

$$R\cdot + O_2 \rightarrow ROO\cdot$$

Equation 3-4 Polymer radical generated via hydrogen abstraction by peroxyl radical

$$ROO\cdot + polymer \rightarrow ROOH + R\cdot$$

Alkoxyl radicals ($RO^{\cdot}$) and hydroxyl radicals ($^{\cdot}OH$) can then be produced by splitting of hydroperoxides in a number of ways.

Equation 3-5 Alkoxyl and hydroxyl radicals generated via hydroperoxides splitting

$$ROOH \rightarrow RO\cdot + \cdot OH$$

Equation 3-6 Alkoxyl and peroxyl radicals generated via hydroperoxides splitting

$$2ROOH \rightarrow ROO\cdot + RO\cdot + H_2O$$

These radicals then continue the reaction to other polymer molecules generating more polymer radicals.

Equation 3-7 Polymer radical generated via hydrogen abstraction by alkoxyl radical

$$RO\cdot + polymer \rightarrow ROH + R\cdot$$

Equation 3-8 Polymer radical generated via hydrogen abstraction by hydroxyl radical

$$HO\cdot + polymer \rightarrow H_2O + R\cdot$$

Termination of the decomposition occurs by radical-radical interaction to create inert products. These termination processes often result in cross-linking between adjacent polymer chains as well as cyclisation. These processes generate carbon rich structures which have higher molecular weights and are less easily volatised [73].

Equation 3-9 Peroxyl radicals react to form unreactive products

$$2ROO\cdot \rightarrow unreactive\ products$$

Equation 3-10 Peroxyl and polymer radicals react to form peroxides

$$ROO\cdot + R\cdot \rightarrow ROOR$$

Equation 3-11 Polymer radicals react to form polymers

$$2R\cdot \rightarrow R$$

3.1.1.2 Epoxy thermal-oxidative decomposition

Extensive research has been carried out into thermal-oxidative degradation/aging of epoxy systems using temperatures in the range 70-200 °C [74-79]. Much work has also been focused on thermal decomposition of epoxy in inert environments [80-83].

Such studies are not particularly relevant to this work given the environment within the fluidised bed recycling system [13].

Many authors have used TGA as means of studying the thermal-oxidative decomposition behaviour of epoxy [84, 85] and carbon fibre reinforced epoxy systems [86-88]. In all cases, a typical two-stage process for epoxy thermal-oxidative decomposition is observed when heating under non-isothermal conditions, as can be seen in Figure 3-1. The initial stage is attributed to devolatilisation where the polymer is decomposed into carbonaceous residue (char). This stage typically accounts for around 60-70% of the mass loss of epoxy [84-86, 88]. The onset and completion temperature for this stage (and all stages) is highly dependent on the heating rate used during analysis. Jiang et al. used a typical heating rate of 10 °C/min and found an onset and completion temperature for the first stage of decomposition to be 320 °C and 460 °C respectively [88]. This is in closed agreement to Chen et al. [84] and Wang et al. [85] when using the same heating rate. Tranchard et al. used TGA with in situ Fourier-transform infrared spectroscopy (FTIR) to characterise the gas released during epoxy decomposition [86]. At the temperature corresponding to the peak reaction rate of stage one of the decomposition, the main peaks observed corresponded to CO_2, CO, COS and SO_2 with H_2O, ε-caprolactam ($(CH_2)_5C(O)NH$) and CH_4 to a lesser extent. Jiang et al. used TGA coupled with mass spectroscopy to also analyse the evolved gases [88]. As well as CO_2, CO and H_2O, eight other organic volatilised including benzene, toluene and styrene were identified.

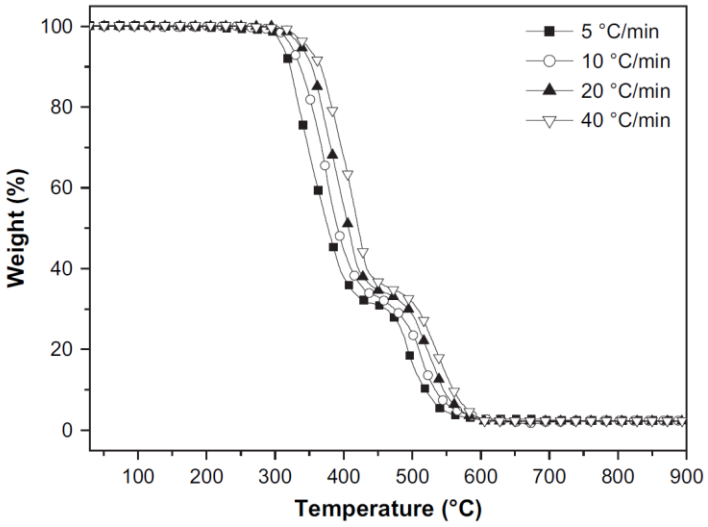

Figure 3-1 TGA thermograms of thermal-oxidative decomposition of epoxy showing 1) two distinct stages of decomposition and 2) influence of heating rate on the temperature required for decomposition, reproduced from [85]

The second stage of the epoxy decomposition involves oxidation of the char residue, which, due to its high thermal stability, requires heating to around 600 °C to decompose (at a heating rate of 10 °C/min) [84, 85, 88]. Despite the similarity in chemical composition, the physical structure of chars greatly influences the thermal decomposition process, and is often the physical characteristic of the char that governor its decomposition [73]. FTIR of products from this stage show a gas rich in a mixture of CO and CO_2 [86]; as would be expected through oxidation of char.

Many authors have used TGA data to evaluate kinetic parameters such as the activation energies, pre-exponential factors, and reaction models, for epoxy decomposition in inert [82, 86, 89, 90] and air atmospheres [84, 85, 87]. Kinetics deals with measurement and parameterisation of process rates, which, when temperature dependant, can be modelled through the Arrhenius equation [91]. From this, many methods for parameterising reaction kinetics have been developed. Typically, the methods utilise data acquired by decomposing under non-isothermal heating programmes at a variety of heating rates. Chen et al. used the Freidman method to determine the average activation energy (Ea) across each stage of epoxy thermal-oxidative decomposition [84]. An Ea of 129.52±91 kJ/mol and 103.02±7.7 kJ/mol were reported for the first and second stage respectively. No comment was made as to the relation between the established kinetic parameters and the fundamental mechanisms of epoxy decomposition. Wang et al. used the Kissinger

differential method; reporting a calculated Ea of 120 kJ/mol and 126 kJ/mol for the first and second stage respectively [85].

Regnier and Fontaine used the Ozawa method to determine the Ea at various values of conversion during epoxy decomposition, both in nitrogen and air atmospheres [87]. The Ea of specific decomposition mechanisms was reported. Their analysis suggests that the initial rates of decomposition in nitrogen and air are controlled by evaporating low molecular mass species, in turn forming a new conjugated carbon polymer, and by the decomposition of peroxide radical into oxygen and a new radical. The Ea for the evaporation of low molecular mass molecules and formation of conjugated carbon polymer was reported to be 100 kJ/mol. The decomposition of peroxide radicals had an Ea of around 130 kJ/mol. It was proposed that in both nitrogen and air environments the second stage of decomposition was dominated by polymer network scission. The Ea of this process was reduced slightly in an air environment, with an apparent Ea of 140 kJ/mol reported. Despite using disparate analytical methods and varying epoxy systems, the reported Ea of thermal-oxidative decomposition of epoxy is similar between the studies sighted [84, 85, 87].

3.1.2 Metal oxide catalysts

3.1.2.1 Catalysis

Catalysis is the increase in the rate of a chemical reaction through the participation of a substance called a catalyst. A catalyst is not consumed during the reaction and can continue to act repeatedly [92]. Homogeneous catalysis refers to catalytic reactions where the catalyst is in the same phase as the reactants. Conversely, in heterogeneous catalysis the phase of the catalyst differs from that of the reactants [93]. Catalytic oxidation is a process where compounds are oxidised with the use of a catalyst(s). Conventional catalysts used for oxidation reactions include metal oxides and noble metals [94]. Metal oxide catalysts are typically oxides of metals located in group 3-12 on the periodic table, which exhibit high electron mobility. The most active single metal oxide catalysts for complete oxidation for a variety of oxidation reactions include oxides of cobalt (Co) and copper (Cu) [94]. Metal ions (such as Co^{2+}/Co^{3+} or Cu^{+}/Cu^{2+}) in solid or liquid phases can catalyse the oxidation

of organic materials by transfer of a single electron [95]. The metal ions function by splitting of hydroperoxides which then form radicals.

3.1.2.2 Copper oxide

Hong and Wang investigated the effect of heating epoxy in contact with copper oxides due to reported delamination of printed circuit boards [96]. It was proposed that copper oxides accelerate the decomposition of polymer materials, resulting in reduced epoxy-copper bond strength. Two forms of copper oxides were investigated, cupric oxide (CuO) and cuprous oxide (Cu_2O). TGA was carried out on epoxy samples containing 0.1% weight copper oxide powders. The resulting derivative curves showed peaks occurring at lower temperatures for samples containing both forms of copper oxides. No conclusion could be made as to which copper oxide was more effective at catalysing the epoxy due to an inconsistency in specific surfaces of the powders.

Hong and Wang propose that the catalytic effect of the copper oxides begins by the abstraction of tertiary hydrogen atoms, which reduces the copper oxide [96]. The copper ions then decompose hydroperoxides (ROOH) formed during the polymer degradation, which generates peroxyl ($ROO^{\cdot}$) and alkoxyl ($RO^{\cdot}$) radicals that can migrate through the polymer, causing radical depolymerisation. Chan and Allara outline a mechanism by which Cu_2O catalyses the thermal degradation of polyethylene [97]. It is suggested that carboxylic acids produced during oxidative degradation of such materials react with the metal surface forming copper salts. It is hypothesised that this copper salt layer acts as catalytic surface generating reactive intermediates (free radicals, hydroperoxides, aldehydes) which can migrate through the polymer matrix resulting in increased oxidation. These salts may also migrate through the polymer aiding the degradation through homogeneous catalysis.

A mechanism for decomposition of hydroperoxides into $ROO^{\cdot}$ and $RO^{\cdot}$ radicals, catalysed by copper ions is outlined by Richardson in Equation 3-12 [98].

Equation 3-12 Chemical reactions involved in the decomposition of hydroperoxides by action of copper ion catalyst [98]

$$Cu^{2+}{}_2 + ROOH \rightleftharpoons Cu^{2+}{}_2(ROOH)_2$$

$$Cu^{2+}{}_2(ROOH)_2 \rightarrow Cu^{2+}Cu^{1+}(ROOH)(H^+) + ROO^{\cdot}$$

$$Cu^{2+}Cu^{1+}(ROOH)(H^+) \rightarrow Cu^{2+}{}_2 + H_2O + RO^{\cdot}$$

The maximum temperature used to investigate the catalytic action of copper oxide was 400 °C and 83 °C in [96] and [97] respectively. It is unclear whether the proposed mechanisms are applicable at typical GRP thermal recycling temperatures. Copper oxide has also been used to increase oxidation of other organic materials such as methane [99], alcohols [100] and soot [101].

3.1.2.3 Cerium (IV) oxide

The major application of the rare earth oxide ceria (CeO2) is in catalysis [102]. Commercial uses of CeO_2 catalysts include as a constituent of three way catalytic convertors to reducing noxious components from automotive exhausts [103, 104], cracking crude oil in refinery operations as well as a hydrocarbon oxidation catalyst in self-cleaning ovens. Much research is focused on the use of CeO_2 as an oxidation catalyst to remove soot from diesel engines [105-107]. Studies have also reported the benefits of using CeO_2 as an oxidation catalyst in wet air oxidation of bisphenol A, a widely used monomer for the production of epoxy [108].

The mechanism of catalytic activity on CeO_2 is a subject under investigation. The catalytic activity is typically attributed to high oxygen storage capability, due to multivalent nature of cerium, as well as high mobility of the oxygen vacancies at the surface of the materials. CeO_2 can accommodate a large number of mobile oxygen vacancies by doping, which improves catalysis. However, this can also be achieved by oxygen removal through annealing [109]. The high mobility of oxygen in the bulk structure and easily reduced surface allow CeO_2 to undergo rapid redox cycles [103]. Tschope et al.describes a general catalytic redox reaction on metal oxides in terms of oxygen transfer in Equation 3-13 [109].

Equation 3-13 General catalytic redox reaction on metal oxides in terms of oxygen transfer [109]

$$Me - O + Red \rightarrow Red - O$$

$$Me + \ Ox - O \rightarrow Me - O + Ox$$

Initially a reductant (Red) reduces the metal oxide surface ($Me - O$). It returns to its original state after re-oxidation by an oxidant ($Ox - O$). The result of this two-stage reaction is the transfer of oxygen from one substance to another. Oxidation of a substances will occur as a result of the metal oxide donating a lattice oxygen,

producing a vacancy on its surface [110]. Oxygen in the atmosphere can re-oxidising the surface oxygen vacancy, facilitating a continuous redox cycle [111].

3.1.2.4 Cobalt (II,III) oxide

The oxidation-reduction properties of cobalt allow valences of I, II or III to be established. Electrons can be easily transferred between these states, accelerating reactions. Ranji-Burachaloo et al. [112] and Ma et al. [113] have investigated the application of cobalt (II,III) oxide (Co_3O_4) as an oxidation catalyst in diesel engine exhaust systems. Ranji-Burachaloo et al. observed increased soot oxidation with the application of Co_3O_4 [112]. It was proposed that soot oxidation is promoted by the transfer of oxygen on the surface of metal oxides to the soot. The mechanism for complete soot/carbon oxidation via metal oxides given in Equation 3-14 [112].

Equation 3-14 Chemical reactions for carbon complete oxidation via metal oxides [112]

$$2C + 3M(O) \rightarrow CO + CO_2 + 3M^*$$

$$CO + M(O) \rightarrow CO_2 + M^*$$

where $M(O)$ and M^* denote a metal oxide and a partially reduced metal oxide respectively. The metal oxide is subsequently regenerated by molecular oxygen in the gas stream as follows:

Equation 3-15 Re-oxidation of metal by molecular oxygen in the gas stream [112]

$$O_2(g) + 2M^* \rightarrow 2M(O)$$

This mechanism is in agreement with Stanmore et al., who state that the role of transition metal catalysts in soot oxidation reaction is oxygen transfer from their surface to the soot [101]. Ma et al. observed increase catalytic activity when Co_3O_4 was doped with indium [113]. It was proposed that doping with indium increased the mobility of lattice oxygen involved in the oxidation reaction. Duan et al. also demonstrated that $Co3O_4$ redox activity can be increased with the addition of noble metals such as Platinum [114].

3.1.2.5 Metal oxide catalysts for polymer thermal decomposition

Several authors have used metal oxides in an attempt to aid thermal decomposition of polymer material [115] and to assist the recovery of glass fibres from GRP [116, 117]. Shinbara et al. reported on the effectiveness of Titanium (IV) oxide (TiO_2) as a catalyst for the decomposition of polycarbonate (PC) [115]. It was claimed that PC rapidly decomposed completely into H_2O and CO_2 at 350 °C when heated in the presence of TiO_2; however, no gas analysis techniques were used to confirm full combustion. Electron spin resonance indicated an increase in radical concentration as the oxidation reaction proceeded, leading to the decrease in molecular weight of PC. It was concluded that the presence of TiO_2 initiated radical formation at the PC-TiO_2 interface, which then propagated through the bulk PC. No data for uncatalysed decomposition was present; therefore, it is difficult to determine the influence of TiO_2 on radical formation and concentration.

Shima et al. used Chromium (III) oxide (Cr_2O_3), Nickel (II) oxide (NiO), Iron (III) oxide (α-Fe_2O_3) and TiO_2 to aid thermal recycling of glass fibres from fibre reinforced polyester (GF-polyester) [117]. GF-polyester plates were sat on a bed of the metal oxide powders and heated at 500 °C. It was stated that the polyester fully degraded within 10 min for each metal oxide. Moreover, the fibres could be recovered at just 350 °C when extending the heating time; no specific value of time was presented. Under SEM, the RGF appeared relatively clean and without surface defects or cracks. It was concluded without actual testing that the fibres were recovered without deterioration or loss of value. Thermally RGF lack commercial value predominantly due to strength loss [8], which was not measure directly in [117]. Feih et al. [31] show that glass fibres are significantly weakened after similar treatment to those used in [117]. Shima et al. provided no control to compare catalysed and uncatalysed GF-polyester thermal recycling. It is therefore unclear to what extent the metal oxides reduced the conditions required to decompose the polyester.

Mizuguchi et al. used Cr_2O_3 to catalyse the thermal recycling of GF-EP [116]. GF-EP plates were sandwiched between Cr_2O_3 coated honeycomb substrates and decomposed at 500 °C; taking just 10 min to recover clean fibres. Glass fibres were characterised using TGA, SEM, X-ray photoelectron spectroscopy and Powder X-ray diffraction. It was concluded that the presence of a sizing on the as received fibres was all that differentiated them from the RGF. Similar to [115, 117], Mizuguchi

et al. provided no data regarding thermal recycling of GF-EP without the action of Cr_2O_3.

3.1.3 Conclusions of literature review

Full decomposition of epoxy typically requires heating up to 600 °C using TGA, depending on heating rate. Similarly, recycling GF-EP in a fluidised bed requires a bed temperature of up to 550 °C. Such high temperatures are required due to the high thermal stability of char, which is formed via polymer cross-linking and cyclisation. It has already been demonstrated that such high temperatures significantly diminish the reinforcement potential of fibres thermally recycled from GF-EP. A catalyst could be used as a means of facilitating the polymer thermal-oxidative decomposition at a lower temperature, mitigating such strength loss and reduce energy input in recycling GRP.

Metal oxides have been demonstrated to function successfully as oxidising catalysts in a variety of applications. It has been demonstrated that copper oxide can accelerate the decomposition of epoxy and degradation of polyethylene. Accelerated decomposition of GF-EP with the action of Cr_2O_3 was also reported as well the catalytic effect of TiO_2, NiO and α-Fe_2O_3 in the decomposition of GF-polyester. Mechanical characterisation of the recovered glass fibres was not performed; therefore, the benefits of using metal oxides to aid thermal recycling glass fibres from GRP were unknown before this work.

3.2 Experiment

3.2.1 Materials

E-glass fibres used in this chapter were from a tri-axial 3-ply mat supplied by Hexcel Reinforcements UK Ltd and PRIME 27 Resin with PRIME 20LV extra slow hardener were supplied by Gurit.

CuO, Co_3O_4 and CeO_2 nanopowders were purchased from SIGMA-ALDRICH with particle size of <50nm (TEM), <50nm (TEM) and 21 nm (TEM) respectively.

3.2.2 Thermogravimetric analysis

3.2.2.1 Epoxy thermal decomposition analysis

Thermal decomposition of epoxy in the presence of the metal oxides was carried using TGA in order to rank the catalysts performance. The epoxy was prepared by mixing the metal oxide nanopowders with the epoxy resin by hand, followed by ultrasonic mixing for 30 min to disperse the particles into the resin system. The hardener was added according to supplier's instruction, then, after mixing until combined, the epoxy was placed in a vacuum chamber to de-gas for 10 min. Metal oxide weight loadings of 0, 1.5 and 5% were investigated in this thesis. This method approximates that outline in [118], where good dispersion of nanopowder in epoxy was observed without negatively affecting the properties of epoxy. SEM was used to observe the dispersion of CuO in the cured epoxy, as shown in Figure 3-2. Some agglomeration of the CuO is present in Figure 3-2, however the dispersion does appear homogenous on the whole. The CuO particle size, measured using SEM, was found to approximate that given by the supplier. Epoxy not containing nanopowders was prepared as above, minus the steps involving the addition and dispersion of nanopowders.

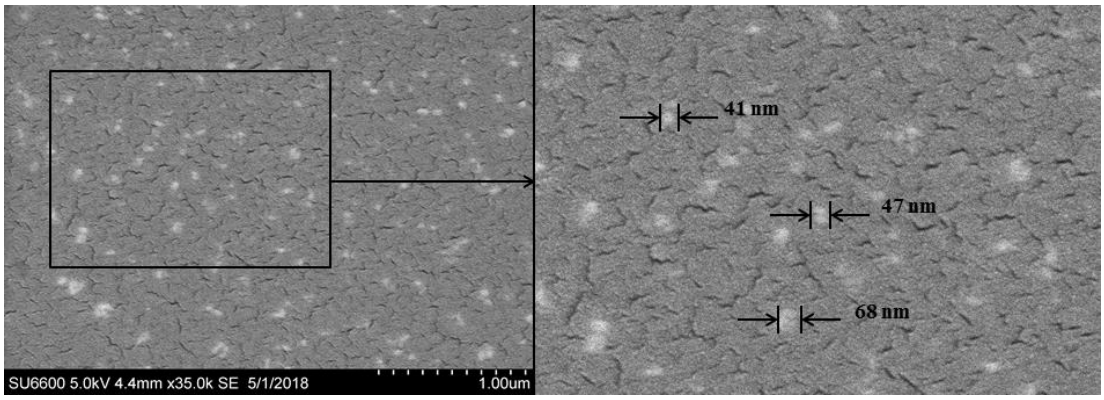

Figure 3-2 SEM image showing CuO nanopowder evenly distributed in an epoxy specimen with particle size approximating that given by the supplier

Using a syringe, small droplets of the uncured epoxy were dropped onto prepreg release film. This created convex disks of epoxy with diameters around 6 mm. This process was carried out multiple times on the same film; giving a large sample size to later choose from. The epoxy disks were then cured at RT for 24 hours; allowing them to harden so they could then be moved without deforming. The samples were

then post-cured at 65 °C for 7 hour following supplier's instruction. The large sample size was initially visually analysed; discarding any epoxy disks that were deformed or were not in the correct diameter range. The final sample selection was then carried out by weighing the remaining samples; any samples out with the range of 11.5 - 12.5 mg were discarded. Figure 3-3 shows an example of epoxy only TGA samples.

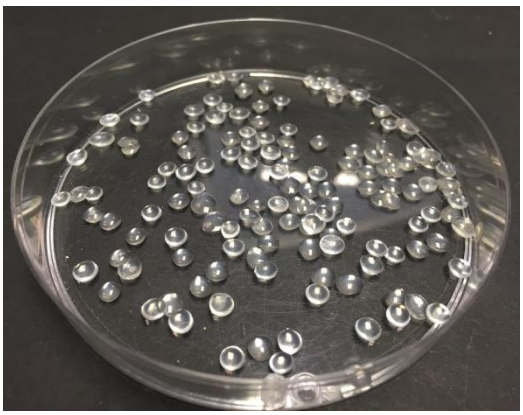

Figure 3-3 Epoxy only TGA samples

Two methods for introducing metal oxides to the epoxy were used while analysing the epoxy thermal decomposition; 1) epoxy only samples sitting on a bed of metal oxide powder and 2) the metal oxide integrated into the epoxy during sample preparation. A schematic of these arrangements in the alumina TGA pan are given in Figure 3-4. Samples with the metal oxide bed were prepared for TGA by applying a 20 mg layer of metal oxide in the base of an alumina TGA pan. The TGA microbalance was then tared with the TGA pan and metal oxide. The flat surface of the epoxy disk was then placed on top of the metal oxide layer. Samples with metal oxides integrated in the epoxy were prepared by taring the TGA microbalance with the TGA pan, then placing the epoxy sample in the pan flat side down.

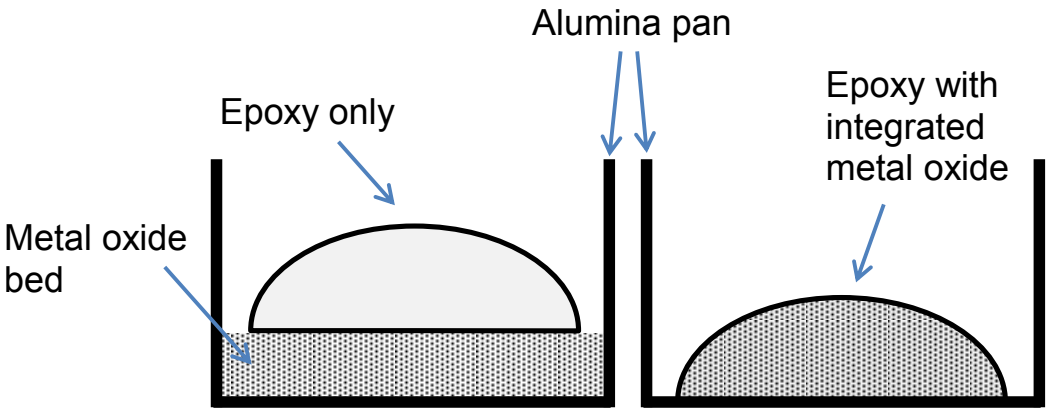

Figure 3-4 Two sample arrangements used during TGA of epoxy thermal decomposition

TGA was performed using a TA Instruments Q50, as shown in Figure 3-5. Isothermal and non-isothermal programs were used at various temperatures and heating rates. Nitrogen and Air atmospheres were used depending on the analysis. The heating programs and atmospheres used for each test will be specified when discussing the results. A kinetic study of the epoxy thermal decomposition was performed using the attained TGA data and the effect of the metal oxides assessed.

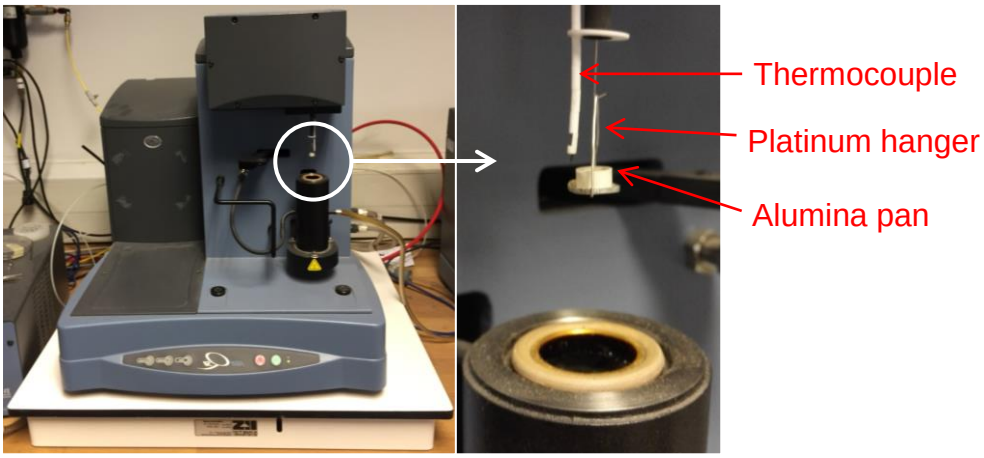

Figure 3-5 TA instruments Q50 used for the TGA of epoxy thermal decomposition

3.2.2.2 Assessing reusability of metal oxide

The reusability of the metal oxide is important in assessing its potential as a catalyst for aiding epoxy decomposition. To do this, a relatively large quantity of bulk epoxy+CuO with 5% weight CuO was produced. This was decomposed in a muffle

furnace at 550 °C in air and the residual CuO was collected. For clarity, the notation CuO(X) will be used, where X is the number of decompositions CuO has previously been subjected. A fraction of this collected CuO(1) was processed into epoxy+CuO(1) TGA samples, as described above, and the rest into more bulk epoxy+CuO(1). The degradation process was repeated on the bulk epoxy+CuO(1) and the residual CuO(2) was again processed into epoxy+CuO(2) TGA samples. Figure 3-6 illustrates the methodology. TGA was performed on the various epoxy+CuO samples at a heating rate of 1, 2, 5, 7 and 10 °C/min from RT to 600 °C in air. The effect of the number of previous uses on the ability of CuO to aid epoxy degradation was compared and quantified by calculating the Ea of epoxy decomposition.

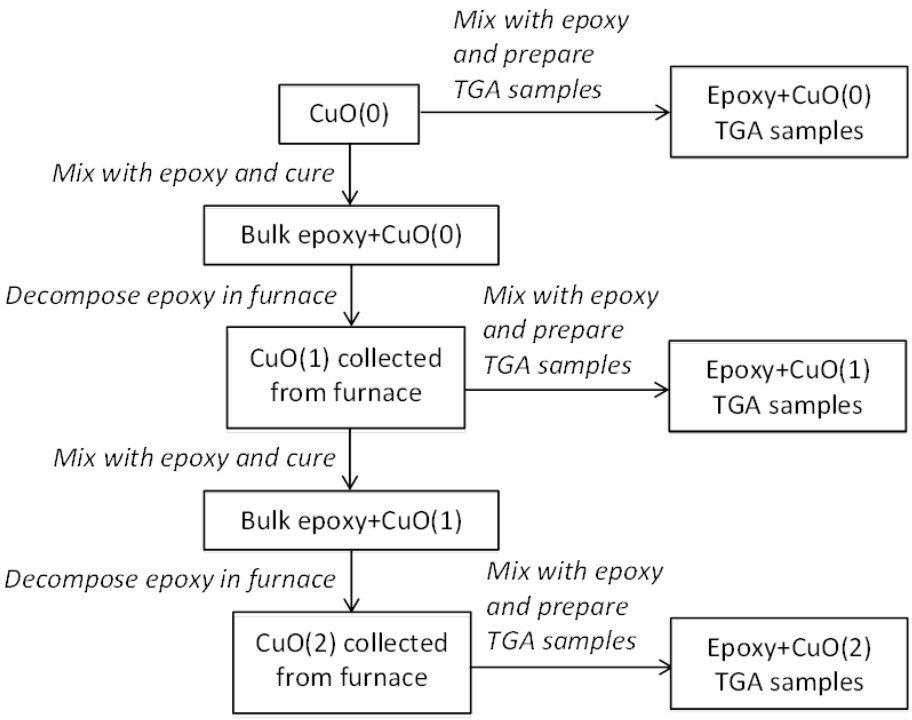

Figure 3-6 Flow chart illustrating the method used to assess the reusability of CuO

3.2.2.3 Glass fibre sizing thermal decomposition

As the commercial sizing on the fibres comprises predominately of a polymeric film former, TGA was used to determine whether the metal oxides used had an impact on the sizing decomposition. The mass of glass fibre far exceeds the mass of the applied sizing. In order to obtain accurate TGA results, a relatively large quantity of fibres was used. 250 mg of glass fibres (chopped to approximately 5 mm) were

mixed with 180 mg of metal oxide and heated from 25 to 600 °C within an alumina beaker. TGA was performed using a NETSZCH STA 449 F1 Jupiter, which provides the ability to analyse larger quantity of samples.

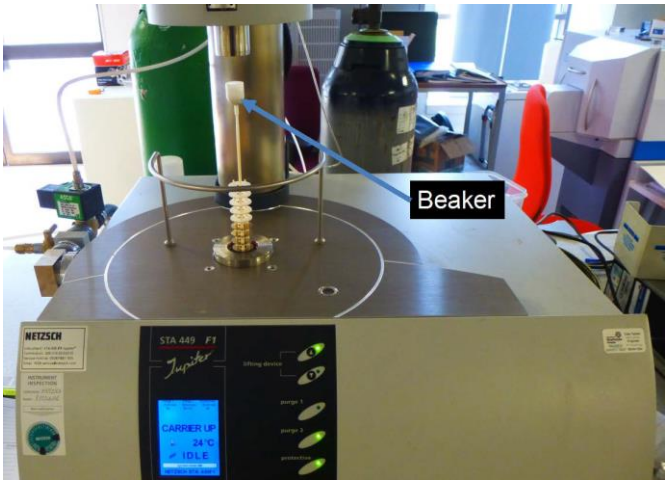

Figure 3-7 NETSZCH STA 449 F1 Jupiter thermogravimetric analyser with beaker attachment, reproduced from [68]

3.2.3 Differential scanning calorimetry for studying epoxy curing

DSC was used to investigate the effect of metal oxide content on the epoxy curing using a TA Instruments Q20. Uncured epoxy was mixed with the metal oxides at 0, 1.5 to 5.0% by weight. Using a syringe, a droplet of the uncured epoxy-metal oxide mixture (in the range 16 - 18 mg) was added to a hermetic aluminium DSC pan and sealed. The samples were heated in the temperature range -10 to 180 °C, then cooled to -10 °C and finally reheated to 180 °C all at a heating rate of 3 °C/min. The reaction enthalpy and glass transition of the cured material were characterised.

3.2.4 Epoxy tensile sample preparation and tensile test

Tensile specimens were prepared in order to investigate the effect of integrating metal oxide nanopowders on epoxy strength. The specimens were prepared and tested following ASTM D638-14. Epoxy with 5% weight metal oxide dispersion was prepared as outlined in 3.2.2.1. Using a syringe, the resin was transferred into a silicone rubber mould as can be seen in Figure 3-8. The epoxy was cured at RT for 24 hour followed by a post cure heat treatment at 65 °C for 7 hour. An Instron 5969

testing machine equipped with a 50 kN load cell was used to perform the tensile test. The strain was recorded with an Instron 2663-821 video extensometer and the displacement rate was set to 1 mm/min.

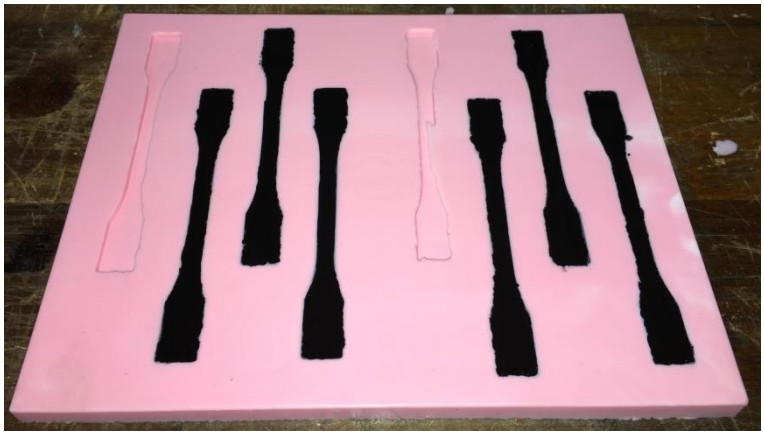

Figure 3-8 Silicone mould with epoxy+CuO specimens prior to curing

3.2.5 Thermally conditioning glass fibres within a furnace

The dependence of heating temperature and time on the glass fibre tensile strength was investigated. Thermal conditioning was performed using a Carbolite CWF 12/13 furnace. The furnace volume was large enough to accommodate simultaneous treatment of large numbers of samples over a wide range of treatment temperatures. Glass fibres were taken from the middle layer of the original mat and subsequently heated within the furnace in air ranging from 300 to 600 °C for up to 240 min. All samples were immediately cooled in RT air after thermal conditioning.

Hereafter, thermal treatments lasting 10 min or less will be described as “brief” treatments and treatments lasting greater than 10 min will be “extended” treatments. The fibres undergoing brief treatments had to be introduced into the furnace without opening the main furnace door to avoid cooling and ensure an accurate thermal loading. This was achieved by rapidly lowering the fibres in through the furnace chimney, which was originally installed to allow flue gas to escape. A precise conditioning temperature was attained by installing an independent thermocouple next to the fibres, as shown in Figure 3-9.

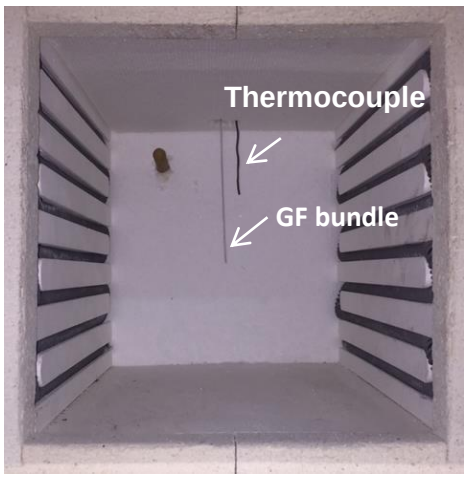

Figure 3-9 Furnace arrangement for brief thermal loading of glass fibre bundle

For extended treatments, the extracted fibre bundle was fixed to a jig, as seen in Figure 3-10. In each case, single fibres were extracted from the bundle for tensile testing after treatment at the desired temperature and time.

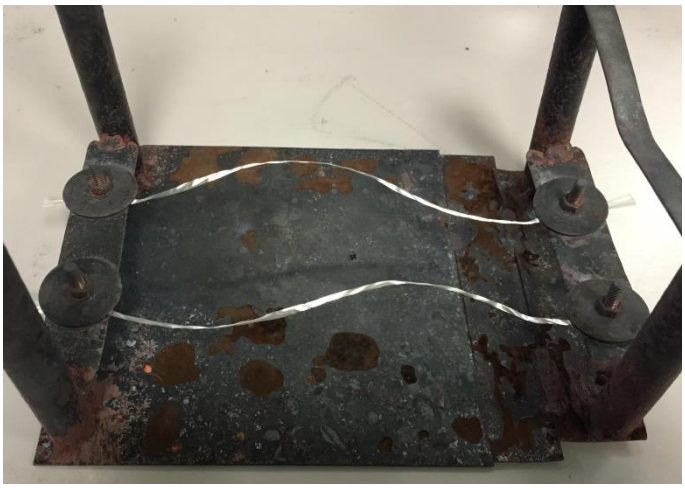

Figure 3-10 Jig used for extended thermal conditioning of bundles with glass fibre bundle attached

3.2.5.1 Thermally conditioning glass fibres in the presence of metal oxides

The effect of physical contact with each of the metal oxides during heating on glass fibre strength was also investigated. Glass fibre bundles were manually separated in order to increase potential fibre exposure. The metal oxide powders were then layered over the fibres and heat-treated in a furnace for 25 min at 400 and 550 °C. A

control sample was also prepared following this procedure with CuO without actually heating to account for possible additional damage to the fibres that could arise from the extra handling involved. After exposing the fibres to the metal oxides for 25 min, single fibre tensile strength was measure as described in Chapter 2.

3.2.6 GF-EP processing

3.2.6.1 Preparing GF-EP recyclate

The GF-EP recyclate used in this chapter was prepared as in Chapter 2. GF-EP with metal oxides integrated within the epoxy matrix was also manufactured in this way. Epoxy with 5% weight metal oxide dispersion was prepared as outlined in 3.2.2.1 and impregnated in the mat. The cured laminates were cut into various dimensions depending on the study as seen in Table 3-1.

Table 3-1 GF-EP dimensions for the various usages

GF-EP use	Dimensions (mm)	Approximate mass (g)
Fluidised bed recyclate	60 x 15 x 2	1.7
Furnace recycling	60 x 60 x 2	6.8

3.2.6.2 Thermal recycling GF-EP within a furnace

Thermal recycling of GF-EP was carried out within a furnace with an air atmosphere. Unlike a fluidised bed, this is a static and discontinuous process. This allowed for a simplified means of initial characterisation while still gaining valuable insight into the effect of the metal oxides on fibre strength and energy consumption in GF-EP recycling.

As with the TGA, two methods for introducing metal oxides to the epoxy were used when thermally recycling GF-EP in the furnace; 1) GF-EP only samples sitting on a bed of metal oxide powder and 2) the metal oxide integrated into the epoxy matrix during sample preparation. A schematic of these arrangements in an aluminium tray are given in Figure 3-11. For samples recycled with the metal oxide bed, the GF-EP plate sat on a 2.7 g bed of metal oxide powder during heating in the furnace.

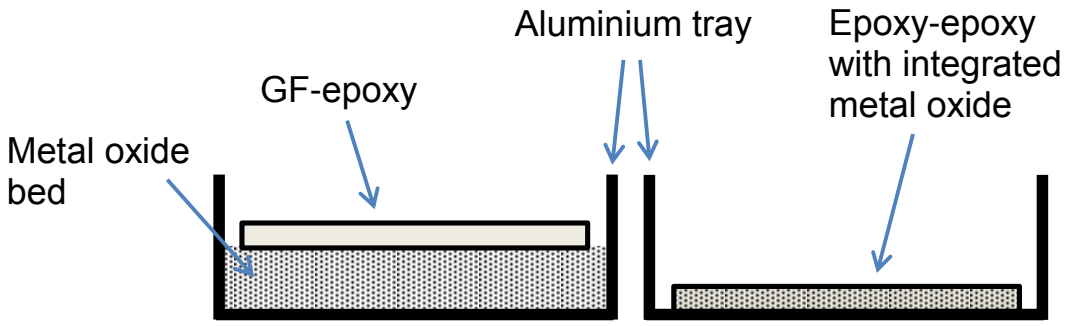

Figure 3-11 Two sample arrangements used during GF-EP thermal recycling in the furnace

An iterative process was employed to find the minimum epoxy decomposition temperature and corresponding minimum treatment time, with each of the metal oxides applied. The treatment time is the duration the sample is heated and the minimum treatment time is defined as the shortest duration of heating required for glass fibre liberation from the matrix, at a given treatment temperature. Initially the minimum decomposition temperature required for epoxy to degrade assisted by each metal oxide was found by heating for extended treatment times. The treatment time was then reduced incrementally until both the minimum temperature and treatment time were evaluated.

In order to assess the effect of the metal oxides on fibre strength retention, the strength of glass fibres thermally recovered from the GF-EP plates with the application of the metal oxide catalysts was measured and compared to those without a catalyst. In addition, the energy consumption of the furnace used during each epoxy decomposition was found using an electricity meter. This allowed a comparison to be made between the catalysing capability of each metal oxide and both recovered fibre strength and the energy input required for recycling fibres.

3.2.6.3 Thermal recycling GF-EP with the fluidised bed process

Other than during characterisation of the fluidised bed performance in Chapter 2, the operating conditions of the fluidised bed were kept consistent throughout this work.

Table 3-2 outlines the fluidised bed operating conditions.

Table 3-2 Operating conditions of the fluidised bed

Feed rate (g/min)	Static bed height (mm)	Fluidisation velocity (m/s)	Bed temperature (°C)
3	150	1.5	500

For consistency through this work, fibres recycled for single fibre tensile testing were also tested at a gauge length of 20 mm. The fibre length degrades when processing in the fluidised bed rig, therefore, 60x15 mm pieces of GF-EP were used to increase the proportion of testable RGF.

3.3 Results and discussion

3.3.1 Effect of integrated metal oxides on epoxy properties

3.3.1.1 Effect of integrated metal oxides on epoxy cure

Table 3-3 gives the reaction enthalpy (ΔH) and glass transition temperature (Tg) of all samples under investigation. There is relatively low variation in both the enthalpy of the curing and Tg of the cured samples. The absolute reaction enthalpy decreases with metal oxide content, however, when normalised to epoxy mass only (i.e. disregarding the mass of the metal oxide in sample) the enthalpy is essentially constant with metal oxide loading. No correlation between the metal oxide used or the loading and Tg was observed. It can be established however that the inclusion of the metal oxides in the epoxy does not appear to negatively affect the curing of the epoxy. The results from this calorimetry study suggest that the addition of metal oxide to aid epoxy thermal decomposition should not be harmful to the epoxy thermal properties at typical operational temperatures.

Table 3-3 Enthalpy of epoxy cure and glass transition temperature found using DSC

Sample	Metal oxide content (%)	Tg (°C)	Absolute ΔH (J/g)	Normalised ΔH (J/g)
Epoxy only	-	80.4	356	356
Epoxy+CuO	1.5	82.3	352	357
	5	83.8	339	356
Epoxy+Co_3O_4	1.5	79.2	354	359
	5	83.1	340	358
Epoxy+CeO_2	1.5	80.2	350	355
	5	79.1	341	359

3.3.1.2 Effect of integrated metal oxides on epoxy mechanical properties

Figure 3-12 gives the mechanical properties of the epoxy+metal oxide systems. The tensile strength [119, 120] and modulus [121] of neat epoxy approximates those found in other studies. Considering the error, integration of metal oxide nanopowder, at 5% weight loading, does not appear to affect the mechanical properties of the epoxy. This mechanical data and the calorimetry study of epoxy cure, suggest that the addition of metal oxides to aid epoxy thermal decomposition should not be harmful to the epoxy thermal or mechanical properties at typical operational temperatures.

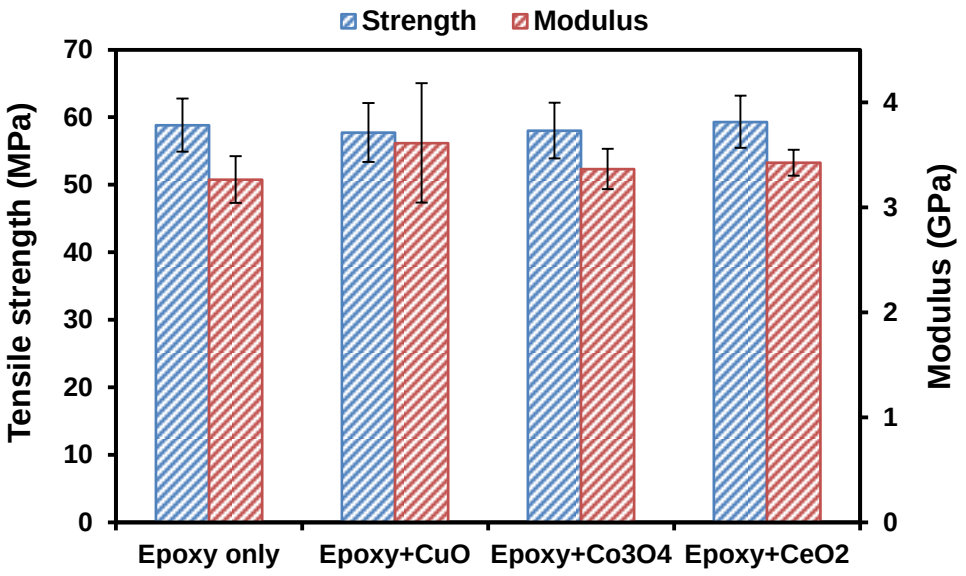

Figure 3-12 Tensile strength and modulus of epoxy with metal oxides integrated at 5% weight loading. The presence of the metal oxides does not appear to affect these mechanical properties of epoxy.

3.3.2 Thermal analysis of epoxy thermal decomposition

3.3.2.1 Isothermal decomposition of epoxy

In this section TGA is used to investigate the effect of metal oxides on epoxy decomposition under isothermal conditions. A temperature range of 375-500 °C was used.

Metal oxide alone

Initially TGA was performed on each of the metal oxides in isolation at 500 °C in air, shown in Figure 3-13. In all cases, there was a small mass loss of no greater than 2%. This mass loss was attributed to impurities in the metal oxide powder and not related to the metal oxide thermally decomposing. As expected no mass gain through oxidation was observed as all metals are at their highest oxidation state. The metal oxides appear stable when heated alone at the temperatures investigated.

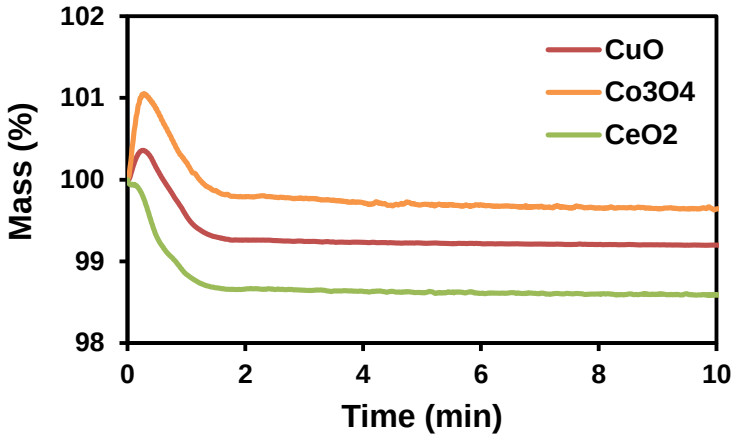

Figure 3-13 Mass as a function of time for metal oxides heated alone at 500 °C

Thermally decomposing epoxy using metal oxide bed under isothermal conditions

Figure 3-14 shows a comparison of the TGA results obtained through isothermal decomposition of epoxy, in air, on metal oxide beds. Epoxy exposed to CeO_2 and Co_3O_4 shows a similar two-stage decomposition process at 500 °C; an initial mass loss of around 90% followed by a decreased rate of mass loss until the epoxy fully degrades. Full decomposition occurs after 14 min for the sample with epoxy alone, while 5 and 4 min are required for complete epoxy decomposition when CeO_2 and Co_3O_4 are used respectively.

Epoxy exposed to CuO, on the other hand, exhibited a completely different behaviour with initial weight loss of 120% followed by a rise to around 0% and final plateau after 5 min. This pattern could be explained by CuO reduction. Since the TGA microbalance was initially tared with the CuO powder and sample pan only, any mass loss below zero should be a result of CuO mass loss. Since thermal oxidation of the epoxy by CuO could cause CuO to reduce to copper (I) oxide (Cu_2O) and/or copper (Cu), this would result in a mass loss of CuO (relative to the initial sample mass) between 17% and 33% according to atomic weight change during this transition. The additional mass loss observed in Figure 3-14 falls into this range and suggests that the rate of oxygen depletion in CuO is much faster than that in its re-oxidation. It is understood that both Cu_2O and Cu can be oxidised to re-form CuO by the hot air in the TGA furnace, which explains the subsequent weight gain in Figure 3-14.

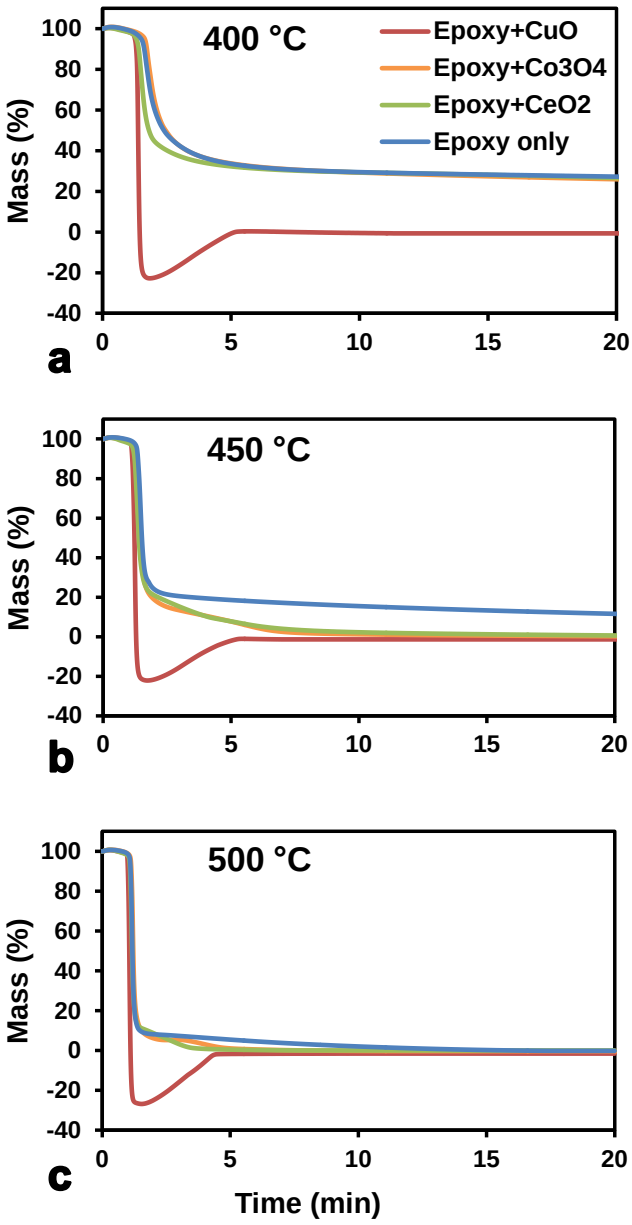

Figure 3-14 Mass as a function of time with metal oxide beds at (a) 400 °C, (b) 450 °C, (c) 500 °C

To test this assertion, epoxy applied with CuO was decomposed using TGA in a nitrogen atmosphere. Figure 3-15 shows the thermogram of the epoxy decomposition isothermally at 500 °C. In this case, the additional mass loss from CuO reduction does not recover under nitrogen until the atmosphere in the TGA furnace was switched to air as shown in Figure 3-15. Based on the above observation, it is reasonably safe to conclude that the mass loss behaviour below the origin in Figure 3-14 should be a result of CuO redox reaction. On the other

hand, similar behaviour is not observed when using CeO_2 and Co_3O_4. This could be an indication of their less catalytic efficiency or function with another mechanism.

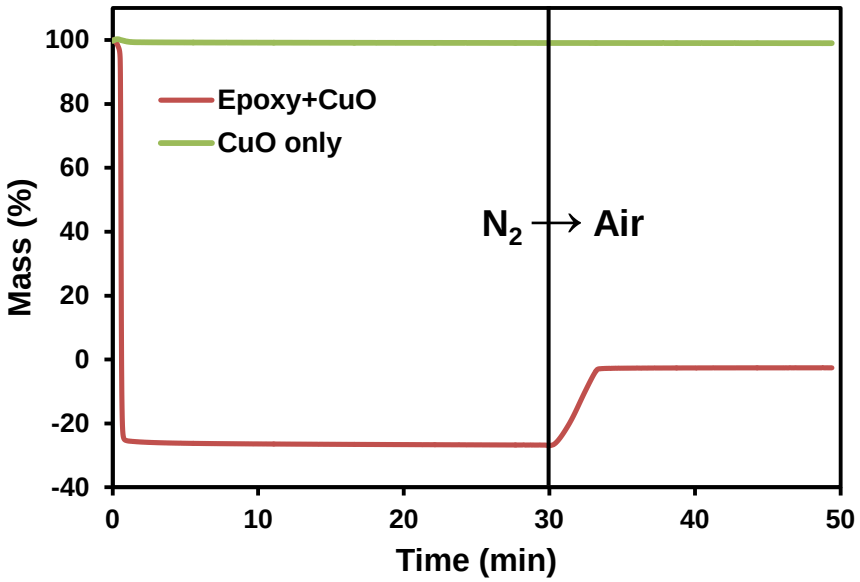

Figure 3-15 Mass as a function of time at 500 °C in both CuO and epoxy with CuO in nitrogen between 0-30 min and in air between 30-50 min

When heating at 450 °C as shown in Figure 3-14, only the uncatalysed epoxy fails to fully decompose within 20 min. Epoxy applied with CeO_2 and Co_3O_4 shows full decomposition within approximately 8 min. In contrast, the temperature reduction appears to have little effect on the catalysing performance of CuO, which produced near identical TGA thermograms to that at 500 °C. Further temperature reduction to 400 °C shows that only the epoxy in contact with CuO can fully decompose within 20 min as shown in Figure 3-14. It was found that the minimum temperature required for epoxy in the presence of CuO to decompose, in air, using TGA was merely 375 °C as indicated in Figure 3-16. This may have important implication in the energy reduction for thermal recycling as well as potential strength preservation for RGF.

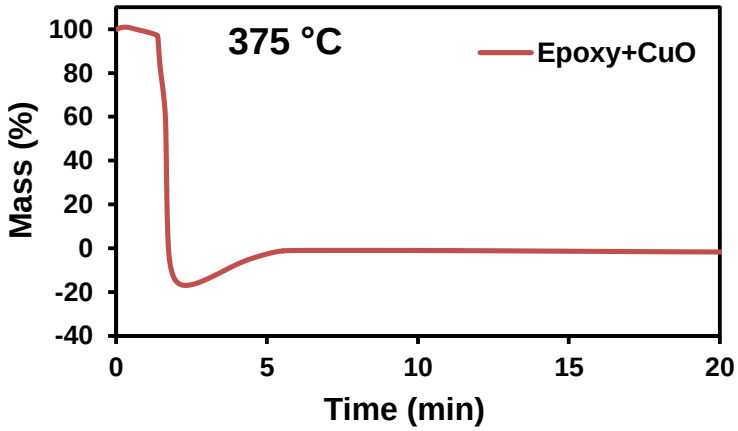

Figure 3-16 Mass as a function of time with CuO bed, showing that epoxy can thermally decompose at just 375 °C in the presence of CuO

Thermally decomposing epoxy using integrated metal oxides under isothermal conditions

Figure 3-17 and Figure 3-18 show the thermograms for isothermal epoxy decomposition with 1.5 and 5% integrated metal oxides respectively. The data has been normalised so the change in mass is relative to only the epoxy mass in the sample. Figure 3-17 and Figure 3-18 show that all metal oxides increase the rate of epoxy decomposition. Under the conditions tested, CeO_2 is consistently the least effective of all the metal oxides at aiding epoxy decomposition. The time for complete epoxy decomposition is reduced with increased CeO_2, however, fails to fully decompose epoxy at 400 °C, regardless of the content. This is in agreement with Figure 3-14 which showed that epoxy cannot fully decompose at 400 °C with a bed of CeO_2. As with CeO_2, the rate of epoxy decomposition increases with Co_3O_4 content. A Co_3O_4 content of 5% facilitates complete epoxy decomposition (within 90 min), unlike 1.5% Co_3O_4 which has relative residual epoxy mass of around 4.3%. As in Figure 3-14, CuO appears to be the most effective at reducing the temperature and time required for epoxy thermal decomposition. It is the only metal oxide able to fully decompose epoxy at 400 °C irrespective of the quantity integrated within the epoxy. The performance of CuO does not appear as dependent on the quantity used, as was observed with Co_3O_4 and CeO_2.

The behaviour of epoxy decomposition with integrated CuO (Figure 3-17 and Figure 3-18) was very different to that observed when using the CuO bed in Figure 3-14. No distinct region of mass increase due to re-oxidation was observed after the

epoxy decomposed. This suggests there is a continuous redox cycle occurring when CuO is integrated in the epoxy. It is likely that the CuO bed sample arrangement restricts air from contacting and re-oxidising the Cu_2O/Cu till after the epoxy has decomposed.

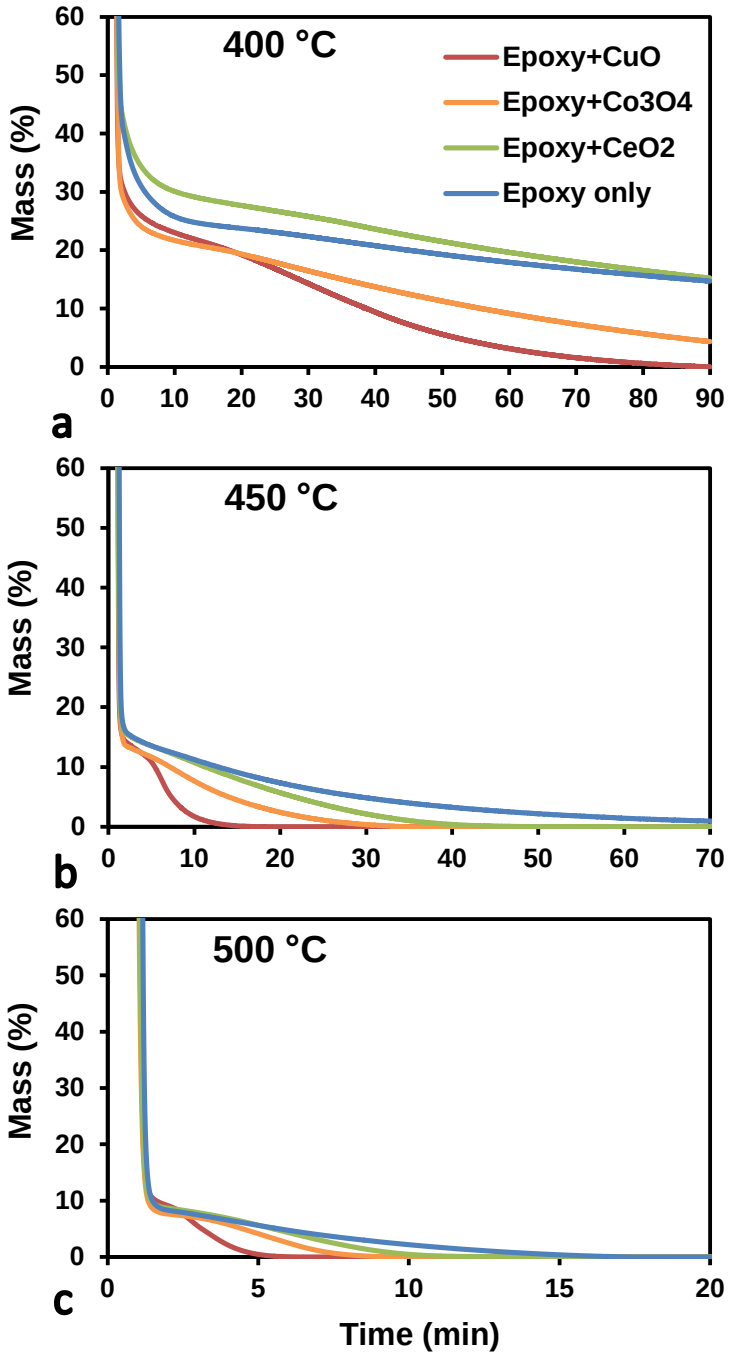

Figure 3-17 Mass as a function of time with 1.5% integrated metal oxide at (a) 400 °C, (b) 450 °C, (c) 500 °C. Time axis scale not consistent between plots.

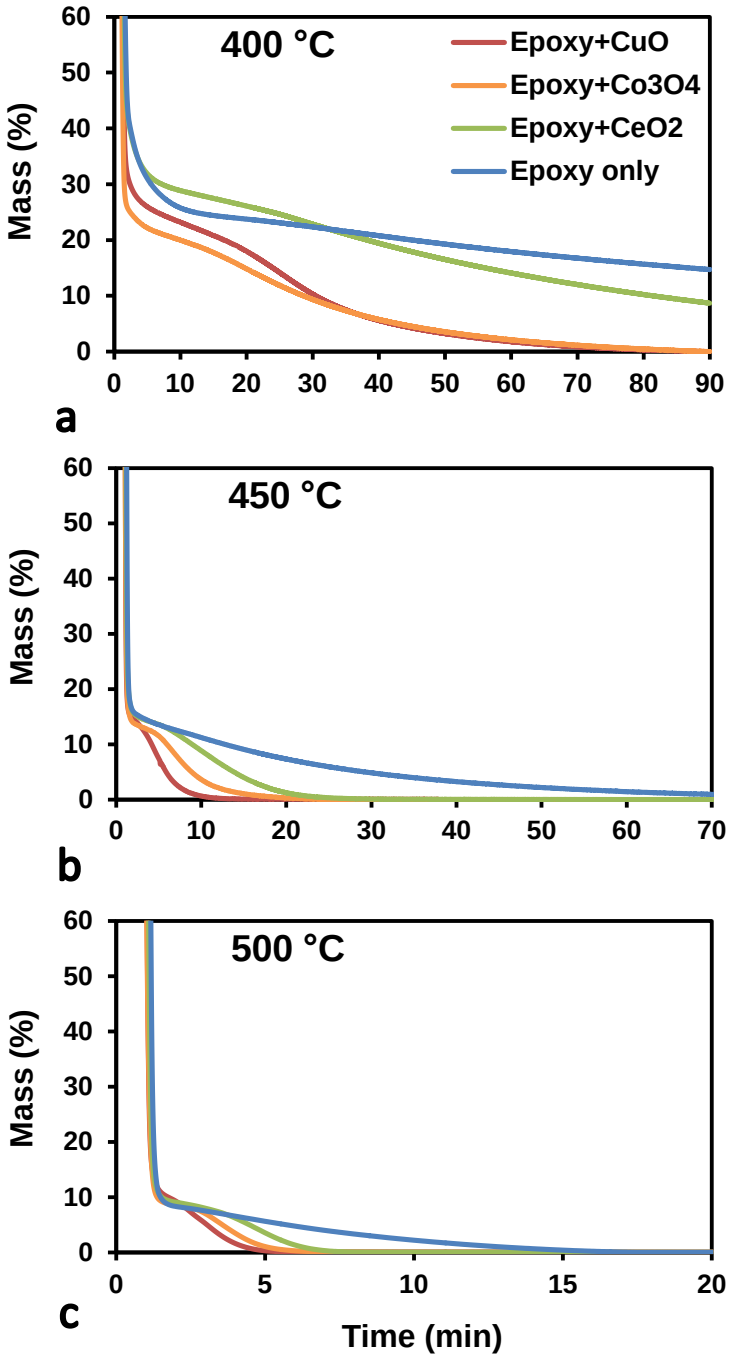

Figure 3-18 Mass as a function of time with 5% integrated metal oxide at (a) 400 °C, (b) 450 °C, (c) 500 °C. Time axis scale not consistent between plots.

Table 3-4 gives the full decomposition time for the various metal oxides, sample arrangements and temperatures used during isothermal thermal analysis. As discussed, the metal oxides are generally more effective when integrated at 5% compared to 1.5%. Table 3-4 also shows that the epoxy decomposition is significantly more rapid when the using the metal oxide bed sample arrangement.

Table 3-4 Full decomposition time for the various samples, arrangements and temperatures used during isothermal thermal analysis. Overall CuO shows the lowest decomposition times and therefore the greatest potential as a catalyst for use within a fluidised bed recycling process.

Metal oxide	Sample arrangement	Full decomposition time (min)		
		400 °C	450 °C	500 °C
Epoxy only		-	80	14
CuO	Bed (+ re-oxidation)	6	6	5
	Integrated – 1.5%	88	16	6
	Integrated – 5%	88	12	5
Co_3O_4	Bed	-	8	4
	Integrated – 1.5%	-	31	8
	Integrated – 5%	89	20	6
Ceo_2	Bed	-	8	5
	Integrated – 1.5%	-	42	12
	Integrated – 5%	-	30	8

3.3.2.2 Non-isothermal decomposition of epoxy

In this section, TGA is used to investigate the effect of metal oxides on epoxy decomposition under non-isothermal conditions. Thermal analysis was carried out in air at five different heating rates; 1, 2, 5, 7 and 10 °C/min. Decomposing epoxy at various heating rates provided data which was further analysed to determine the activation energy of the epoxy decomposition which is outlined and discussed in 3.3.2.3.

Thermally decomposing epoxy using metal oxide bed under non-isothermal conditions

Figure 3-19 gives the thermograms of epoxy decomposition using metal oxide beds at heating rates of 2 °C/min and 10 °C/min. The two stage process of epoxy thermal-oxidative decomposition shown in Figure 3-19 is typical in the literature [122]. CuO appears to have the largest impact on epoxy decomposition. In each case there is a large initial mass loss, especially at a heating rate of 10 °C/min. Over 90% of the initial mass is lost when the sample reaches just 400 °C, whereas the epoxy only sample has a residual mass of around 40%. Thermal decomposition does appear to be aided with Co_3O_4 and CeO_2, especially the second stage of decomposition.

In light of the behaviour of CuO in Figure 3-14, it is plausible that the substantially greater mass loss of epoxy with CuO in Figure 3-19, between 300-400 °C, is the result of epoxy decomposition facilitated by CuO and simultaneous CuO reduction. The extent of CuO contribution to the mass loss in this region could be estimated to be up to 20% based on Figure 3-14.

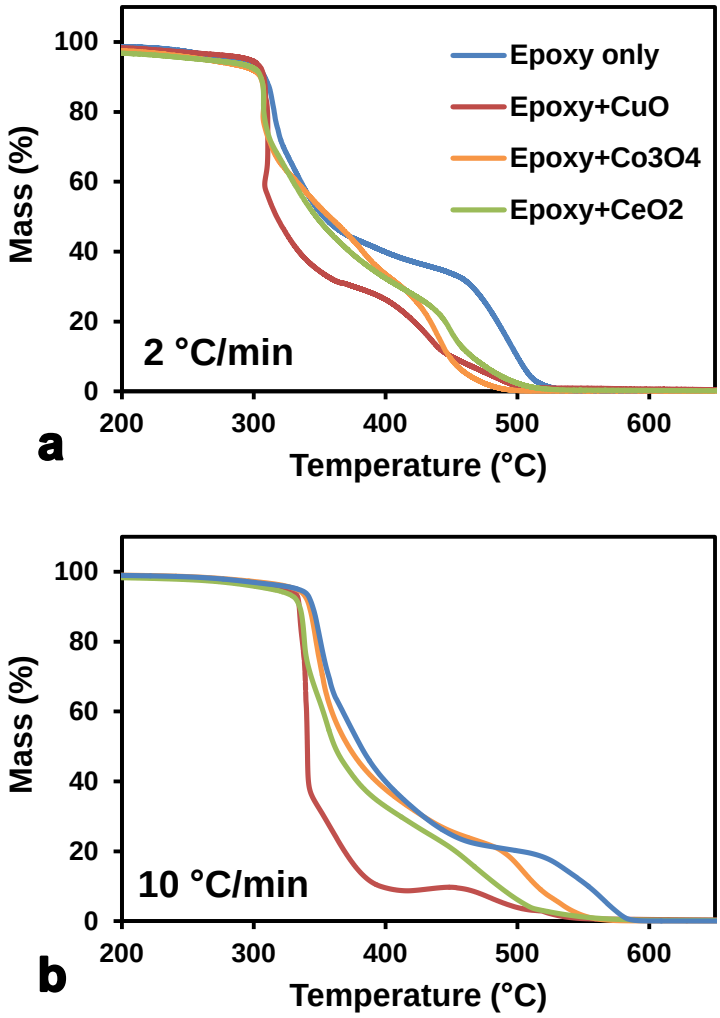

Figure 3-19 Mass as a function of temperature with metal oxide beds at (a) 2 °C/min (b) 10 °C/min. All metal oxides provide a reduction in thermal stability of epoxy under non-isothermal heating conditions, with CuO showing the greatest catalytic activity.

Figure 3-20 gives the average reduction in first and second stage of decomposition onset temperatures, as well as the average reduction in complete decomposition temperature. The metal oxides have little effect on the first stage onset temperature however, all reduce the second stage onset and complete decomposition temperature. The effectiveness of CuO, over Co_3O_4 and CeO_2, at aiding epoxy decomposition is not so clear under non-isothermal conditions, compared with Figure 3-14. Given the large error bars (representing a 95% confidence), there is no significant difference between the metal oxides at reducing the second stage onset and complete decomposition temperature of epoxy.

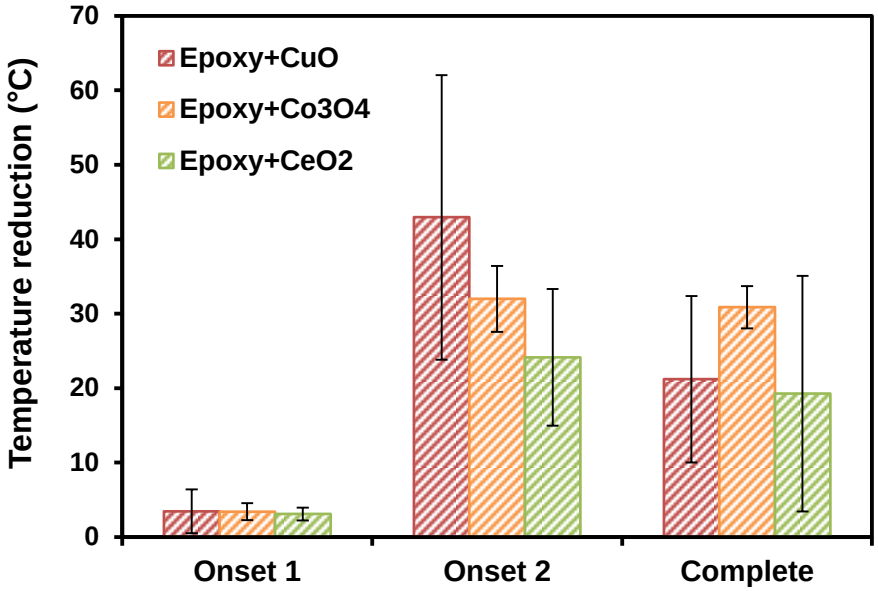

Figure 3-20 Average reduction in first and second stage onset and complete decomposition temperature with metal oxide beds. All the metal oxides tested successfully reduce the second stage onset and complete decomposition temperatures of the epoxy.

Thermally decomposing epoxy using integrated metal oxides under non-isothermal conditions

Figure 3-21 gives the thermograms of epoxy decomposition using 1.5% and 5% integrated metal oxide at heating rates of 2 °C/min. The first stage of epoxy decomposition is relatively consistent between samples. However, Figure 3-21 shows a reduction in the second stage onset temperature as well as the temperature required to decompose the epoxy. Unlike in Figure 3-19, there are no major abrupt drops in mass in samples containing CuO. As was seen when decomposing isothermally with TGA, it is likely a continuous redox cycle occurs when CuO is integrated in the epoxy.

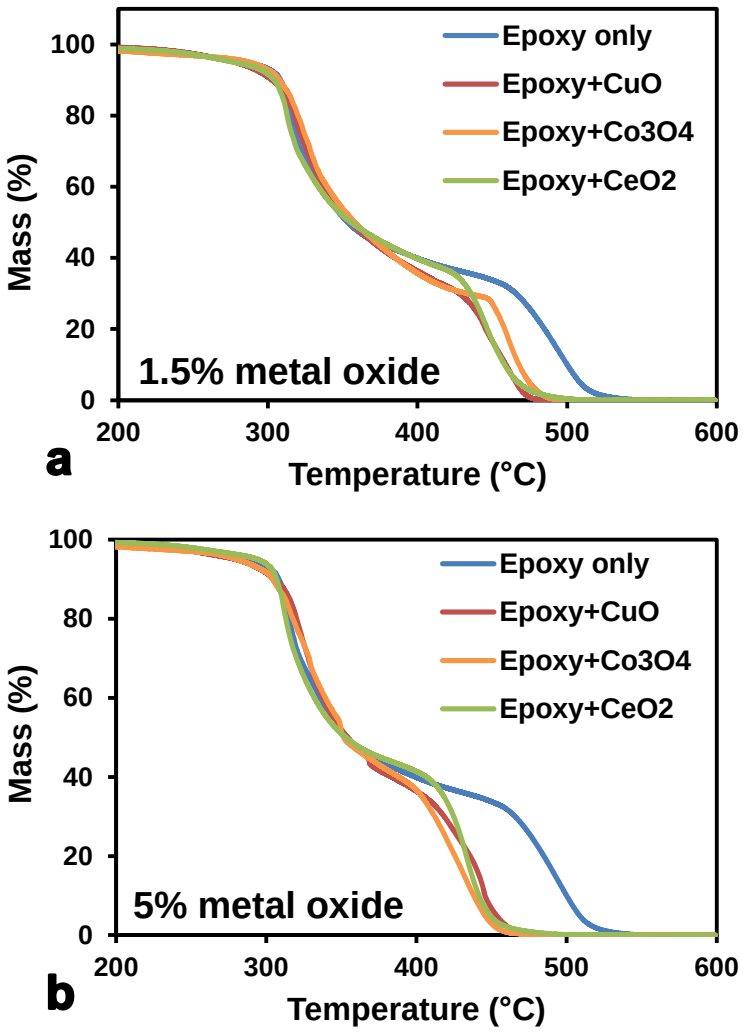

Figure 3-21 Mass as a function of temperature at a heating rate of 2 °C/min with (a) 1.5% and (b) 5% integrated metal oxide. All metal oxides provide a reduction in thermal stability of epoxy under non-isothermal heating conditions.

Figure 3-22 and Figure 3-23 gives the average reduction in first and second stage of decomposition onset temperatures, as well as the average reduction in complete decomposition temperature for integrated metal oxides. Similarly when using the metal oxide bed arrangement (Summarised in Figure 3-20), the metal oxides have a negligible effect on the first stage onset temperature when integrated within the epoxy. The second stage onset and complete decomposition temperature are reduced in all cases when metal oxides are used. Similar to Figure 3-20, the error bars are large such that there is no significant difference in the average temperatures between metal oxides in Figure 3-22 and Figure 3-23.

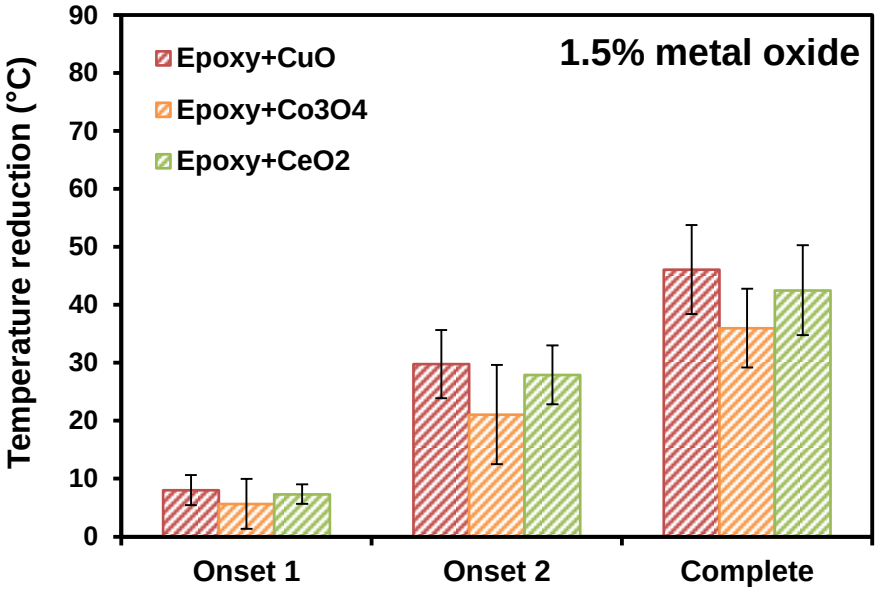

Figure 3-22 Average reduction in first and second stage onset and complete decomposition temperature with 1.5% integrated metal oxides. All the metal oxides tested successfully reduce the second stage onset and complete decomposition temperatures when integrated into epoxy at 1.5%.

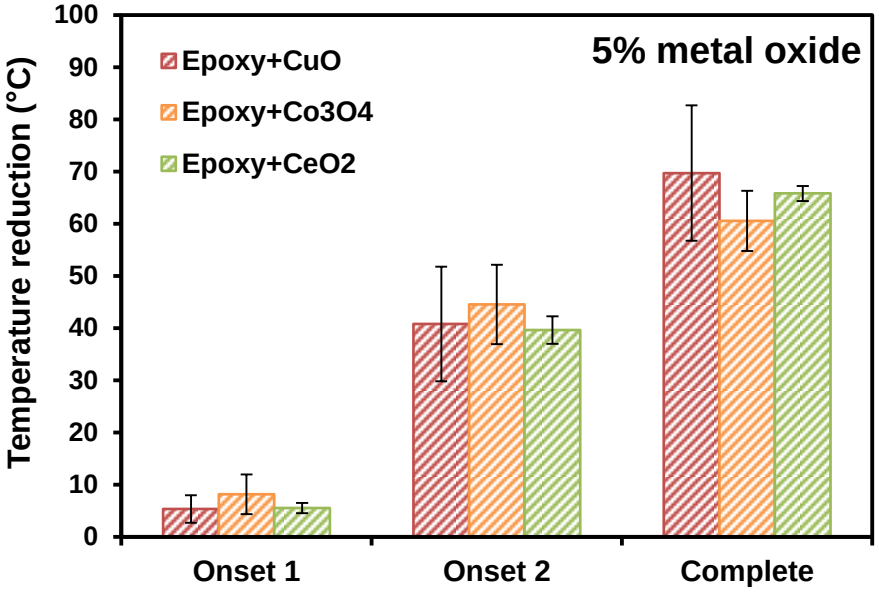

Figure 3-23 Average reduction in first and second stage onset and complete decomposition temperature with 5% integrated metal oxides. All the metal oxides tested successfully reduce the second stage onset and complete decomposition temperatures. Increasing metal oxide content to 5% provides larger reduction in thermal stability compared to Figure 3-22

Figure 3-24 shows effect of metal oxide content on second stage onset and complete decomposition temperatures. In all cases, the temperature reduction increases with metal oxide content. This is in agreement with data in Table 3-4 that concludes there is a reduction in thermal stability with increased metal oxide content under isothermal heating programs.

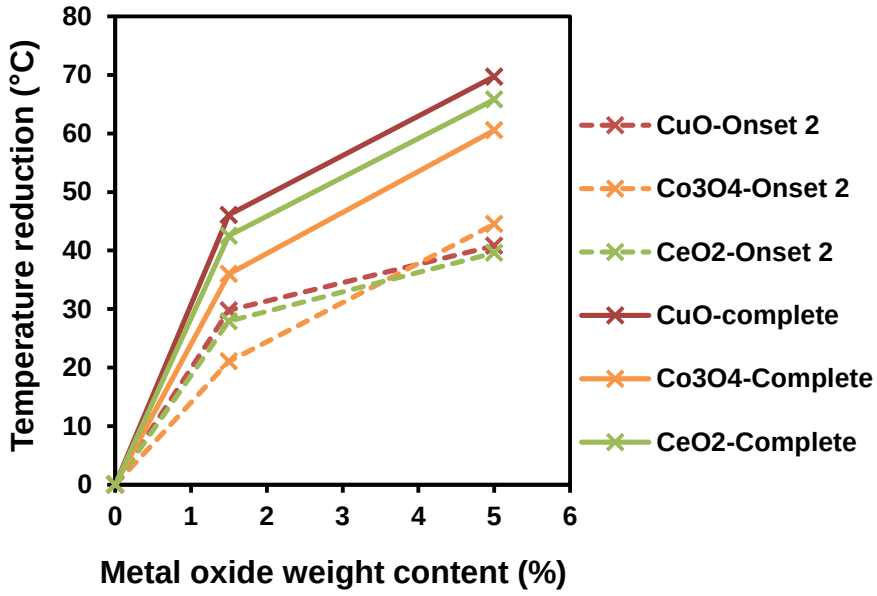

Figure 3-24 Effect of metal oxide content on second stage onset and complete decomposition temperatures

Figure 3-25 compares the reduction in average complete decomposition temperature for the various sample arrangements when using non-isothermal heating programs. There is a significant reduction in epoxy decomposition temperature when the metal oxides are introduced into the epoxy matrix over the bed arrangement. When heating with the metal oxide bed, highly porous char could build up and act as a barrier between the metal oxide bed and residual epoxy. This would restrict the metal oxides from contacting the remaining un-decomposed epoxy/char, which would then decompose at the rate of uncatalysed samples. This separation does not occur in samples with integrated metal oxides, allowing for full epoxy decomposition at lower temperatures.

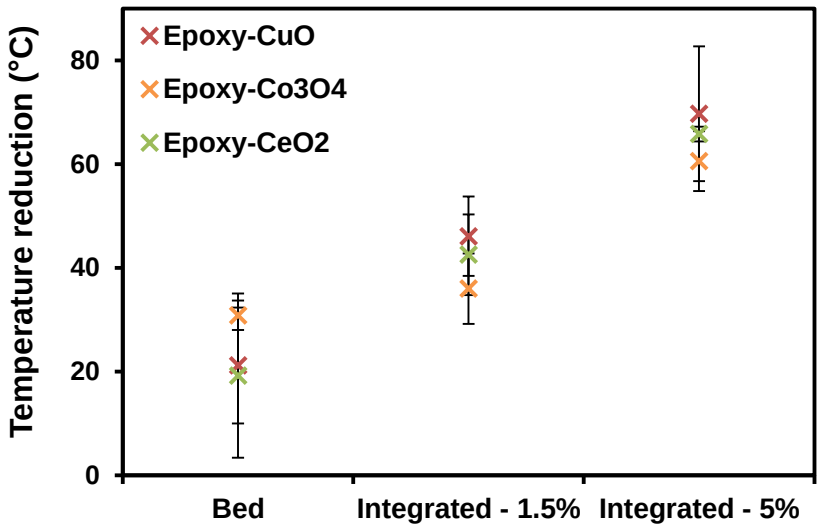

Figure 3-25 Reduction in average complete decomposition temperature for the various sample arrangements. Integrating metal oxides in epoxy at 5% provides the lowest thermal decomposition temperature.

Under isothermal heating schedules, it was concluded that the metal oxide bed arrangement significantly reduced the time required for epoxy thermal decomposition, as seen in Table 3-4. This is inconsistent with the results obtained from non-isothermal decomposition in Figure 3-25, the cause for which is still unclear. Before resolving the apparent contradiction, a fuller understanding of the underlying mechanisms of epoxy decomposition, and how the metal oxides affect this would be required.

3.3.2.3 Epoxy thermal decomposition kinetic study

A means of measuring the thermal stability of epoxy is calculating its decomposition Ea; a reduction in the Ea in the presence of the metal oxides indicates the decomposition is catalysed. The Ea was found for epoxy with the metal oxides integrated at 1.5% and 5% weight loadings.

A summary is given below outlining how the Ea can be found from TGA data. Using a non-isothermal TGA heating programme the remaining epoxy mass can be plotted as a function of temperature assuming a linear temperature-time relation such that $\beta = dT/dt = constant$, where β is the heating rate. The rate of conversion is a linear function of the rate constant, k, and a function of conversion, α, as shown in Equation 3-16:

Equation 3-16 Rate of conversion as a linear function of k and $f(x)$

$$\frac{d\alpha}{dt} = kf(\alpha)$$

The temperature dependence rate constant is given by the Arrhenius equation in Equation 3-17:

Equation 3-17 Arrhenius equation

$$k = Aexp\left(\frac{-Ea}{RT}\right)$$

Where A is the pre-exponential factor, R is the universal gas constant and T is absolute temperature. Combining Equation 3-16 and Equation 3-17 yields the following:

Equation 3-18 Rate of conversion

$$\frac{d\alpha}{dt} = Af(\alpha)exp\left(\frac{-E}{RT}\right)$$

For constant heat rate the extent of conversion can be analysed as a function of the temperature:

Equation 3-19 Rate of conversion for constant heating rates

$$\frac{d\alpha}{dT} = \frac{A}{\beta}f(\alpha)exp\left(\frac{-E}{RT}\right)$$

There are many methods for determining the Ea from TGA data. The Kissinger–Akahira–Sunose (K-A-S) method uses the integral isoconversional principle; it is assumed that the reaction rate at constant extent of conversion is only a function of temperature. Equation 3-20 gives the integral form of the reaction model, $g(\alpha)$:

Equation 3-20 Integral form of the reaction model

$$g(\alpha) = \int_0^{\alpha} \frac{d\alpha}{f(\alpha)} = \frac{A}{\beta}\int_0^{T} exp\left(\frac{-Ea}{RT}\right)dT$$

It was derived by integration of Equation 3-17 with the rate of conversion being a linear function of the rate constant and conversion. Since Equation 3-20 does not have an analytical solution, integral isoconversional methods typically make approximations of the temperature integral in linear form. The approximations given by the K-A-S method is shown in Equation 3-21.

Equation 3-21 Approximation of temperature integral used in K-A-S method

$$ln\left(\frac{\beta_i}{T^2{}_{\alpha,i}}\right) = Constant - \frac{-Ea_\alpha}{RT_\alpha}$$

This method allows the Ea at various extents of conversion to be found by plotting $ln\left(\frac{\beta_i}{T^2{}_{\alpha,i}}\right)$ vs. $1/T_\alpha$ for a variety of heating rates [91]. Figure 3-26 shows the thermograms of epoxy decomposition at 0%, 1.5% and 5% CuO loading using the various heating rates. The lagging effect caused by varying the heating rate can be seen clearly. From the TGA data, the temperature at various values of conversion was found and plotted as in Figure 3-27. From the gradient of line of best fit, the Ea can be calculated. As can be seen in Figure 3-26, the epoxy decomposition thermograms tended to overlap towards the end of the first stage of decomposition, therefore, the Ea was only found for $0 \leq \alpha \leq 0.4$ and $\alpha \geq 0.8$.

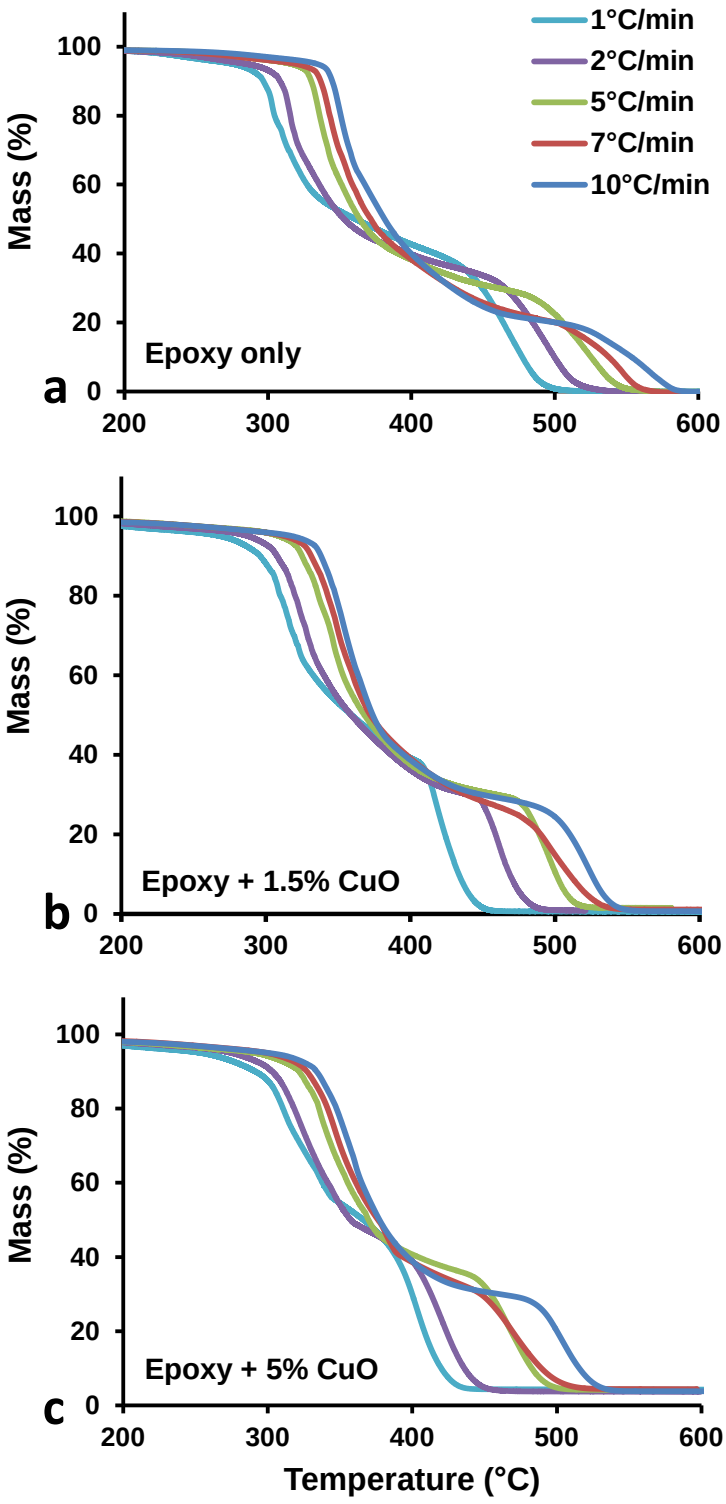

Figure 3-26 Thermograms of epoxy decomposition at various heating rates for a) epoxy only, b) 1.5% CuO and c) 5% CuO

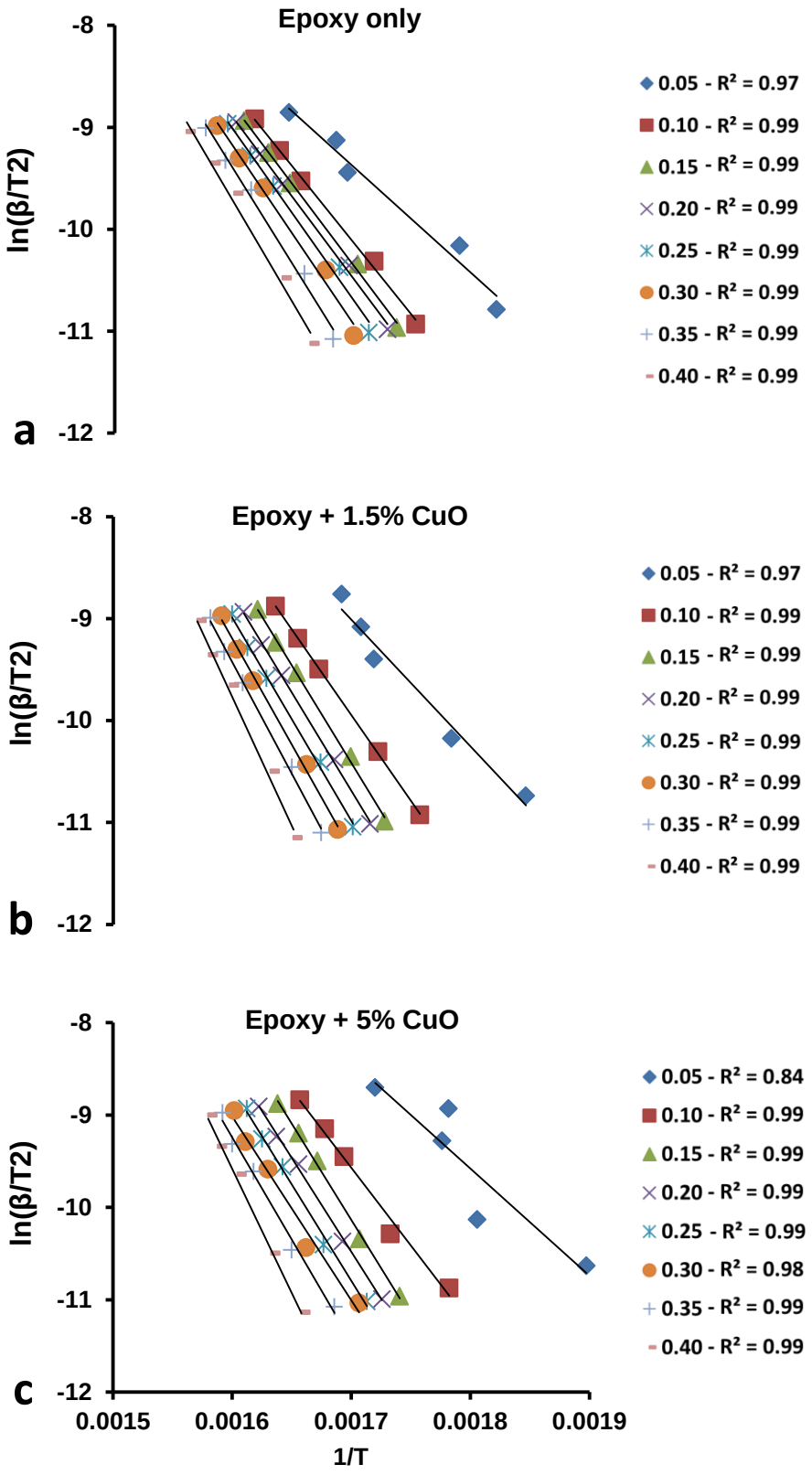

Figure 3-27 Example of plot with straight lines of best fit used to find the Ea using K-A-S method at conversions up to 0.4 for a) epoxy only, 1.5% CuO and c) 5% CuO

The concept of Ea is typically identified as the energy barrier that has to be overcome during the transformation of reactant to product. However, much discussion regarding the actual meaning of Ea in terms of solid decomposition is present in the literature, in particular between Galwey and Vyazovkin [123-125]. When analysing with isoconversional methods (such as K-A-S), a potentially complex multi-step process is treated as a single-step. The Ea obtained is therefore "apparent" and does not have any mechanistic significance.

Figure 3-28 gives the calculated apparent Ea across both ranges of conversion for each specimen. All metal oxides (and loadings) appear to increase the apparent Ea of the epoxy decomposition within the conversion range $0 \leq \alpha \leq 0.4$. This increase is particularly high for specimens containing CuO and Co_3O_4. From the TGA thermograms in Figure 3-21, as well as TGA data in Figure 3-22 and Figure 3-23, it is understood that integrating the metal oxides in the epoxy had negligible effect on the first stage of epoxy decomposition. An increase in apparent Ea was also reported by Zabihi and Somayyeh when integrating CuO nanopowders in epoxy at similar loadings, which was attributed to nanoparticles increasing the crosslinking density during curing [118]. Given the decomposition thermograms are similar between specimens up to 0.4 conversion, one may expect parity in the calculated Ea. From this work, no conclusive statements can be made as to the cause for the disparity in the Ea within the conversion range $0 \leq \alpha \leq 0.4$ however it is indicative of disparate chemical processes occurring.

Figure 3-28 shows the Ea for $\alpha \geq 0.8$ is significantly lower for specimens containing CuO and CeO_2 at both 1.5% and 5% weight loading.

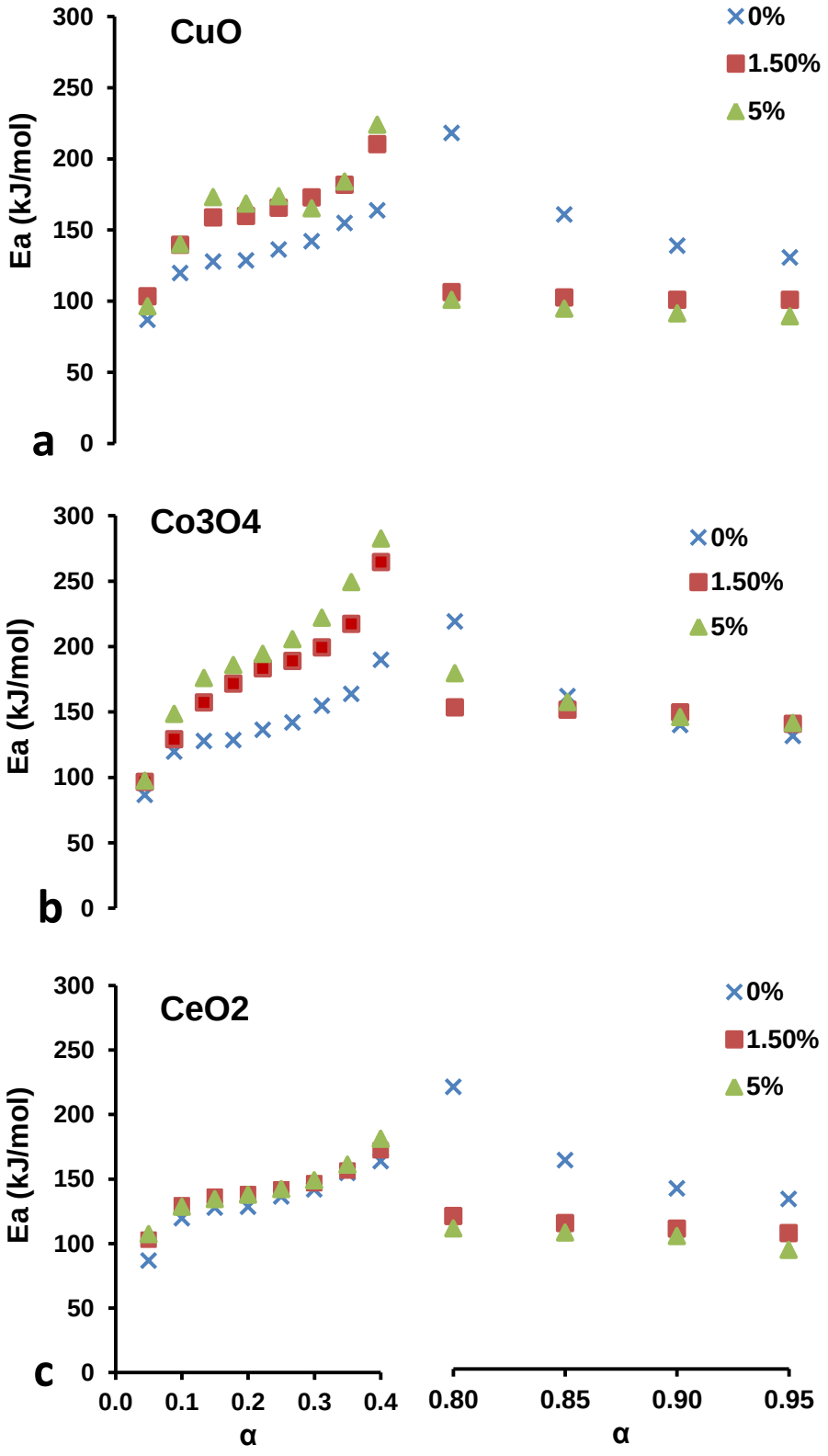

Figure 3-28 Ea of epoxy decomposition at various values of conversion found using K-A-S method with integrated a) CuO, b) Co_3O_4 and c) CeO_2. CuO and CeO_2 provide a significant reduction in the Ea of the second stage of epoxy decomposition.

Figure 3-29 gives the average reduction in Ea with the use of the metal oxides nanopowders across both conversion ranges. The reduction in apparent Ea suggests that the metal oxides are able to catalyse the thermal decomposition of the residual char typically present after the first stage of epoxy decomposition without compromising the epoxy thermal stability at lower temperatures. Given it is the char residue that requires typical high GF-EP recycling temperatures, reducing Ea of its decomposition could be important to reducing operating conditions within the fluidised bed reactor. This decrease in second stage Ea along with the reduction in complete decomposition temperature, shown in Figure 3-25, has real world implications and alludes to potentially lower energy input required for composites thermal recycling.

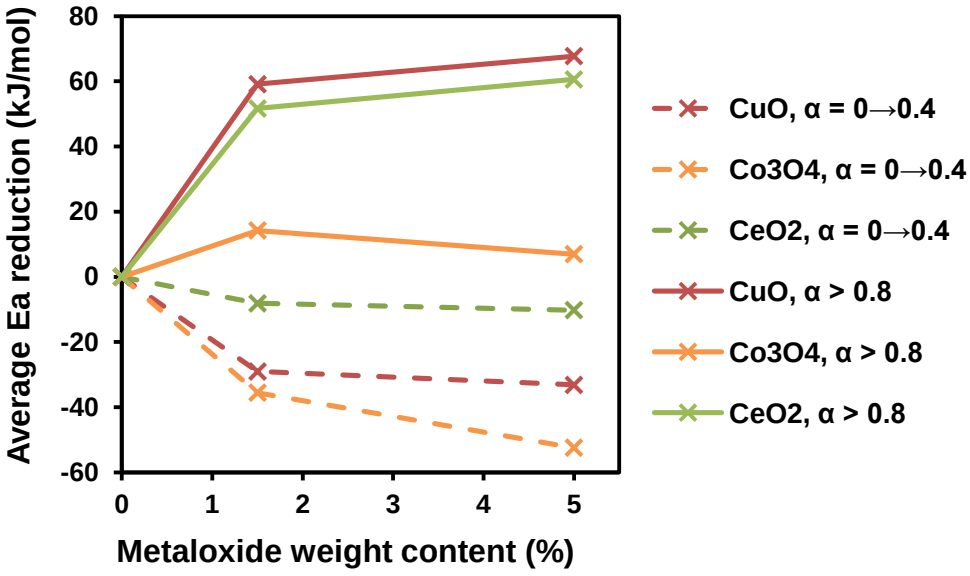

Figure 3-29 Average reduction in Ea with the use of the metal oxides across the conversion ranges. CuO integrated at 5% loading provides the overall largest reduction in Ea of second stage epoxy decomposition, within the conversions investigated.

The model-free isoconversional K-A-S method allows the apparent Ea to be evaluated without determining the reaction model. The Ea found using such methods can be used in determining both the reaction model and pre-exponential factor, under the condition that the process can be reasonably approximated as single-step kinetics [91]. Vyazovkin et al. state that significant variation in Ea with conversion (when found using isoconversional methods) indicates the process cannot be described adequately by a single reaction model and a single pair of

Arrhenius parameters [91]. Figure 3-28 clearly shows that the isoconversional kinetic modelling of epoxy decomposition yields Ea values that vary considerably with conversion. Moreover, there are clearly two distinct stages during the epoxy decomposition process as shown Figure 3-26.

To accurately determine the reaction model, a multi-step kinetic analysis needs to be employed to yield an individual reaction model and a pair of Arrhenius parameters for each of the reaction steps. The TGA thermograms of each region were separately normalised within conversion of 0–1 interval using the Equation 3-22[126].

Equation 3-22 Normalised conversion for individual stages of a multi-step kinetic process

$$\alpha = \frac{m_i - m}{m_i - m_f}$$

Where m is the percentage residual mass of the specimen at a given temperature/time; m_i and m_f are the initial and final masses of the sample.

Figure 3-30 gives an example of splitting the two-stage epoxy decomposition process for epoxy only specimen decomposed at 1°C/min. The Ea was then found again for each stage independently using the K-A-S method as outlined above.

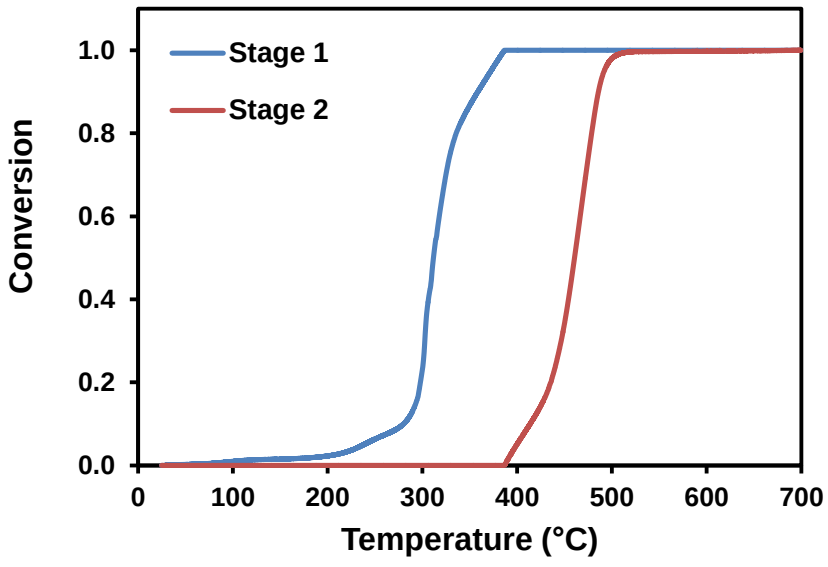

Figure 3-30 Example of splitting the two stage epoxy decomposition process (example specimen is epoxy only at 1 °C/min)

Figure 3-31 shows the Ea of epoxy only decomposition found for each stage independently. Despite using multi-step kinetic analysis, the Ea across the conversion remains inconsistent. This was also observed when analysis specimens with integrated metal oxides. Galwey discusses various possibilities as to why this variation in Ea may occur within an apparent single-step process [123]. It is suggested that if decomposition occurs via multiple simultaneous pathways, changes in conversion or temperature may alter their relative contribution from each process, in turn varying the apparent Ea. Similarly, considerable overlap of consecutive reactions within a sample during decomposition would also likely result in significant variation in apparent Ea. In both cases, the kinetic characteristics found would contain contributions from multiple individual chemical processes. Even the kinetics of some single step reactions have been shown to vary with temperature [123]. Inconsistent apparent Ea would therefore be expected when calculated using rate data across the temperature where the change happens. A comprehensive understanding of the decomposition kinetics overall necessitates characterisation of all contributing processes and their dependency with conversion.

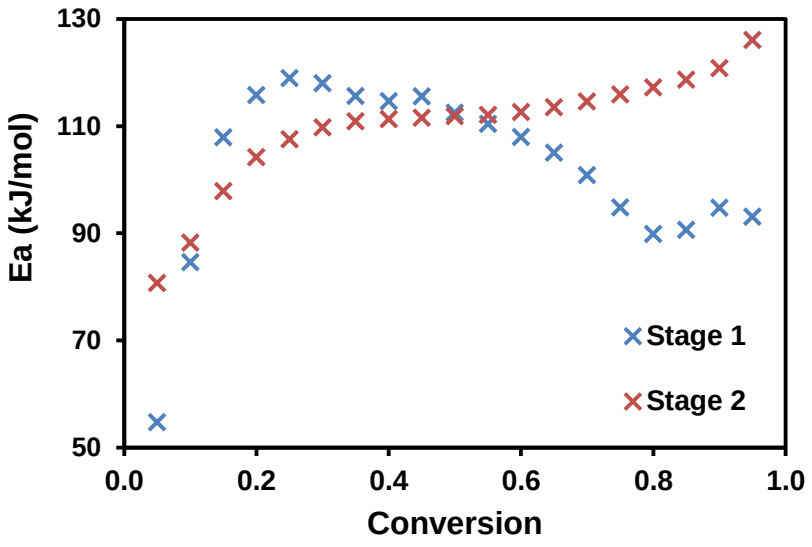

Figure 3-31 Epoxy only decomposition Ea found using K-A-S method for each stage independently. Ea still not constant across conversion indicating the process cannot be described adequately by a single reaction model [91].

3.3.3 GF-EP recycling within a furnace

3.3.3.1 Effect of metal oxides on GF-EP recycling using furnace

Recycling GF-EP in a furnace using metal oxide bed

Table 3-5 gives the epoxy matrix decomposition temperature and time found qualitatively for GF-EP samples decomposed in the furnace using metal oxide beds. Multiple recycling temperatures and times were found when using CuO and as such are given in Table 3-5. The recycling time is defined as the quantity of time required for glass fibre liberation from the matrix at a given treatment temperature. This is of course not a fixed value over the entire 60x60x2 mm sample. Visually it was observed that the extent of the epoxy decomposition within a given layer varied slightly. More variation in epoxy decomposition was observed through the thickness of the sample. It is not surprising for example that the epoxy on the top surface of the composite (which is directly exposed to the furnace atmosphere) decomposed faster than the centre of the composite. This is also true for the lower surface of the composite as it is exposed to the metal oxide. This means that fibres could be recovered from these layers, before the epoxy had decomposed sufficiently to allow the fibre in the centre to be liberated. Fibres were always taken from the middle layer of the composite, ensuring the epoxy had decomposed throughout the thickness.

Table 3-5 Heating parameters and energy required for glass fibre liberation with metal oxide bed

Sample	Furnace temperature (°C)	Required recycling time (min)	Furnace energy consumption (kJ)
GF-EP	500	80	6420
GF-EP+CuO [1]	430	65	3720
GF-EP+CuO [2]	400	180	6030
GF-EP+CuO [3]	380	330	20200
GF-EP+Co3O4	450	65	4000
GF-EP+CeO2	450	60	4090

Initially an attempt was made to find a value for the percentage of the epoxy matrix mass loss to allow glass fibre liberation. This would give a numerical definition to “recycling time”. It was found however that even minimal quantities of residual epoxy matrix could result in fibres still being bonded together (i.e. could not be removed manually without force). A consistent value could not be established most likely because it was so small and was affected by the nonhomogeneous nature of the epoxy decomposition throughout the sample. It was found that typically over 90% of the epoxy matrix mass was decomposed during the initial violent combustion. Even with the vast majority of the epoxy being decomposed there was a substantial layer of char residue prohibiting the fibres from being removed and they were of course extremely dirty. The vast majority of the recycling time was required for decomposing this relatively small mass of residual char, which joined the fibres together.

In agreement with the results obtained from isothermal TGA in Figure 3-14, CuO provided the largest reduction in the required temperature for the epoxy matrix to fully degrade. CuO, CeO_2 and Co_3O_4 can decrease the recycling temperatures by 120, 50 and 50 °C respectively. These results are consistent with those observed using isothermal TGA in Figure 3-14. Table 3-5 also shows that the heating period required is considerably extended as the temperature is reduced even including the case of the use of CuO. Such phenomenon may seem to be expected from typical temperature dependence of reaction kinetics. However, the results in Figure 3-14 and Figure 3-16 have clearly demonstrated that similar temperature reductions scarcely affect the period of epoxy decomposition when using CuO. It implies that the extended period of GF-EP decomposition observed in the furnace is likely to be caused by up-scaling effect compared to very small amount of epoxy samples used in TGA.

Figure 3-32 shows a comparison between GF-EP heat-treated with and without CuO. Both samples were heated at 380 °C for 330 min. It can clearly be seen that GF-EP decomposition assisted with CuO returned significantly cleaner RGF.

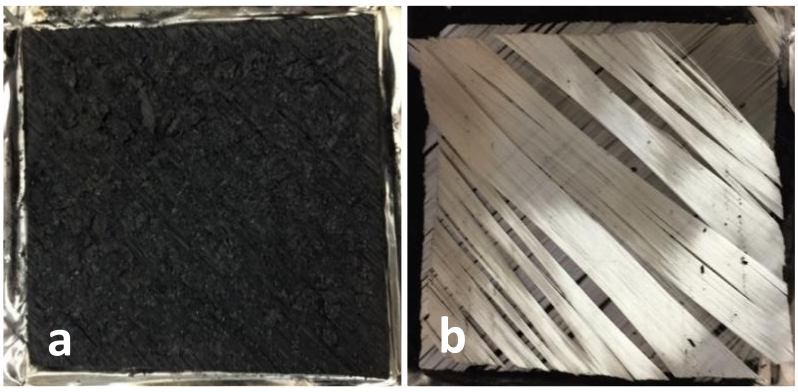

Figure 3-32 Image of GF-EP after heating at 380 °C for 330min (a) without and (b) with CuO bed. Epoxy char residue is clearly decomposed more successfully with the use of CuO.

Recycling GF-EP in a furnace using integrated metal oxides

Table 3-5 gives the epoxy matrix decomposition temperature and time found qualitatively for GF-EP samples degraded in the furnace using integrated metal oxides. Again, the temperatures required for thermal decomposition are similar to those found using isothermal TGA in Figure 3-18. The exception to this is recycling using Co_3O_4, which requires a higher furnace temperature than was found using TGA. As with the metal oxide bed, the reduction in furnace temperature is 120, 50 and 50 °C when using CuO, CeO_2 and Co_3O_4 respectively. The time required for furnace recycling with Co_3O_4 and CeO_2 are comparable whether introduced as a metal oxide bed or integrated in the matrix. The recycling time using integrated CuO is significantly lower than the CuO bed, and is comparable to the decomposition time found in Figure 3-18, using TGA. It appears feasible that integrating the metal oxide within the matrix of GF-EP does not lead to the same scaling up problems as with using the metal oxide bed. However, it is still unclear why the recycling conditions required when using Co_3O_4 and CeO_2 do not more closely match those found in with TGA in Figure 3-18.

Table 3-6 Heating parameters and energy required for glass fibre liberation with 5% integrated metal oxides

Sample	Furnace temperature (°C)	Required recycling time (min)	Furnace energy consumption (kJ)
GF-EP	500	80	6420
GF-EP+CuO [1]	450	15	870
GF-EP+CuO [2]	400	40	1370
GF-EP+CuO [3]	380	80	4890
GF-EP+Co3O4	450	50	3500
GF-EP+CeO2	450	60	4080

Table 3-5 and Table 3-6 also give the total energy required to recycle each of the samples within the furnace, measured using an electricity meter. It can be shown that all metal oxides can reduce the energy consumption of the furnace by around 40% compared to uncatalysed GF-EP recycling. The total furnace energy consumption is reduced by up to 85% when recycling with integrated CuO.

The energy values calculated are specific only to the furnace used in this investigation and may not be generalised for different operations. It should also be noted that the energy consumption of the furnace is dominated by its heat loss with little influenced from the exothermic reaction taking place inside. The calorific value of the GF-EP processed is likely to be around 12 kJ/g [127] and therefore insignificant compared to the furnace energy consumption figures given in Table 3-5 and Table 3-6. The established furnace parameters (temperature and time) required for thermal decomposition therefore dictates the measured energy consumption. Nevertheless, a simple comparison of energy consumption between heating parameters should reflect the potential energy benefit from the employment of decomposition catalysts.

3.3.3.2 Effect of thermal conditioning temperature and time on glass fibre strength

In this section the effect of thermal conditioning temperature and time on glass fibre strength is discussed. Glass fibres were conditioned at 300, 400, 430, 450, 470, 500, 550 and 600 °C. Figure 3-33 gives the tensile strength of fibres conditioned in the range of temperatures for 25 and 60 min. In agreement with the literature [31, 32, 35], the residual fibre strength significantly reduces with conditioning temperature. The strength loss also increases with conditioning time beyond 300 °C, before converging at 600 °C. Figure 3-33 demonstrates that reducing the recycling temperature of GF-EP could improve strength retention of recycled glass fibre. Moreover, where the recycling temperature is less than 600 °C, reducing the recycling time could also decrease thermal damage to RGF.

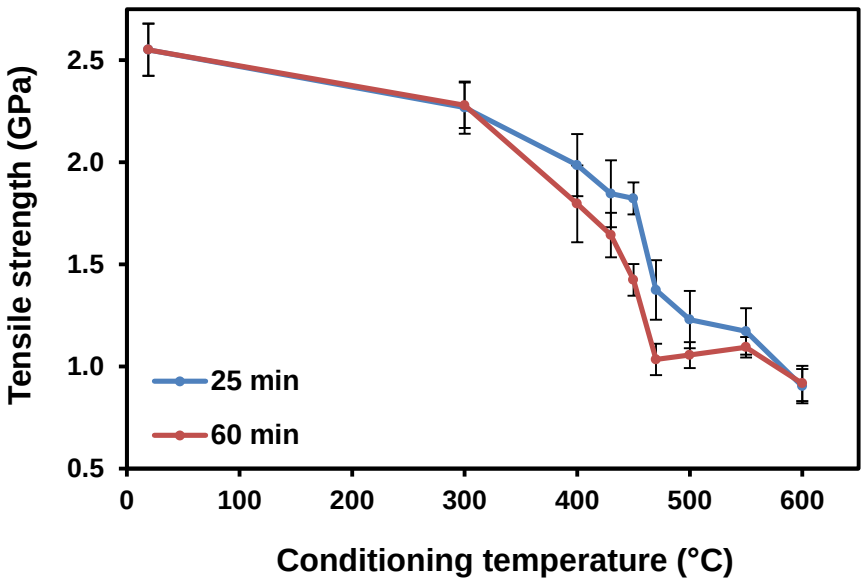

Figure 3-33 Tensile strength of glass fibre thermally conditioned for 25 and 60 min at various temperatures from 300 °C to 600 °C. As observed throughout the literature, both temperature and exposure time significantly weaken the glass fibres.

Glass fibres were also thermally conditioned at 400 °C and 500 °C for up to 240 min in order to compare with the fibres recycled in the furnace using the heating schedules given in Table 3-5 and Table 3-6. Although an extensive range of conditioning temperatures was investigated in Figure 3-33, the treatment time was

limited to 60 min. Given the recycling time used to recycle GF-EP in the furnace was up to 330 min, additional data on extended thermal conditioning was required.

Figure 3-34 shows the residual fibre tensile strength after heating at 400 °C and 500 °C for 10, 25, 60, 120 and 240 min. Glass fibres exposed to a temperature of 400 °C lost around 25% of their strength after 25 min. Prolonged exposure of 120 and 240 min led to approximately 40% strength loss. When heated at 500 °C, the glass fibre strength diminishes to around 50% of its original value within the first 25 min and levels off at around 40% within 60 min. Clearly, both heating temperature and time influence the fibre strength, however, the residual strength plateau increases in value with decreasing treatment temperature as seen in Figure 3-34. The rate of strength loss is greater for the higher treatment temperatures; suggesting that composite recycling time is more detrimental to fibre strength retention at higher temperatures.

Overall, Figure 3-33 and Figure 3-34 confirm the notion that reducing the typical recycling temperature/time of GF-EP by means of catalysed epoxy decomposition could potentially yield glass fibres with increased strength retention.

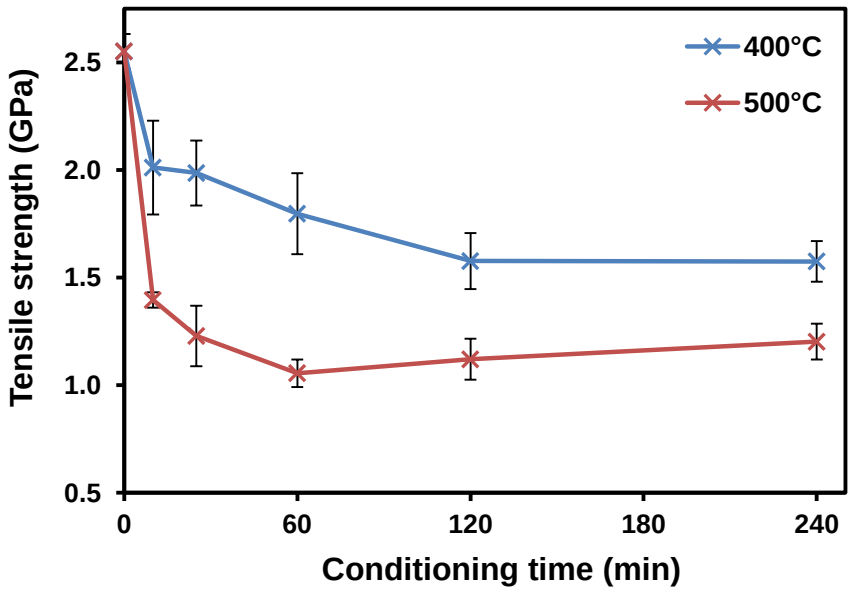

Figure 3-34 Strength loss of glass fibres after thermal conditioning in the range of recycling temperatures and times. For both conditioning temperatures, the plateau in the data clearly shows the steady state fibre strength when heating for extended periods.

Additional research into the influence of thermal conditioning testing parameters on the strength of glass fibres can be found in Appendix B, along with a phenomenological model of glass fibre strength loss as a function of conditioning temperature and time.

3.3.3.3 Tensile strength of glass fibres recycled in a furnace

Glass fibres recycled using metal oxide bed

Figure 3-35 shows the tensile strength of the glass fibres thermally recycled from GF-EP with the use of the metal oxide beds. These results are compared to the strength of fibres after thermally conditioning glass fibres at the same temperature and approximate times, as indicated in Figure 3-35 and Figure 3-33. No estimated strength retention could be made for GF-EP recycled at 380 °C since glass fibres have not been thermally conditioned at this temperature.

Strength loss was sustained in all cases given an as received strength of 2.55 GPa. The GF-EP only sample heated at 500 °C yielded fibres with a strength of 0.94 GPa, which is slightly lower than was observed for glass fibres directly heated at a similar schedule. This suggests that the additional processing and handling involved in manufacturing and retrieving fibres from the degraded GF-EP may have resulted in additional fibre damage.

Despite the high anticipation for potential strength retention indicated by the results obtained from direct fibre thermal conditioning (in Figure 3-33 and Figure 3-34), the use of metal oxides showed much less effect on improving strength retention of RGF as seen in Figure 3-35. The average tensile strength of glass fibres recycled using CuO, Co_3O_4 and CeO_2 are respectively 1.11, 0.99 and 1.14 GPa; giving a maximum additional strength retention of 21%.

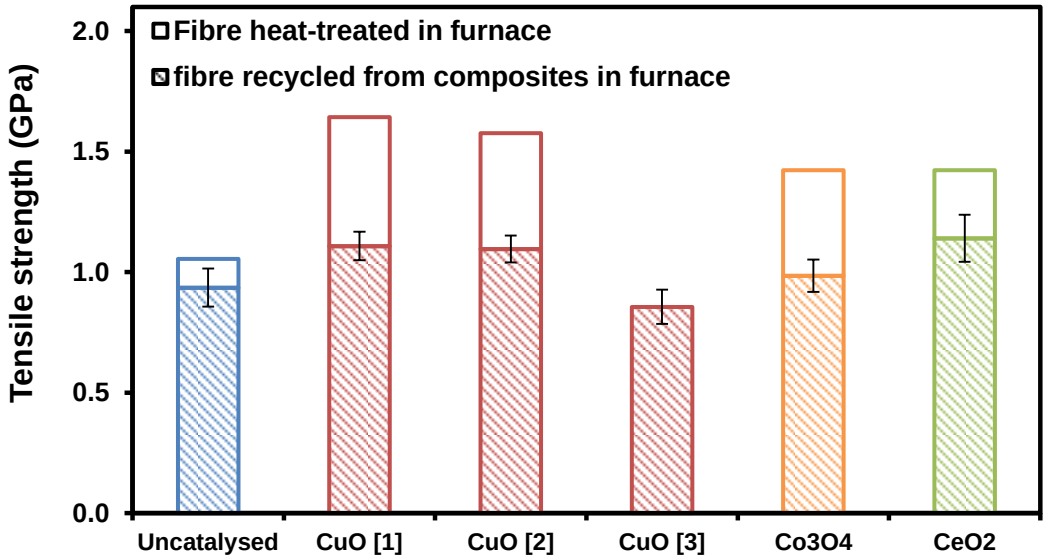

Figure 3-35 Tensile strength of glass fibres recycled from GF-EP composites with metal oxide bed

Glass fibres recycled using integrated metal oxides

Figure 3-36 shows the tensile strength of the glass fibres thermally recycled from GF-EP with the use of integrated metal oxides. These results are again compared to the strength of fibres after thermally conditioning glass fibres at the same temperature and similar times, where no estimated strength retention could be made for GF-EP recycled at 380 °C. Fibres recycled with integrated Co_3O_4 and CeO_2 exhibit similar strength retention as in Figure 3-35, when the metal oxide bed arrangement was used. The recycling parameters, temperature/time given in Table 3-5 and Table 3-6, were comparable for both arrangements therefore this is to be expected. Despite the substantial reduction in recycling parameters, the average strength of fibres recycled with integrated CuO is up to 1.5 GPa lower than the strength of fibres thermally conditioned in the furnace under the same heating schedule. It appears unlikely that this discrepancy can simply be attributed to additional damage during sample manufacture or when retrieving fibres from the decomposed GF-EP.

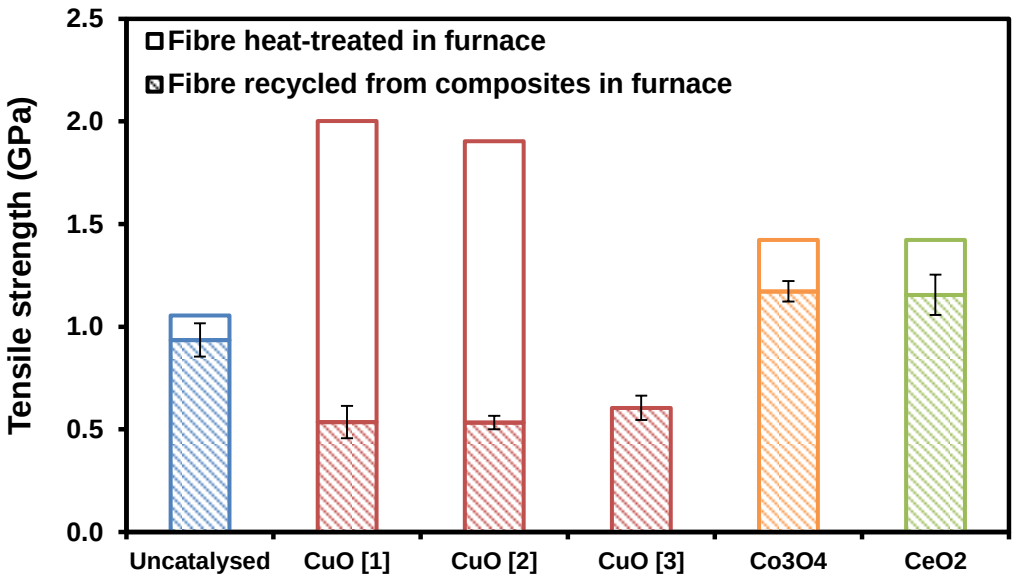

Figure 3-36 Tensile strength of glass fibres recycled from GF-EP composites with integrated metal oxides

Two possibilities may account for this under-delivered performance in strength retention. Firstly, the actual thermal loading experienced by the fibres during GF-EP recycling inside the furnace is higher than the actual furnace set point temperature. This is to be expected given that epoxy thermal decomposition is exothermic. The thermal loading experienced during thermal recycling of GF-EP and the effect on glass fibre strength is further explored in 3.3.3.4 and 3.3.3.5 respectively. Alternatively, physical contact between the glass fibre and metal oxides during heating may result in additional damage beyond purely thermal weakening. This is especially relevant to glass fibres recycled using integrated metal oxides and is investigated further in 3.3.4.

3.3.3.4 Temperature local to glass fibres during recycling

Figure 3-37 shows a comparison of surface temperature of GF-EP samples with and without the presence of CuO. The temperature was measured by an independent thermocouple placed directly on the GF-EP during thermal recycling in the furnace. As it can be seen in Figure 3-37, the surface temperature of the GF-EP increases substantially in all cases before it gradually drops down to corresponding set temperatures. Although CuO increases the rate of epoxy decomposition, this did not result in transitory heating of fibres beyond that experienced in uncatalysed samples

during furnace recycling. The fibres recycled using CuO, however, experienced over 550 °C for around 35 s with a maximum temperature of around 660 °C for integrated CuO. This sharp temporary rise in temperature is due to the exothermic nature of epoxy decomposition. The effect of this rapid thermal loading on the glass fibre strength was further investigated by heating glass fibre bundles at 600 °C for 15, 30 and 60 s within the same furnace.

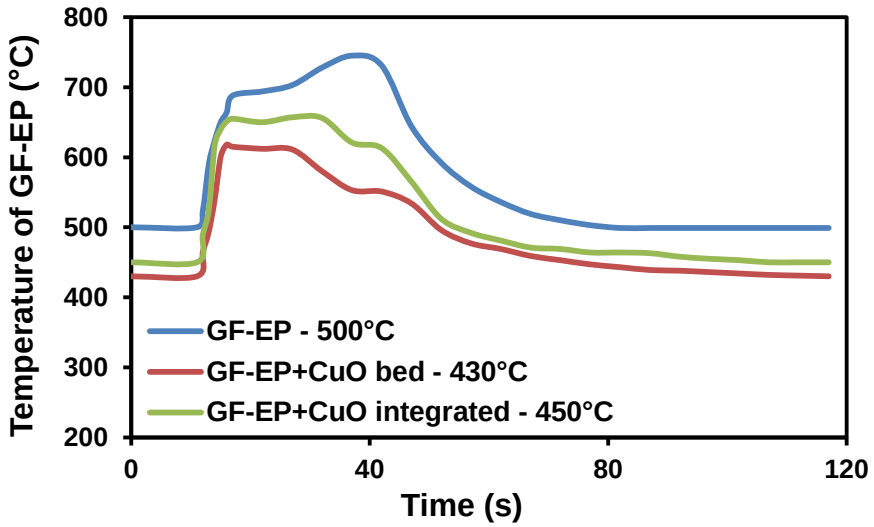

Figure 3-37 Temperature measured directly on GF-EP composites surface during thermal recycling in furnace, showing substantial increase in temperature above furnace set point due to exothermic epoxy decomposition.

3.3.3.5 Effect of rapid thermal loading on the glass fibre strength

Figure 3-38 shows a dramatic reduction in fibre strength to 1.35 and 1.16 GPa after exposure to 600 °C for merely 30 and 60 s respectively. It is therefore clear that the brief increase in thermal loading caused by the epoxy decomposition could cause substantial weakening of the fibres. By recycling statically within the furnace, the rise in temperature as the epoxy decomposes could not be adequately regulated. Simply halting energy input when the furnace temperature is above the set point is insufficient and may result in significant fibre weakening. The overshoot may be better controlled within a dynamic process such as a fluidised bed reactor by distributing areas of localised heating.

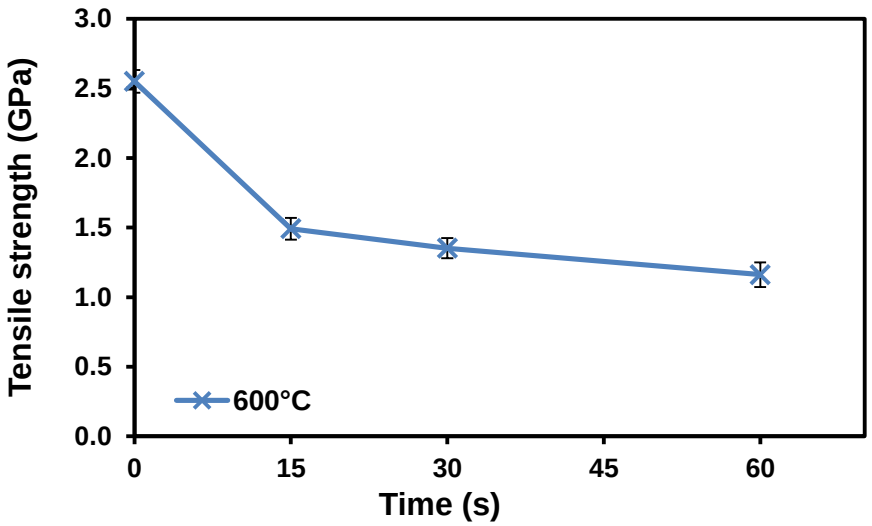

Figure 3-38 Tensile strength of glass fibres after heating at 600 °C, indicating that even short periods of heating can cause substantial weakening of glass fibres.

The spike in thermal loading observed during GF-EP recycling may cause the disparity in estimated and measured strength in most cases in Figure 3-35 and Figure 3-36; however, it cannot account for the magnitude of strength loss sustained by fibres recycled with integrated CuO, in Figure 3-36. It should be noted that the temperature measured in Figure 3-37 was only from an independent thermocouple placed on the surface of the GF-EP. Compared to the in-built furnace thermocouple, this is a more accurate measurement of the temperature local to the fibres during recycling. However, the temperature in the bulk of the material may in fact be higher than that found in Figure 3-37. Further work could be done to investigate this by integrating the thermocouple within the bulk of the GF-EP prior to curing the epoxy.

3.3.4 Glass fibres thermally conditioned in contact with metal oxides

Another possible explanation for the lack in strength retention could be related to the glass fibres being in physical contact with the metal oxides during recycling. Figure 3-39 shows the extent of CuO nanopowder present on the surface of fibres recycled using integrated CuO. To ensure the residue on the fibre surface in Figure 3-39 was CuO, opposed to char, the fibre was thermally conditioned at 550 °C for 120 min. Such treatment has been demonstrated to fully thermally clean uncatalysed fibres from char residue, therefore the observed residue in Figure 3-39 must be attributed to CuO nanopowder.

A reaction between glass and the metal oxides, which could lead to chemical changes to the surface or bulk glass fibre, could not be found in the literature. Sizing decomposition may have been promoted by the metal oxides, which could lead to a reduction in fibre strength. This section investigates the effect of metal oxides on sizing decomposition using TGA and the strength of fibres after heating in direct contact with the metal oxides.

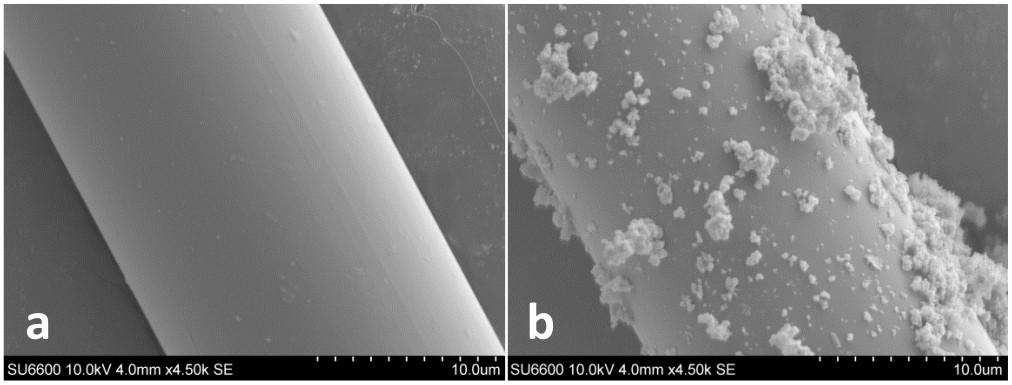

Figure 3-39 SEM of glass fibres recycled in the furnace; (a) without CuO (b) with integrated CuO, confirming that CuO is present on the surface of RGF

3.3.4.1 Effect of metal oxides on glass fibre sizing decomposition

Figure 3-40 presents the results obtained from TGA with glass fibre with and without the presence of the metal oxides. Figure 3-13 showed however that the metal oxides alone also lose mass when heated to 500 °C. Accounting for this, Table 3-7 gives the relative mass loss of the glass fibre at 500 °C. The observed glass fibre mass loss in Table 3-7 are within the range (0.2-2%) of commercial sizing content on glass fibres [128, 129], suggesting the sizing is indeed thermally decomposing.

Table 3-7 Relative mass loss of glass fibres when thermally conditioned using TGA

Specimen	GF only	GF+CuO	GF+Co_3O_4	GF+CeO_2
Glass fibre mass loss (%)	0.43	1.27	0.93	1.51

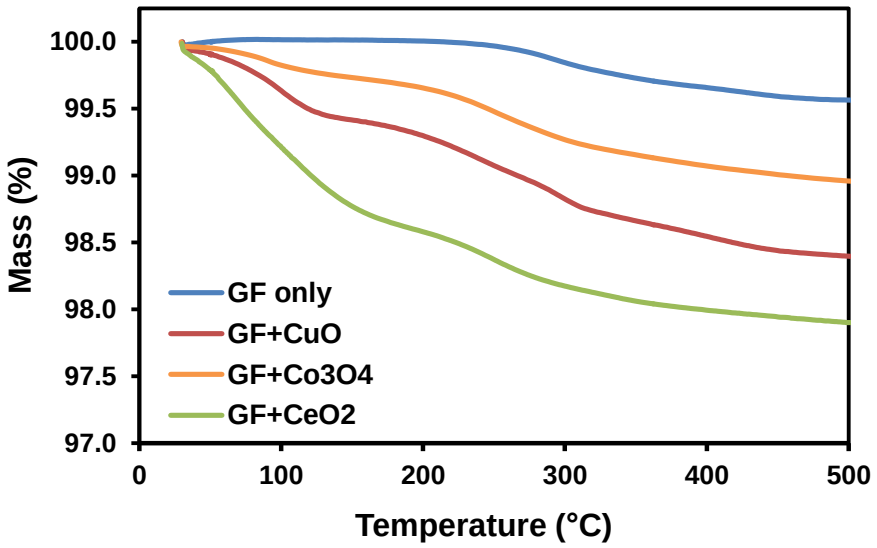

Figure 3-40 Mass loss of glass fibres assisted by metal oxides as a function of temperature

Given that the same glass fibres are thermally conditioned throughout Figure 3-40, it may be expected that the relative glass fibre mass loss in Table 3-7 would be the same for each specimen. Other authors however have observed that a temperature range of 550-650°C is required to fully thermally decompose silane coupling agents/film formers in an air atmosphere [32, 59]. The exact sizing composition is proprietary and cannot be made readily available however; it appears plausible that further heating of the glass fibre alone would result in additional mass loss in line with the catalysed specimens. Disparity in glass fibre mass loss between the tested metal oxides used may be a result of differences in catalytic activity. It is interesting to see that CeO_2 proves to be most effective in promoting decomposition of the sizing and implies that catalytic efficiency of these selected metal oxides is also dependent on targeted material/polymer. It is clear from Figure 3-40 that all the metals oxides do indeed increase the rate of the sizing decomposition.

3.3.4.2 Strength of glass fibres thermally conditioned in contact with metal oxides

Figure 3-41 shows a comparison of the strength of glass fibres after heating in direct physical contact with each of the oxide catalysts. No reduction in the strength of fibres applied with CuO was observed when they did not undergo any heating regimes. This simply rules out the possibility of the mechanical effect of application

of the oxides on fibre strength. At elevated temperatures, however, lower strength is exhibited by fibres heated in the presence of all the metal oxides. It is interesting to point out that the rate of strength loss presented in Figure 3-41, seems to correlate with the results in Figure 3-40. The more efficiently an oxide catalyst is able to promote sizing decomposition, the more strength loss is caused by that oxide. As the temperature of the conditioning continues to increase, fibre strength presented in Figure 3-41 tends to converge regardless of the type of the oxides and their presence. This observation shares the similarity with that in [32], where it showed the effect of sizing decomposition on the difference in strength loss of heat-treated glass fibres diminished as higher temperatures (e.g. 500-600 °C) are reached. This supports the observation from Figure 3-41; however, the additional strength loss caused by the oxides does not seem sufficient to account for the total strength loss shown in Figure 3-35 and Figure 3-36.

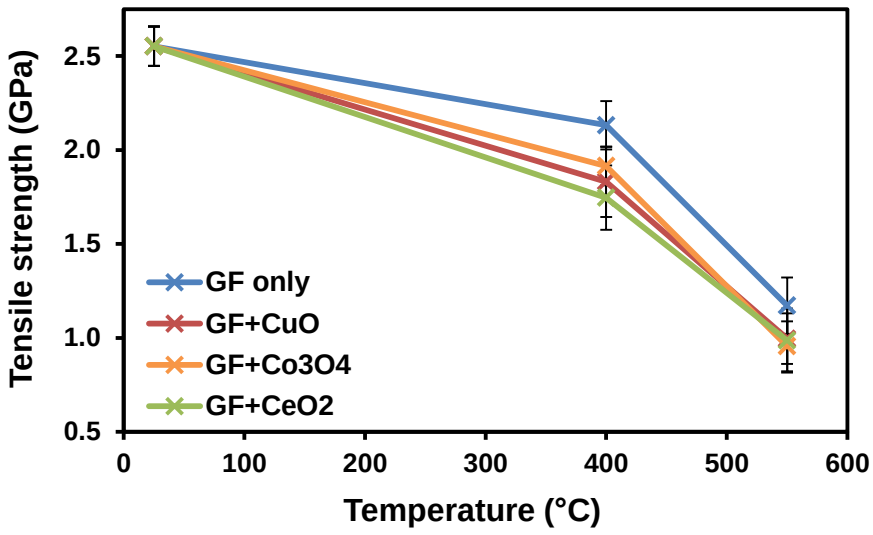

Figure 3-41 Tensile strength of glass fibres after direct thermal conditioning with metal oxides at different temperatures for 25 min. In all cases, fibre strength is lower when thermally conditioned in the presence of the metal oxides.

3.3.5 Catalysed fluidised bed

In this section an investigation into the use of CuO as a catalyst for GF-EP recycling within the fluidised bed was carried out. CuO integrated within the GF-EP matrix was used throughout the study; Figure 3-42 shows a comparison between the GF-EP with and without CuO. Introducing the catalyst into the process as the/a

constituent of the fluidised bed particles would be more practical and better simulate an industrial scale catalysed fluidised bed. This arrangement would closer align with the metal oxide bed arrangement used throughout the thermal analysis. It is understood however that nanoparticles are intrinsically difficult to fluidise therefore the CuO could not simply be integrated within the fluidised bed rig in this form. Future work should be carried out into integrating the catalyst within the bed particulate itself, which would negate the need for it to be introduced into the material during production.

As outlined in Chapter, the recyclate was initially fed into the fluidised bed for 45 min, after which the system was ran for a further 15 minutes without inputting any more recyclate.

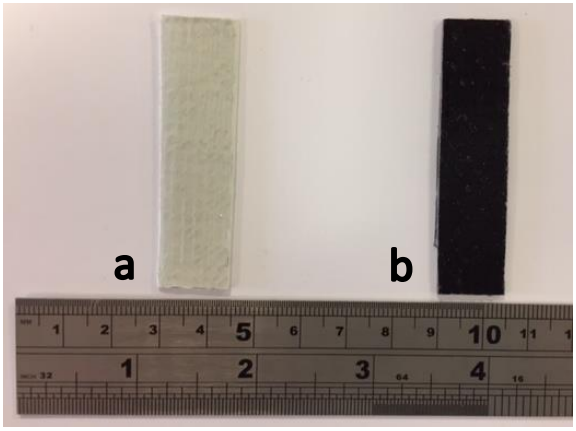

Figure 3-42 Comparison of composite recyclate (a) GF-EP (b) GF-EP+CuO

3.3.5.1 Yield efficiency of recycled glass fibres

Figure 3-43 gives the obtained fibre yields when recycling GF-EP in the fluidised bed at 400, 450 and 500 °C and compares the results with and without integrated CuO. It is clear that the application of CuO significantly improves the yield efficiency of RGF, particularly at lower temperatures. When recycling at 400 °C the yield increases from 6% to 40% when using CuO. As would be expected, the yields appear as though they will converge at higher temperatures since the epoxy rapidly thermally decomposes without the need for an oxidising catalyst. This could be confirmed by recycling at higher temperatures, however, this work is centred on reducing the temperature required for recycling.

Almost no residual glass fibres were found in the sand bed after recycling at 500 °C with CuO, suggesting that the cyclone separator has an upper limit of around 70% yield efficiency. The cyclone separator efficiency is presumed to be independent of CuO presence in recyclate material therefore; discrepancy between yields (for a given temperature) is the result of improved rates of fibres exiting the bed. It appears CuO can aid epoxy decomposition within the fluidised bed, increasing fibre liberation, in turn improving yield efficiency at lower operating conditions.

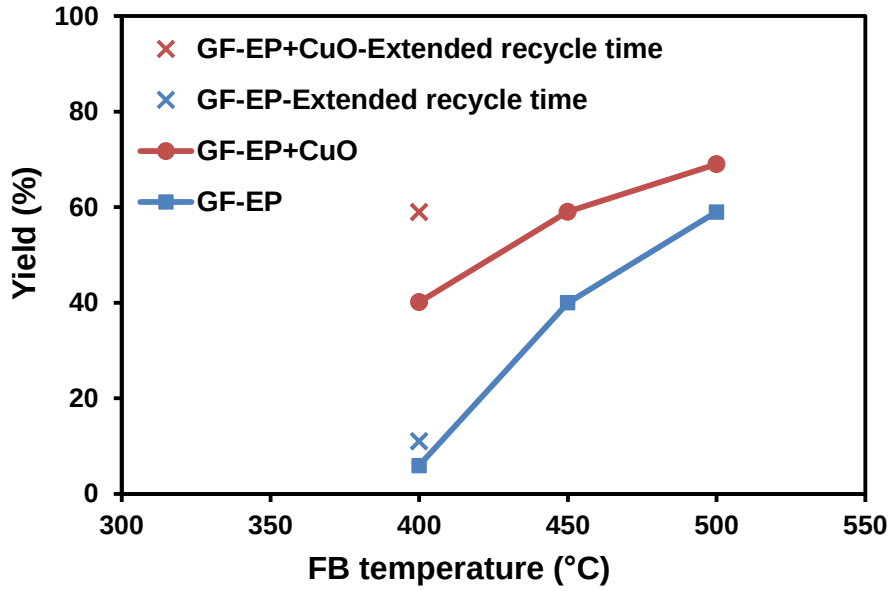

Figure 3-43 Yield efficiency of glass fibres recycled from GF-EP in the fluidised bed at various temperatures. At all fluidised bed temperatures the fibre yield efficiency is improved with the use of CuO catalyst.

Figure 3-44 shows an image of glass fibres which remained in the sand bed after recycling at 400 °C. The fibres on the left are from GF-EP only composites, whereas the right had CuO integrated within the epoxy matrix. It is clear there is substantially more residual char present on the fibres processed without CuO present; they are too heavy to leave the bed, and hence why they cannot be recovered at such a low temperature. In contrast, the fibres processed with CuO are significantly cleaner. These fibres are clearly liberated from the epoxy matrix and should be able to leave the bed given enough time.

Recycling GF-EP with and without integrated CuO at 400 °C was therefore repeated. In this case, the additional run time (above the first 60 min of material

input) was increased from 15 to 45 min while the total material input remained constant. As shown in Figure 3-43, the resulting yield efficiency was found to be approximately 60%, the same as recycling at 500 °C without the addition of CuO. On the other hand, there was a comparatively small increase in yield efficiency to 11% by extended operating time without the use of CuO.

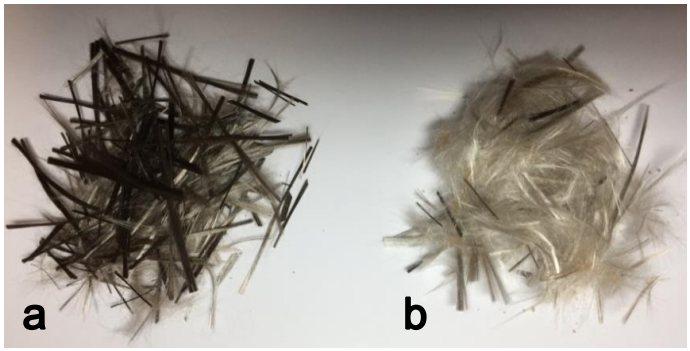

Figure 3-44 Char residue remaining on glass fibres remaining in fluidised bed reactor after recycling at 400 °C (a) without CuO (b) with integrated CuO. Visually, CuO provides significantly cleaner RGF.

3.3.5.2 Strength of recycled glass fibres

Figure 3-45 shows the tensile strength of fibres recycled in the fluidised bed at 400, 450 and 500 °C, with and without integrated CuO. The recycling temperature does not appear to influence the tensile strength of the RGF as was suggested in Chapter 2. Reducing the temperature required for the epoxy decomposition therefore does not appear to have the added benefit of increasing the strength retention of glass fibres recycled using the in-house fluidised bed rig. As discussed in Chapter 2, Kennerley et al. did in fact observe a relation between fluidised bed temperature and recovered fibre strength [14]. Figure 3-45 may not truly represent the possible strength retention when using the catalyst in other fluidised bed recycling processes, which, for example, use less aggressive separation systems than the cyclone separator.

On the contrary, it was observed that using integrated CuO when thermally recycling GF-EP (Figure 3-36) in the furnace led to significant additional fibre weakening. For all the temperatures investigated, the strength of fibres recycled with CuO are only slightly lower than those recycled without, as shown in Figure 3-45. This difference is not significant given the size of the error bars. CuO may indeed cause additional

damage to the glass fibres however; damage sustained while processing through the fluidised bed rig could overwhelm any observable difference. This explanation is in line with that given for the lack in trend between bed temperature and RGF strength. Alternatively, fibres weakened by recycling with CuO would be more likely to suffer length degradation during processing in the rig and would be too short to make into single fibre tensile test samples. This could result in a bias toward selecting fibres for testing which were not substantially weakened by CuO given the lack in length degradation of those fibres. This could artificially increase the average tensile strength of the fibres recycled with CuO.

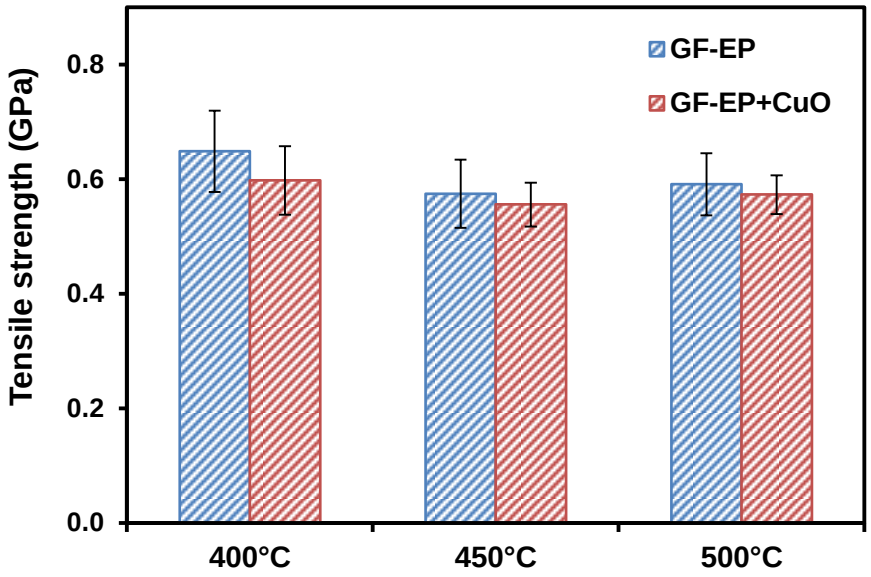

Figure 3-45 Effect of thermal recycling temperature on glass fibre tensile strength. No significant difference in strength of RGF was observed with the use of CuO catalyst.

3.3.5.3 Reusability of CuO as an oxidation catalyst

Figure 3-46 compares the effect of re-using CuO, up to three times, on its ability to aid thermal decomposition of epoxy using TGA at 5 °C/min. Multiple uses results in little deviation from the decomposition thermogram obtained from epoxy containing fresh CuO.

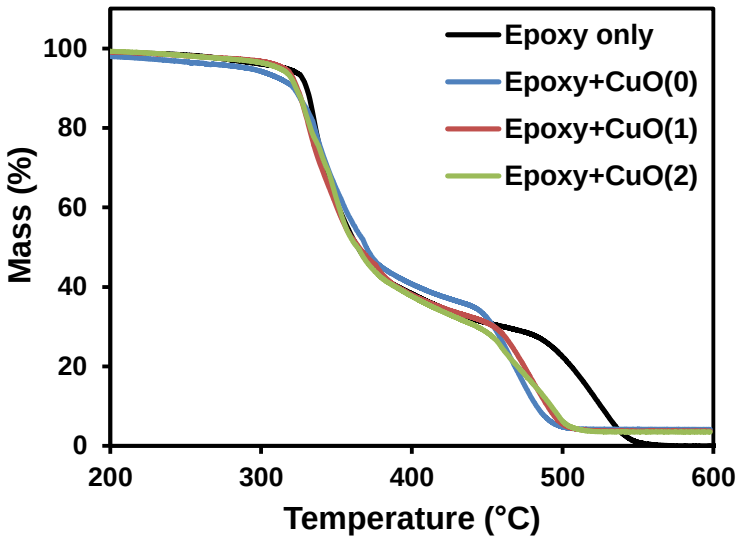

Figure 3-46 Epoxy thermal decomposition thermograms demonstrating the reusability of CuO as an aid for epoxy decomposition

The samples were also decomposed at 1, 2, 7 and 10 °C/min to determine the Ea of thermal decomposition. For brevity, the Kissinger method was used, which allows the Ea to be found at peak derivatives of conversion. Given the epoxy decomposition is a two stage process, with two maximum rates of conversion, an Ea for each is found. The Kissinger equation (Equation 3-23) below can be derived from the Arrhenius equation under conditions of the maximum rate [91]:

Equation 3-23 Kissinger equation

$$ln\left(\frac{\beta}{T^2{}_{m,i}}\right) = ln\left(-\frac{AR}{Ea}f'(\alpha_m)\right) - \frac{Ea}{RT_{m,i}}$$

where β is the heating rate, α is conversion, i denotes various temperature programs and m denotes the values related to the maximum rate. In the Kissinger method, at maximum rates, $ln(\beta/T^2{}_{m,i})$ is plotted against $1/T_m$ giving rise to a straight line whose slope yields Ea. Figure 3-47 gives the plots and straight-line

equations used to calculate the Ea of both stages of decomposition using the Kissinger method.

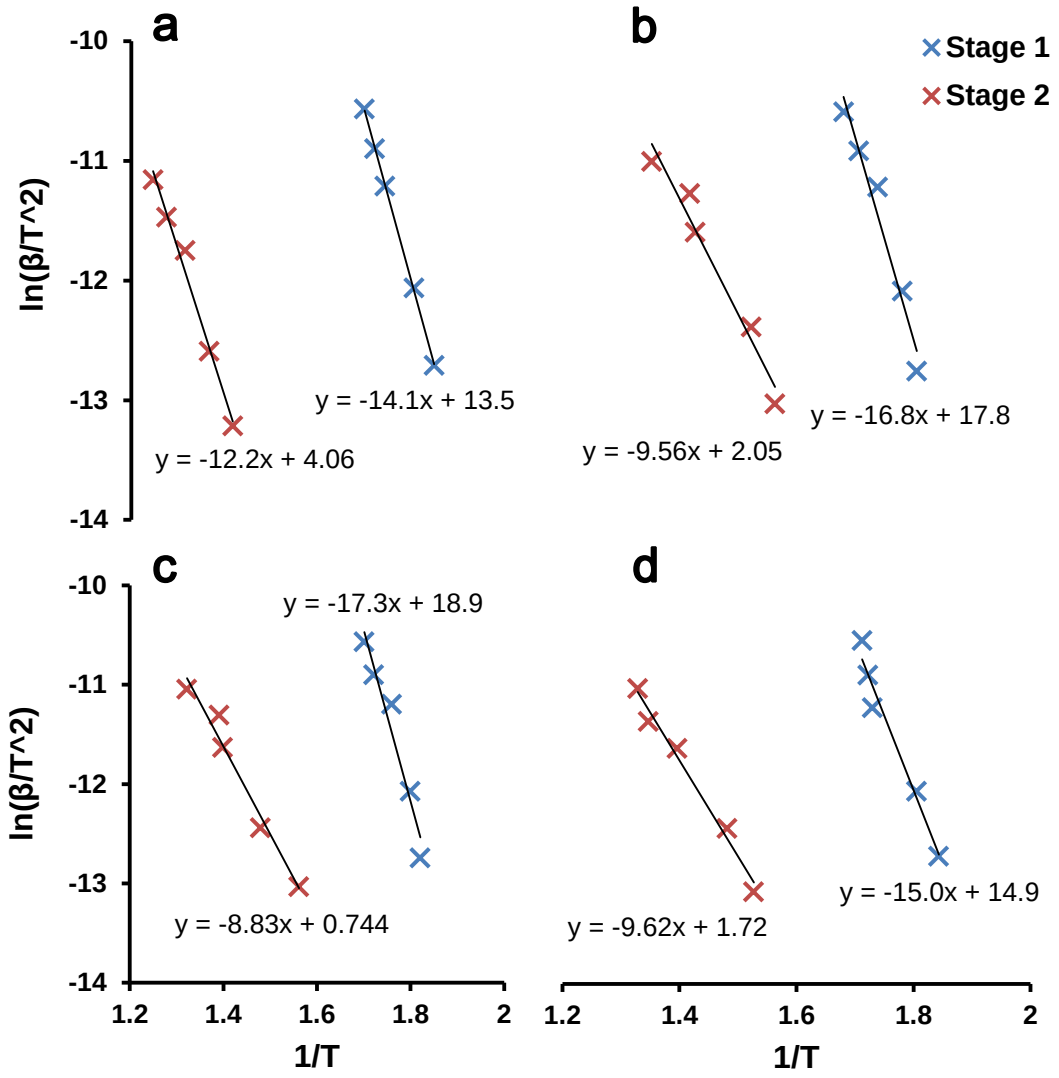

Figure 3-47 Plots used to calculate CuO thermal decomposition activation energy using the method of Kissinger (a) Epoxy only, (b) Epoxy+CuO(0), (c) Epoxy+CuO(1), (d) Epoxy+CuO(2)

Table 3-3 gives the Ea for each sample found using the Kissinger method. In agreement with Figure 3-46, there is a relatively consistent reduction in second stage Ea, indicating that the performance of CuO is not diminished when utilised repeatedly. Since the CuO was introduced into the matrix as a nanopowder, it could not easily be recovered after using to aid GF-EP recycling in the fluidised bed rig. For scaling up, it is proposed that the catalyst could be integrated within the recycling system as a permanent constituent of the fluidised bed particles. Under

these conditions, the CuO would be under a redox cycle, where it is reduced by epoxy molecules then re-oxidised by the high temperature fluidising air stream, following the mechanism outline in Equation 3-13. Pickering et al. modelled the economics of a commercial fluidised bed plant to thermally recycle GRP waste, operating at a nominal bed temperature of 550 °C [13]. It was concluded that with a throughput greater than 9000 ton of scrap GRT per annum, such a plant could be commercially viable. Given the dramatic reduction in temperature required to recycling GF-EP using the metal oxide catalyst, even if relatively high quantities of oxides are initially required, the cost benefit of long-term reduction in operating conditions could be realised.

Table 3-8 Activation energy of epoxy thermal decomposition when CuO is re-used up to three times

	Activation energy (kJ/mol)		Correlation coefficient	
	Stage 1	**Stage 2**	**Stage 1**	**Stage 2**
Epoxy only	118	101	-0.999	-0.993
Epoxy+CuO(0)	140	79.5	-0.983	-0.988
Epoxy+CuO(1)	144	73.4	-0.969	-0.985
Epoxy+CuO(2)	125	80.0	-0.992	-0.989

3.4 Conclusions

In this chapter the effect of three metal oxides on GF-EP thermal recycling were investigated. Initially DSC was used to investigate the cure of epoxy with and without the application of each of the metal oxides. All metal oxides had negligible effect on the Tg and normalised ΔH of the epoxy cure and was concluded that the addition of metal oxide should not be harmful to the epoxy thermal properties at typical operational temperatures. TGA was used to study the thermal decomposition of epoxy in the presence of the metal oxides. It was found that CuO is superior at reducing epoxy thermal stability, enabling full decomposition at just 375 °C under isothermal heating in air.

An investigation into thermal weakening of glass fibre indicated that reducing the thermal recycling temperature/time could significantly increase the strength retention of RGF. The applicability of the metal oxides on GF-EP thermal recycling within a furnace was established in terms of recycling temperature, energy consumption and recycled fibre strength. CuO, CeO_2, and Co_3O_4 successfully reduced the epoxy matrix decompostion temperture required for glass fibre liberation by 120, 50 and 50 °C respectively. This was followed at least a 40% reduction in energy consumption when recylcing with the metal oxides. It was found that all metal oxides could increase strength retention of furnace RGF by around 20%, depending on sample arrangement and recycling conditions. This was significantly lower than anticipated and additional causes for the strength loss were investigated.

It was found that the thermal loading on fibres within GF-EP during recycling increased conciderably above the target recycling temperature due to exothermic epoxy decompostion. It was demonstrated that similarly brief high temperature treatments could significantly weaken fibres and is likely a contributor to the lack in recycled fibre strength. Direct application of metal oxides on glass fibres during thermal conditioning caused greater weakening than was observed through thermal effects alone and it was confirmed that the metal oxides under investigation accelerate sizing decomposition during heating. Consequently, sizing removal faciliated by the metal oxides may also contribute to diminished fibre strength retention.

GF-EP with integrated CuO was thermally recycled in the fluidised bed rig. Glass fibres could be recycled at 400 °C with 60% yield, which was comparable to uncatalysed at 500 °C. The strength of RGF was around 0.6 GPa regardless of the recycling conditions. Despite this, it is postulated that such a decrease in bed temperature would reduce the energy required to recycle GF-EP. Finally, it was demonstrated that multiple uses of CuO did not reduce its ability to facilitate thermal decomposition of epoxy.

Although the focus of this thesis is directed at thermal recycling of GRT, both glass and carbon fibres are typically used with analogous thermosetting matrix materials and similar thermal recycling processes have been proposed for both. Appendix C studies the feasibility of using metal oxides during the recycling of carbon fibre reinforced thermoset composites, and determines if the same benefits seen for GRT can be translated to recycling carbon fibre based composites.

4. Regenerating recycled glass fibres

In this chapter thermally recycled glass fibres are subject to various chemical and water treatments in order to improve their strength and interface properties with PP and epoxy. The effect of sodium hydroxide (NaOH), hot water, water vapour and hot APS treatments on fluidised bed recycled glass fibres is investigated as a means for regenerating RGF strength. A variety of treatment times are investigated as well as a range of NaOH concentrations. The effect on fibre strength and diameter reduction is measured. The surface morphology of glass fibres after selected treatments is assessed using SEM. Fluidised bed recycled glass fibres are also treated in hydrochloric acid (HCl) in an attempt to improve fibre surface functionality, by increasing surface silanol density. RGF are also treated in APS to improve the interface adhesion with polymer matrices. The effect of HCl and APS treatments on glass fibre tensile strength and IFSS with PP and epoxy are measured. Table 4-1 gives a summary of the regeneration treatments investigated in this chapter.

Table 4-1 Summary of the regeneration treatments, property targeted and technique used for characterisation

Regeneration treatment	Property regeneration	Testing technique
NaOH Hot water Water vapour Hot APS	Tensile strength	Single fibre tensile test
RT APS HCl	IFSS	Microbond test

4.1 Literature review

In this section the concept of the fibre-matrix interface is introduced, along with technologies used to improve adhesion between glass fibres and polymers. An overview of the research into the use of chemical treatments to 1) regenerate the strength and 2) regenerate surface functionality of glass fibres exposed to typical recycling temperatures is presented and critiqued.

4.1.1 Regeneration of glass fibre strength

Given the detrimental effects of thermal recycling on the reinforcement potential of glass fibres, it was concluded that the fibre strength should be regenerated. Methods for increasing the strength of glass fibres are typically focused on the surface flaws, since it is widely believed that these are a strength-limiting factor.

4.1.1.1 Applying sizing to increase glass fibre strength

Zink et al. investigated the influence of a variety of applied sizings on the tensile strength of new glass fibres [130, 131]. It was found that a combination of both a coupling agent (APS) and film formers provided the largest increase in fibre strength [131]. It was concluded that the sizings could diminishing separation as well as severity of surface flaws. It was estimated that flaw length reduced from 200-400 nm to 75 nm with the application of APS/PP film former sizing [131]. Typically called “flaw healing” theory, it is suggested that the mechanism for improved strength involves the creation of polysiloxane network, which can fill the flaws on the fibre surface [130]. Sáez-Rodríguez et al. [132] and Thomason et al. [35] attempted to use APS and MethacryloxyPropyltrimethoxySilane (MPS) coatings to regenerate the strength of thermally conditioned glass fibres. The silane treatments were used in conjunction with diluted HCl treatments in order to improve APS and MPS adhesion to the glass fibre. Although an increase in strength was observed in each study, the change was minor and considered insignificant by Sáez-Rodríguez et al. when allowing for error bars [132]. Yang et al. observed a small, but statistically significant increase in the strength of thermally conditioned glass fibre after treating in APS [5]. Similarly, Thomason et al. reported APS treatment increasing thermally conditioned glass fibre strength [15]. It was observed that the level of regeneration was inversely

related to the conditioning temperature. The cause for the disagreement between [5, 15, 35, 130-132] is currently unexplained. However, when observed, the strength regeneration was consistently very low and insufficient to add significant value to the weakened fibres. The above APS treatments were all carried out at RT; however, Sáez-Rodríguez et al. recently filed a patent claiming that hydrolysing the APS and performing the treatment at 83 °C (in conjunction with other chemical treatments) can successfully regenerate thermally conditioned glass fibre [133]. It is suggested that crosslinking increases when APS is hydrolysed at elevated temperatures, which can heal the surface flaws more effectively [134].

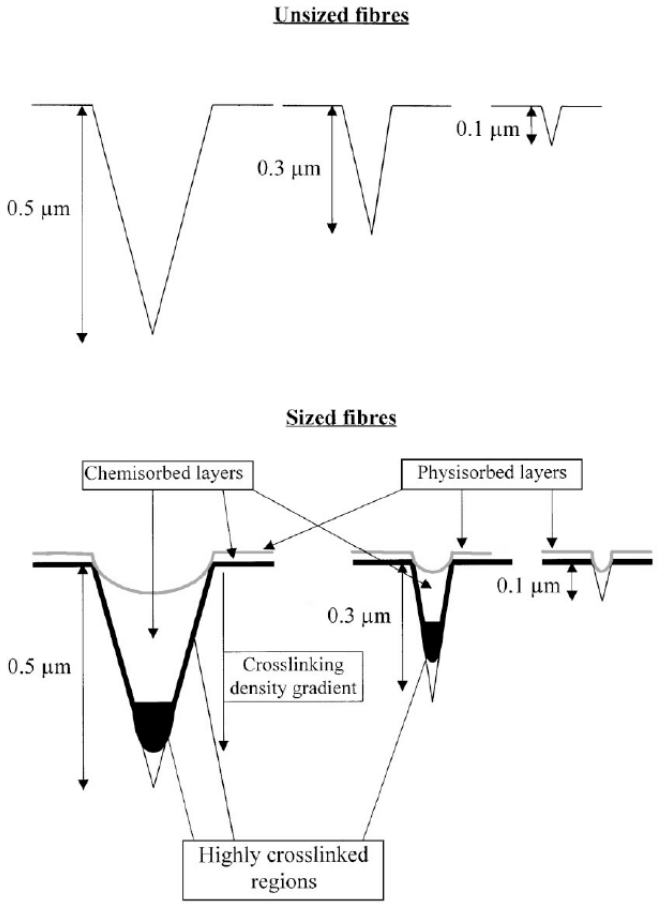

Figure 4-1 Schematic representation of flaws and the effect of a surface treatment, reproduced from [130]

4.1.1.2 Acid and basic treatments to increase glass fibre strength

Serval authors have shown that acid or basic treatments can etch the surface of thermally conditioned glass fibres and regenerate the fibre strength [5, 15, 34, 49,

135]. It is suggested that etching the outer surface of the glass fibre can remove or smooth serve flaws induced during thermal conditioning.

Aslanova [135] and Sakka [136] demonstrated that treating thermally conditioned glass fibres in hydrofluoric acid (HF) can significantly improve their tensile strength. Sakka was able to completely regenerate the fibre strength after thermally conditioning at temperatures up to 660 °C [136]. The HF treatment was less effective above 660 °C. It was observed that treating glass fibres that were conditioned above 660 °C caused the fibre surface to become irregular. It was proposed that such high temperatures created an inhomogeneous structure on the glass fibre surface, leading to irregular etching. More recently, Yang et al. showed that HF could increase the strength of glass fibres thermally conditioned at 500 °C from around 0.6 GPa to 1.7 GPa [5]. It is unclear why Yang et al. could not fully regenerate the fibre strength like in [136]. In each case a similar treatment time was used, however, HF concentration use by Sakka was 10 vol% compared to just 1 vol% used in [5]. Treating the fibres in a higher concentrated HF solution may provide further improvements to the fibre tensile strength in [5].

Both Aslanova [135] and Yang et al. [5] reported a reduction in fibre diameter during treatment in HF which was indeed correlated to an increase in glass fibre strength, as can be seen in Figure 4-2.

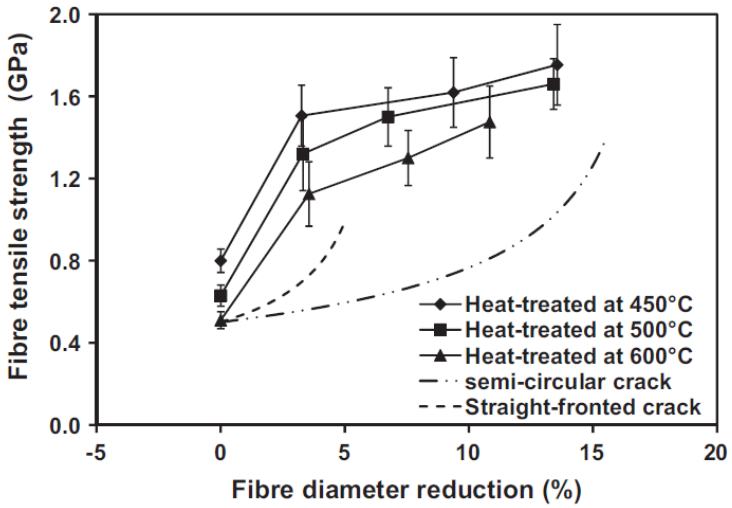

Figure 4-2 Strength increase of thermally conditioned (heat-treated) glass fibres as a function of fibre diameter reduction, showing that HF increases the strength of glass fibres through an etching mechanism, reproduced from [5]

It is widely understood that Equation 4-1 presents the chemical reaction between HF and silica. Given that the tensile strength of glass fibres is dictated by the size and geometry of the surface flaws [48], it is concluded that etching with HF modifies or reduces these strength-determining defects, in turn increasing the fibre strength [5, 135].

Equation 4-1 Chemical reaction between SiO_2 and HF [137]

$$SiO_2 + 4\mathrm{HF} \rightarrow SiF_4 + 2H_2O$$

Despite its effectiveness at regenerating the strength of glass fibres, HF is highly toxic and using it in an industrial environment would likely be problematic [5].

Other authors have used alkaline solutions to regenerate the strength of thermally conditioned glass fibres. Bashir et al. reported an increase in fibre strength from around 0.7 GPa to 1.2 GPa after treating with 1.5 mol/L NaOH at 95 °C for 10 min [34]. A similar increase was achieved using potassium hydroxide; however, a higher concentrated solution was required. Lithium hydroxide was shown to be ineffective at the concentrations and treatment time tested. Fibre strength data from [34] can be seen in Figure 4-3. Unlike HF treated fibres [5], there was no discernible reduction in diameter associated with an increase in the fibre strength after NaOH treatment. However, it is well established that NaOH dissolves glass [138]. Bashir et al. used optical microscopy to measure the fibre diameter, which may not have been accurate enough to detect a slight change in the fibre diameter. Bashir et al. conditioned the fibres at 450 °C to replicate the temperature of a typical thermal recycling process [34]. Less thermally stable thermosets like polyester may be able to be decomposed at this temperature; however, it may underestimate the temperature required for other materials such as epoxy [7].

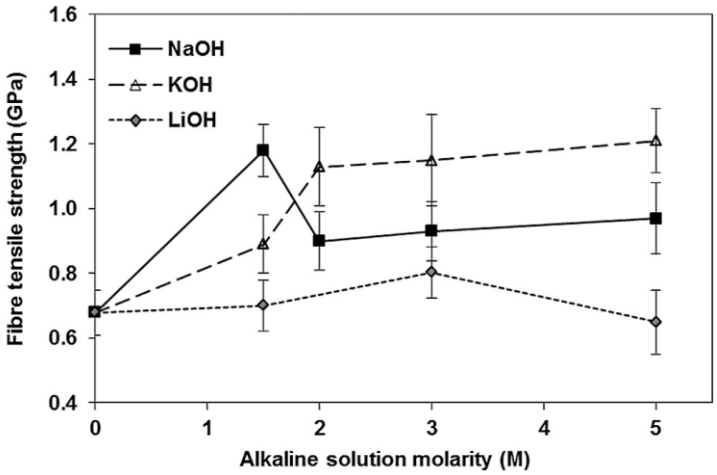

Figure 4-3 Average strength of fibres thermally conditioned at 450 °C and treated in various concentrations of alkaline solutions for 10 min, reproduced from [34]

Thomason et al. also used NaOH to re-strengthen glass fibres thermally conditioned at 450, 500 and 600 °C [34]. Figure 4-4 shows the effect of treating the thermally conditioned glass fibres in 3 mol/L NaOH solution at 90 °C for 10 min. Thomason et al. observed similar levels of strength regeneration to 1.4 - 1.5 GPa, irrespective of thermal conditioning temperature. In contrast with several other authors [30, 31, 40, 46], there is no significant difference in strength loss of glass fibres conditioned between 450 °C and 600 °C [34]. The cause for this is not clear; however, similar levels of regeneration could be expected between the conditioning temperatures, given that the initial degree of thermal weakening sustained is comparable. There is however a significant disparity between the achieved strength regeneration of fibres conditioned at 450 °C in [15] (Figure 4-4) and those in [34] (Figure 4-3). Despite using the same solution concentration and treatment time, the strength of fibres treated with NaOH are 40% stronger in [15]. There is only a small difference in the initial strength of the weakened fibres prior to treating in NaOH. The only reported variation between treatments is a 5 °C difference in NaOH temperature. It is unclear how sensitive the treatment is to variation in temperature and if this is the cause for the disparity.

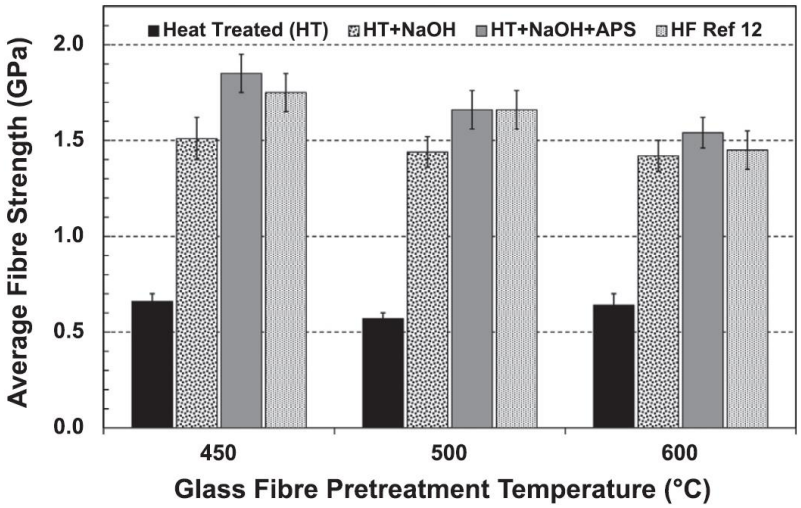

Figure 4-4 Influence of thermal conditioning temperature and chemical treatments on the average glass fibre strength, reproduced from [15]. Both NaOH and HF can substantially increase the strength of thermally conditioned glass fibres, however, the degree of regeneration is dependent on conditioning temperature.

The glass fibre corrosion in alkaline media is dominated by dissolving the silica network (SiO_2) [138, 139]. The hydroxide ions in the solution cleave the siloxane bonds in the glass fibre as shown in Equation 4-2. Aluminium oxide (Al_2O_3), which accounts for 12-14% of the weight of E-glass fibre [140], can also react with hydroxyl ions similar to SiO_2 as shown in chemical Equation 4-3.

Equation 4-2 Mechanism of hydroxide ion attacking SiO_2 network [141]

$$[-Si-O-Si-]+OH^- \xrightarrow{\Delta} [-SiO]^- + [-Si-OH]$$

Equation 4-3 Mechanism of hydroxide ion attacking Al_2O_3, reproduced from [141]

$$[-Al-O-Al-]+OH^- \xrightarrow{\Delta} [-AlO]^- + [-Al-OH]$$

Calcium oxide (CaO) and magnesium oxide (MgO), which account for around 22% and 3% of E-glass fibre weight, are basic and will therefore not react directly with NaOH [141]. They are soluble in alkaline solution however which could result in further disruption of the glass network [141]. The key chemical reactions between NaOH and the glass fibres are therefore as follows [142]:

Equation 4-4 Chemical reaction between SiO_2 and NaOH [142]

$$SiO_2 + 2\mathrm{NaOH} \rightarrow Na_2SiO_3 + H_2O$$

Equation 4-5 Chemical reaction between Al_2O_3 and NaOH [142]

$$Al_2O_3 + 2\mathrm{NaOH} + 3H_2O \rightarrow 2NaAl(OH)_4$$

Bashir et al. studied the kinetics of dissolution of glass fibre in hot alkali solution, and found significant etching of the glass fibre surface, concluding that the diameter reduction increases linearly with time, and the rate increases as a function of concentration [141], as shown in Figure 4-5. Similarly to the observations made when treating in HF, it is concluded that fibre surface modification through etching is the underlying mechanism for the observed increase in the strength of thermally conditioned fibres after treating in hot alkali solutions [15, 34].

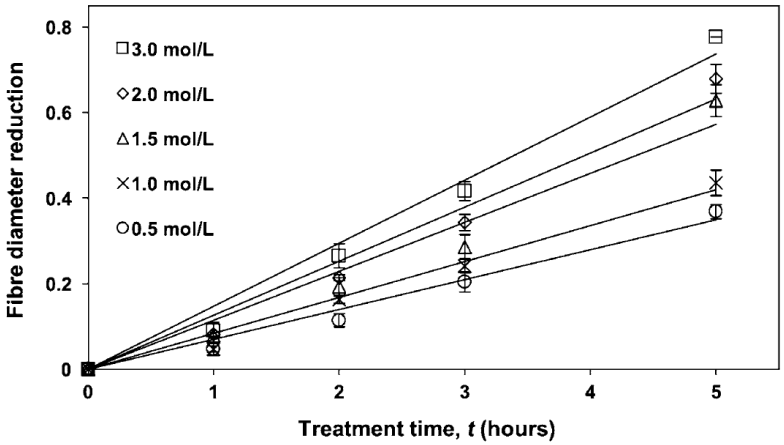

Figure 4-5 Glass fibre diameter reduction as a result of treating in NaOH solution at various concentrations and durations, showing the etching effect NaOH has on the glass fibre surface, reproduced from [141]

4.1.1.3 Water treatments to increase glass fibre strength

Several authors have demonstrated an increase in the strength of abraded glass after exposure to water under various conditions [50-52]. Mould observed the strength of abraded laboratory microscope slides increased after storing in water or water vapour at various relative humidities [50]. Soaking in distilled water for one day provided a 50% increase in strength; the largest observed under the conditions tested. Exposure to water vapour proved less effective and was highly dependent on humidity. No further improvements in strength were observed after treating for more than one day. The water and water vapour temperatures used for storing the glass slides were not given in [50]. Ito and Tomozawa abraded 3 mm high-silica glass

rods then stored in RT water and 88 °C water for up to 500 hour [51]. A near linear strength-treatment time relation was observed when soaking in the 88 °C water for up to 360 hour. After 360 hour, a 30% increase in strength was observed compared to abraded only specimens. The rate of strength increase for storage times greater than 360 hour was diminished and, given the large error bars, insignificant. Immersion in RT water yielded no increase in strength of the glass rods. Li and Tomozawa continued this work by storing abraded glass rods in saturated water vapour at 250 °C for up to 4 days [52]. A 200% increase in strength was observed after storing for 4 days. It is unclear whether further improvements could be attained with longer exposure; however, the rate of strength increase appears to be plateauing after 4 days.

The mechanism for the strength increase is as yet unclear; however, several have been proposed and dismissed. Mould suggested that the strength increase is unlikely to involve the reduction in crack depth [50]. Using fracture mechanics it was determined that the crack length must be reduced by half to account for the observed strength increase in [50]. It was also suggested by Mould that there is a lack of evidence showing that cracks can be “healed” with water. Mould states it is more likely that water would contaminate the surface preventing the re-formation of “glassy bonds” across crack rather than re-joining crack surface. Glassy bonds are not defined in [50], however are likely a reference to siloxane bonds given that high silica glass is under investigation. Mould does not propose a mechanism that would prevent re-formation of such bonds in the presence of water [50]. It is further suggested by Mould that any healing of cracks by closing would have to involve a bonding across the crack by a water-containing material, possibly a form of silica gel, which would be weaker than the original glass.

This was further confirmed by Li and Tomozawa who, using optical microscopy, observed no change in the crack length on the fracture surface of glass rods after storing in water vapour [52]. All authors concluded that a reduction in crack radius or “crack blunting” causes the improved strength of abraded glass [50-52]. It is hypothesised that the mechanism for this involves either 1) dissolution of the glass in the region of crack tips or 2) dissolution and subsequent re-precipitation of silica around the crack tip. Figure 4-6 illustrates the geometry of the crack tip following each of these processes. Ito and Tomozawa measured the rate of dissolution of high-silica glass rods in water [51]. Using fracture mechanics it was found that the mass loss of the rod was insufficient to account for the required increase in crack tip

radius, if uniform dissolution was the only mechanism involved. It was therefore concluded that dissolution and re-precipitation better explained the strength increase of the abraded glass [51].

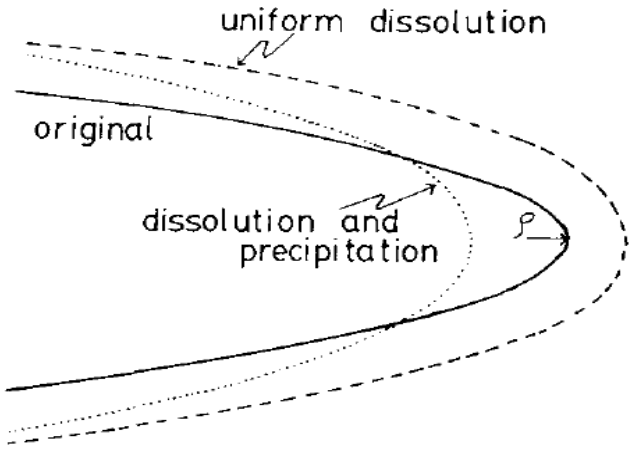

Figure 4-6 Schematic of crack tip, comparing the geometry of uniform dissolution and dissolution with re-precipitation, reproduced from [51]

Rather than crack blunting, Wiederhorn et al. [143], Fett et al. [144] and Wiederhorn et al. [145] suggest that the strengthening mechanism involves diffusion of water into the crack surface, which generates swelling around the crack tip. Compressive stresses are generated around the tip since the material is constrained from expanding by the surrounding glass. It is proposed that this causes a fracture mechanics shielding of cracks present in the glass surface and increases the toughness. Based on this mechanism, Fett et al. developed a model to estimate the strengthening of hot soaked glass rods [144]. Using Ito and Tomozawa [51] data as a comparison, the strength predicted by Fett et al. fell well within the error bars of the actual measurement. It is suggested by Wiederhorn et al. however that this mechanism would not apply to the submicron flaws present on the surface of glass fibres [145]. The stress enhancement through swelling depends on the level of stress in the water-penetrated region of the glass. For high-strength glass fibre, the failure stress may be an order of magnitude higher than that of the glass rods [144]. Hence, the level of compressive stress around the crack will have little effect on the strength of fibres [145].

To the best of the author's knowledge, the literature lacks any investigations into water treatments as a means of regenerating the strength of thermally recycled

glass fibres. Cracks present in the glass rods discussed in [52] are several order of magnitude larger than those found in thermally conditioned glass fibres [47]. Moreover, [50-52] used high content silica glass whereas E-glass is typically composed of around just 60% silica, with metal oxides accounting for the remaining constituent [140]. Further research into this area could lead to the development of a relatively inexpensive method for regenerating the strength of thermally recycled glass fibres.

4.1.2 Glass fibre interfacial adhesion

The interfaces present within composites exist due to the inherent heterogeneous nature of such materials, and is defined as the region that links the various phases within a composite. This boundary facilitates the transfer of loads from the matrix phase to the reinforcement phase, and as such, plays a critical role in determining the overall mechanical properties of composites. In the case of fibre-polymer composites, the term adhesion is commonly used to describe the interactions occurring at the interface. It is a simplified term that encompasses a combination of complex mechanisms. Typical examples of such interactions include adsorption, wetting, electrostatic attraction, chemical bonding, polar attraction, physical and mechanical interactions [146, 147]. Interfaces is not the foremost focus of this thesis, therefore the literature is not comprehensively reviewed. In this section, the use of silane coupling agents as a means of improving interfacial adhesion between glass fibre and polymer matrices is explored.

4.1.2.1 Sizing and silane coatings

A key step in the production of glass fibre is the application of a sizing. Glass fibre sizings are typically water-based formulation containing a film former, a coupling agent and additional auxiliary components [148]. This sizing is applied for several reasons including; to reduce fibre damage during processing, protect surface against contact and diffusion of water, give the fibres anti-static properties and to enhance adhesion with composite matrices [149]. Organofunctional silanes are molecules prepared from a silicon compound, which contains both organic and inorganic reactive groups, allowing them to function as a coupling agent [150]. Silane based coupling agents are commonly used as they have the ability to join

glass fibres with a range of different matrices. Silane based coupling agents have a typical chemical structural of R-Si(OR')$_3$ where; R' is a hydrolysable group and R is the functional group which is selected to bonds with a desired matrix. Amino-silanes are the most widely used silane coupling agents [149]; in particular APS, the structure of which can be seen in Figure 4-7.

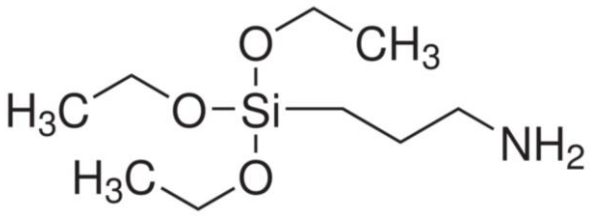

Figure 4-7 3-Aminopropyltriethoxysilane molecule

In order to bond the silane to the glass substrate the silane monomers are mixed in aqueous solution. Hydrolysis of silane then occurs yielding the corresponding silanol. Siloxane is then produced by self-condensation of the silanols [151], as shown in Figure 4-9. After the hydrolysis and self-condensation reactions occur, the final stage is a reaction between the remaining hydroxyl groups of the siloxane and those present on the surface of the substrate. Initially they bond via hydrogen bonding. After drying, water is removed yielding a polysiloxane layer covalently bonded to the surface [151]. This then creates an outer surface of functional groups allowing it to react with the polymer matrix.

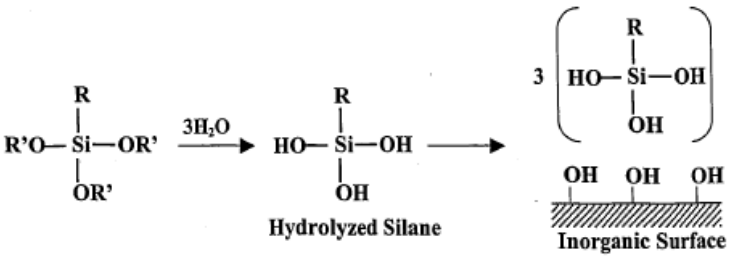

Figure 4-8 Hydrolysis of silane coupling agent, reproduced from [152]

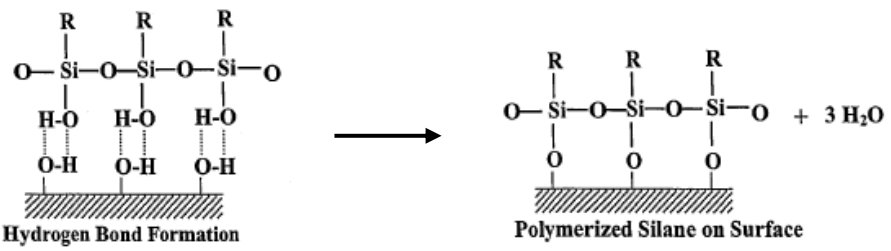

Figure 4-9 Reaction of silane adhesion promoters on substrate, reproduced from [152]

The single polymerised layer on the fibre surface represented in Figure 4-9 is a rather simplistic representation of the structure of the condensed silane. It is now understood that silane coupling agents are present as a multi-layered structure on the glass fibre with 1) chemically bonded polymerised silane, 2) chemisorbed and 3) physisorbed oligomeric silane layers [153, 154], as represented in Figure 4-10.

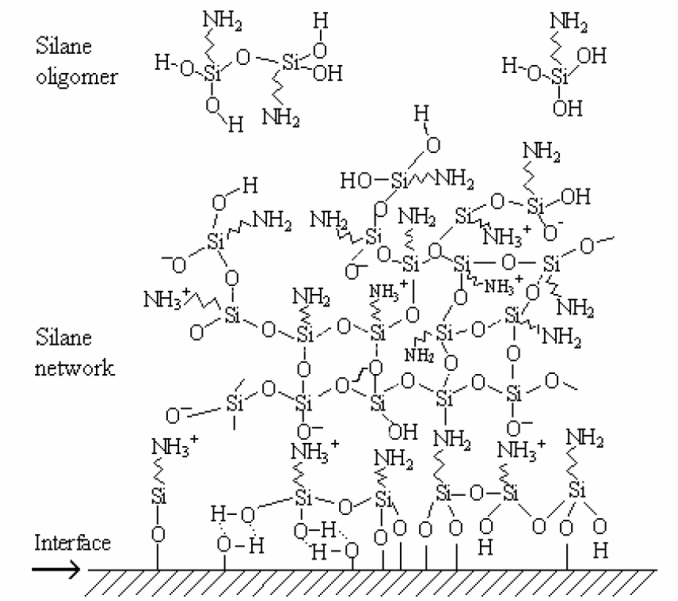

Figure 4-10 Chemical structure of hydrolysed APS on glass fibre surface, reproduced from [154]

4.1.2.2 Glass fibre – polypropylene interface and interfacial adhesion

There is conflicting data in the literature as to the effectiveness of silane coupling agents at increasing IFSS between glass fibre and unmodified PP. Yang et al. [5] and Thomason et al. [15] used the microbond technique to measure the IFSS between unmodified PP and glass fibre. The IFSS of fibres with 1) sizing thermally

removed and 2) fibres with sizing thermally removed followed by coating with APS were compared. In both cases, the APS significantly increased adhesion with unmodified PP. Other authors suggest however, that sizing alone does not necessary improve IFSS with PP.

Microbond tests [155], single fibre pull out tests [156, 157] and fibre fragmentation tests [158] show that IFSS cannot be increased when silane coupling agents are used in combination with unmodified PP. The nonpolar nature of unmodified PP is cited as the cause for the lack of adhesion.

Serval authors observe that the PP must be modified with acidic groups in order to improve the IFSS with silane coupling agents [155-158]. It is proposed that the basic functional group of the silane can react with the acidic groups of the modified PP [155]. Figure 4-11 illustrates the reaction mechanism between amino groups of the silane coupling agent and maleic anhydride molecule grafted on PP. The benefit of modifying PP on adhesion is further demonstrated directly by measuring the IFSS using the microbond test [55, 159]. Nagel reported around 70% increase in IFSS when maleic anhydride grafted polypropylene (MAPP) loading of 1-12% was used in combination with APS coated fibres [55]. Jannerfeldt et al. observed around 30% increase in IFSS when using 2% MAPP loading however the sizing on the fibre was not specified [159]. Several authors also reported improvement in the strength of GF-PP when the PP was modified with acidic group, which was attributed to increased IFSS [55, 160-163].

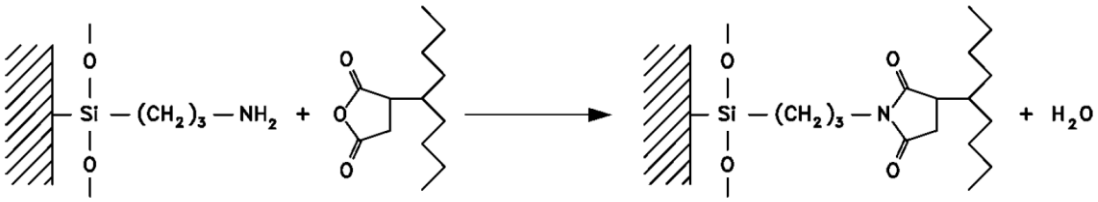

Figure 4-11 Chemical reaction between the amino group and the maleic anhydride molecule grafted on PP, reproduced from [158]

Several studies also observe an increase in IFSS when using maleic anhydride modified PP with unsized glass fibres [155-157] or with glass fibres which have had their sizing thermally removed [55]. The surface of glass fibre is acid which suggests that acid-base reactions are not possible. The maleic anhydride is polar thus may

interact with the hydroxyl group on the fibre surface via intermolecular bonds such as hydrogen bonding. This mechanism is just speculative and further work is required to understand the interaction between MAPP and unsized glass fibre.

It is understood that other factors such as intermolecular entanglement [155, 158, 164, 165], transcrystallinity [160, 165-171] and residual stress [172] also affect the adhesion between glass fibre and PP, however these are out with the scope of this thesis.

4.1.2.3 Glass fibre – epoxy interface and interfacial adhesion

Several authors in the literature show that application of silane coupling agents significantly increase the level of adhesion with epoxy matrices [173-175]. Gao et al. observed an approximately 40% increase in IFSS with epoxy when glass fibres were prior coated in the silane coupling agent 3-glycidoxypropyltrimethoxysilane [174]. Using the pull out test, Ramezanzadeh et al. observed an approximately 40% and 55% increase in adhesive strength between epoxy and steel wire treated with tetraethylorthosilicate and APS respectively [175]. Langroudi et al. reported significant increase in peel strength of GF-EP systems when fibres were treated in APS prior to composite preparation. This phenomenon was attributed to increased interfacial adhesion when APS is used [173]. Using the fragmentation technique on single filament glass fibre epoxy composites, Berg and Frank actually report a reduction in IFSS with APS surface loading [176]. This was however attributed to polymeric–oligomeric silane deposit on the fibre, creating an interphase of reduced shear yield strength. It is believed that this is formed because silane was deposited under laboratory conditions [176].

The mechanism underlying the chemical bonding between amino-silane coupling agents and epoxy is less controversial compared to interactions with PP matrices. It is proposed by Walker [177] that the amino-silane and uncured epoxy matrix chemically bond by the reaction between the amine and epoxide functional groups, as outline in Figure 4-12. A similar reaction process is also described in [173].

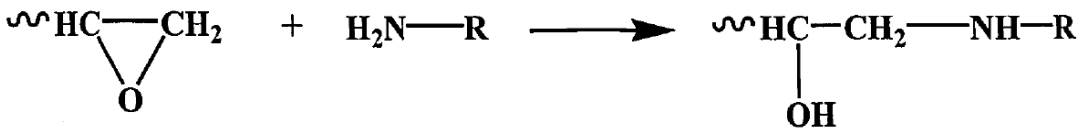

Figure 4-12 General reaction between amino-silane and epoxy resin, reproduced from [177]

The level of adhesion between unsized glass fibres and epoxy [174] appears greater than with PP matrices [55]. This is most likely a result of greater polar interaction between epoxy and the hydroxyl ions on the fibre surface. Epoxy shrinkage during curing may also generate additional compressive stress on the glass fibre that increase stress transfer and improve the IFSS [178, 179].

4.1.3 Regeneration of glass surface functionality

4.1.3.1 Effect of applying sizings on glass fibre – polymer interfacial adhesion

It was established in Chapter 2 that the organic sizings present on fibres decompose at typical thermal recycling temperatures. The removal of this sizing reduces the adhesion between fibre and the polymer matrix, ultimately reducing the properties of GRP. Serval authors re-applied coupling agents to thermally conditioned glass fibres and investigated the resulting interfacial adhesion. Bikiaris et al. observed the micrographs of fracture surfaces, showing that thermally cleaned fibres treated with APS and MPS had significantly more matrix residue present on the fibre surface compare to un-silanised fibres [57]. It was concluded that composites with silanised fibres failed at the matrix due to an increase in interfacial adhesion. Lee and Jang used the fragmentation test to characterise the interface between thermally cleaned glass fibres and PP matrix [180]. It was found the fibre fragmentation length was shorter when fibres were applied with the coupling agent N-β-(N-vinylbenzyl aminoethyl)-γ-aminopropyl trimethoxy silane. As with [57], analysis of the fracture surface revealed that pull-out fibres had more matrix residue when the coupling agent was used.

Yang et al. [5] and Nagel [68] used the microbond test to directly measure the IFSS between glass fibre and PP matrix. Yang et al. found that reapplying APS after thermal conditioning fully regenerated the IFSS to that of as received fibres. Nagel

also observed full regeneration of IFSS with PP matrix when thermally conditioned glass fibres were coated with APS [68].

4.1.3.2 Methods for glass fibre surface rehydroxylation

Several authors have attempted to restore hydroxyl groups on the surface of previously dehydroxylated glass fibres [62, 63] and silica [64, 66] by treating in water vapour, liquid water or other aqueous solutions. Young found that complete rehydroxylation with water vapour can be achieved for samples of silica which were subjected to thermal conditioning at temperatures below 400C° [66]. After conditioning at a higher temperature, only partial rehydroxylation of the silica surface was possible. Liu et al. exposed glass fibres to 80% relative humidity at RT after thermally conditioning at 600 °C [62]. In agreement with Young, the hydroxyl concentration was only partially restored, to around 90% of unconditioned fibres. Contrary to Young, Zhuravlev reported full rehydroxylation of silica gel that was previously conditioned up to 1100 °C by subjecting to 100 °C water for 5-10 hour [64].

Gonzalez-Benito et al. investigated the use of boiling water and 10 vol% HCl treatments as a means of restoring hydroxyl on the surface of thermally conditioned glass fibres [63]. Using FTIR it was observed that soaking the fibres in HCl for 1 and 3 hour increased the O-H stretching band from silanol groups. It is unclear what proportion of new silanol are surface groups or within the fibre itself. Furthermore, it was observed that acidic treatment leads to a more hydrophilic surface, which was observed by an increase in free surface energy. Water treatment for 1 hour provided no change in O-H band intensity and in fact reduced the free surface energy of the fibres. Reduced polar contribution to the overall free surface energy was observed after applying APS to fibres treated in HCl; suggesting increased APS coating.

No work come be found in the literature directly measuring the IFSS of fibres before and after rehydroxylation and re-sizing treatments. It is therefore unclear how significant increasing the hydroxyl concentration on the fibre surface is to increase fibre adhesion.

4.1.4 Conclusions of literature review

Several methods for regenerating the strength of thermally conditioned glass fibres have been reported. Applying organosilane coupling agents increased the strength of thermally conditioned glass fibres, however, the improvement was minimal and insufficient to use as a reinforcement commercially. Hot water and water vapour treatments have been effective at improving the strength of bulk glass but no research has been done on applying this technique to thermally conditioned or recycled glass fibres. Treatments in basic or acid solution function by etching the glass fibre surface, which either removes or modifies the surface flaws. Etching with HF is well established as a means for increasing fibre strength after thermal conditioning. A newly proposed method for fibre strength regeneration is etching in hot NaOH, which provided similar levels of regeneration as HF without the associated handling dangers. No strength regeneration techniques have been used on thermally RGF as of yet. Re-application of APS on thermally conditioned glass fibres has been shown to fully regenerate the interfacial adhesion with polymer matrix. To conclude, regeneration of strength and surface functionality have proven to be effective at increasing the reinforcement potential of thermally conditioned fibres; however, little work has been done towards regenerating the strength of fibre thermally recycled from GRT.

4.2 Experimental

4.2.1 Materials

In this chapter, two different composites were recycled in the fluidised bed 1) in-house prepared GF-EP and 2) an end-of-life offshore wind turbine blade. The in-house prepared GF-EP was prepared as described in Chapter 2. These composites were made from E-glass fibres from a tri-axial 3-ply mat supplied by Hexcel Reinforcements UK Ltd infused with PRIME 27 Resin with PRIME 20LV extra slow hardener supplied by Gurit.

A 25 kg section of an end-of-life offshore wind turbine blade was also sourced and used as the recyclate for this work, which can be seen in Figure 4-13. The blade structure comprised of continuous glass fibre reinforced epoxy sandwiching a wood centre. By ashing a small amount in a furnace, it was established that the fibre

weight fraction of the part was 68%, with the remaining mass a combination of wood and epoxy. Since delivered in a single piece, the blade required size reduction prior to recycling in the fluidised bed rig. Suitable size reduction equipment such as shredder or hammer mill were not available in house, therefore the blade section was cut into regular pieces using a water jet cutter, as shown in Figure 4-13.

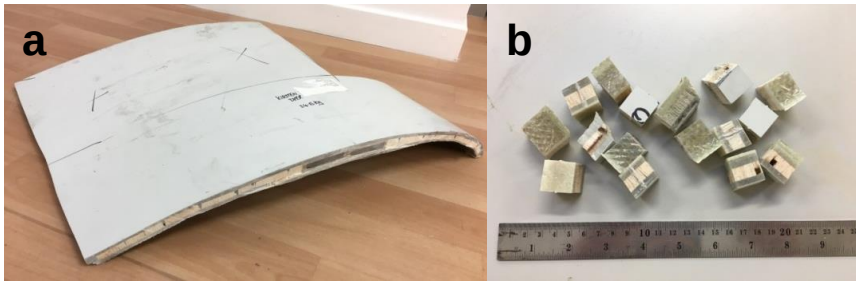

Figure 4-13 End-of-life offshore wind turbine blade (a) as received before downsizing and (b) after downsizing before recycling

PP used in this chapter was DA3/6 PP fibres, purchased from Goonvean Fibres Limited. The PP fibres were received chopped with a nominal length of 6 mm and a nominal linear mass of 3.3 dtex. The method used to prepare GF-PP composites in Chapter 5 require the PP to be in fibre form, for consistency the same PP was used in this chapter also.

Epoxy used to characterise the adhesion with RGF was IN2 Epoxy Infusion Resin and AT30 slow hardener supplied by Easy Composites Ltd.

NaOH pellets and 37% HCl were supplied by VWR and APS by Sigma-Aldrich.

4.2.2 Glass fibre chemical treatments

In this section the methodology for each of the regeneration treatments is outlined. For the sake of brevity, Table 4-2 summarises various parameters of each of the treatments. After each of the treatments, the fibres were dried in an oven at 105 °C for 30 min.

Table 4-2 Summary of various parameters used when preparing and carrying out each of the regeneration treatments

	Fibre mass (g)	Solution vol. (mL)	Conc.	Temp. (°C)	Time
NaOH	0.3	500	1.5-10 mol/L	95	10-180 min
Hot water	0.3	500	/	90	8-336 hour
Water Vapour	0.3	5 (ambient conditions)	/	250	4-96 hour
Hot APS	0.3	500	1 vol%	83	0.25-240 hour
RT APS	0.3	100	1 vol%	RT	15 min
HCl	0.3	500	10 vol%	RT	1, 3 hour

4.2.2.1 NaOH treatment

RGF were treated in a hot NaOH solution in an attempted to regenerate their tensile strength. 0.3 g of glass fibres were treated in 500 mL of NaOH solution. NaOH pellets were dissolved in deionised water to produce a solution with the desired concentration. The solution was prepared in a PP storage container and (with the lid on) was placed in an AX60 carbolite oven pre-heated to 95 °C. After 4 hour, the solution was taken out of the oven and poured over the fibres. The container was then returned to the oven and the fibres treated in the NaOH solution for the desired length of time. It was late found that the ratio of NaOH solution to glass fibres could be reduced without influencing the NaOH treatment; however, for consistency this ratio was used throughout this chapter.

After the treatment, the fibres were drained using a nylon sieve. The glass fibres were then rinsed in order to remove residue produced during the NaOH treatment, the procedure for which is outlined in Table 4-3.

Table 4-3 Rinsing procedure after NaOH treatment for single fibre tensile test/microbond test specimens

Order	Repetitions	Rinse	Volume (mL)	Temperature (°C)	Time (s)
1	1	37% HCl solution	500	RT	60
2	1	Water	500	95	60
3	2	Water	500	RT	60

4.2.2.2 Hot water treatment

As discussed, it has been demonstrated that the strength of abraded bulk glass can be regenerated after soaking in hot water. A similar process was used in this work in an attempt to improve the strength of thermally RGF. 500 mL of deionised water was poured into a PP storage container and sealed with a lid. The container was placed in an AX60 carbolite oven at 90 °C for 4 hour; the water temperature was measured with a thermocouple to ensure it had reached 90 °C. 0.3 g of fluidised bed RGF were submerged in the water. The container was resealed and returned to the oven. A variety of treatment times ranging from 8-336 hour were studied.

4.2.2.3 Water vapour treatment

Observations were made that storing abraded bulk glass in water vapour could significantly improve its strength. In an attempt to improve the strength of thermally RGF, a similar process was used. 5 mL of deionised water was syringed into a Parr Instrument Co. Teflon(PTFE)-lined acid digestion bomb. A stand was placed in the vessel and 0.3 g of fluidised bed RGF were placed on the stand inside the vessel. The stand was used to avoid fibres contacting any liquid water during the treatment. The vessel was sealed and placed in an AX60 carbolite oven at 250 °C for various treatment times. After the allotted times the vessel was removed from the oven and allowed to cool for 30 min before removing the glass fibres.

4.2.2.4 Hot APS treatment

It has been proposed that APS may be used to regenerate the strength of thermally conditioned glass fibres when the APS is hydrolysed at 83 °C. In this work, fluidised bed RGF were also treated in hot APS in an attempt to regenerate their strength.

The preparation of the hot APS solution was the same as is outlined in [142]. In a PP storage container, APS was mixed with deionised water to prepare 500 mL of 1 vol% solution. The container was sealed with a lid and placed in an AX60 carbolite oven at 83 °C. The solution was allowed to hydrolyse in the oven for a total of 5 hour. The lid was opened twice during hydrolyses; first after 1.5 hour then after 3 hour, each for 15 min. It was suggested by Saez-Rodriguez that doing this allowed for the evaporation of ethanol vapour that is a by-product of the APS hydrolysis [142]. After the APS solution was prepared, 0.3 g of fluidised bed RGF were submerged in the APS. The lid was returned to the container and was treated in the oven for various treatment times.

4.2.2.5 RT APS treatment

The glass fibres were treated with RT APS in an attempt to improve the compatibility between fibre and polymer matrices. APS was mixed with RT deionised water to prepare a 1 vol% solution. The solution was allowed to fully hydrolyse by leaving for 24 hour at RT. 100 mL of APS solution was prepared a small PP storage container, the APS solution was poured over 0.3 g of glass fibres and the lid closed. After 15 min, the fibres were drained and dried.

4.2.2.6 Hydrochloric acid treatment

RGF were subject to a HCl treatment as a means of increasing silanol concentration on the fibre surface. A 10 vol% solution was prepared by diluting 37 vol% HCl with deionised water. The HCl solution was poured over the fibres in a PP storage container then the lid closed and treated for the desired time. After HCl treatment, the fibres were twice rinsed in water before drying.

4.2.3 Fourier transform infrared spectroscopy

FTIR was carried out to characterise RGF after various treatments. An Agilent Technologies 4100 Exoscan with diffuse interface was used. Each spectrum consisted of 128 scans with 8 wavenumbers resolution for solids with depth penetration from 200 – 400 μm. For each condition, the spectra of 10 different fibre bundles were measured and OriginPro software was used to average and normalise the data.

4.2.4 Microbond sample preparation and test

The microbond test was performed to assess the IFSS between glass fibre and polymer matrices. The sample preparation differed depending on the polymer under investigation.

4.2.4.1 Preparation with polypropylene matrix

A preconsolidated layer of DA3/60 PP was produced by mixing and preconsolidating 31.36 g of Goonvean DA3/60 PP fibres as described in Chapter 5. The preconsolidated PP was then cut into pellets. The pellets were heated on a glass slide which was placed on a hot plate set at 200 °C. After 45 s, the PP pellets melted and were drawn using tweezers to form PP fibres.

Figure 4-14 outlines the procedure for preparing microbond samples. A single glass fibre was attached to a small piece of double-sided tape using tweezers to avoid contaminating the fibre surface. A PP fibre was knotted around the glass fibre and the ends stuck to adjacent pieces of tape. Vanna's-Type micro-scissors (straight 80 mm, purchased from Agar scientific) were used to trim the PP fibre. The PP fibre was fixed at each end to minimise movement while cutting, allowing the fibre to be cut closer to the knot. Trimming close to the knot produced smaller PP droplets, which require lower loads to debond, and reduces the probability of the glass fibre breaking during testing. This was especially important since the RGF under investigation have low strength after thermal recycling.

After trimming the PP fibre, the glass fibre with PP knot was glued onto a washer using Araldite epoxy adhesive and cured for at least 8 hour at RT. The samples were suspended on metal wire frames and placed in an OV-11 vacuum oven.

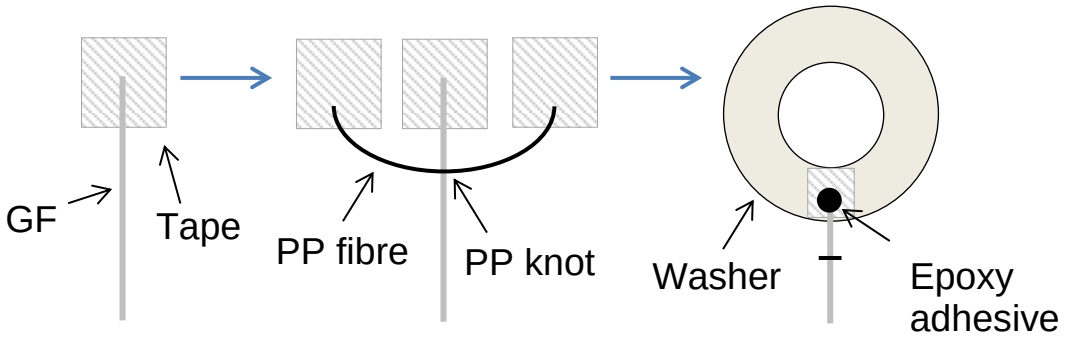

Figure 4-14 Sample preparation of microbond test

The oven was purged with nitrogen, heated up to 220 °C then allowed to slowly cool to RT. Figure 4-15 gives the oven temperature profile used.

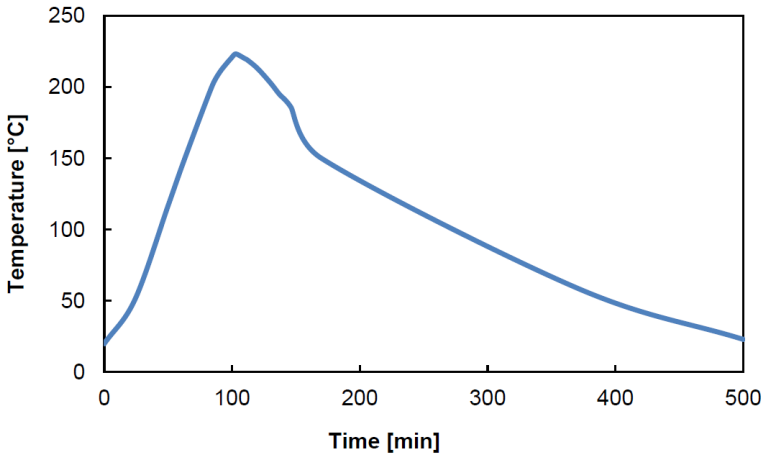

Figure 4-15 Temperature profile of vacuum oven used to prepare microbond samples, reproduced from [68]

4.2.4.2 Preparation with epoxy matrix

The procedure for preparing the microbond samples with epoxy polymer differed from PP, primarily in the way the polymer was applied to the fibre. The process began by fixing the glass fibres to a 5 mm gauge length card template using Loctite super glue (cyanoacrylate). Care was taken to ensure that the fibre surface was not touched or exposed to contaminants during preparation. 2 g of epoxy was then prepared by mixing resin with hardener at 100:30 by weight. After mixing for 5 min the epoxy was degassed in a vacuum chamber for 10 min. Epoxy droplets were applied to the fibre surface using a modified scalpel, which utilised a piece of 50 µm

steel wire attached to the end of the blade, as shown in Figure 4-16. The wire was dipped into the epoxy and several small droplets were then applied to each fibre. The epoxy was cured at RT for 24 hour followed by a post cure treatment at 60 °C for 6 hour, in line with supplier's instruction.

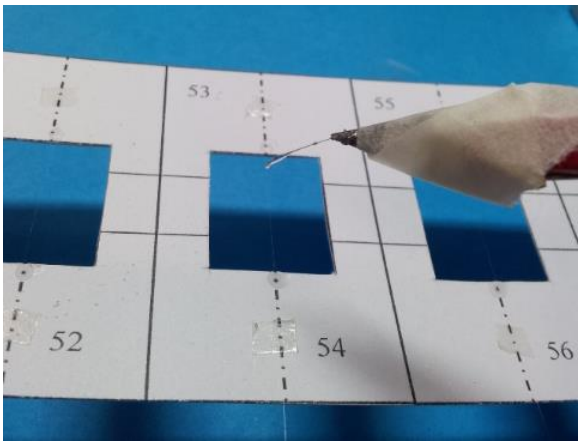

Figure 4-16 Modified scalpel used to apply epoxy microbond droplets on glass fibres

4.2.4.3 Microbond test procedure

Before measuring the IFSS using the microbond test, the fibre diameter, droplet diameter and the embedded fibre length of the microbond samples were determined using a Leitz Ergolux optical microscope and ImageJ software. Only samples with symmetric droplets were tested. Table 4-4 gives the range of droplet diameters and embedded lengths used for microbond test with epoxy and PP. Figure 4-17 shows a typical PP droplet and the dimensions measured using ImageJ.

Table 4-4 Range of microdroplet geometries used for microbond test with epoxy and PP

Polymer	Embedded length (µm)	Droplet diameter (µm)
Epoxy	100-130	40-80
PP	120-200	80-180

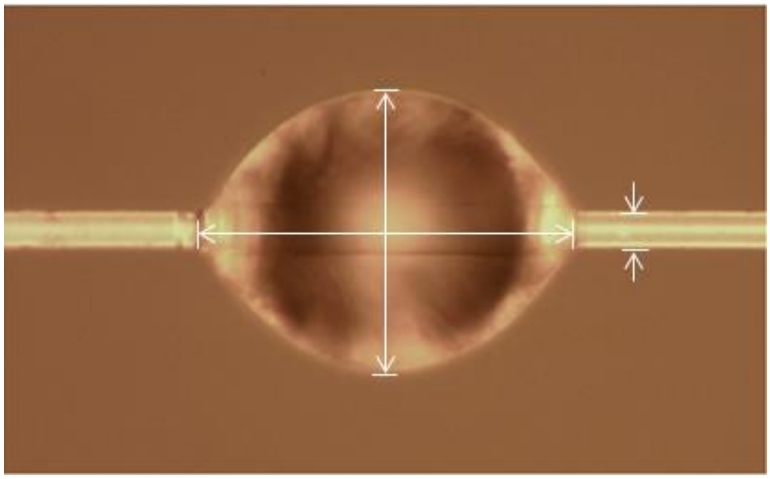

Figure 4-17 Typical PP droplet on GF with dimensions measured for microbond test

Figure 4-18 shows the microbond test set-up. An Instron 3342 universal testing machine equipped with a 10 N load cell was used to apply load to the microbond samples. The washer/card (PP/epoxy respectively) was placed on the hook with the fibre hanging vertically downward. The adjustable shear blades were moved toward the fibre then the height of the droplet was moved so that it was below the shear blades. A 45x magnification microscope with a DCM140 video camera were used to view the samples and shear blades.

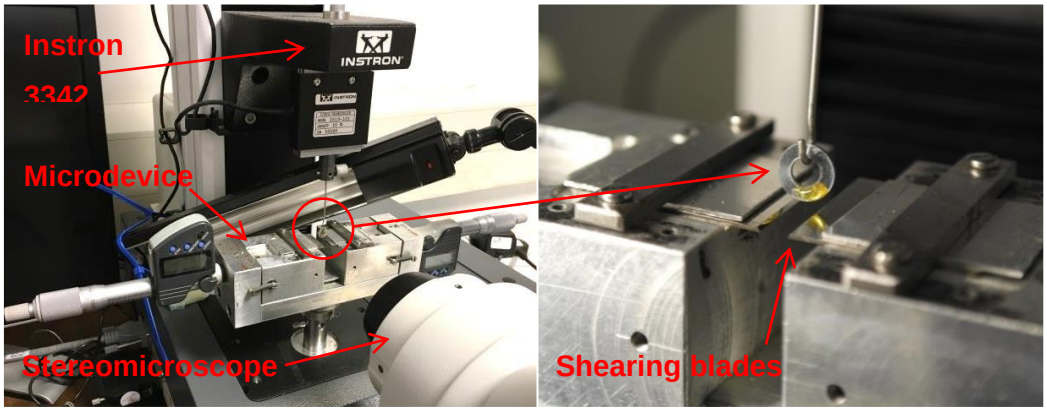

Figure 4-18 Microbond test setup

Figure 4-19 shows a stereomicroscopy view of a microbond droplet. A test speed of 0.1 mm/min was used and all tests were carried out at RT. The load was recorded

as a function of displacement. The test was stopped after the load reached a peak followed by a drop to a plateau.

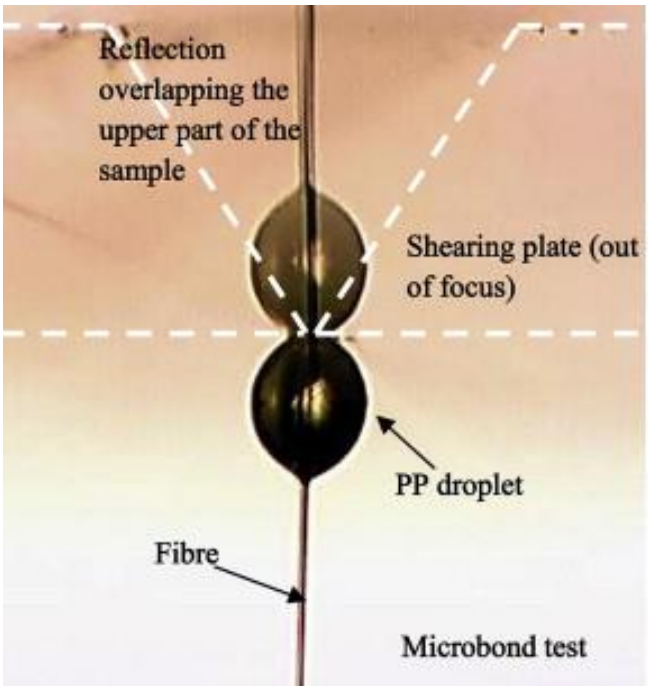

Figure 4-19 Stereomicroscopy view of microbond of PP droplet, reproduced from [181]

Figure 4-20 gives an example of a typical load-extension plot obtained during a microbond test.

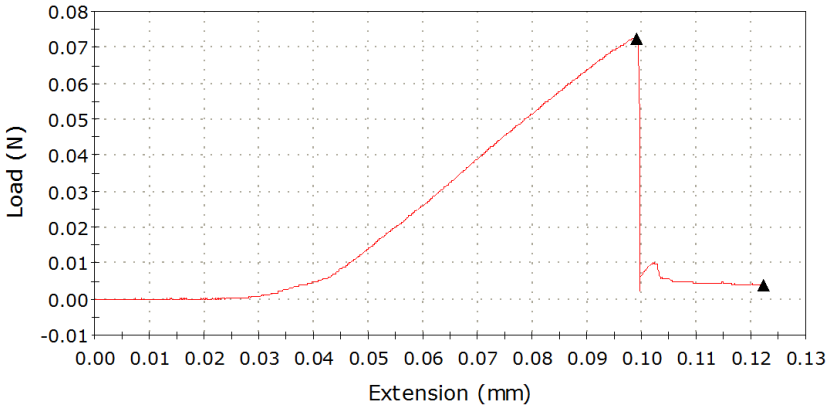

Figure 4-20 Example of a typical load-extension plot output from Instron Bluehill 2 software

The IFSS was then calculated by dividing the peak load at droplet de-bond by the fibre-matrix contact area as shown in Equation 4-6.

Equation 4-6 Equation used to calculate IFSS from microbond test data

$$IFSS = \frac{F_{db}}{\pi D l_d}$$

Where F_{db}, D and l_d are the load at droplet de-bond, glass fibre diameter and embedded length respectively.

4.3 Results and discussion

4.3.1 Tensile strength of regenerated glass fibres

4.3.1.1 Effect of NaOH on glass fibres recycled from in-house recyclate

Initially NaOH treatments were performed on glass fibres after three thermal treatments:

- Thermally conditioned in the furnace
- Thermally recycled in the furnace
- Thermally recycled in the fluidised bed

The thermal history in each case is shown in Table 4-5. The NaOH treatment time was kept constant at 10 min and solution concentrations of 1.5, 3 and 5 mol/L were used. The treatment time was initially selected as Thomason et al. observed a 130% increase in tensile strength of glass fibres thermally conditioned at 500 °C when treated with 3 mol/L NaOH solution for 10 min [15]. Bashir et al. also showed that higher concentrations of NaOH (in the range of 1.5, 3 and 5 mol/L) resulted in increased strength of thermally conditioned glass fibres after NaOH treatment for 10 min [34].

Table 4-5 Thermal history of glass fibres treated with NaOH at 1.5, 3 and 5 mol/L for 10 min

Sample	Material	Temperature (°C)	Time (min)
TC in Furnace	Glass fibre	500	25
Recycled in furnace	In-house prepared GF-EP	500	80
Recycled in fluidised bed	In-house prepared GF-EP	500	Est. 15-20

Figure 4-21 gives the single fibre tensile strength of the various thermally weakened fibres following treatment in the NaOH solutions. The strength of thermally conditioned fibres increases with NaOH concentration, similar to that observed in [34]. Treating with 1.5, 3 and 5 mol/L solution yields a 14, 33 and 48% increase in tensile strength respectively, compared to fibres not treated with NaOH. Higher concentrations may continue to improve the strength of these fibres since a plateau does not appear to have been reached in the range of concentrations studied.

The relative increase in strength for thermally conditioned fibres found in this work is significantly lower than was observed by Thomason et al. [15]. This is likely due to the large disparity in the baseline thermally conditioned fibre strength; given as less than 0.6 GPa in [15] compared to 1.2 GPa found in this work. Thomason et al. thermally conditioned APS only coated fibres whereas the fibres used in this work have a commercial sizing on them. This could be the cause for the significantly higher strength loss observed by Thomason et al., which is further investigated in, Appendix B. Nagel also performed NaOH treatments on glass fibres thermally conditioned at 500 °C for 25 min and reported a strength of around 1.2 GPa after thermal conditioning alone [68]. Nagel used commercially sized glass fibres and, similar to this work, observed around a 33% increase in fibre strength after treating with 3 mol/L NaOH solution for 10 min [68].

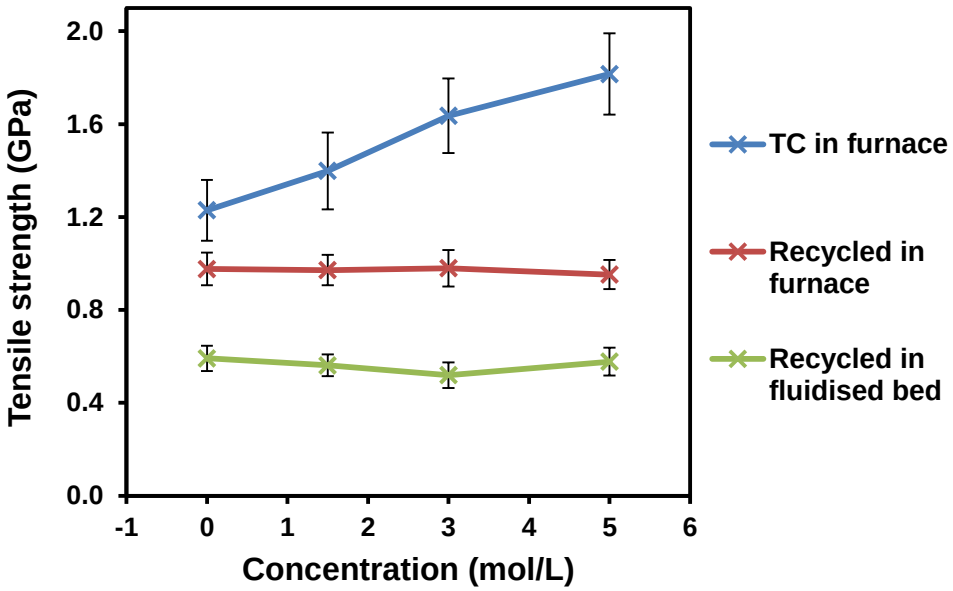

Figure 4-21 Tensile strength of glass fibres thermally conditioned in the furnace, recycled in the furnace and recycled in the fluidised bed then treated with NaOH at 1.5, 3 and 5 mol/L for 10 min. Only thermally conditioned glass fibres show any improvement in strength after the NaOH treatments.

The NaOH treatments used in Figure 4-21 show little effect on the strength of furnace and fluidised bed RGF, with a relatively consistent single fibre strength of 1.0 GPa and 0.5-0.6 GPa respectively. It has been hypothesised that the reaction of silica in the glass fibre with hydroxide ions from the NaOH solution smooths and/or removes the severe surface flaws that manifest during exposure to elevated temperatures, and thus increases the tensile strength of the fibre [15, 34]. It is likely that there are more severe flaws present on the surface of the thermally RGF compared to the thermally conditioned, given their significantly lower strength. The same is true for fibres recycled in the fluidised bed versus within the furnace. In light of this, the efficacy of NaOH at increasing recycled fibre strength could be reduced due to the presence of more severe flaws on the surface of these fibres. This explanation is not fully satisfying given Thomason et al. did in fact observed an increase in the strength of fibres with a tensile strength of less than 0.6 GPa [15], which is similar to that of the fluidised bed RGF in Figure 4-21. With comparable strengths, it could be expected that the flaws on both fibre surfaces would have similar severity. It is therefore not entirely clear why the NaOH treatments were effective at increase the strength of fibres thermally conditioned in [15], but not the RGF from composites as shown in Figure 4-21.

Figure 4-22 gives the average diameter of the various thermally weakened fibres following the treatments used in Figure 4-21. Considering the error bars, and that the diameters were measured using optical microscopy, there appears to be no significant change in average diameter of RGF. Thermally conditioned fibres show a consistent reduction in average diameter of around 8%. Again, it is unclear how significant this reduction is and SEM would be a more accurate technique to measure such small variations in diameter.

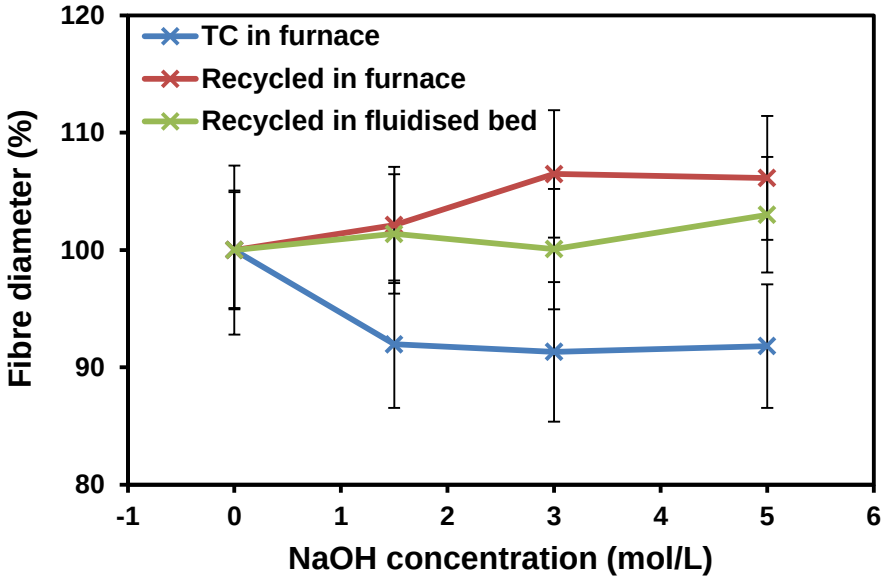

Figure 4-22 Diameter of glass fibres thermally conditioned in the furnace, recycled in the furnace and recycled in the fluidised bed then treated with NaOH at 1.5, 3 and 5 mol/L for 10 min. Only thermally conditioned glass fibres exhibit a reduction in fibre diameter after the NaOH treatments.

As seen in Figure 4-21 and Figure 4-22, only fibres with a reduction in diameter exhibit an increase in strength after the NaOH treatments. This gives weight to the hypothesis that NaOH treatment increases fibre strength by etching the glass fibre surface and removing the flaws; similar to treatment with HF [15].

Linear-elastic fracture mechanics can be used to estimate the flaw length in the glass fibres. The flaw length (c) is proportional to the measured fibre tensile strength ($\sigma_{f,av}$) via Equation 4-7, where K_{IC} is the mode I fracture toughness and Y is a geometric stress concentration factor [47].

Equation 4-7 Critical flaw length in the glass fibres [47]

$$c = \frac{1}{\pi}\left(\frac{K_{IC}}{\sigma_{f,av}Y}\right)^2$$

K_{IC} of E-glass fibre was found by Feih et al. to be approximately 0.91 MPam$^{1/2}$ [47]. Y is dependent on the shape of the flaws on the glass surface, which is unknown with and without thermal/mechanical weakening. Halfpenny ($Y = 0.73$) and straight ($Y = 1.12$) flaw geometries represent the minimum and maximum values of Y, where any intermediate flaw shape will be $0.73 < \mathrm{Y} < 1.12$ [47]. In this study, both Y values were used and a range of flaw lengths for each sample based on the average tensile strength was estimated. Assuming the fibre is uniformly etched radially, the reduction in diameter required to remove a flaw of length, c is given in Equation 4-8, where D_o is the initial fibre diameter.

Equation 4-8 Relative reduction in diameter required to remove flaw with length c

$$Diameter\ reduction = \frac{2c}{D_o} \times 100$$

Table 4-59 gives the range of estimated flaw lengths on the surface of the various glass fibre samples as well as the relative reduction in diameter required to remove them. As expected, flaw length and diameter reduction increase significantly with a drop in fibre strength. The reduction in average diameter of thermally conditioned fibres (8%) in Figure 4-22 is substantially higher than found using fracture mechanics in Table 4-6. This suggests that the most severe flaws present on the fibre surface after thermal conditioning may have been removed at all concentrations. If the surface flaws govern the fibre strength, it is unclear why the strength of these fibres continues to increase with concentration. As state above, the error in diameter measurement is relatively large and the reduction could be due to variation in fibre diameter within the mat used to prepare the GF-EP recyclate, rather than a result of the NaOH treatment.

Table 4-6 Range of estimated flaw lengths on the surface of the various glass fibre samples and the relative reduction in diameter to remove the flaws

Sample	Flaw length (nm)	Diameter reduction (%)
As received	22-51	0.25-0.59
Thermally conditioned in furnace	93-220	1.1-2.6
Recycled in furnace	150-350	1.7-4.1
Recycled in fluidised bed	400-950	4.7-11

Given the lack in strength increase under the conditions used in Figure 4-21, fluidised bed RGF were treated with NaOH for extended times. Figure 4-23 gives the strength and relative diameter of fluidised bed RGF after treatment with a 5 mol/L solution of NaOH for 5, 10, 20, 60, 120 and 180 min. There is a clear increase in tensile strength with treatment time when treating for longer than 20 min. The strength increase appears to begin to plateau around 180 min at 1.25 GPa, however, longer treatments may yield fibres with even higher strength.

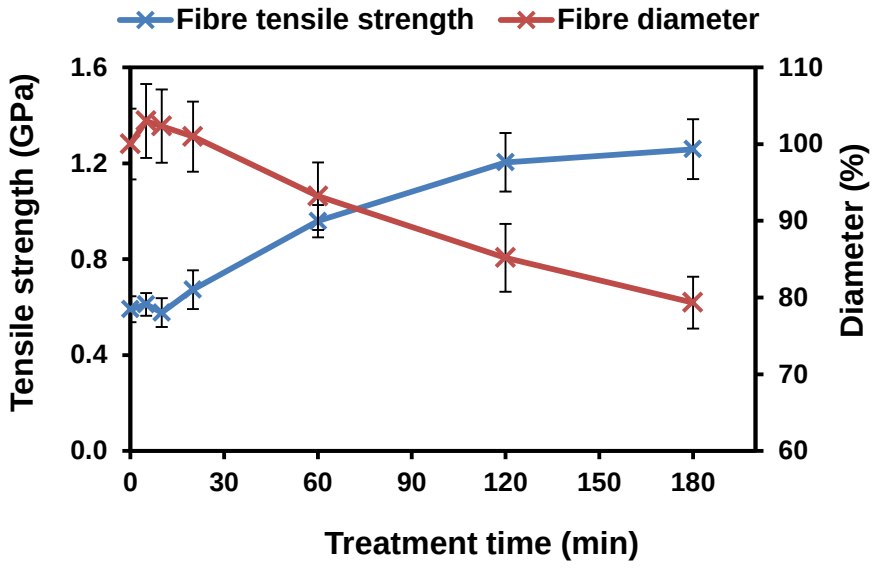

Figure 4-23 Tensile strength and relative diameter of glass fibres recycled in the fluidised bed treated with NaOH at 5 mol/L for various treatment times. Increasing NaOH treatment time beyond 30 min provides regeneration of the RGF strength.

Figure 4-23 also shows the change in glass fibre diameter after the NaOH treatment. The reduction in fibre diameter with treatment time is more pronounced when extending the range of NaOH treatment times. Similar to the tensile strength, the effect of the NaOH is not observed for treatments shorter than 60 min. In further agreement with Figure 4-21 and Figure 4-22, fibre strength only significantly increases with a reduction in fibre diameter. There is a slight increase in fibre strength after treating for 20 min without any reduction in diameter, however, when considering the error this increase in less significant.

In an attempted to further improve their strength, additional concentrations of NaOH solutions were applied to fluidised bed RGF at extended treatment times. NaOH concentrations of 1.5, 3, 7 and 10 mol/L were used for 60, 120 and 180 min. Figure 4-24 gives the tensile strength of glass fibres recycled in the fluidised bed then treated with NaOH at the various concentrations and times. All concentrations investigated, except 1.5 mol/L NaOH solution, increase the strength of fluidised bed RGF. In agreement with Figure 4-21, the effectiveness of NaOH tends to increases with NaOH concentration. Fibres treated with 1.5 mol/L NaOH solution may exhibit an increase in strength if the treatment times were extended further; given the dependence of rate of strength increase on NaOH concentration.

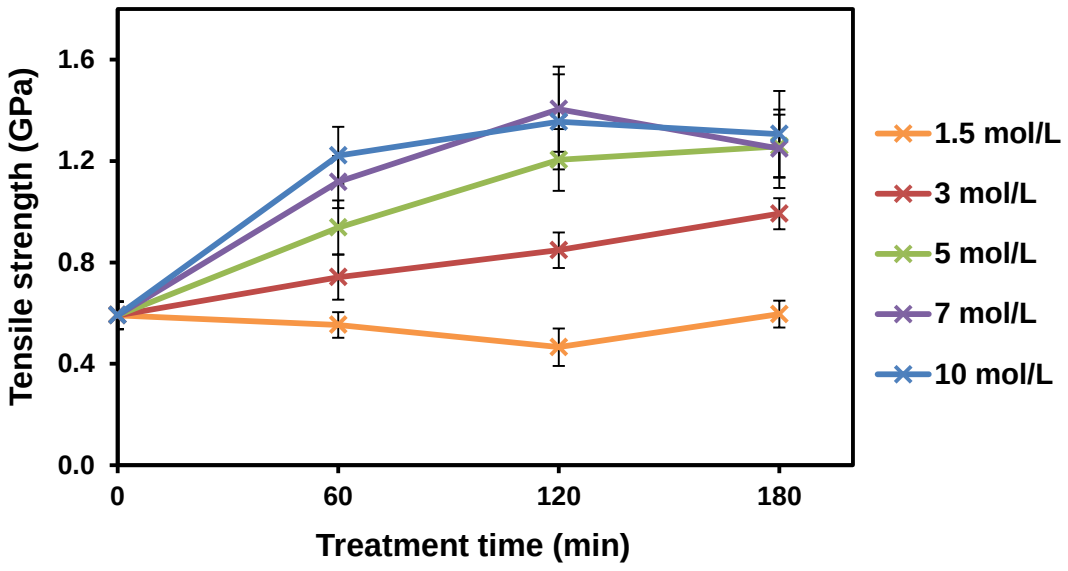

Figure 4-24 Tensile strength of glass fibres recycled in the fluidised bed then treated with NaOH at various concentrations and times. Under the conditions investigated, increasing both NaOH treatment concentration and time result in superior regeneration of RGF strength.

It appears there is a maximum strength increase for 7 and 10 mol/L treatments, where extending the treatment time does not improve the fibre strength. This plateau occurs more rapidly when higher concentrations are used. Figure 4-24 shows the strength of fibres treated at 7 and 10 mol/L appear to plateau after treatments lasting 120 and 60 min respectively. No plateau is observed for 5 mol/L treatments, however, the rate of strength increase appears to reduce after treatment of 120 min. Furthermore, no plateau is observed for 3 mol/L treatments which approximate a linear increase in strength within the treatment times studied. Extended treatments at 3 and 5 mol/L are required to determine if/when the fibre strength plateaus when using these concentrations.

The maximum possible strength increase may be the same for all concentrations, with lower concentrations requiring longer treatments to converge. This is better seen in Figure 4-25 which plots tensile strength against NaOH concentration. It is clear from 4-20 that the rate of strength regeneration increases with concentration and there does seem to be asymptotic strength value as time elapses.

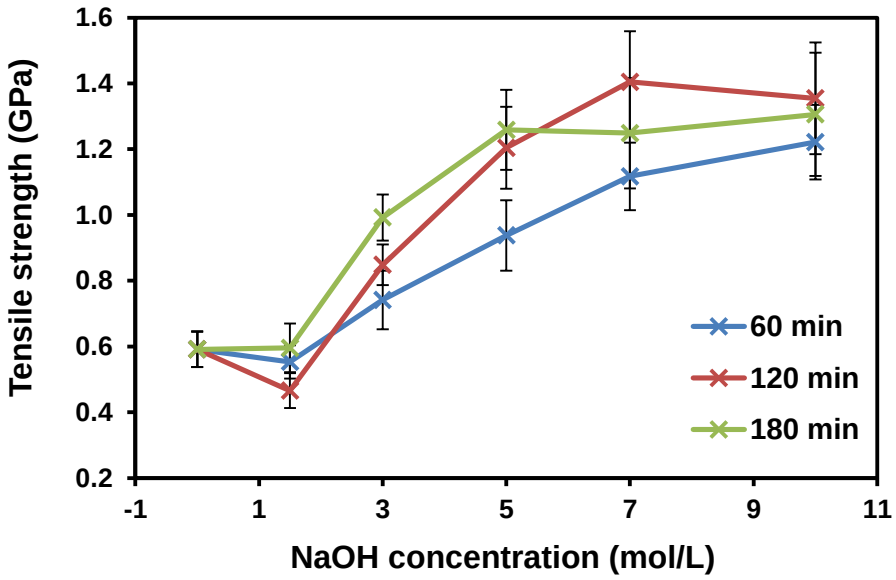

Figure 4-25 Tensile strength of glass fibres recycled in the fluidised as a function of NaOH concentration for 60, 120 and 180 min treatments

Under the conditions investigated, the maximum fibre tensile strength attained was approximately 1.4 GPa after treating for 120 min at 7 mol/L. While this is a significant increase in the fibre strength, it is still considerably lower than the original

strength of 2.55 GPa. It was previously demonstrated by Thomason and Kalinka that the actual average strength of fibres in a commercial 4 mm chopped glass product was as low as 1.5 GPa at a gauge length of 2 mm [182]. It is well established that there is an inverse relation between fibre tensile strength and gauge length, therefore, the regenerated strength of 1.4 GPa at 20 mm gauge length found in this work may provide a fibre strength distribution that is higher than that obtained in typical commercial discontinuous glass fibre products.

Figure 4-26 shows the fibre diameter after NaOH treatment at the various times and concentrations used in Figure 4-24. The trend lines represent second order polynomials with a minimum R^2 value of 0.91. Fibres treated with 1.5 mol/L solution exhibit no significant change in diameter until treated for 180 min. All treatments which exhibit an increase in fibre strength in Figure 4-24, also show a significant reduction in fibre diameter. Both fibre diameter reduction and rate of reduction tend to increase with treatment time as shown in Figure 4-26. Yang et al. observed an inverse relation between rate of fibre reduction and treatment time when etching glass fibre with HF [5]. This was attributed to the build-up of insoluble residue particles on the fibre surface, which masked the fibre surface and impeded the etching process over time. However, this does not seem to occur when using NaOH within the treatment times studied.

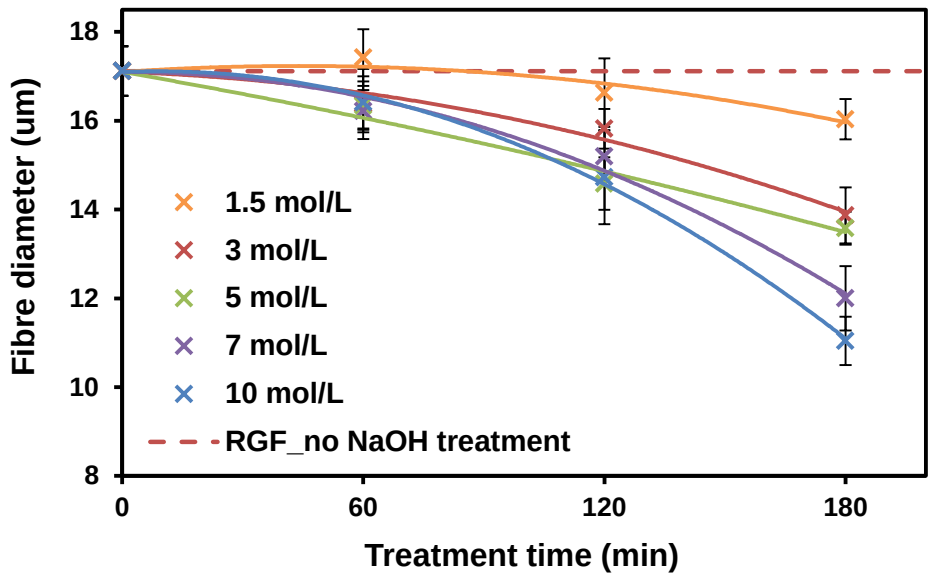

Figure 4-26 Glass fibre diameter after treating with NaOH at various concentrations and times, showing that higher NaOH concentrations more rapidly etch the RGF surface.

Scheffler et al. propose a glass fibre corrosion process in NaOH solution [183]. When glass fibres are introduced into NaOH solution, the hydroxide ions attack the silica network at areas on the fibre surface that include large defects. Over time, this creates a thin “corrosion shield” completely covering the fibre surface that is penetrated by water molecules, causing it to swell. Using EDX, Liu et al. concluded that a “passivation Ca-Si layer” is formed on the fibre surface. This shell irregularly peels from the fibre surface, exposing the new surface underneath and reducing the fibre diameter [183]. Such layers can be seen under SEM in [138, 139, 183]. On the contrary, Bashir et al. examined the kinetics of dissolution of glass fibres in NaOH solution and found that a radial diffusion model does not describe the reaction well [141]. It was concluded that during the reaction, a product layer was formed on the surface, likely to have been comprised of sodium silicates. Due to the corrosive NaOH solution it is likely that the diffusion of hydroxide ions through this layer occurred rapidly (i.e. not a rate-determining step). Furthermore, the product silicates are highly soluble and are unlikely to sufficiently increase in thickness to impede the glass dissolution reaction [141]. Figure 4-26 clearly shows that the rate of dissolution of the RGF used in this work does not diminish within the treatment time investigated, suggesting that no passivation layer (as proposed in [183]) is formed. Given the contradictory conclusions drawn between studies, further work investigating the mechanism(s) of glass fibre dissolution in alkali solutions is required. Figure 4-26 shows that, in general, higher concentration treatments more rapidly remove the glass fibre surface. This can be attributed to an increase in hydroxide density with NaOH concentration. Higher hydroxide density increases the probability that more collisions with silica (of the glass surface) will be sufficiently energetic to cause a reaction and cleave the silica network.

Figure 4-27 - Figure 4-30 show SEM images of fluidised bed RGF after NaOH treatment at 3, 5, 7 and 10 mol/L for 2 hour. The NaOH appears to substantially modify the glass fibre surface, which is more prominent on fibres treated with higher concentrated solutions. This can be attributed to hydroxide ions corroding the silica network as outline in [138, 139, 184]. The corrosion appears to be irregular on the fibre surface, creating the pits seen most clearly in Figure 4-29 and Figure 4-30. No corrosion shell can be seen on the surface of the fibres in Figure 4-27 - Figure 4-30, as was observed in other studies [138, 139, 183]. Scheffler et al. suggest that eventually the remaining shell will be only slightly bonded to the fibre surface, therefore, if present, the corrosion shell/layer may be removed during the rinsing

process used after NaOH treatment. No reference to pitting on the surface of alkali treated glass fibre could be found in the literature. Further studies should be done to understand the cause for such features and their influence on the mechanical properties of glass fibres.

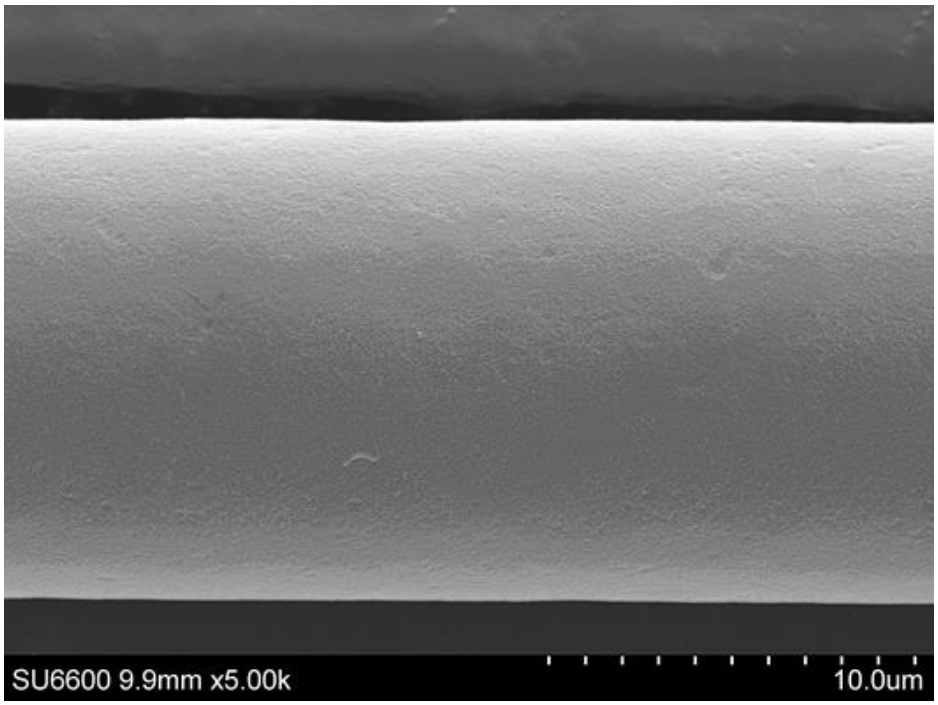

Figure 4-27 SEM image of fluidised bed recycled glass fibre treated with NaOH at 3 mol/L for 2 hour

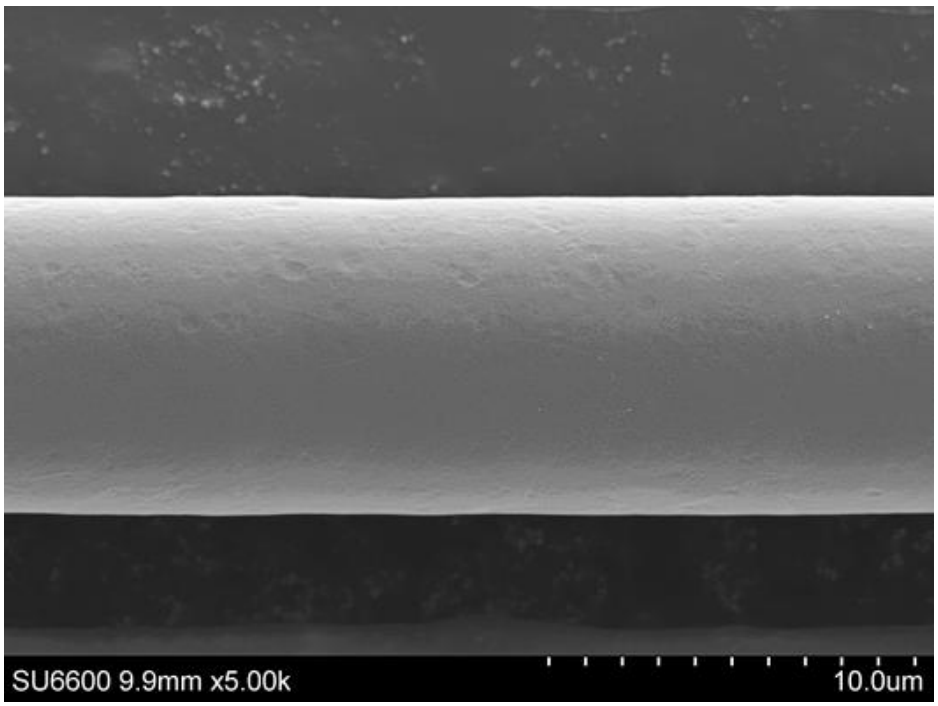

Figure 4-28 SEM image of fluidised bed recycled glass fibre treated with NaOH at 5 mol/L for 2 hour

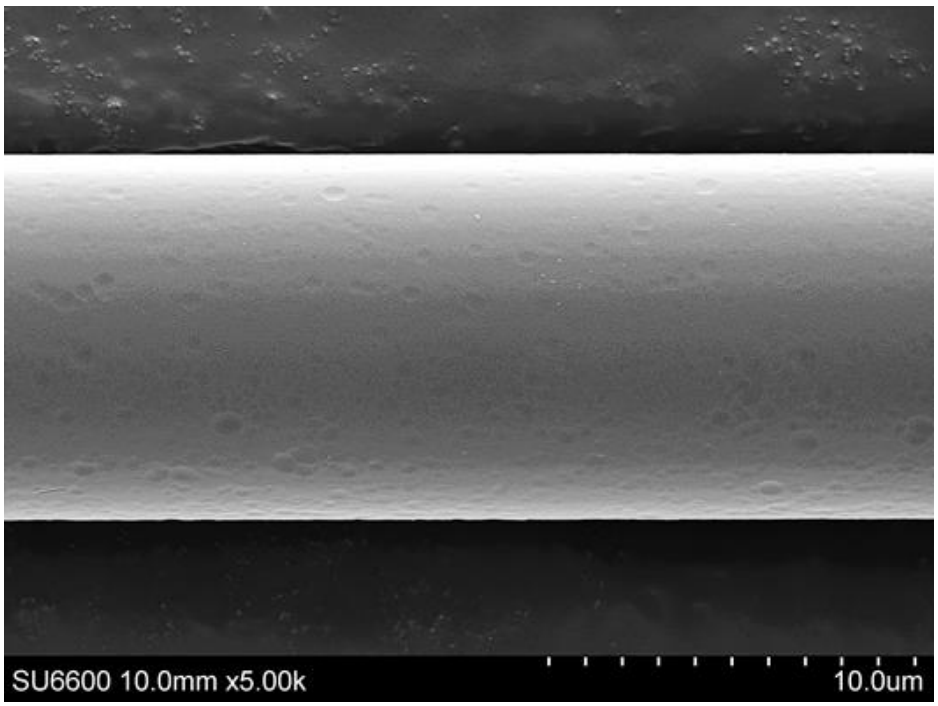

Figure 4-29 SEM image of fluidised bed recycled glass fibre treated with NaOH at 7 mol/L for 2 hour

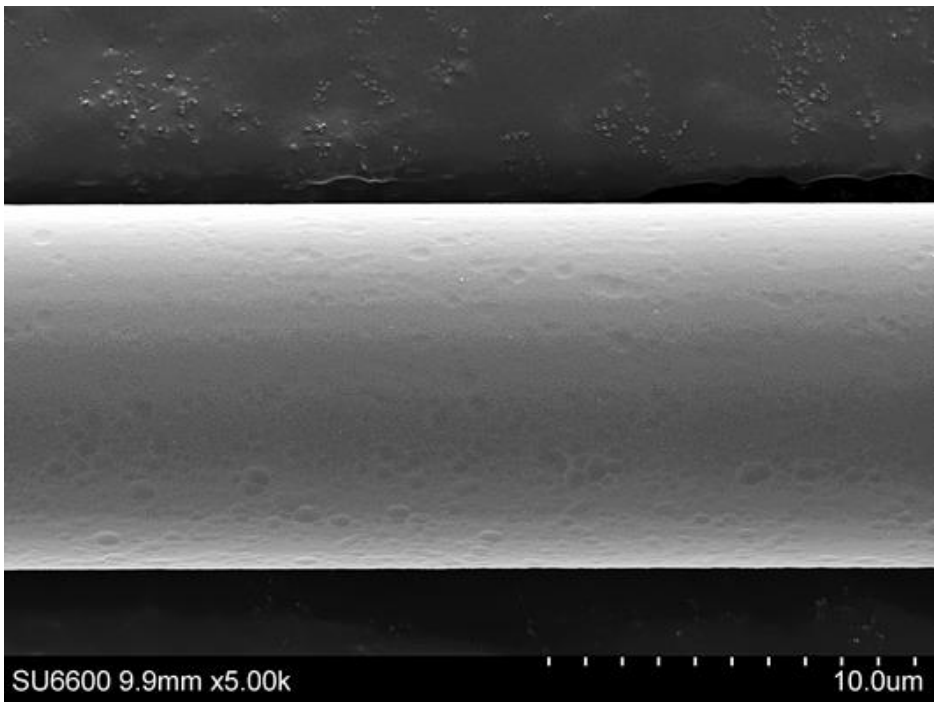

Figure 4-30 SEM image of fluidised bed recycled glass fibre treated with NaOH at 10 mol/L for 2 hour

Figure 4-31 shows the surface of the fibre in Figure 4-28 under higher magnification. Unlike recycled only fibres, the surface of fibres treated with NaOH appear uneven and could be due to the glass surface itself becoming rough after being etched by NaOH. This observation is in agreement with Bashir et al. who, using atomic force microscopy, measured surface roughness of thermally conditioned glass fibres rise from around 2 to 23 nm after treating in a 3 mol/L NaOH solution for just 30 min [34]. As with the pitting seen in Figure 4-27 - Figure 4-30, it is unclear how these features affect the mechanical properties of the glass fibres.

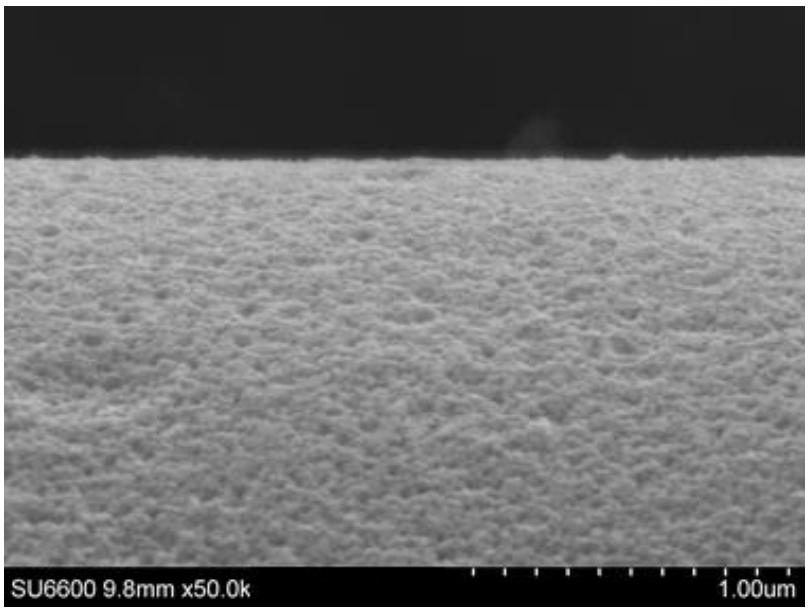

Figure 4-31 SEM image of fluidised bed recycled glass fibre treated with NaOH at 5 mol/L for 2 hour, exhibiting a roughened surface which was not observed for untreated RGF.

Figure 4-32 gives a plot of the regenerated strength of fibres recycled in the fluidised bed as a function of fibre diameter reduction by NaOH treatments. The range of diameter reductions required to remove the flaws given in Table 4-6 have also been added to Figure 4-32. Fibres treated with 1.5 mol/L solution have been omitted, as they do not show any improvement in strength. In agreement with [5], this work demonstrates that removal of the surface layer of thermally recycled glass fibre can significantly improve its tensile strength. Higher concentrated treatments reach a maximum regenerated strength, after which additional removal of the glass surface is no longer beneficial. This may also be the case for 3 and 5 mol/L treatments however the rate of diameter reduction at these concentrations is lower and was not observed within 180 min.

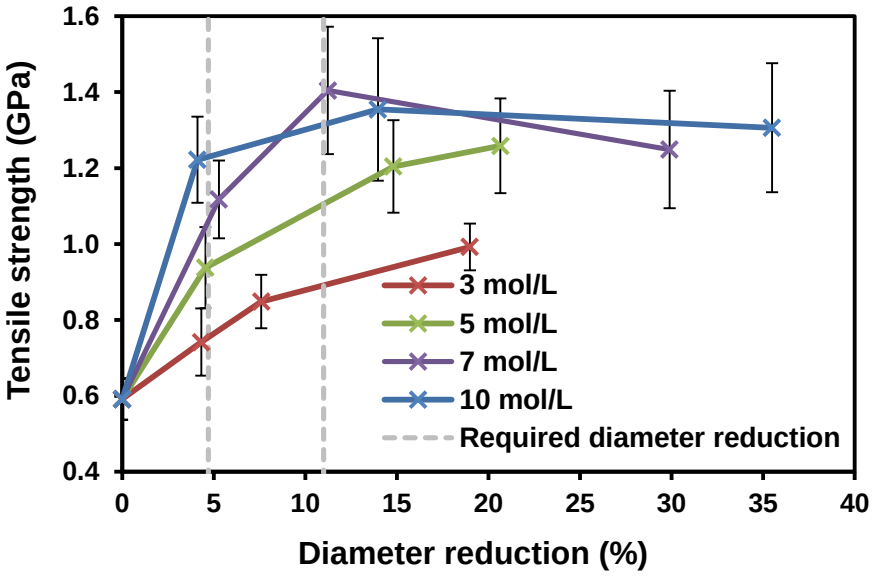

Figure 4-32 Tensile strength of glass fibres as a function of diameter reduction after various NaOH treatment concentrations and times. Tensile strength of RGF treated in NaOH is not merely proportional to the quantity of surface material etched, illustrated by the plateau in strength observed when higher NaOH concentrations are used.

Although there appears to be a trend between tensile strength and diameter reduction, this is only distinct within a given concentration of NaOH. The inconsistency in strength increase and diameter reduction between concentrations can be observed in Figure 4-32. The first data point for all concentration in Figure 4-32, representing treatment for 60 min, occurs around 4-5% reduction in fibre diameter. However, the tensile strength values are widely different, and increases with NaOH concentration. If the strength increase mechanism solely involved removal of the surface flaws, it would be expected that the strength of fibres treated at each concentration would be similar, given that approximately the same amount of material has been removed. According to fracture mechanics, these data points are in the range where flaws on the surface are still likely to be present, as seen in Figure 4-32. The disparity in tensile strength may therefore be due to flaw modification rather than complete removal. Higher concentrated NaOH solutions may smooth the serve flaws on the surface more rapidly, reducing stress concentrations during testing [185]. This is in agreement with Bashir et al. and Nagel who observed no detectable reduction in diameter when regenerating the strength of thermally conditioned fibres with NaOH [34, 68].

In Figure 4-32 the strength of fibres treated in 7 and 10 mol/L NaOH do plateau at approximately the diameter range given in Table 4-6. Enough of the surface has

been removed to eliminate all surface flaws caused during thermal recycling. The reason for the apparent upper limit on strength regeneration is still unclear. One may expect the resulting glass fibre surface to be absent of flaws and the strength approach that of pristine fibres [48]. It is well established in the literature however that NaOH solution is a corrosive environment for glass fibre, which can substantially weaken the fibre [138, 139, 183, 184]. Jianxun Liu et al. propose hydroxide ions can disrupt the continuity of the glass network therefore reducing the fibre strength [138]. Treating with NaOH may therefore improve the strength of RGF by removing the highly damaged outer surface while creating features on the new exposed outer surface (as seen in Figure 4-27-Figure 4-31), which limits the ultimate potential for strength regeneration. Figure 4-32 shows that fibres treated with 3 and 5 mol/L continue to increase in strength beyond the estimated diameter reduction required to remove all flaws induced during recycling. With the serve flaws removed, it is unclear why the strength of fibres treated with the lower concentrated NaOH do not converge with those treated in 7 and 10 mol/L solution. It would appear that fibres treated with lower concentrated solutions require additional removal of surface material to replicate the strength increase provided by higher concentrated treatments.

Figure 4-33 gives a plot of all the tensile strength data in Figure 4-32 without differentiating between concentrations. There remains a general trend of increasing strength with diameter reduction; however, there is more of a scatter when considering the data as a whole. The trend line in Figure 4-33 represents a second order polynomial with a low R^2 value of 0.39. When assessing the data from each concentration discretely, the R^2 value for second order polynomial trend lines are in the range 0.75 - 0.99.

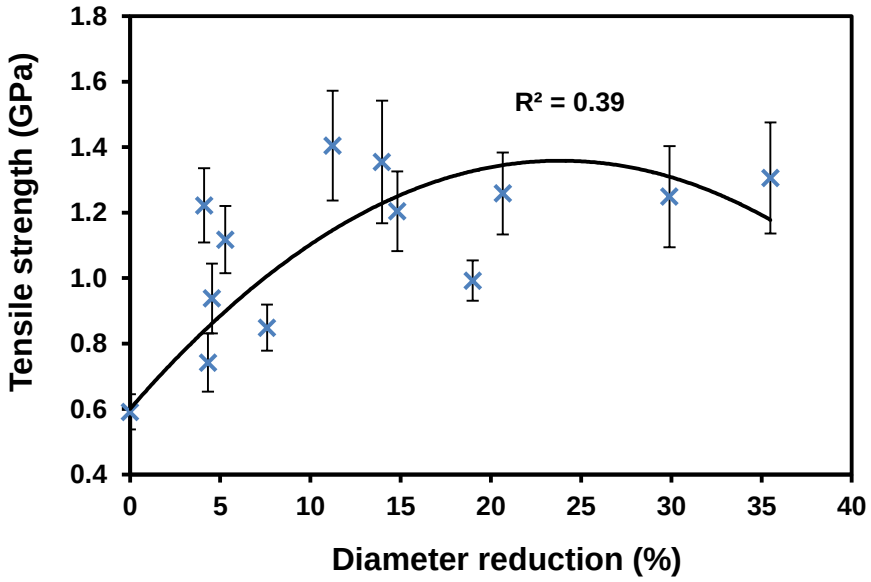

Figure 4-33 Tensile strength of glass fibres as a function of diameter reduction after various NaOH treatment concentrations and times

As shown in Figure 4-32, higher concentration treatments will continue to remove material without the benefit of improving the fibre strength. This should be avoided in order to preserve the yield of recycled and regenerated glass fibres. The relation between diameter and mass loss of the fibres is given in Equation 4-9, assuming material is only removed radially and uniformly during NaOH treatment.

Equation 4-9 Relation between diameter and mass loss of glass fibre

$$\Delta m \propto \Delta(D)^2$$

The relative mass reduction for the fibres after each treatment were calculated using Equation 4-10 with the fibre diameter values in Figure 4-26, where D_o is the average diameter of fluidised bed RGF and D is the average diameter of these fibres after NaOH treatment.

Equation 4-10 Relative mass reduction after NaOH treatment in terms of the change in fibre diameter

$$Mass\ reduction = \frac{{D_o}^2 - D^2}{{D_o}^2} \times 100$$

Figure 4-34 gives a plot of the regenerated strength of fibres as a function of fibre mass reduction by NaOH treatments, calculated from Figure 4-26 using Equation 4-10. The relative mass reduction is significantly higher than the diameter reduction, which is to be expected given the relation in Equation 4-9.

It appears from Figure 4-34 that the lower concetration treatments are not optimal in terms of strength regenration, mass loss and treatment time. Relative to the strength increase, glass fibre mass loss decreases significantly with treatment concentration. The treatment time required for sufficient strength regenration is also substantially shorter when using a higher concentrated solution. From Figure 4-34, the optimal conditions for treating fluidised bed RGF in terms of strength increase and mass loss is 7 mol/L for 120 min. These conditions yield the strongest glass fibres with a relatively low mass loss of around 20%. This treatment is simply the optimal based on the set of parameters used during this study, and the range of concentrations and treatment times investigated. The treatment may be further improved by investigating other factors such as:

- Treatment temperature
- Agitating fibres during treatment
- Alternate alkali/basic solutions
- Ratio between volume of NaOH solution and mass/surface area of the fibres

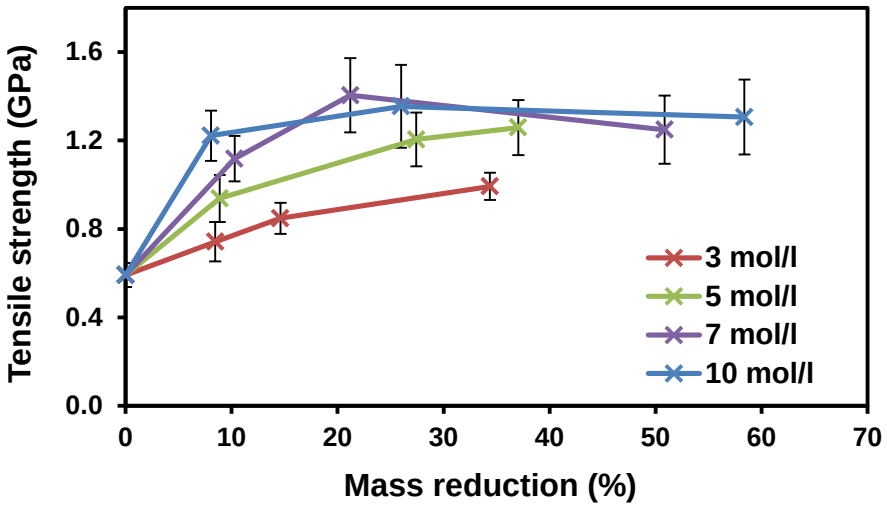

Figure 4-34 Relative mass reduction of NaOH treated fibres, calculated from change in diameters in Figure 4-26. As would be expected, glass fibre mass loss (as a result of etching in NaOH) depends on NaOH treatment time and concentration.

4.3.1.2 Effect of hot water on glass fibres recycled from in-house recyclate

Glass fibres recycled in the fluidised bed at 500 °C were soaked in deionised water at 90 °C for up to 336 hour in an attempt to increase their strength. Figure 4-35 shows the tensile strength of the fibres after the water treatment. Soaking in water for up to 32 hour provides no discernible improvement to the fibre strength. After soaking for 96 hour, the fibre strength increases to around 1 GPa, reflecting a 67% increase in strength.

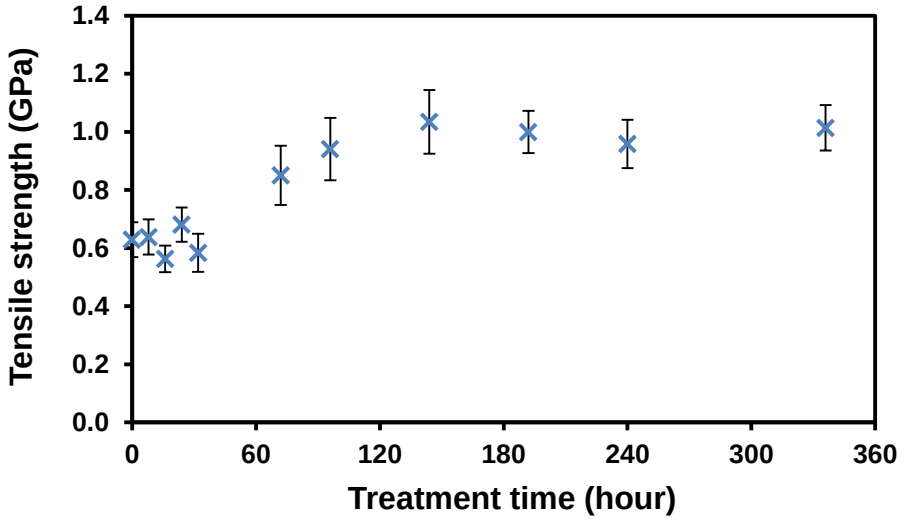

Figure 4-35 Tensile strength of fibres recycled in the fluidised bed followed by treatment in 90 °C water for 8, 16, 24 and 32, 72, 96, 192, 240 and 336 hour. Slight increase in RGF strength is observed in water treatments lasting 72 hour and greater.

This relative increase in strength is markedly higher than was observed by Ito and Tomozawa when performing water treatments on silica glass rods [186]; only a 12% and 20% increase in strength was attained after soaking for around 100 hour and 240 hour respectively. Figure 4-35 also shows that extending the treatment time for glass fibres above 96 hour does not lead to further improvement in strength. In contrast, the reported strength increase of silica glass rods does not plateau until soaking in water for 360-480 hour. The disparate behaviour may be caused by the difference in geometry of flaws/cracks present on the surface of the glass fibres compared to the rods. The length of the crack present on the surface of silica glass rods after abrading in [186], was found to be around 180 um. In contrast, the crack length on fluidised bed RGF (as given in Table 4-6) was estimated using fracture mechanics to be 400-950 nm, depending on flaw geometry. The flaw length of the

glass fibres is therefore likely to be three orders of magnitude less than those present on the silica rods in [52, 186]. As discussed previously, crack blunting, through dissolution and precipitation, has been proposed as a mechanism for improving the strength of glass after water soaking [50, 52, 186]. With this in mind, the smaller flaws present on the surface of fibres may explain the enhanced effect water soaking has on the relative strength improvement of glass fibres over glass rods. Less precipitated material would be required to reduce the tip radius of flaws on glass fibres, therefore, a reduction in tip radius sufficient to observe an increase in strength may occur more rapidly in the case of glass fibres.

An alternative mechanism for strength increase involving the formation of compressive stress around the crack tip, in turn “shielding” the crack, was also proposed [143-145]. Despite predicting that water treatments would not improve the strength of fibres having submicron flaws, Figure 4-35 clearly suggests otherwise. Wiederhorn et al. were referring to pristine glass fibres (estimated strength of 5 GPa), concluding that any benefit from the compressive stress around the crack tip would be obfuscated by the inherent high strength of the fibre. For the case of fluidised bed recycled glass fibre (or fibre treated at sufficiently high temperature) the residual strength is significantly reduced and is in fact closer to that of the abraded glass rods [186]. The strength increase in Figure 4-35 may therefore arise through the mechanism outlined in [143-145].

Figure 4-36 shows the change in diameter of the glass fibres after the water treatments. There is a general trend of increasing diameter loss with treatment time, which closely follows a second order polynomial. No relation was observed for treatment times that failed to yield any improvement in fibre strength. Figure 4-36 also includes the diameter change of silica rods (3 mm diameter) observed by Ito and Tomozawa [186], when treated in water under similar conditions. The relative change in diameter is slightly higher for glass fibres; however, given the error bars it is not significant. No error was present for the silica rods in [186].

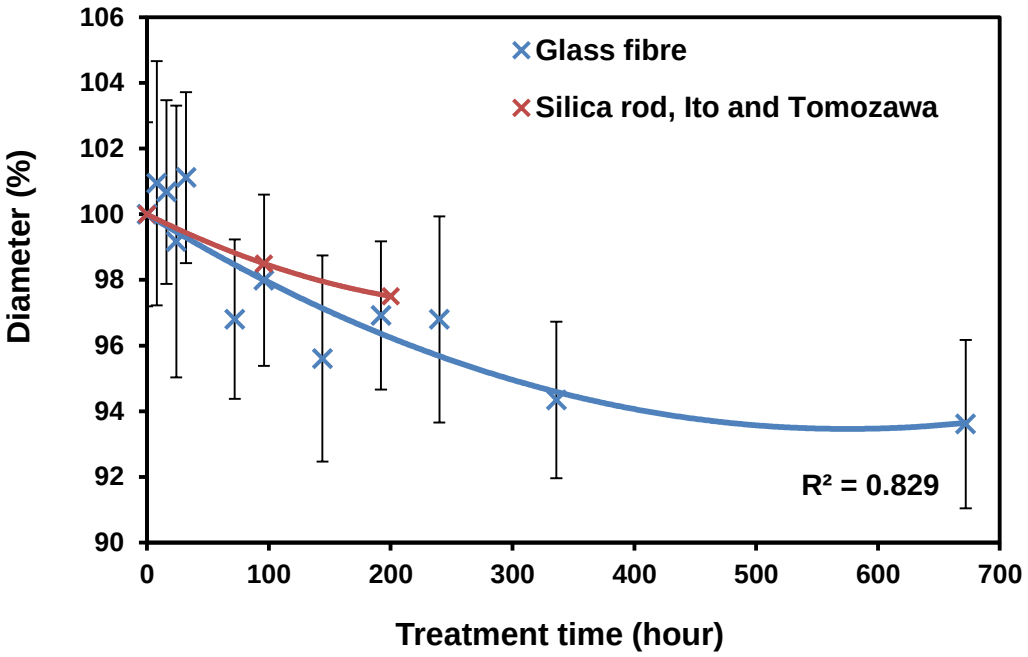

Figure 4-36 Change in diameter of glass fibres recycled in the fluidised bed followed by treatment in 90 °C water for 96, 192 and 240 hour compared to that of silica rods, reproduced from [80]

Unlike the high-silica rods used in [186], the E-glass fibres used in this work only contain around 60% silica, with the remaining constituent material comprising various metal oxides [140]. Al_2O_3, TiO_2 and Fe_2O_3 are unreactive with hot water and are insoluble/sparingly soluble in water. The oxides of alkaline earth metals CaO and MgO will react with water as shown in Equation 4-11 and Equation 4-12 respectively.

Equation 4-11 Chemical reaction between calcium oxide and water

$$CaO + H_2O \rightarrow Ca(OH)_2$$

Equation 4-12 Chemical reaction between magnesium oxide and water

$$MgO + H_2O \rightarrow Mg(OH)_2$$

The hydroxides of Ca and Mg are only sparingly soluble in water. The oxides of alkali metals Na_2O and K_2O will react with the water as shown in Equation 4-13 and Equation 4-14.

Equation 4-13 Chemical reaction between sodium oxide and water

$$Na_2O + H_2O \rightarrow 2NaOH$$

Equation 4-14 Chemical reaction between potassium oxide and water

$$K_2O + H_2O \rightarrow 2KOH$$

The hydroxides of alkali metals will readily dissolve in water; however, they are present in very low quantities in E-glass fibres and are unlikely to significantly alter the pH of the water during the treatment. The lower silica content may result in more rapid relative mass loss of the glass fibres and precipitation of the insoluble metal oxides. The measured reduction in diameter (used to produce Figure 4-36) was in the range 0.35-0.56 μm. Given the estimated flaw lengths in Table 4-6, even removing such little material would significantly reduce the length of flaws present on the recycled fibre surface. The mechanism for the strength increase in Figure 4-35 is yet to be conclusive; however, reducing the flaw length through dissolution of the glass surface may contribute.

Although there is an apparent trend of diameter reduction with water treatment time, there is a large variation in diameter within each data point. This results in a large error relative to the change in diameter, therefore, no definitive conclusion can be made as to the significance of the change in average diameter observed in Figure 4-36. To resolve this, a technique outline by Bashir et al. could be employed which involves measuring the same glass fibre under SEM before and after the treatment [141]. This removes the large error induced by the variation in initial diameter between fibres as well as obtains a more accurate diameter measurement due to the enhanced magnification provided by SEM.

Figure 4-37 - Figure 4-40 show SEM images of fibres after treatment in 90 °C water for various durations. The small particles on the surface of the fibres may be attributed to residues from the recycling process, presumably un-decomposed epoxy in the form of char. The degree of contamination on the fibre surface appears to diminish after water treatment. If the residue is carbonaceous char, it will not dissolve in water therefore it is likely removed purely through physical forces during the treatment process. There does not appear to be any change to the surface morphology of the glass fibres after the various water treatments. Therefore, no

further inferences can be made as to the strengthening mechanism of hot water treatments base on the SEM images of the fibre surface.

Although the effect of hot water is positive, the resulting fibre strength is still low at around 40% of the as received fibre strength. Despite the long treatment time, in an industrial continuous process this may not necessarily be an issue. RGF can be continuously treated in one or many water baths, which will then continuously supply regenerated fibres for next processing stages. Undoubtedly, an advantage of the water treatments over NaOH is the inexpensive material cost and few processing steps.

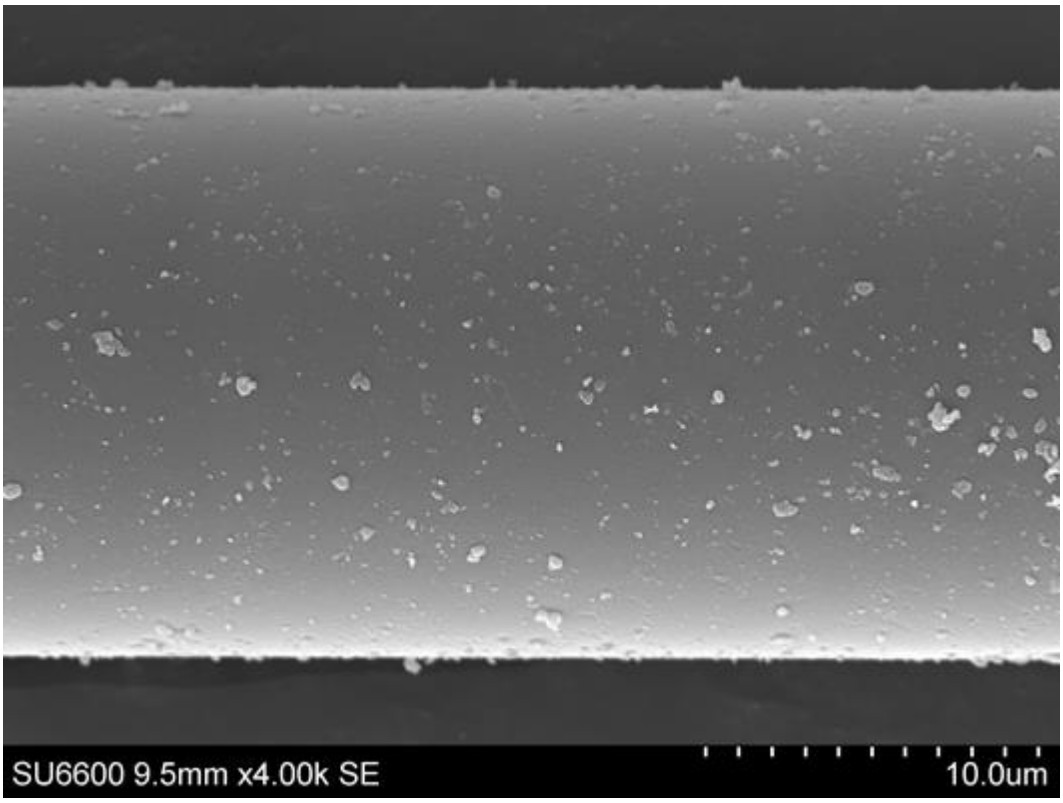

Figure 4-37 SEM image of fluidised bed recycled glass fibre without water treatment

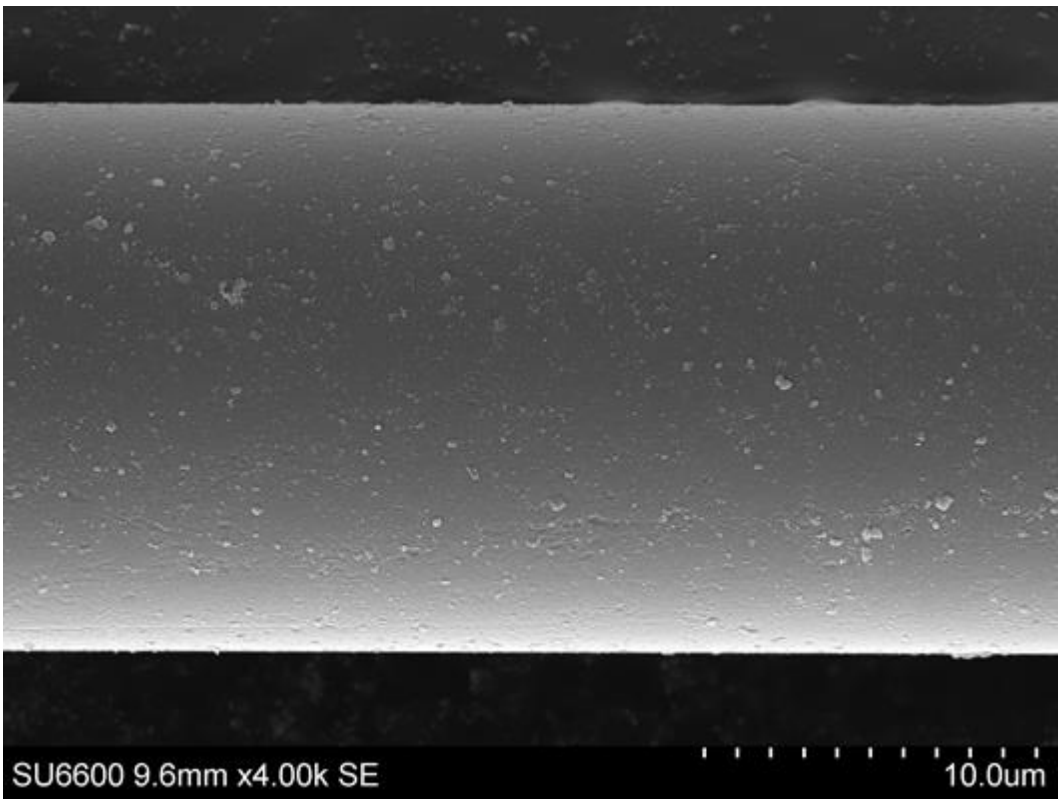

Figure 4-38 SEM image of fluidised bed recycled glass fibre treated with 90 °C water for 96 hour

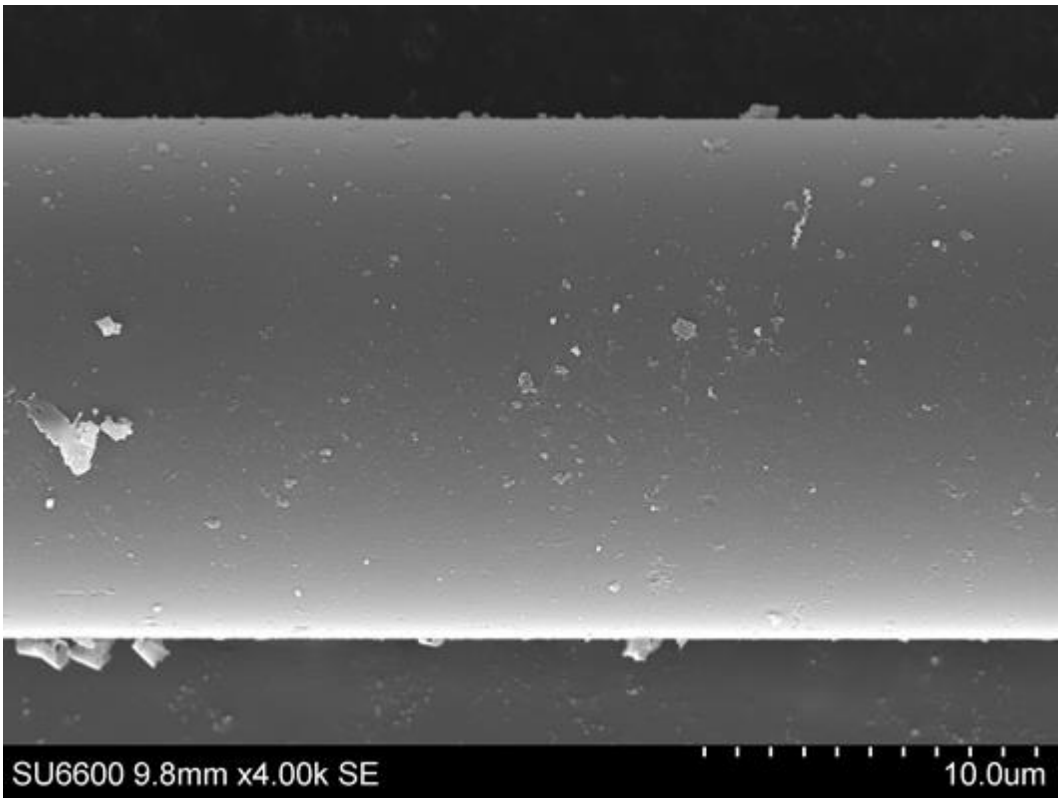

Figure 4-39 SEM image of fluidised bed recycled glass fibre treated with 90 °C water for 240 hour

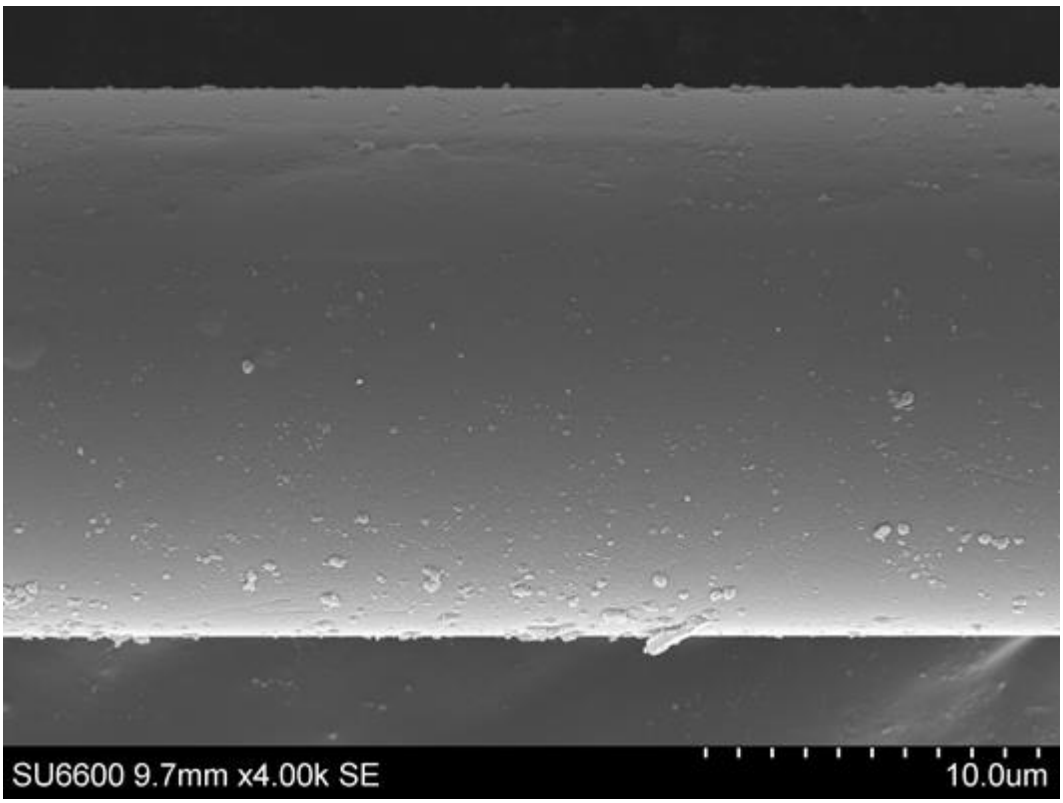

Figure 4-40 SEM image of fluidised bed recycled glass fibre treated with 90 °C water for 336 hour

4.3.1.3 Effect of water vapour on glass fibres recycled from in-house recyclate

Glass fibres recycled in the fluidised bed at 500 °C were treated in saturated water vapour at 250 °C for up to 96 hour in an attempt to increase their strength. Figure 4-41 shows the tensile strength of the fibres after the water vapour treatment. In the range of treatment times tested, the water vapour has showed no effect on the strength of the RGF. Contrary to this, it was observed by Li and Tomozawa [52] that water vapour treatments were far more effective than hot water treatments at increasing the strength of abraded silica rods [186]. Similarly to Li and Tomozawa [52], no reduction in glass fibre diameter was observed when treating the fibres in water vapour.

Given that the mechanism for strengthening with water/water vapour is still unclear, the cause for water vapour not affecting the fibre strength is as yet unknown. Li and Tomozawa conclude that the strengthening mechanism for water vapour is crack blunting via either 1) dissolution or precipitation of material at the crack tip or 2) water diffusion reducing the glass viscosity, leading to viscous flow of the surface layer near the crack tip [52]. These mechanisms are similar to that given for

strengthening glass in hot water. Since soaking in hot water was effective in partially regenerating the strength of recycling fibres as shown in Figure 4-30, it is unclear why the vapour treatments were ineffectual.

As is widely understood, and demonstrated in Chapter 3, that temperature is a key factor in determining the strength of thermally conditioned glass fibres. In this work, glass fibres were not subject to such a low conditioning temperature within an air environment. It is therefore unclear what effect prolonged exposure to a 250 °C environment alone will have on the strength of glass fibre. Feih et al. thermally conditioned glass fibres at 250 °C in air for 2 hour [31]. It was observed that the strength of the fibres was around 95%, relative to as received fibres. No other treatment times were presented so it is unclear whether this is the steady state strength of the fibres at 250 °C. It was shown by Feih et al. that fibres take longer to reach a steady state strength value when exposed to lower temperatures, therefore, further damage may be caused to the fibres by extending the vapour treatment up to 96 hour.

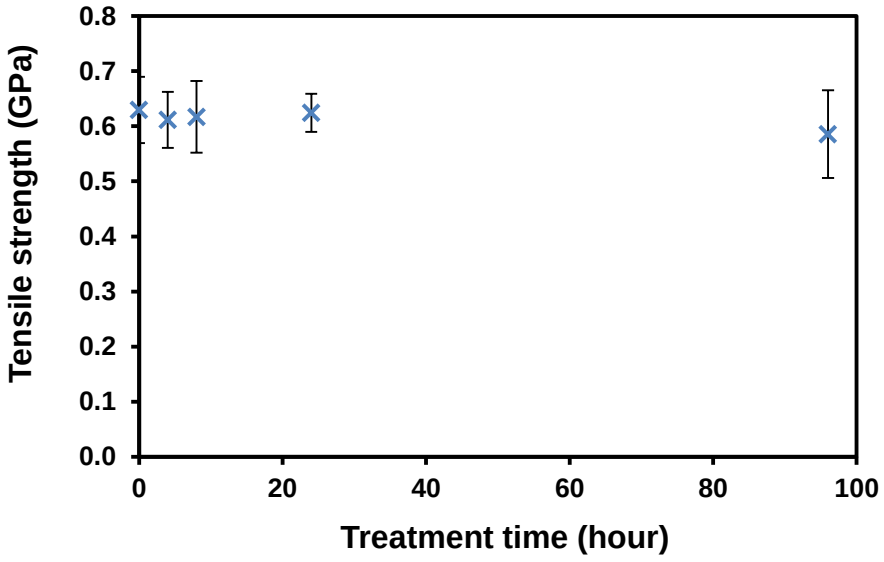

Figure 4-41 Tensile strength of fibres recycled in the fluidised bed followed by treatment in 250 °C water vapour for 4, 8, 24 and 96 hour. No change in RGF tensile strength was observed as a result of exposure to water vapour under the conditions tested.

4.3.1.4 Effect of hot APS on glass fibres recycled from in-house recyclate

In accordance with the method outlined by Saez-Rodriguez [142], fluidised bed RGF were initially treated in hot APS solution for just 15 min. Table 4-7 shows that there is no observed improvement in fibre strength after the hot APS treatment. Saez-Rodriguez reported an increase in strength from 0.98±0.05 GPa to 1.22±0.09 and 0.64±0.06 GPa to 0.89±0.05 GPa when treating fibres in hot APS that were thermally conditioning at 500 °C and 600 °C respectively [142]. The strength of fluidised bed RGF are comparable to those thermally conditioned at 600 °C in [142]. If flaws control the fibre strength, it would follow that the surface of these fibres exhibit similar degrees of damage; therefore, it is unclear why fluidised bed recycled fibre exhibit no increase in strength after hot APS treatment. As can be seen in Figure 4-22, processing in the fluidised bed causes substantial mechanical damage to the fibres, in addition to thermal weakening. Since fibres were thermally conditioned in a furnace in [142], it is likely the predominant mechanism for strength loss is related to thermal effects. It is unknown if/how flaws generated through thermal and mechanical damage differ in terms of scale or geometry, or how this would influence the effectiveness of the hot APS treatment.

Table 4-7 Tensile strength of fibres recycled in the fluidised bed followed by treatment in 83 °C APS for 15 min

Sample	Tensile strength (GPa)
Recycled glass fibre	0.63±0.06
Recycled glass fibre+ hot APS for 15 min	0.58±0.05

The effect of hot APS on recycled fibre strength was further investigated by extending the duration of the treatment. It is understood that solution of hydrolysed APS is basic, with a natural pH of 10-11 [187]. Given the increase in strength after treating in NaOH solution, it was postulated that extending the treatment in basic APS could also yield improvements in fibre strength. It is thought that the hydrolysed APS could react with water in the solution to produce hydroxide ions, as shown in Figure 4-42. The hydroxide ion could then react with the silica network in the glass fibre as shown in Equation 4-2.

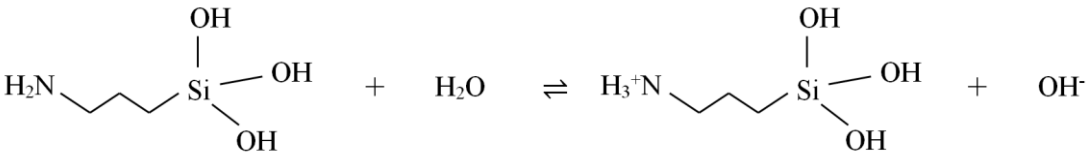

Figure 4-42 Reaction between APS and water to produce hydroxyl ion

Figure 4-43 gives the strength of the RGF after the hot APS treatment for 24, 120 and 240 hour. No strength regeneration was observed as a result of increasing the treatment times. The NaOH solutions used in Figure 4-24 are substantially more basic with a pH>14 for all treatments. The APS solution might not have been basic enough to disrupt a significant portion of the silica network, as was observed when treating in NaOH. No significant change in fibre diameter was observed across the range of treatment times investigated. This is in agreement with Yue and Quek who observed that immersion time is not a key factor in silane deposition on glass fibre surface [188].

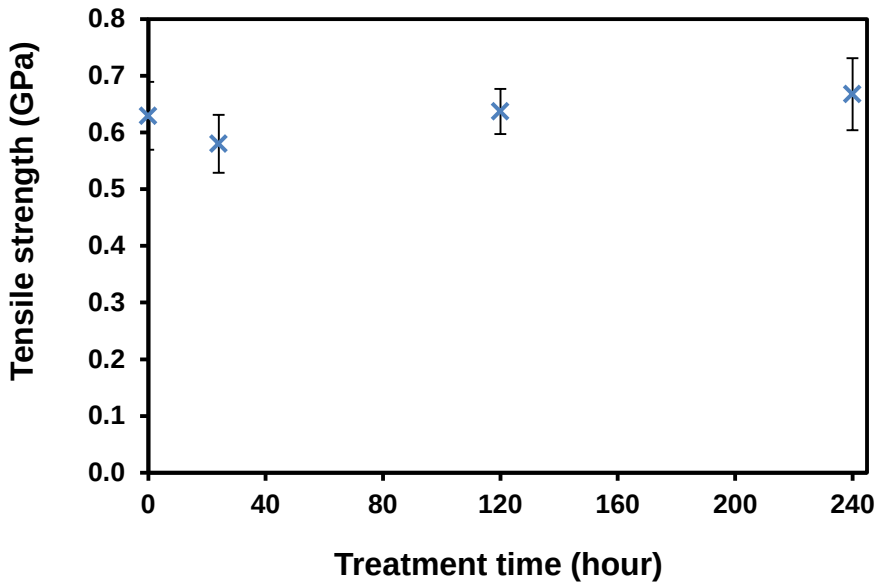

Figure 4-43 Tensile strength of fibres recycled in the fluidised bed followed by treatment in 83 °C APS for 24, 120 and 240 hour. Hot APS provided no improvement in the strength of RGF under the conditions investigated.

The solution used to treat the fibres in Figure 4-43 is very dilute at only 1 vol% APS. If the presence of APS itself does not increase fibre strength, one may presume that soaking in hot water would still improve the fibres strength to a level seen with the hot water treatment in Figure 4-35. The temperature used for the APS treatment was lower than the hot water treatment. The difference is slight however, and not an entirely satisfying explanation as to the disparity in the fibre strength data. This could be examined by also carrying out the hot APS treatment at 90 °C, in line with the hot water treatment, then comparing the fibre strength. It was observed that after drying, the APS treated fibres were firmly stuck together in a bundle. This is likely due to a silane network forming and bonding adjacent fibres together during drying. This made extracting a single glass fibre for tensile testing difficult. It is therefore plausible that the fibres sustained additional mechanical damage during sample preparation, which obfuscates any strength improvement gained during the hot APS treatment. To confirm this, RGF could be separated prior to hot APS treatment and avoid contact with other fibres until after the drying processes.

4.3.1.5 Glass fibres recycled from wind turbine blade

Table 4-8 outlines the recycling conditions and various regenerative treatments applied to the fibres recycled from real world scrap GRP. NaOH and hot water treatment were selected since only these demonstrated any fibre strength regeneration when applied to fibres recycled from the in-house recyclate.

Table 4-8 Outline of the various regeneration treatments used on fibres recycled from wind turbine blade

Treatment	Description
RGF	Glass fibres recycled in Fluidised bed at 500 °C with fluidisation velocity of 1.5 m/s
APS	1 vol% APS solution for 15 min at RT
NaOH	7 mol/L NaOH solution for 2 hour at 95 °C
Water	Deionised water for 4 days at 90 °C

Figure 4-44 gives the tensile strength of RGF before and after treatment in NaOH and hot water. Given the size of the recyclate, single fibre tensile testing was carried out at a gauge length of 5 mm. The strength of RGF from in-house prepared recyclate was also tested at 5mm for a comparison and the data is included in Figure 4-44. The tensile strength of fibres recycled from the end-of-life turbine blade, in Figure 4-44, approximates those recycled from in-house prepared GF-EP recyclate. Treatment in NaOH solution significantly increases the strength of these RGF. With an average tensile strength of 1.7 GPa, the fibres recycled from real world scrap respond even more favourably to the NaOH strength regeneration treatment than fibres recovered from the in-house recyclate. Figure 4-44 helps to validate the effectiveness, and potential for, NaOH solution to be used as a strength regeneration treatment on glass fibres recycled from commercial GRP scrap.

Soaking in hot water for 4 days yielded the same strength regeneration when applied to the fibres recycled from the scrap turbine blade. No further improvement in fibre strength was observed for water treatments extended longer than 4 days in Figure 4-35; therefore, no additional soaking times were explored in this section.

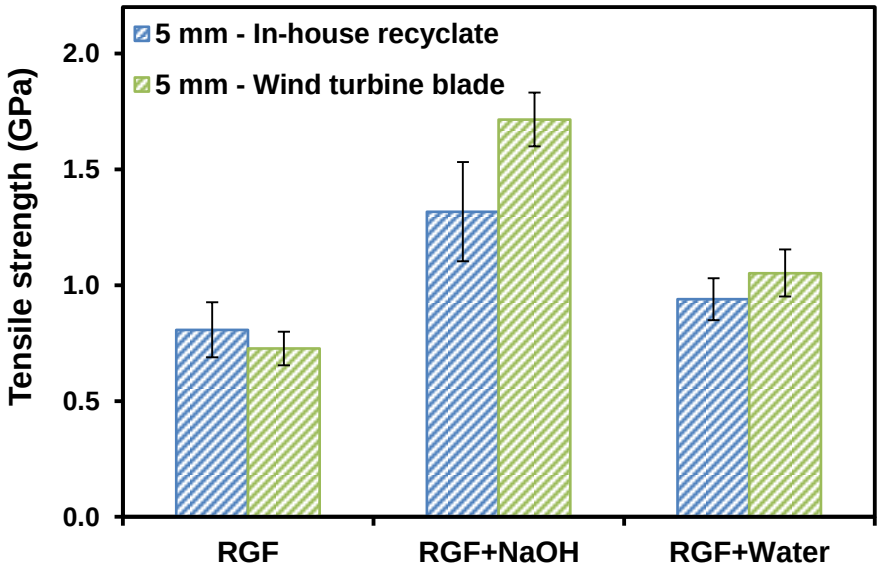

Figure 4-44 Strength of RGF from both recyclate before and after various strength regeneration treatments at a gauge length of 5 mm. As was observed when using the in-house prepared recyclate, glass fibres recycled from the real world scrap also show an increase in strength after treating in NaOH and hot water.

Figure 4-45 gives the relative diameter of both recyclate after the NaOH and hot water treatments. The diameter reduction of RGF from the wind turbine blade after NaOH treatment is approximately 35%, which is significantly higher than was observed when treating fibres recycled from the in-house produced GRP. All fibres previously recycled were E-glass, however, it is unknown what grade of glass fibre was used in the production of the turbine blade. It is understood that C-glass and D-glass exhibit far poorer durability to alkali solution (Na_2CO_3), with an order of magnitude greater mass loss observed relative to E-glass fibres [189]. E-glass is more widely used however, and is the main fibre used in the production of wind turbine blades and GRP in general [190]. It is therefore probable that the glass fibres from the scrap wind turbine blade are indeed E-glass and similar in composition to the fibres used to prepare the in-house recyclate. It would therefore be expected that the etching rates between these fibres would be comparable under identical alkali conditions.

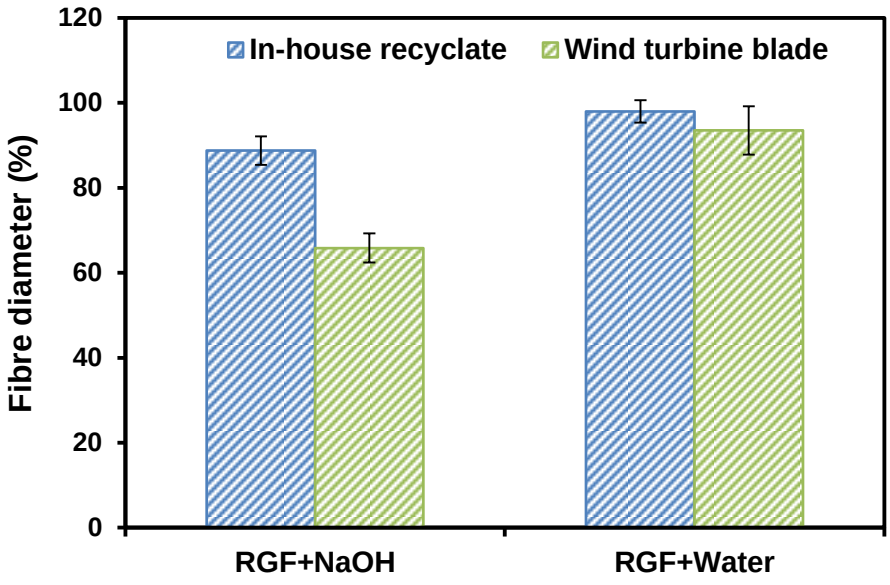

Figure 4-45 Relative diameter for both recyclate after various strength regeneration treatments, showing that glass fibres recycled from the real world scrap exhibit higher surface etching rates.

The fibre layup within the turbine blade was examined by ashing a small section of the blade material. It was observed that plies of varying architecture were present through the thickness of the blade; comprising unidirectional, woven and chopped strand mat. The source of these fibres is unknown, or whether they are produced by

differing manufactures. Further work could be carried out to find the average diameter of fibres within each layer independently. The apparent fibre diameter reduction in Figure 4-45 would be inaccurate if inadvertently comparing fibres from plies of differing initial diameters. A controlled study focusing specifically on the etching rate of RGF (similar to Bashir et al. [34]), as well as an investigation into whether this varies between GRP recyclate/glass fibre composition and manufacturer is required. As before, there appears to be a slight decrease in fibre diameter after the water treatment however, this cannot be established given the diameter distribution within the recyclate.

4.3.1.6 Influence of gauge length on glass fibre strength

Figure 4-46 compares the strength of RGF after various treatments at a gauge length of 20 mm and 5 mm. The initial recyclate dimensions were 60x15 mm and 10x10 mm for the RGF tested at 20 mm and 5 mm respectively. Figure 4-46 shows that only the RGF without subsequent regeneration treatments exhibit any significant variation in fibre strength with gauge length. It is widely understood that the strength of glass fibres is dependent on the gauge length used, since the probability of a flaw of a given severity being present increases with the surface area of the fibre sample [48]. An increase in strength when testing at 5 mm would therefore be expected for each specimen. It was observed that the recycled only fibres frequently failed when mounting into the tensile tester. The short gauge length meant that any movement of the sample during mounting resulted in significant straining, and often failure of the fibre. The recycled only fibres failed around 50% more often during mounting than the fibres treated with NaOH and hot water. This may inadvertently select for the strongest fibres contributing to the average strength, since only these fibres can survive the mounting process. The value for the average RGF strength could therefore be artificially increased. It is currently unclear whether this, or if the reduced probability of a strength determining flaw being present, is the cause for the increase in fibre strength. Since all the fibres tested in Figure 4-44 are, to varying degrees, weaker than as received fibres, they are more populated with surface flaws. If the flaws are ubiquitous on the fibre surface, they may still be statistically likely to be present on the fibre at both gauge lengths tested. The effect of gauge length on virgin fibre strength is well understood in the literature; however, less is reported for weakened fibres.

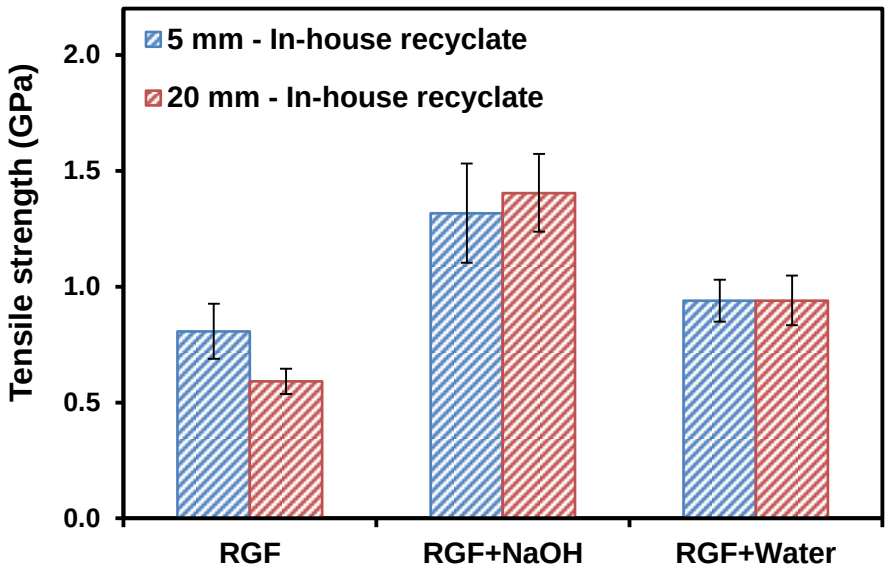

Figure 4-46 Strength of fibres recycled from in-house prepared recyclate after NaOH and hot water treatment at 5 and 20 mm gauge length

Throughout this, and previous chapters of this thesis, a gauge length of 20 mm was used to measure the single fibre tensile strength. The length of RGF used to produce GRP in Chapter 5 are considerably shorter than 20 mm, given the recyclate is cut into 10x10 mm pieces prior to processing in the fluidised bed. (This level of downsizing was carried out because the process used in Chapter 5 to prepare GRP demands so.) The strength of fibres recyclate from the 10x10 mm recyclate using a gauge length of just 5 mm is therefore more representative of the actual fibre strength within GRP in Chapter 5.

4.3.2 Recycled glass fibre – polymer interface

In this section the interfacial adhesion between RGF and 1) PP matrix and 2) epoxy matrix are investigated. Two interface regeneration treatments, RT APS and HCl, are also explored. Table 4-9 summarises this information and shows the fibres used to study each matrix material.

Table 4-9 Summary of the matrix material, source of recycled fibre and regeneration treatment used to investigate the IFSS between polymer and RGF

Matrix material	Source of RGF	Interface regeneration treatment investigated
PP	In-house prepared GF-EP	RT APS HCl
Epoxy	Scrap wind turbine blade	RT APS

4.3.2.1 IFSS between recycled glass fibre and polypropylene

The IFSS between fibres recycled from the in-house prepared recyclate and PP were measured using the microbond technique. RGF treated with and without NaOH were tested, where the NaOH treatment used was 7 mol/L solution for 2 hour. Other than NaOH, two treatments were applied to the RGF in an attempt to improve their adhesion with PP: 1) HCl treatment and 2) APS treatment. As discussed in the literature, exposing glass fibres to elevated temperatures has been demonstrated to remove surface hydroxyl groups [62, 64], whereas subsequent soaking in HCl has been reported to rehydroxylate the fibres [63].

Figure 4-47 shows the IFSS between PP and RGF after the various treatments. As a control, Figure 4-47 also gives the IFSS when using new glass fibres supplied by Owens Corning, denoted “New”. New glass fibres were supplied by Owens Corning in a roving. These were selected as a control in this work as they were either unsized or coated with APS alone, opposed to a commercial sizing blend. For reference, the IFSS with and without APS applied to thermally conditioned (at 500°C) fibres, found by Nagel has also been included [68].

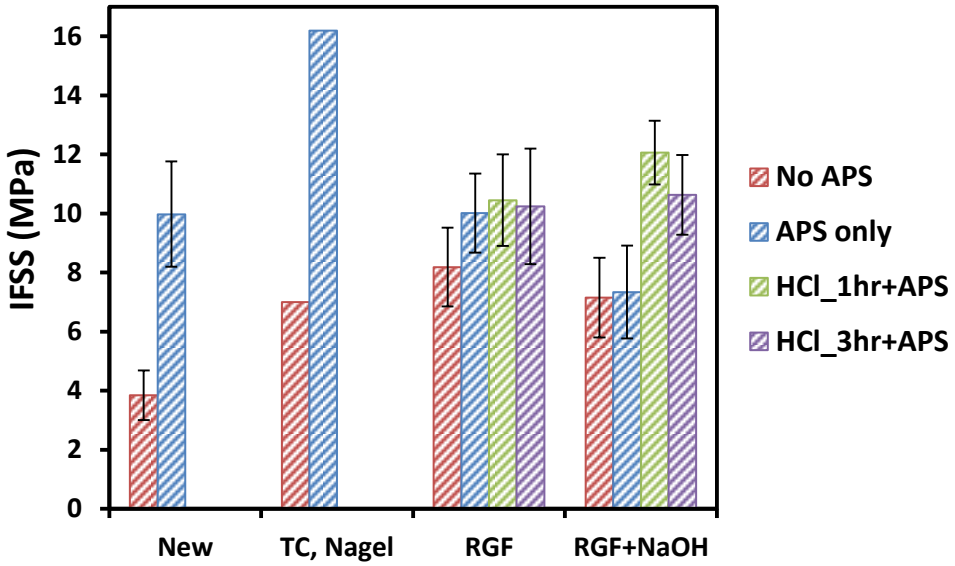

Figure 4-47 IFSS between PP and glass fibres after the various treatments, Nagel data reproduced from [68]

The IFSS of the RGF prior to any treatment approximates that reported by Nagel [68]; however, is slightly less than was observed by Thomason et al. after thermally conditioning fibres at the same temperature [15]. The new, unsized glass fibres, exhibit significantly weaker interfacial adhesion than both the thermally conditioned fibres in [68], and the fluidised bed RGF. The measured value for IFSS with bare glass fibres closely matches that reported by Thomason [191] and Min et al. [192]. With a fluidised bed temperature of 500 °C, the organic portion of the silane coupling agent present on the fibres in the recyclate will decompose during recycling [32]; however, the silane network which is deposited on the fibre surface will remain, given the high thermal stability of such material. Although there no longer remains amino functional groups for the polymer to interact with chemically, it is yet unclear how this deposited silane layer (after thermal conditioning/recycling) influences the IFSS with PP.

APS treatment alone slightly increases the IFSS of RGF, however, given the error; it is not clear how significant the apparent rise in IFSS is after coating in APS. This is in contrast with new glass fibres, which, when treated with APS, exhibit a near threefold increase in IFSS. Thomason et al. [15], Yang et al. [5] and Nagel [68] (shown in Figure 4-47) also observed a significant increase in IFSS between thermally conditioned glass fibres and unmodified PP when APS was used. This is contradicted by other studies [155-158], which found that amino-silane coupling

agents alone do not improve the adhesion with unmodified PP; concluding that PP has to be modified with an acidic group to interact with APS. Although PP may not chemically bond with APS, weaker intermolecular forces (such as van der waals forces) may increase adhesion, specifically via the electronegative amino functional group.

No increase in IFSS for NaOH treated RGF (RGF+NaOH) was observed when using APS alone. According to the literature, a product of etching with NaOH is silanol on the glass surface, caused by the cleaving of siloxane [141]. It may therefore be expected that RGF+NaOH would have higher IFSS (than RGF) when coated in APS, due to higher hydroxyl group concentration and better APS bonding. This was not observed; moreover, the IFSS with RGF is significantly higher than with RGF+NaOH when APS is used.

When comparing the effect of APS on IFSS with PP in Figure 4-47, it is worth reiterating that fibres used for the new, thermally conditioned [68] and RGF data points are all from different sources/suppliers. As such, comparing the exact values for IFSS may be less valuable than observing the trends themselves. It is clear from Figure 4-47 that using APS significantly improves the IFSS when used with new and thermally conditioned fibres [68], whereas RGF do not respond so favourably.

Figure 4-47 shows that treating RGF in HCl prior to applying APS provides no additional improvement to IFSS with PP. There is little difference in RGF IFSS for all four samples tested (particularly when accounting for relatively large errors) which suggests that 1) the APS is not bonded to the glass surface, or 2) the APS is bonded to the glass surface however the amino functional group of APS has limited interaction with the PP. The cause for the lack in IFSS regeneration cannot be established from the data given in Figure 4-47 and is further explored using FTIR below.

Treating the RGF+NaOH in HCl significantly improves the IFSS with PP. Whether this is caused by rehydroxylation of the glass surface by action of the HCl, as proposed by González-Benito et al. [63], cannot yet be established. Since the HCl was ineffective when applied to RGF, an alternative cause for the rise in RGF+NaOH IFSS may simply be removal of NaOH treatment residues that were contaminating the fibre surface. Poorly adhered residue on the surface may block APS/PP from interacting with the glass fibre leading to a low apparent IFSS with PP. This could be indirectly tested by applying HCl rinse for a brief amount of time

(rather than hours); given that HCl and NaOH reaction can readily happen. Comparing the IFSS between shorter and longer HCl treatments could give insight into whether surface residue is in fact present and influencing adhesion. The predominant residue that would be expected on the RGF+NaOH surface are NaOH and Na_2SiO_3, both of which would interact with HCl through acid-basic reactions shown in Equation 4-15 and Equation 4-16 respectively.

Equation 4-15 Chemical reaction between sodium hydroxide and hydrofluoric acid

$$HCl + NaOH \rightarrow NaCl + H_2O$$

Equation 4-16 Chemical reaction between sodium silicate and hydrofluoric acid

$$2HCl + Na_2SiO_3 \rightarrow 2NaCl + SiO_2 + H_2O$$

Sodium chloride (NaCl) will readily dissolve in the HCl solution while SiO_2 would precipitate. An SEM image of the surface of RGF treated in 7 mol/L NaOH for 2 hour is given in Figure 4-29. It cannot be conclusively determined through SEM alone whether the surface is contaminated with residue. Further investigation into the RGF+NaOH surface and adhesion with APS is further explored with FTIR below.

4.3.2.2 Investigation into glass fibre surface functionality after chemical treatments using FTIR

FTIR was used to analyse the effect of HCl treatment on the composition of the surface of RGF as well as the interaction between APS and the fibre surface. All fibres treated under the conditions in Figure 4-47 were characterised using FTIR. Additionally, RGF with and without NaOH treatment (7 mol/L for 2 hour) were characterised after HCl treatment for 1 and 3 hour. Figure 4-48 - Figure 4-51 show the IR spectra of the various RGF. The broad band of 3650 - 3000 cm^{-1} correlates to the presence of hydroxyl groups, with silanol specifically around 3650 cm^{-1} . The signal that appears in each spectra around 2340 cm^{-1} represents O=C=O stretching and appears commonly in IR spectra. The apparent large peak at 1250 cm^{-1} for each spectrum is a point of inflection as a consequence of the reststrahlen effect [193], where features at lower wavenumbers from this point are all negative primarily

due to concomitant changes in refractive index with IR absorbance. As a result, the siloxane peak centred around 900–1100 cm^{-1} appears inverted.

Figure 4-48 is the IR spectra for RGF treated only with HCl. Treating with HCl, for 1 and 3 hour, does not significantly affect the absorbance of silanol/hydroxyl in the spectra. This is in contrast to González-Benito et al. who observed an increase in silanol/hydroxyl intensity after treating in HCl [63]. Siloxane absorbance is slightly lower after HCl treatments suggesting there may be some break-up of the silica network. Figure 4-49 shows the IR spectra for the fibres in Figure 4-48 after the application of APS. RGF treated only with APS exhibit significantly higher silanol/hydroxyl concentration with a corresponding low siloxane absorbance, which suggests the APS is poorly polymerised. Some organic peaks also appear (CH_2/CH_3) which come from the APS and are not well resolved, suggesting poor bonding of APS to the glass fibre. HCl treatment prior to the application of APS results in lower silanol/hydroxyl absorbance and greater intensity of the siloxane peak than APS treatment alone. This suggests greater polymerisation of the APS. Also, the APS peaks are better resolved, indicating better attachment of the APS to the glass surface.

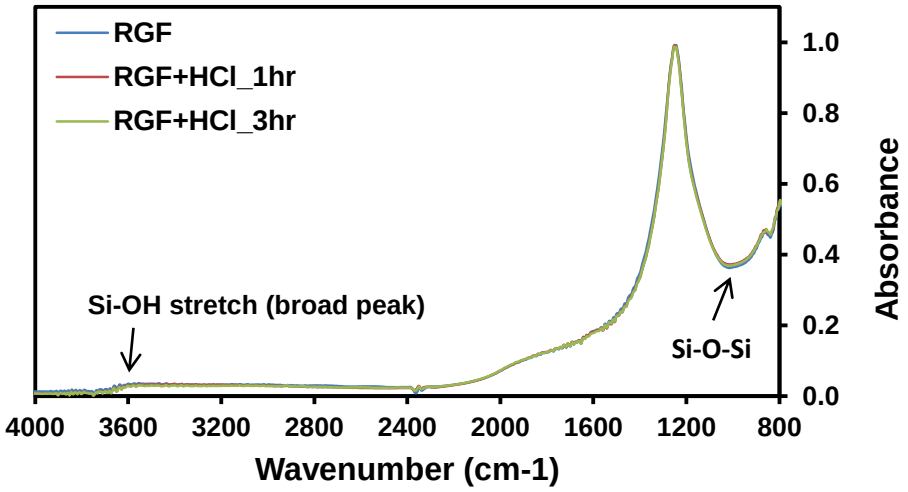

Figure 4-48 IR spectra of RGF and RGF+HCl

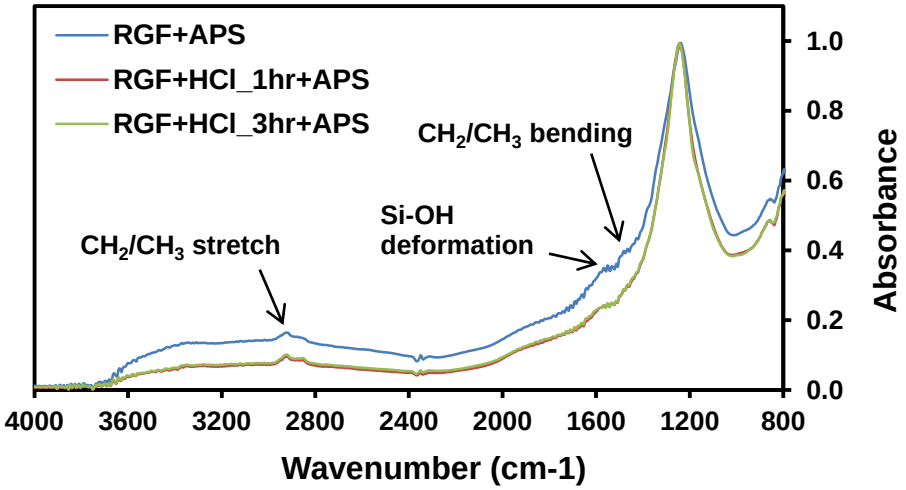

Figure 4-49 IR spectra of RGF+APS and RGF+HCl+APS

Figure 4-50 shows the IR spectra for RGF treated with NaOH and compares the effect of HCl treatments. NaOH treatment alone increases silanol/hydroxyl absorbance and decreases siloxane absorbance of the glass fibres. This suggests the siloxane network is attacked by the hydroxide (from the NaOH solution) to form silanol, which is typically given as the product in the literature [141]. The increase in apparent silanol/hydroxyl absorbance may however be a result of hydroxide groups from NaOH residue on the fibre surface. The silanol/hydroxyl absorbance decreases with HCl treatment time which is again contrary to González-Benito et al., who observed hydroxylation of the glass surface after HCl treatment [63]. However, because these fibres were NaOH treated, the decrease in silanol/hydroxyl absorbance after HCl soaking could be due to the removal of residual NaOH rather than silanol.

Figure 4-51 gives the IR spectra for the fibres in Figure 4-50 after the application of APS. Treating the fibres in NaOH then APS increases silanol/hydroxyl and decreases siloxane absorbance. This is likely due to several reasons such as, hydroxide attack of the glass during NaOH treatment, NaOH residue, and un-polymerised APS.

When these fibres are treated in HCl prior to coating with APS, the silanol/hydroxyl absorbance is lowered and the siloxane absorbance increases. There are also better resolved organic peaks around 2960 – 2850 978 cm^{-1}, suggesting better attachment of APS to the glass and greater degree of polymerisation than without

HCl treatment. It appears that the 1 hour HCl treatment decreases the silanol/hydroxyl and increases the siloxane absorbance greater than the 3 hour HCl treatment.

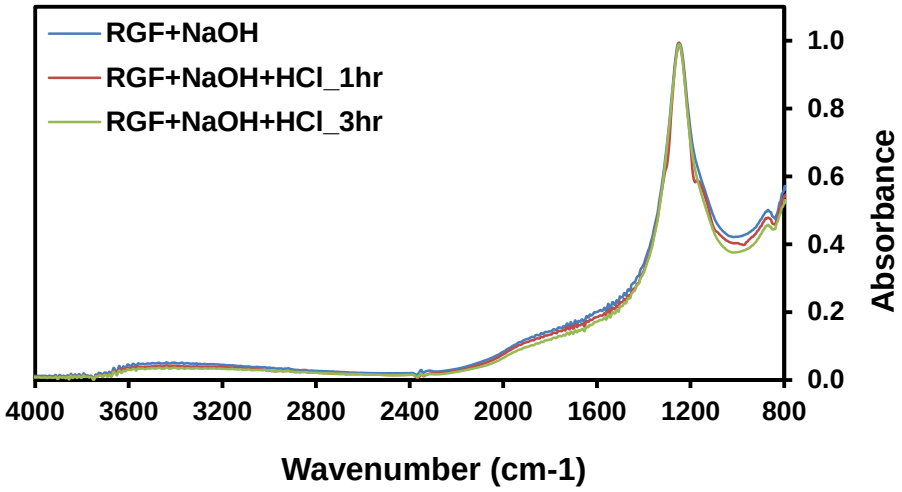

Figure 4-50 IR spectra of RGF+NaOH and RGF+NaOH+HCl

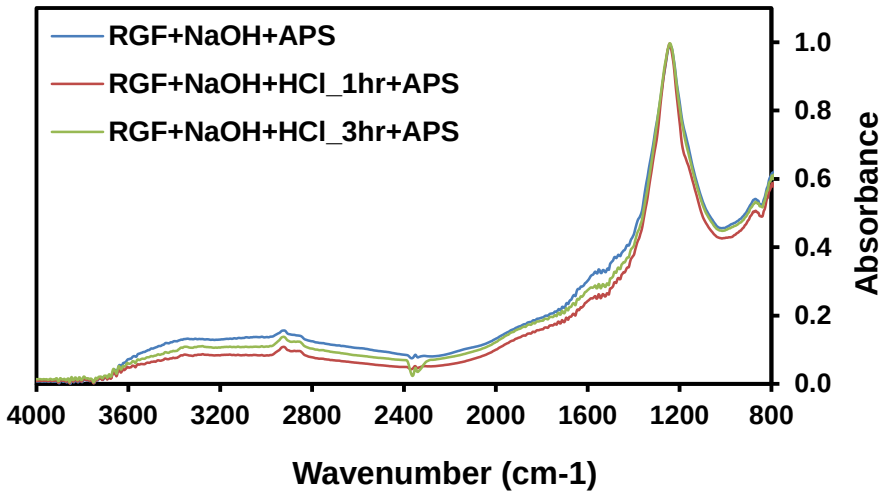

Figure 4-51 IR spectra of RGF+NaOH+APS and RGF+NaOH+HCl+APS

Reviewing the IFSS and FTIR data together, some deductions can be made as to the effectiveness of HCl treatment at hydroxylating the fibres surface as well as the adhesion of APS to the fibre surface. Initially it can be concluded that HCl treatments did not increase silanol concentration on the surface of the RGF used in

this work, as demonstrated in Figure 4-48. This is further established in Figure 4-50, where a reduction in Hydroxyl/silanol concentration on RGF+NaOH was observed after HCl treatments, indicating the removal of hydroxide ions opposed to rehydroxylation.

It is yet unclear why there appears to be a higher degree of APS polymerisation and adhesion to the RGF surface after HCl treatments in Figure 4-49. From Figure 4-47 however it can be seen that no change in IFSS resulted from the HCl treatment. This suggests that the degree of APS polymerisation may not be controlling the apparent IFSS with PP. Figure 4-47 shows increased IFSS for RGF+NaOH after HCl treatment, however, this does not appear to be through rehydroxylation, and may be attributed to removal of surface residue. Reduced hydroxyl band intensity in Figure 4-49 and Figure 4-51 does suggest polymerisation of the APS on the glass surface. The mechanism typically proposed for APS polymerisation involves interaction with the glass surface followed by APS condensation and polymerisation. This would indicate that the APS has bonded to the fibre surface however this cannot be concluded with the current data.

4.3.2.3 IFSS between recycled glass fibre and epoxy

The IFSS between fibres recycled from the scrap wind turbine blade and epoxy were measured using the microbond technique. Fibres treated with and without NaOH were tested, where the NaOH treatment used was 7 mol/L solution for 2 hour. Figure 4-52 gives the IFSS of RGF with epoxy, before and after NaOH and APS treatments. Again, Owens Corning unsized and APS sized fibres were used as the “New” control.

Although a different epoxy system was used in [194], the IFSS with APS coated new glass fibres given in Figure 4-52 approximates that reported by Minty et al. [194]. RGF without any post-treatments exhibit a significant reduction in IFSS with epoxy; approximately 60% of new glass fibres sized with APS. It is shown in the literature that exposure to typical thermal recycling temperatures degrades silanes present on glass fibres [32, 55, 59-61]. The sizing present on fibres in the GRP recyclate has been rendered ineffective as a coupling agent after recycling, given that the IFSS with these fibres approximates that of unsized new fibres. In agreement with the literature, it appears that the silane present in the recyclate has, to some degree, thermally degraded during recycling. The IFSS measured with the untreated RGF is

in fact slightly lower than that found with unsized new fibres. Undecomposed epoxy residue (likely char) on the surface of the RGF may be the cause for this disparity. This surface residue can be seen under SEM in Figure 4-53. Although chemical bonding at the interface is not expected without a coupling agent, the epoxy and surface silanol groups can still experience polar interaction, via hydrogen bonding [195]. Residue on the fibre surface may inhibit such interactions and in turn reduce the measured IFSS. Factors such as wetting, adsorption and diffusion may also be affected by the presence of surface residue contamination. It should be noted that the fibres under comparison are not of the same origin and as such may have difference in composition and production history. It is feasible that such inconsistencies alone could also account for the discrepancy in IFSS.

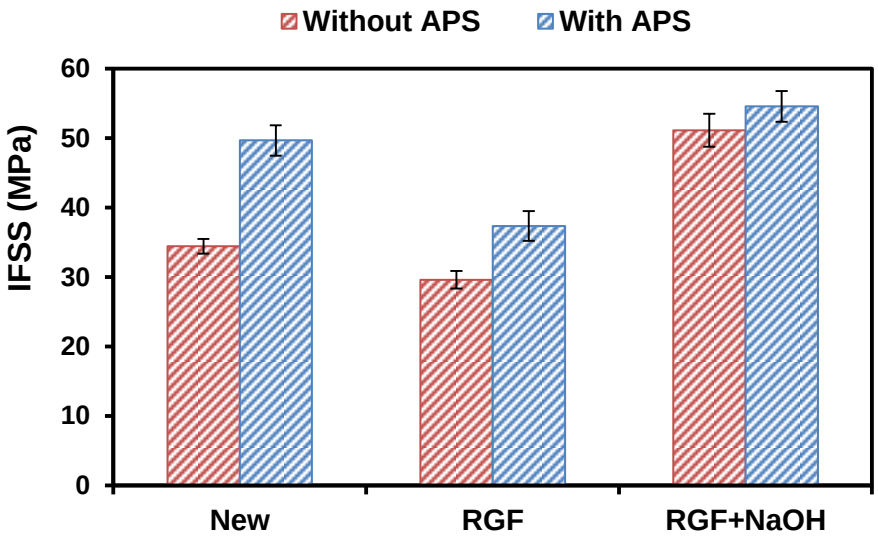

Figure 4-52 IFSS of various new and RGF with epoxy, measured using the microbond technique. The IFSS with epoxy is significantly reduced as a result of recycling in the fluidised bed; however, can be regenerated with both NaOH and APS treatments.

Figure 4-52 shows that RGF treated in NaOH solution yield an IFSS comparable to that of APS coated new glass fibres. The increase in IFSS must be induced by treating the RGF in NaOH solution; however, it is unclear if the improvement in IFSS is due to chemical or physical interaction (or both). It was observed under SEM in Figure 4-27-Figure 4-30 that etching in concentrated NaOH solution resulted in significant pitting on the fibre surface. Moreover, Bashir et al. observed a significant increase in the roughness of glass fibre surfaces after soaking in NaOH solution [34]. Figure 4-53 and Figure 4-54 show SEM images of the fibres recycled form the

wind turbine blade, without and with NaOH treatment respectively. In agreement, there appears to be pitting forming on the surface of these fibres after NaOH treatment. As shown in Figure 4-53, these features were not found on the surface of untreated RGF. It appears plausible that the introduction of surface pitting and/or higher surface roughness could increase mechanical interaction between the glass fibre and epoxy. An increase in friction would produce a higher IFSS and provide one possible explanation for the observations in Figure 4-52. Similarly, oxidation of carbon fibre can produce pits and corrugations on the fibre surface, which can be used to mechanically anchor polymer matrices and improve stress transfer to the fibre [146].

Figure 4-47 shows that, unlike epoxy, the IFSS is not increased with PP as a result of NaOH treatment. If mechanical anchoring due to surface pitting causes improved adhesion with epoxy, one could deduce the same phenomenon would be observed with PP matrices. As discussed above, the level of adhesion is controlled by a combination of complex mechanisms acting collectively at the polymer/fibre interface. Factors such as increased wettability and/or chemical interactions with epoxy may work in parallel with mechanical anchoring to produce the increase in IFSS observed in Figure 4-52. It is also understood that epoxy undergoes shrinkage during curing [178]; when used as a matrix medium this cure shrinkage can produce residual radial compressive stresses on the reinforcement fibre. It has been proposed that this can increase stress transfer to the fibre in turn increasing the IFSS between fibre and matrix [179]. With the introduction of surface pitting, the contribution of such forces may be enhanced, further increasing the measured IFSS.

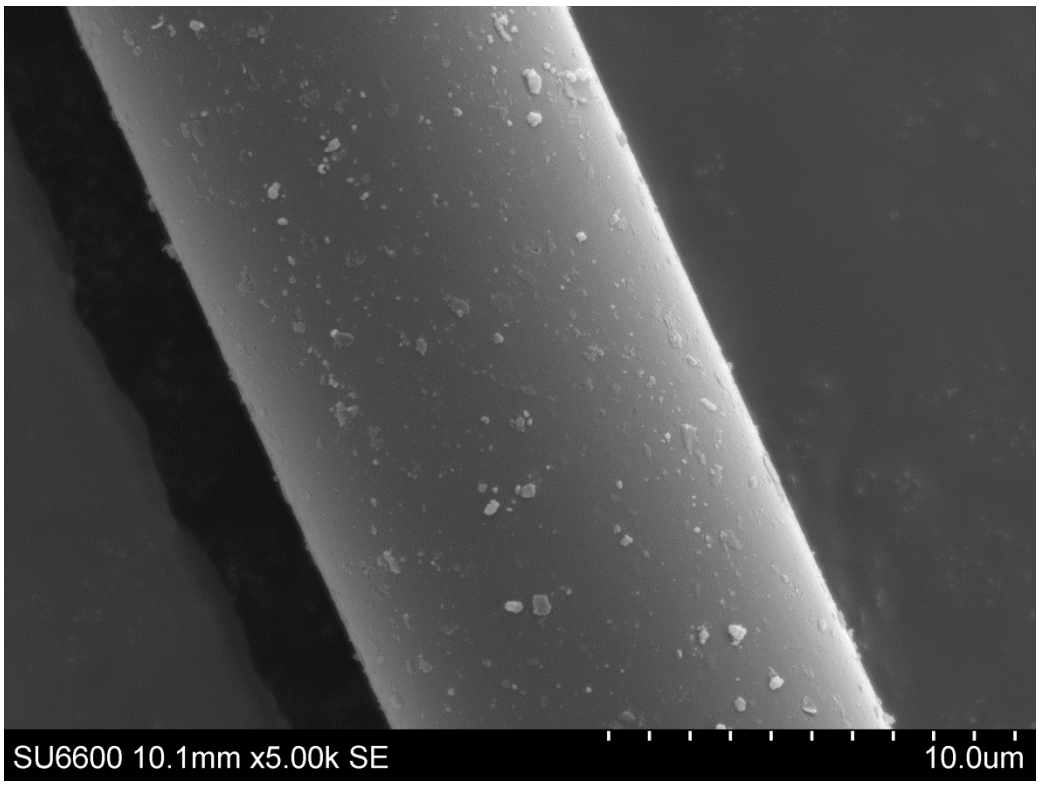

Figure 4-53 SEM image of glass fibre recycled from end-of-life wind turbine blade

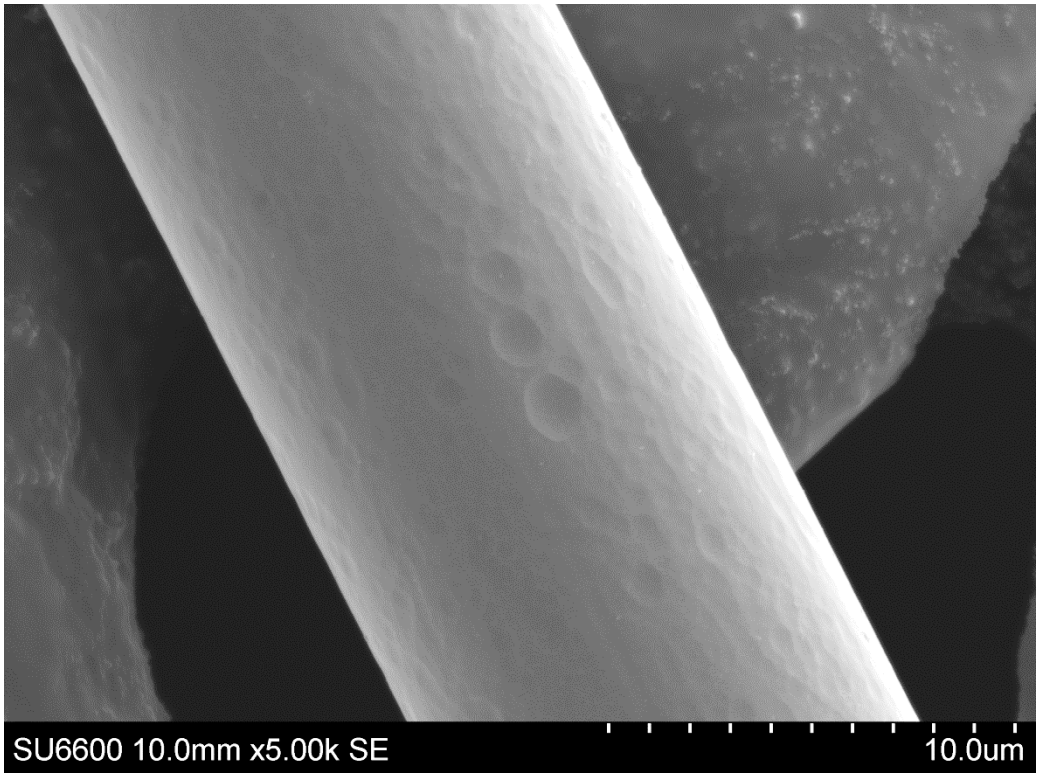

Figure 4-54 SEM image of glass fibre recycled from end-of-life wind turbine blade treated in 7 mol/L NaOH solution for 2 hour showing significant surface pitting

In Figure 4-27 - Figure 4-30, it is shown qualitatively under SEM that the apparent pitting on the fibre surface was a function of NaOH solution concentration. Measuring the IFSS of fibres treated in a variety of NaOH concentrations may provide further insight into the mechanism behind the improved stress transfer. A proportional relation between IFSS and NaOH concentration would suggest that increase mechanical interaction might be occurring.

The surface chemistry of NaOH treated fibres is not yet understood therefore improved adhesion through chemical bonding/interaction with epoxy cannot be dismissed as the cause for the rise in IFSS. Given the known reactions between NaOH and compounds that compose glass fibre (Equation 4-4 and Equation 4-5), there is no evident mechanism for increased chemical bonding after the NaOH treatment. A proposed mechanism for silica network attack via hydroxide ions results is the formation of silanol groups on the fibre surface [141]. Given the polar nature of epoxy, an increase in silanol density may improve the IFSS through increases polar interaction. It remains unclear whether the silanol density on the fibre surface does indeed rises after treating in NaOH. No firm conclusions could be made using FTIR in Figure 4-51-Figure 4-52. Chemical interactions should therefore not be overlooked; however, determining the mechanism(s) that result in the apparent IFSS in Figure 4-52 is out with the scope of this thesis and requires additional work to fully understand.

Finding the IFSS of RGF treated only with APS proved problematic using the current microbond methodology. Over 60 specimens were prepared; however, in all cases, the fibre itself failed prior to droplet de-bonding during testing. This is most definitely a consequence of the weakness of these fibres. This phenomenon was not observed as frequently for untreated RGF, suggesting the IFSS is improved with the application of APS. Using the peak force prior to the fibre failure, a “minimum” value for average IFSS of these specimens was found to be 37.4±2.16 MPa. It is this average “minimum” IFSS which has been added to Figure 4-52. Although this quantitatively demonstrates an increase in IFSS with application of APS, it is unclear what the true IFSS value is, or whether it would approach that of the new APS coated glass fibre.

Applying APS to NaOH treated fibres yield an insignificant increase on IFSS. This apparently contradicts the observations made when measuring the IFSS of new and RGF treated only in APS. It was also found that these fibres failed (opposed to

droplet de-bonding) at a higher rate during testing, however, there were a sufficient number of successful de-bonded specimens to express an average IFSS. It is plausible however that the average IFSS was also limited by specimens with higher IFSS failing due to fibre breakage (rather than de-bonding). The apparent average IFSS would therefore be diminished since the IFSS of these specimens was not included in the average value in Figure 4-52. This would mean that the value given for the APS coated RGF+NaOH in Figure 4-52 would be a “minimum average”, as in the case of APS coated RGF. Given the significantly higher fibre strength, the measured IFSS of RGF+NaOH may indeed be closer to the true average IFSS.

Further research into the fibre surface composition and morphology after NaOH treatment, as well as how this effects physical and chemical interaction with APS/epoxy, would first be required before understanding the key mechanisms contributing to the measured IFSS. Despite this incomplete understanding, Figure 4-52 shows that the IFSS of recycled and regenerated fibres using NaOH can compete with that of APS sized new glass fibres. Further improvements in IFSS may be achieved by applying a suitable commercial sizing to the RGF. Such blends typically contain film formers that are tailored for use with epoxy matrices, and may enhance chemical interaction at the fibre-matrix interface.

4.3.2.4 Effect of interface regeneration treatments on glass fibre strength

The effect of RT APS and HCl treatments on the strength of RGF was investigated. The was carried out to ensure these treatments did not adversely impact the strength of the fibres. All fibres tested were recycled from the in-house prepared GF-EP recyclate.

Effect of RT APS treatment on glass fibre strength

The strength of fluidised bed RGF treated with APS is shown in Figure 4-55. Fibres with and without strength regeneration were treated within APS, where NaOH treatment was 7 mol/L for 2 hour. The data in Figure 4-55 shows that resizing RGF with APS does not lead to any improvement in fibre strength. This is in agreement with Nagel who also observed no significant change in the strength of thermally conditioned glass fibres treated with APS [68]. Figure 4-55 establishes that an

increase in composite properties when using APS should be attributed to improved glass fibre-polymer adhesion and not stronger reinforcing fibres.

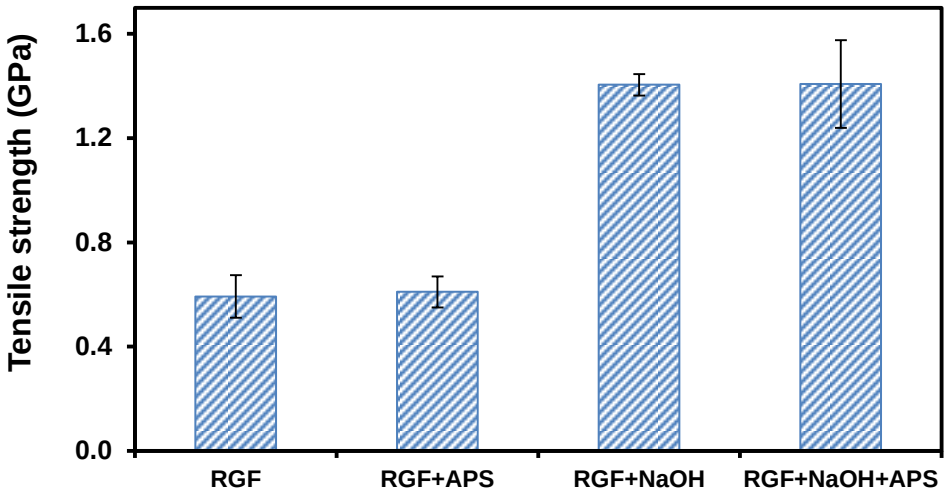

Figure 4-55 Tensile strength of glass fibres is unaffected by treating in 1 vol% APS for 15 min

Effect of HCl treatment on glass fibre strength

Figure 4-56 shows the effect of the HCl treatments on the strength of fluidised bed RGF. HCl was applied to fibres with and without strength regeneration. The NaOH treatment used in Figure 4-56 was 7 mol/L for 2 hour. Both durations of HCl treatment do not affect the strength of recycled only fibres. The strength of NaOH treated fibres drops by 0.1 GPa for both 1 and 3 hour treatments. Saez-Rodriguez also reported a 0.1 GPa reduction in tensile strength of thermally conditioned fibres after treating with 10% HCl solution for 1 hour [142]. However, considering the error in Figure 4-56, the change in strength after HCl treatments is not significant. It appears that using HCl as means of increasing glass fibre-polymer adhesion should have little, if any, effect on the reinforcing ability of the fibres.

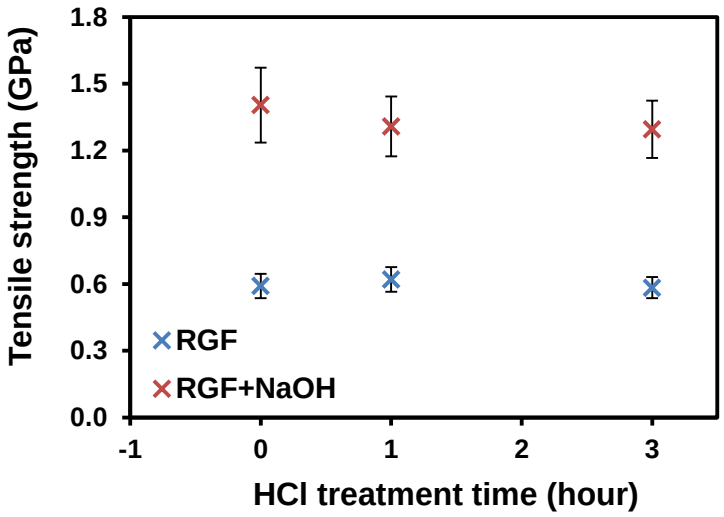

Figure 4-56 Tensile strength of glass fibres after treating with 10 mol/L HCl for 1 and 3 hour. RGF treated in NaOH show a slight reduction in strength after HCl treatment; however, given the error bars, it is unclear how significant this reduction is.

4.4 Conclusions

In this chapter, several chemical treatments were investigated as a means of regenerating the strength of fluidised bed RGF, as well as their IFSS with PP and epoxy. Four different treatments to improve the strength of fibres recycled from in-house prepared GF-EP recyclate were examined 1) hot NaOH solution, 2) hot water, 3) water vapour and 4) hot APS.

It was found that soaking in hot NaOH solutions, with concentration of 3 mol/L or greater, can significantly increase the tensile strength of RGF. The treatment time required for strength regeneration was significantly higher for fibres recycled in the fluidised bed, compared to fibres thermally conditioned in a furnace at the same temperature. This was attributed to fibres sustaining a greater degree of damage during the recycling processes, therefore, requiring more etching to remove/sufficiently modify the surface flaws. It was found that the rate of strength regeneration increases with NaOH concentration. Treatment in 7 and 10 mol/L solution yield fibres with tensile strength of around 1.4 GPa; the highest observed under the conditions examined in this study. This is apparently due to highly concentrated solutions providing rapid etching of the fibre surface. For higher concentration treatments (7 and 10 mol/L) it was observed that the strength increase plateaus. This was not observed for 3 and 5 mol/L treatments within the examined treatment times, however, may be the case if treatment time was extended. The

tensile strength of NaOH treated fibres could not be characterised purely as a function of diameter reduction, which may be expected since flaw removal/smoothing is typically the proposed strength regeneration mechanism. Indeed, even when sufficient material was etched from the fibre surface to remove the largest flaws, the strength does not reach that of pristine/virgin fibres. This is likely due to NaOH creating features on the new exposed outer surface, limiting the potential for strength regeneration.

Soaking in hot water for extended periods also yielded an improvement in the strength of RGF. As with treatment in NaOH, the strength increase appears to eventually plateau. Treating for between 96 and 336 hour produced fibres with a strength of around 1 GPa. While still low, the relative increase in fibre strength is far higher than was observed in studies on water treated bulk glass. The hot water treatment is especially encouraging given the low material cost and minimum processing steps.

The strength of RGF did not show any improvement when treating in hot APS or water vapour for extended durations. It was observed that the APS treated fibres were strongly adhered together after drying, and as a consequence, may have sustained significant mechanical damage during sample preparation. Given the reported benefits when used on bulk glass, no conclusion could be made as to the cause for the ineffectiveness of the water vapour treatment when applied to glass fibres.

A scrap offshore wind turbine blade was sourced and used a recyclate in the fluidised bed process. This gave the opportunity to test the regeneration treatments on real life scrap GRP. These RGF exhibited significant strength improvement (up to 1.7 GPa) when treated in NaOH. Hot water treatment for 4 days yielded the same strength regeneration as was observed when treating fibres recycled for in-house prepared recyclate. This work shows that these treatments can also regenerate the strength of real waste composites.

The IFSS between 1) RGF and 2) RGF treated in NaOH (RGF+NaOH) and PP was measured using the microbond technique. The IFSS with RGF/RGF+NaOH was approximately 8 MPa, which was similar to that given by Nagel for thermally conditioned GF-PP system [68]. However, unlike Nagel, no significant improvement in IFSS was observed with the addition of APS. This suggests either 1) the APS is not bonded to the glass surface, or 2) the APS is bonded to the glass surface

however, the amine functional group of APS has only weak interaction with the PP. RGF and RGF+NaOH were also soaked in HCl as a means of improving IFSS with PP by increasing silanol concentration and therefore APS bonding with RGF surface. Only RGF treated in NaOH exhibited an increase in IFSS after HCl treated. FTIR showed that HCl treatment does not increase silanol concentration on the fibre surface. The mechanism responsible for the increase in IFSS when HCl is used with NaOH treated RGF is yet unclear, however the FTIR results suggests it is not addition of silanol groups.

IFSS with epoxy was reduced by approximately 40% after fibres were recycled in the fluidised bed. Applying APS increased the adhesion, however, the actual IFSS could not be measured due to the weak RGF breaking during microbond testing. An alternative test methodology may be required to attain an accurate IFSS measurement. It was found that NaOH treatment alone, originally intended to increase fibre strength, could regenerate the IFSS with epoxy to that observed with new, APS coated glass fibres. It is proposed that mechanical anchoring, facilitated by surface pitting induced by NaOH etching, may contribute to this rise in IFSS. Further work is required to fully understand the mechanism of adhesion and whether chemical bonding/interaction also contribute.

5. Reusing recycled and regenerated glass fibres

In this Chapter, fluidised bed RGF are reused as a reinforcement material in GF-PP and GF-EP. For consistency with the interface work in Chapter 4, new GF-PP and GF-EP are prepared with the RGF obtained from both the GF-EP composite made in-house and wind turbine blade recyclate respectively. This, along with the regeneration treatments used are summarised in Table 5-1.

The extended Kelly-Tyson model is used to investigate the influence of fibre strength and IFSS on GF-PP, using the fibre length distribution measured from GF-PP prepare with fluidised bed RGF. The effect of the various fibre strength and interface regeneration treatments was investigated in terms of the resulting GF-PP tensile, flexural and impact properties. The influence of NaOH treatment concentration is explored in terms of GF-PP tensile strength. GF-PP reinforced with a mix of both new and fluidised bed RGF are produced and the tensile strength is characterised.

Glass fibres recycled from the scrap wind turbine blade are used to prepare GF-EP composites. The effect of NaOH treatment and coating with APS on the tensile properties of the GF-EP was investigated.

Table 5-1 Summary of the GRP prepared and the source of RGF and regeneration treatment used

Composite	Source of RGF	Regeneration treatments
GF-PP	In-house prepared GF-EP	RT APS HCl NaOH
GF-EP	Scrap wind turbine blade	RT APS NaOH

5.1 Literature review

In this section the challenges of reprocessing thermally recycled fibres are discussed. Studies investigating GRP prepared with thermally weakened (thermally conditioned or thermally recycled) glass fibres are reviewed in terms of the resulting mechanical properties. The influence of strength and surface functionality regeneration treatments on mechanical properties of GRP prepared with thermally weakened glass fibres is summarised.

5.1.1 Reprocessing thermally recycled glass fibres

Several limitations restrict the processing methods that can be used for manufacturing GRP with thermally RGF. New glass fibres are produced into roving or yarns with sizing applied to bind the fibres together. In this form, the fibres are suitable for producing continuous mats and textiles. However, for ease of transport and efficient reactor loading, scrap GRP requires size reduction prior to recycling. Thermally RGF therefore have a distribution in fibre length; meaning they can only be used as discontinuous reinforcement in GRP. The sizing, which binds new glass fibres together is also decomposed during recycling. This allows the fibres to move and separate during processing. The fibre strand integrity and alignment are therefore lost and fibres become entangled and fluffy. Studies by Feih et al. [31, 65] and Kennerley et al. [30] produce continuous fibre composites using thermally conditioned fibres. Although interesting in terms of investigating the effect of fibre strength on GRP properties, these composites will not comply with the architecture of commercial GRP based on thermally recycled discontinuous fibres. Several authors have processed thermally RGF into GRP [14, 23, 37, 53, 196]. Åkesson et al. produced randomly orientated mats with RGF, which were then infused with polyester [37]. Li et al. extruded RGF with PP into threads using a screw extruder which was then injection moulded [53]. Most of the studies however produced a dough moulding compound (DMC) by dispersing the RGF in unsaturated polyester resin [14, 23, 196]. Other authors have processed thermally conditioned fibres into discontinuous GRP using methods that may be suitable for thermally RGF [15, 56, 180]. Roux et al. also used a twin-screw extruder to process GF-PP with thermally conditioned fibres. Thomason et al. used a wet deposition and papermaking process to mix thermally conditioned chopped glass fibre with PP fibres to produce glass mat thermoplastic (GMT), which was subsequently compression moulded to form GF-PP plates [15]. A similar papermaking process was used by Lee and Jang, however, the

PP matrix was introduced in powder form [180]. It has therefore been demonstrated that thermally RGF are suitable to be used in discontinuous, randomly orientated GRP using extrusion, papermaking and DMC processes.

Improved mechanical properties can be achieved when fibres are aligned in FRP. The optimal mechanical properties of FRP are typically attained with fibre volume fractions of around 60%, which can only be achieved using aligned fibres [197]. Several authors have investigated methods for re-aligning short thermally recycled fibres to improve the properties of composites reinforced using recycled fibres [197-200]. Numerous alignment methods have been proposed however “wet” fibre alignment methods appear the most promising in terms of level of alignment and fibre volume fraction that can be achieved [200]. The process involves suspending fibres in a liquid and accelerating the mixture through a converging nozzle. The alignment is achieved by forcing the fibres to follow the fluid streamlines [198]. The fibres can be used to create aligned tapes, veils or re-woven yards, and used in composite preparation methods such as infusion processes or as prepregs [201]. To the best of the author’s knowledge, all reported studies focus on re-aligning recycled carbon fibres. Kacir et al. demonstrated that wet alignment techniques could successfully align 90% of new glass fibres within a tolerance of ±15° [202]. Further work is required; however, it may be feasible to use such methods to produce aligned glass fibre composites with improved mechanical properties.

5.1.2 Mechanical properties of GRP reinforced with thermally weakened glass fibres

A number of authors have reported the mechanical properties of GRP reinforced with either thermally conditioned [5, 15, 30, 31, 56] or thermally recycled [14, 23, 37, 196] glass fibres; Table 5-2 and Table 5-3 give a summary of the properties of these respectively. The “Initial composite strength” is the strength of composites based on new glass fibres to use as a comparison to those prepared with thermally degraded fibres. As can be seen is Table 5-2, the composite properties suffer when using thermally conditioned glass fibres. Kennerley et al. [30] and Feih et al. [31] observed an inverse relation between the fibre conditioning temperature and tensile strength of GRP based on these fibres.

Table 5-2 Properties of GRP based on thermally conditioned glass fibres

Matrix material	Initial GRP strength	Thermal history	GRP strength based on conditioned fibres	Strength retained (%)	Property	Ref.
PP	75 MPa	500 °C 25 min	38 MPa	51	Tensile	[55]
PP	51 MPa	500 °C 10 hour	28 MPa	55	Tensile	[56]
PP	68 MPa	500 °C 25 min	40 MPa	59	Tensile	[15]
Polyester	250-350 MPa	375 °C 20 min	200 MPa	57-80	Tensile	[30]
		500 °C 20 min	170 MPa	49-68		
		625 °C 20 min	75 MPa	21-30		
Epoxy	220 MPa	500 °C 30 min	80 MPa	36	Tensile	[5]
Vinyl ester	100%	450 °C 2 hour	/	40	Tensile	[31]
		550 °C 2 hour	/	20		
		650 °C 2 hour	/	20		

The tensile and flexural strength of GRP based on thermally RGF also tend to be inferior to those made with virgin fibres, irrespective of the thermal recycling method used, as seen in Table 5-3. Many authors attempt to mitigate this performance drop by reinforcing with both recycled and virgin fibres. “Virgin fibre content” in Table 5-3

gives the weight percentage of virgin fibre used out of the total fibre weight. Most studies summarised in Table 5-3 use thermosetting polyester resin as the matrix material for the RGF. Cunliffe and Williams [23] and Marco et al. [196] report high strength retention of GRP, however only 25% and 15% of the fibre content is replaced with recycled glass fibre. More notably, Kennerley et al. observed no change on GRP strength when replacing up to 50% of fibre content with those recycled using the fluidised bed.

Table 5-3 Properties of GRP based on thermally RGF

Matrix material	Initial GRP strength	Recycling method	Thermal history	GRP strength based on RGF/ retained strength	Virgin fibre content	Property	Ref
Polyester	22-26 MPa	Fluidised bed	450 °C < 60 min	15 MPa / 58-68%	0%	Tensile	[14]
				25 MPa / 96-114%	50%		
Polyester	96 MPa	Pyrolysis	450 °C 90 min	89 MPa / 93%	75%	Flexural	[23]
Polyester	190 MPa	Microwave pyrolysis	Non-isothermal 440 °C max	157 MPa / 83%	75%	Flexural	[37]
				104 MPa / 55%	50%		
Polyester	22.9 MPa	Pyrolysis	500 °C 30 min	24.0 MPa / 105%	85%	Tensile	[196]
PP	/	Pyrolysis	Non-isothermal 500 °C max	38 MPa	0%	Tensile	[53]
	/			42 MPa		Flexural	

The drop in composite properties observed in Table 5-2 and Table 5-3 is likely a result of strength loss of the glass fibres and/or reduced adhesion between the fibres and the matrix. Feih et al. established that the tensile strength of continuous glass fibre reinforced vinyl ester is solely controlled by the fibre strength, with the relative strength loss of thermally conditioned fibres mapping that of composites based on those fibres [31]. In contrast, Nagel et al. attributed the drop in tensile strength of injection moulded PP composites to the loss of adhesion, when using thermally conditioned glass fibres [55]. It is understood that the interfacial shear strength has a larger effect on the strength of composite reinforced with shorter fibres [203], which could explain the conflicting observations in [31] and [55].

5.1.3 Mechanical properties of GRP reinforced with regenerated glass fibres

Yang et al. investigated the effect of using thermally conditioned and regenerated glass fibres in GF-EP [5], as seen in Figure 5-1. Using HF etched fibres increased the strength of GF-EP from around 80 MPa to 120 MPa, compared to using only thermally conditioned fibres. A comparable improvement in GF-EP strength was achieved by simply re-silanising the glass fibres with APS. Combining HF treatment followed with APS application further increased the GF-EP strength to around 160 MPa. A significant increase in GF-EP flexural strength was also observed when thermally conditioned fibres were treated in HF then coated with APS [5]. Despite the increase in strength, the GF-EP based on regenerated fibres is significantly weaker than those made with as received fibres. This may be due to differences in fibre strength, given that the strength of regenerated fibres (around 1.7 GPa) is still significantly lower than the as received (around 2.4 GPa).

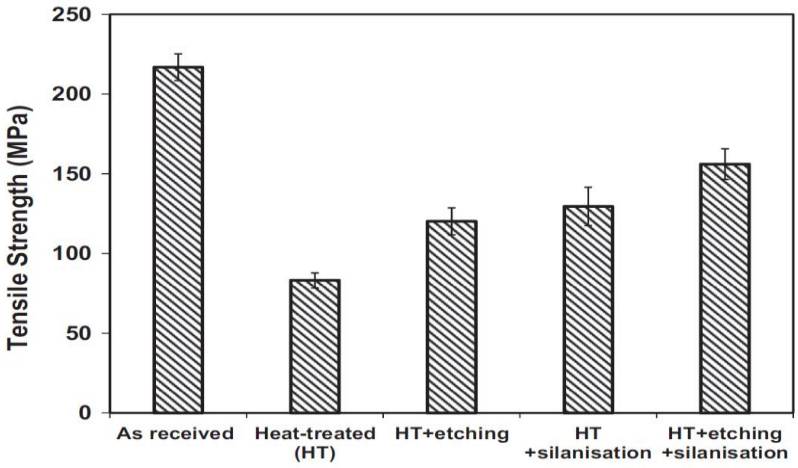

Figure 5-1 Tensile strength of GF-EP composites reinforced with thermally conditioned glass fibres treated in hydrofluoric acid (etching) and/or APS (silanisation), reproduced from [5]

Thomason et al. investigated the effect of using thermally conditioned and regenerated glass fibres in GF-PP [15], as seen in Figure 5-2. A 44% increase in the strength of GF-PP was observed when reinforced with fibres regenerated using NaOH solution. Applying APS further improved the GF-PP strength, giving a strength increase of 74%. Thomason et al. observed using the microbond technique that re-silanising with APS fully regenerated the IFSS between thermally conditioned fibres and PP matrix. Similar to Yang et al. [5], it therefore appears that a lack in full fibre strength recovery limits the strength of composites based on thermally conditioned and regenerated fibres. Thomason et al. presented no tensile data for GF-PP based on fibres thermally conditioned and subsequently only coated in APS. It is therefore unclear to what degree the overall improvement in GF-PP strength is simply a result of increased interfacial adhesion.

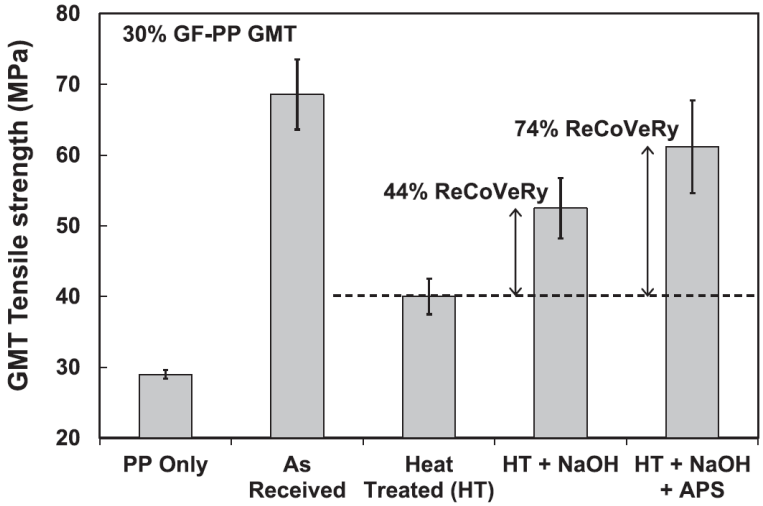

Figure 5-2 Tensile strength of GF-PP composites with glass fibres receiving various regeneration treatments, reproduced from [15]

Nagel investigated the effect of MAPP content on injection moulded GF-PP prepared using thermally conditioned fibres, as seen in Figure 5-3 [68]. (In Figure 5-3, “TD” is used to denote glass fibres thermally conditioned in a furnace at 500 °C for 15 min). GF-PP tensile strength increased from 36 MPa to 44 MPa with the addition of 4% MAPP. No further improvement was observed with the addition of more MAPP. Treating the thermally conditioned fibres in APS prior to GF-PP preparation however significantly improvement in the strength of GF-PP when used in connection with MAPP modified PP matrix. Over 50% of the strength loss was recovered with APS treatment and just 1% MAPP content, as can be seen in Figure 5-3. It was concluded that treatment of the fibres with APS is more effective in improving the GF-PP tensile strength than solely the addition of MAPP to the matrix [68].

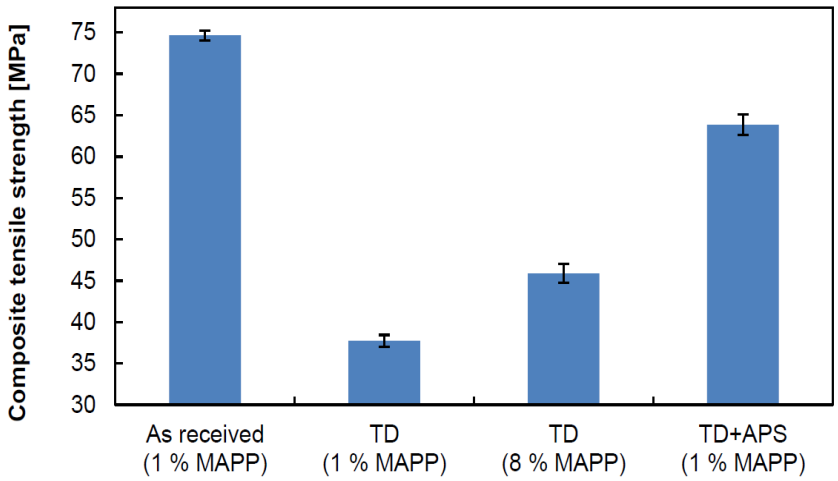

Figure 5-3 Effect of fibre APS coating and MAPP content on the tensile strength of injection moulded GF-PP, reproduced from [68]

Kennerley et al. was the only study found in the literature that investigated the effect of using a coupling agent on thermally RGF [14]. MPS was applied to fluidised bed RGF which were used in a polyester based DMC. The addition of MPS made no discernible improvement in tensile, flexural or impact strength. This suggests that either the coupling agent present in the recyclate material was not removed during recycling, or the MPS did not function as expected. Kennerley et al. did not specify what coupling agent was present in the recyclate; however, it is likely it significantly degraded according to the thermal stability of commonly used coupling agents reported in [61]. Iglesias et al. prepared GF-EP with fibres thermally cleaned at 450 °C for 1 hour [195]. The effect of coating the reinforcement fibres with various amino-silane coupling agents on composite tensile strength was investigated. The influence of fibre thermal weakening on GF-EP properties could not be deduced, since no strength data was given for composites prepared with non-thermally conditioned fibres. Iglesias et al. obtained no increase in composite strength when applying any of the silanes investigated, suggesting that the IFSS was not increased as a result [195]. It was proposed that low amine group density reduced the contribution of chemical bonding to the overall adhesion; however, this was never confirmed through direct measurement or observation.

5.1.4 Conclusions of literature review

Due to the architecture of thermally RGF, reprocessing into second life GRP can be problematic. RGF are typically reprocessed into discontinuous and randomly orientated composites, often a polyester based DMC. Several authors attempt to align short recycled fibres however the focus is on carbon rather than glass fibre. The mechanical performance of GRP reinforced with thermally conditioned/RGF is therefore relatively poor and not competitive with new composite properties.

Several authors have attempted to improve the performance of composites based on thermally RGF by regenerating the glass fibre strength or the interfacial adhesion between fibre and matrix material. It was demonstrated that the composite strength could be improved by using glass fibres strengthened with HF treatment. Given its toxicity, it is unlikely that HF could be used in a commercial fibre regeneration process. Using RGF treated in NaOH significantly increased the strength of GRP without the associated handling dangers. Re-application of APS on thermally conditioned fibres has proven to improve the strength of GF-PP. In contrast, coating fibres recycled in the fluidised bed process with MPS yield no improvement in strength of polyester based DMC. Modification of PP based composites (reinforced with thermally conditioned fibres) with MAPP showed significant increase in tensile strength when used in combination with APS surface coating. To the best of the authors knowledge, no research has been carried into the mechanical properties of PP reinforced with recycled and regenerated glass fibres.

5.2 Experiment

5.2.1 Materials

In this chapter, two different composites were recycled in the fluidised bed 1) in-house prepared GF-EP and 2) an end-of-life offshore wind turbine blade. These are the same composites as described in Chapter 4. The recyclate was cut into 10x10 mm pieces. It was found that longer fibres are difficult to disperse within the scale of current wet deposition process used to prepare GRP. The recyclate was therefore cut to this size so the RGF are short enough to be able to be processed into GRP without further size reduction.

For the preparation of GF-PP, DA3/6 PP fibres were purchased from Goonvean Fibres Limited. MAPP added to the GF-PP was purchased from Sigma-Aldrich and had an 8-10% weight maleic anhydride content. The MAPP was received in pellet form and was ground to a powder with particle size ≤200 μm before using in GF-PP preparation. This was done by briefly submerging the MAPP pellets in liquid nitrogen, processing in a coffee grinder then passing through a sieve with a 200 μm aperture.

For the preparation of GF-EP, IN2 Epoxy Infusion Resin and AT30 slow hardener supplied by Easy Composites Ltd.

As well as fluidised bed RGF, new glass fibres were also used in the production of GF-PP. PPG 8069 chopped glass fibres were supplied by PPG Fibreglass Company. The fibres were received non-dried with a sizing that is optimized for the dispersion in aqueous media. The nominal fibre diameter was 10 μm and the nominal fibre length 9 mm. NaOH pellets and 37% HCl were supplied by VWR and APS by Sigma-Aldrich.

5.2.2 Glass fibre chemical treatments

5.2.2.1 NaOH treatment

RGF were treated in NaOH as in Chapter 4. This was done on a larger scale when treating fibres that were to be processed into GRP. Table 5-4 summarises the conditions used to treat fibres with NaOH on a large scale.

Table 5-4 Conditions used for large scale NaOH treatment

Treatment	Fibre mass (g)	Solution volume (L)	NaOH conc. (mol/L)	Temp. (°C)	Treatment time (hour)
NaOH	55 - 80	5	3 - 10	95	2

The rinsing procedure used in Chapter 4 was originally developed by Nagel [68] and was initially used when investigating the effect of NaOH treatments on single fibre strength. It was later found however that this procedure was not sufficient in removing the entire residue produced. GRP produced with these fibres were poorly

mixed and the fibres tended to bundle together during wet deposition with PP fibres when preparing GF-PP. It is thought that the presence of reaction residue between the glass fibres inhibits their dispersion with the PP fibres. Nagel [68] used a relatively low NaOH concentration and substantially shorter treatment times compared to those in this work. As a result, less residue is likely to have accumulated and would have been more readily removed. An extended rinsing procedure (Table 5-5) was therefore developed for fibres used in GRP production in order to attain a well-mixed and homogeneous RGF preform for making composite.

Table 5-5 rinsing procedure for RGF soaked in NaOH to ensure effective treatment residue removal prior to processing into GRP

Order	Repetitions	Rinse	Volume (L)	Temperature (°C)	Time
1	4	10% HCl solution	4	RT	90 s
2	1	Water	5	RT	90 s
3	1	Water	5	95	10 min
4	2	Water	5	RT	90 s

Figure 5-4 shows GF-PP pre-consolidates which have been backlit to evaluate the extent of fibre dispersion. A significant improvement in fibre dispersion was observed when increasing the number of HCl rinses and decreasing the HCl concentration. This allowed improved dispersion while using approximately the same quantity of HCl. After rinsing, the NaOH treated fibres were dried at 105 °C for 8 hour.

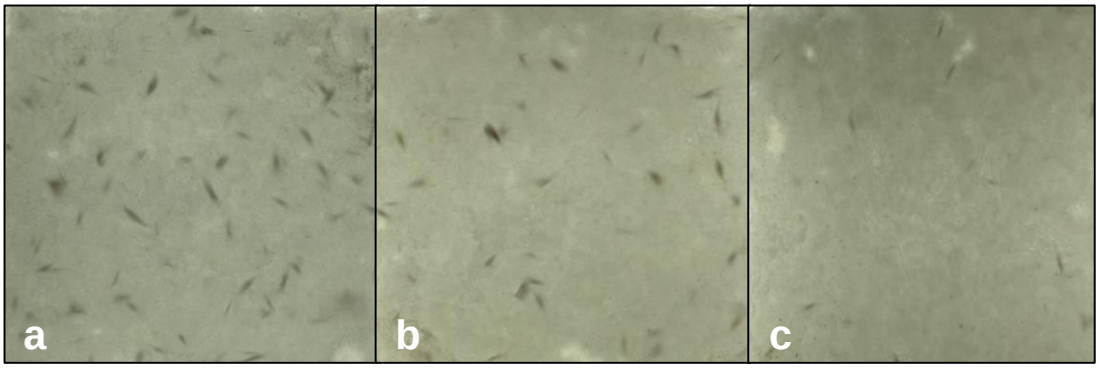

Figure 5-4 Improving GF-PP dispersion with various rinses each lasting 90 s: a) 1x 37 vol% HCl, b) 2x 20 vol% HCl and c) 4x 10 vol% HCl

5.2.2.2 Hydrochloric acid treatment

RGF were subject to a HCl treatment as it was observed, in some circumstances, to increase IFSS as shown in Chapter 4. This was done on a larger scale when treating fibres that were to be processed into GRP. Table 5-6 summarises the conditions used to treat fibres with HCl on a large scale.

Table 5-6 Conditions used for large scale HCl treatment

Treatment	Fibre mass (g)	Solution volume (L)	Temperature (°C)	Treatment time (hour)	Drying time (hour)
HCl	60	4	RT	1	8

5.2.2.3 RT APS treatment

RGF were treated with RT APS in an attempt to improve the compatibility with polymer matrices. These treatments were perform slightly differently when preparing GF-PP and GF-EP. During each preparation however, the APS was allowed to hydrolyse for 24 hour as outlined in Chapter 4.

RT APS treatment for the preparation of GF-PP

To treat glass fibres used for production of GF-PP, 4 L of APS solution was prepared. 1 L of solution was used for 13.44 g of fibres. In a PP storage container, the APS solution was poured over the fibres and the lid closed. After 15 min, the

fibres were drained and immediately processed into composites without drying. Nagel [68] found that drying the APS treated fibres made subsequent dispersion during composite processing more difficult. The fibre content of GF-PP (13.44 g / layer) could be controlled by weighing the fibres before treating with the APS.

RT APS treatment for the preparation of GF-EP

Treating glass fibres with APS to prepare GF-EP was similar to that when producing GF-PP. In this case, 6 L of APS solution was prepare and 3 L of solution was used to treat 30 g of glass fibres at a time. Again, fibres were not dried prior to processing into composites.

5.2.3 Preparation of GF-PP

5.2.3.1 Wet deposition process

31.36 g of DA3/6 PP fibres and 13.44 g of glass fibres were dispersed in a Premier International KCL type hand sheet former to prepare one GF-PP mat. The sheet former was filled with approximately 20 L water and an electrical stirrer was used to mix the dispersion at a stirring speed of 1250 rpm for 6.5 min, after which the dispersion was strained through the nylon sieve of the sheet former. When producing GF-PP with modified PP matrix, MAPP powder was added to the wet deposition process for the last 2 min of mixing. It was found that adding the MAPP powder too early in the wet deposition process inhibited fibre dispersion. The wet mat of glass fibres and PP fibres (200x200 mm) was dried for 8 hour in a Sanyo Convection MOV 212 oven at 105 °C.

5.2.3.2 Pre-consolidation and compression moulding

A Polystat 400S heated press was used to preconsolidate the mats at a pressure of 10 bar and a temperature of 200 °C for 1 min. The preconsolidated material was cooled outside of the press under a 20 kg mass for 15 min. After cooling, the preconsolidated sheets were trimmed to squares with dimensions 165x165 mm to fit tightly in the mould shown in Figure 5-5.

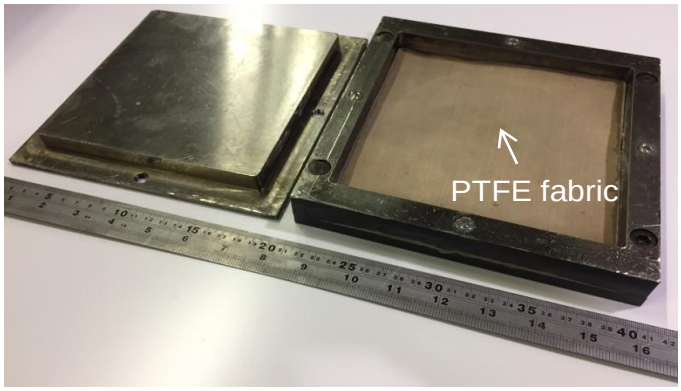

Figure 5-5 Mould used to prepare GF-PP laminates

Four preconsolidated sheets were stacked in the mould to produce one laminate. To prevent the composite from sticking to the mould a PTFE glass fibre fabric (Biscor Fluorofab® Fabric 100-6) was placed above and below the stack of preconsolidated sheets. Chemlease 2203 W release agent was also applied to the sidewalls of the mould. The compression moulding was performed at 200 °C, at a pressure of 20 bar for 4 min. The mould was rapidly transferred to a second press and the material was quenched cooled at 20 bar. The final dimensions of the laminates were approximately 165x165x4 mm. Figure 5-6 shows the various stage of the GF-PP preparation. Mechanical test specimens were water jet cut from the moulded laminates to dimensions according to the relevant standards; ISO 527, ISO 179 and ISO 14125 for tensile, flexural and impact tests respectively.

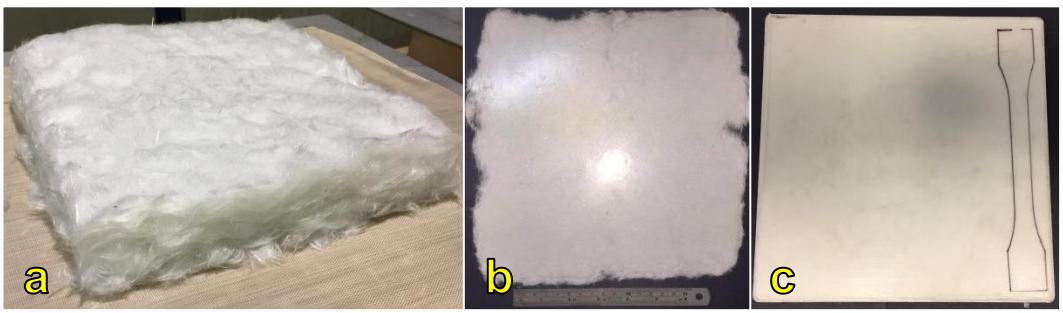

Figure 5-6 Various stages of GF-PP fabrication: a) dried GF-PP mat, b) preconsolidated layer, c) final compression moulded GF-PP laminate with tensile specimen geometry outlined

5.2.4 Preparation of GF-EP

The RGF were processed into randomly orientated discontinuous fibre mats before infusing with epoxy under vacuum. The RGF mats were prepared in a similar method used to produce the GF-PP mats. 30 g of RGF were dispersed in 20 L of water in a Premier International KCL type hand sheet former. The fibres were mixed using an electrical stirrer at 1200 rpm for 6.5 min prior to straining the dispersion through a nylon sieve. The 200x200 mm mats were dried for 8 hour in a Sanyo Convection MOV 212 oven at 105 °C. An example of the glass fibre mats can be seen in Figure 5-7.

Figure 5-7 Randomly orientated discontinuous glass fibre mats used to prepare GF-EP with RGF

After drying, two mats were stacked on top of one another and a vacuum infusion process was used to infuse the RGF with epoxy. Prior to infusion, the epoxy was degassed under vacuum for 10 min. A schematic of the vacuum infusion layup is given in Figure 5-8. A rigid plastic plate was places within the vacuum bagging layup to ensure a flat upper surface on the GF-EP was produced.

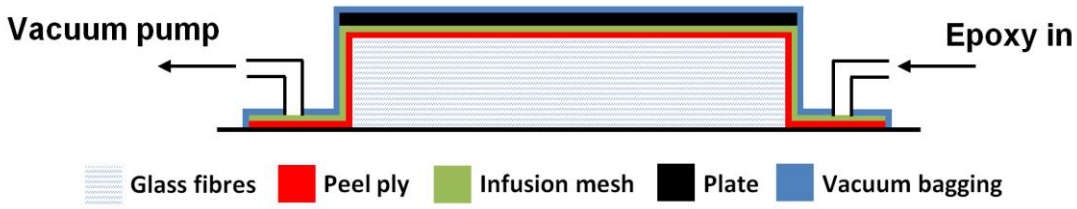

Figure 5-8 Schematic of vacuum infusion layup used to prepare the GF-EP

Figure 5-9 shows the vacuum infusion process set up used to prepare the GF-EP, using mats of RGF. All equipment and consumables used in the vacuum infusion process were purchased from Easy Composites Ltd.

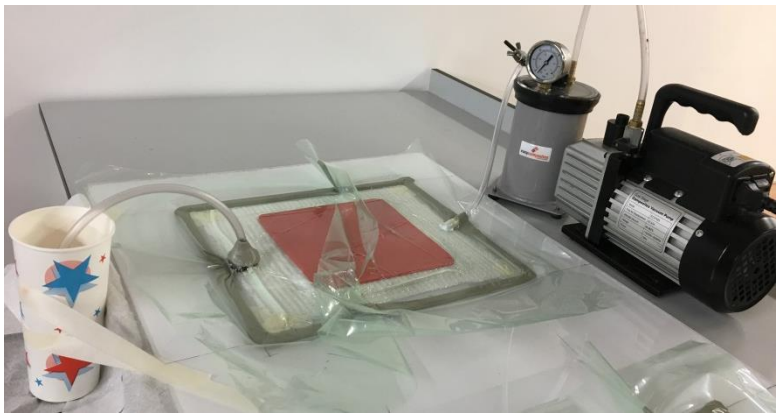

Figure 5-9 Image of vacuum infusion process set up used to prepare the GF-EP

After infusion, the epoxy was cured for 24 hour at RT. Following suppliers instruction, the GF-EP was then de-bagged and placed in an oven at 60 °C for 6 hour to post cure treat the epoxy. Tensile test specimens were then cut from the GF-EP using a water jet cutter following ISO 527. The average thickness of the specimens was measured to be 5.0±0.14 mm. Unlike the preparation of GF-PP, no mould was used in the preparation of GF-EP which resulted in a larger deviation in thickness between specimens.

5.2.5 Composite characterisation

5.2.5.1 Tensile test

Tensile testing of the GRP was performed following ISO 527 standard. An Instron 5969 testing machine equipped with a 50 kN load cell was used to perform the tensile test. The strain was recorded with an Instron 2663-821 video extensometer and the displacement rate was set to 1 mm/min. Figure 5-10 shows the tensile testing equipment used.

Figure 5-10 Tensile test set up on Instron 5969 testing machine

5.2.5.2 Three-point flexural test

Three-point flexural testing of the GRP was performed following ISO 178 standard. An Instron 5969 testing machine equipped with a 50 kN load cell and in-house jig was used to perform the flexural testing. The strain was recorded with an Instron 2663-821 video extensometer and the displacement rate was set to 2 mm/min. Figure 5-11 shows the flexural testing equipment used.

Figure 5-11 Three-point flexural test set up on Instron 5969 testing machine

5.2.5.3 Unnotched charpy impact test

Unnotched charpy impact testing of the GRP was performed following the ISO 179 standard. A Tinius Olsen Impact 503 impact tester was used, equipped with a 25 J hammer. All specimens had dimensions of 80x10x4 mm and were tested edgeways. Figure 5-12 shows the impact testing equipment used.

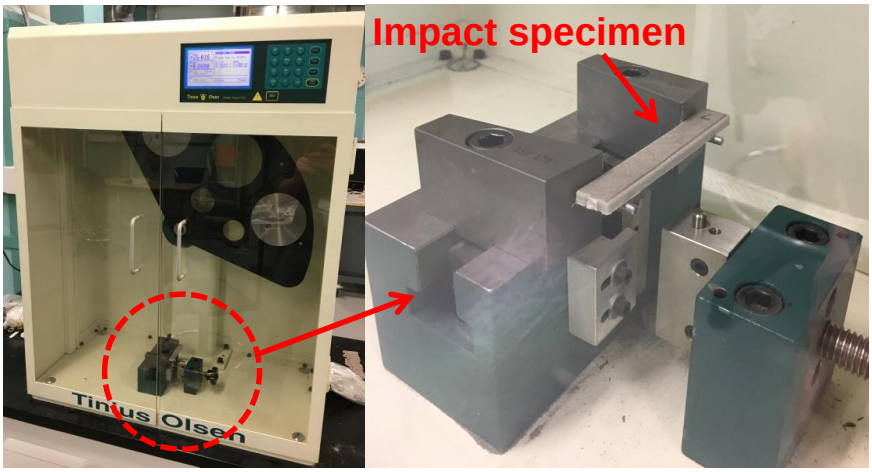

Figure 5-12 Unnotched impact test set up

5.2.5.4 Fibre content measurement

The GRP test specimens were ashed in order to find the fibre content. This process involves thermally decomposing the polymer matrix leaving only the glass fibres. The fibre content can be found by measuring the composite mass before ashing and the residual fibre mass. Equation 5-1 shows how the fibre weight fraction is calculated. Ashing was performed using a Carbolite CSF 1200 furnace at 550°C for 2 hour and the samples weighed using a Sartorius AX224 analytical balance.

Equation 5-1 Glass fibre weight fraction of composite

$$Glass\ fibre\ weight\ fraction = \frac{Residual\ glass\ fibre\ mass}{Initial\ composite\ mass}$$

5.2.5.5 Fibre length measurement

Glass fibres were extracted from tensile bar specimens by ashing using a Carbolite CSF 1200 furnace at 550°C for 2 hour. Approximately 25 mg of the fibres were extracted from the middle (test section) of the bar and dispersed in 500 mL distilled water in a glass beaker. 250 mL of the dispersions was then diluted with another 250 mL of distilled water in another beaker. 2 drops of glycerine were added to the water, reducing the surface tension of the fluid and making it easier to disperse the fibres. The dispersion was mixed manually before pouring a small quantity into different petri-dishes. An IDM FASEP fibre length measurement system was used to capture an image of the dispersion. Figure 5-13 shows that various components of the system.

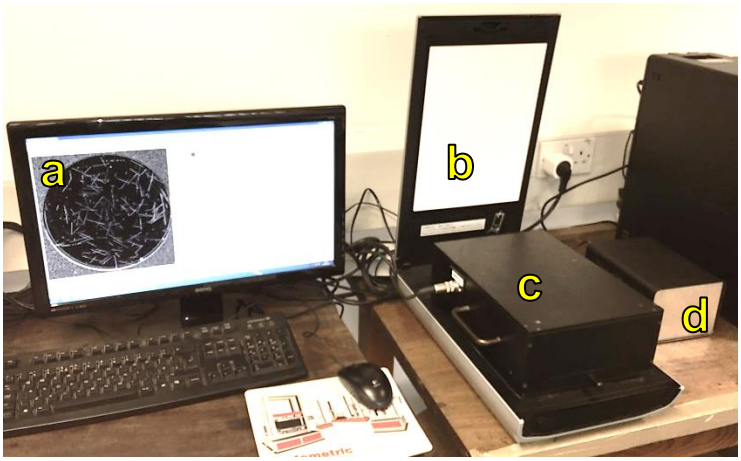

Figure 5-13 IDM FASEP fibre length measurement system: a) FASEP software, b) scanner, c) dark field box, d) controller

The petri-dishes were put in the dark field box, placed on a Canon ScanoScan 9000F high-resolution scanner. The dark field box was illuminated to improve the contrast between fibres and the black background. An Image Pro macro of the IDM FASEP fibre length measurement system was then used to analyse the captured images. The scanned images were analysed using the Image Pro software. The detected objects were classified into dust, single fibres and crossing or curved fibres depending on their width. The FASEP software used an algorithm based on the Hough Transformation to analyse crossing and curved fibres as illustrated in Figure 5-14. The classified objects were measured by the FASEP software.

As average fibre length increases in a dispersion, so does the concentration of crossing fibres. This leads to clusters, where fibres cross multiple other fibres as seen in Figure 5-14. This can increase inaccuracy in fibre detection and produce an incorrect output of fibre length distribution. In Figure 5-14, eight fibres have been detected by the FASEP software where in fact there are twelve present. For this reason, all clusters and curved fibres were manually evaluated and corrected if necessary before including in the data set.

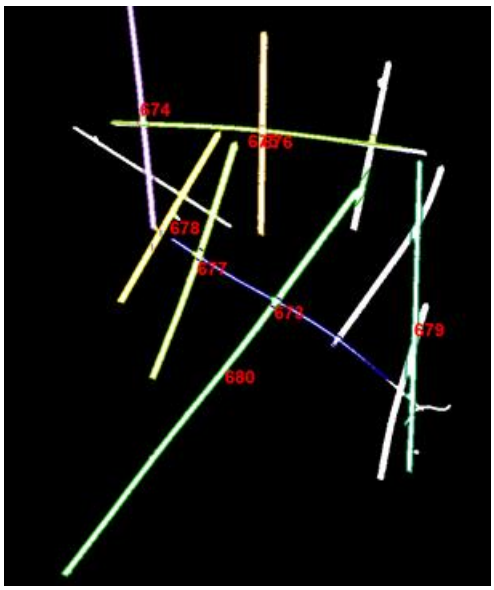

Figure 5-14 Detection of crossing fibres by the FASEP software

5.3 Results and discussion

5.3.1 Mechanical properties of GF-PP

In this section, fluidised bed RGF are treated with APS and HCl and used to prepare GF-PP in order to determine the effect of such treatments on GF-PP tensile properties. The effect of modifying the PP matrix with MAPP is also investigated. The Kelly Tyson model is also used as a means of estimating the tensile strength of GF-PP prepared with recycled and regenerated glass fibres.

5.3.1.1 Kelly-Tyson model for estimating GF-PP tensile strength

The extended Kelly-Tyson (K-T) model describes the tensile strength of discontinuous fibre composites. A derivation of the K-T model can be found in Appendix E. The model allows the influence of parameters such as fibre strength, fibre length, IFSS, fibre orientation and fibre diameter on GF-PP strength to be found. It is therefore used in this work to estimate the potential increase in strength of GF-PP prepared with fluidised bed RGF when regeneration treatments are used.

Effect of fibre strength and IFSS on GF-PP tensile strength

Figure 5-15 gives the estimated tensile strength of GF-PP using K-T model at various fibre strengths and IFSS. The fibre length distribution used to calculate the strength values was measured from a GF-PP tensile specimen prepared with fluidised bed RGF, which had received no other treatments (fibre length distribution can be found in Appendix D). The observations and conclusions made from Figure 5-15 may therefore not apply to other discontinuous fibre composite systems with varying parameters such as fibre diameter, length distribution and fibre and matrix properties. An orientation factor (η_o) of 0.335 was used throughout Figure 5-15 as it was found by Nagel to best represent the fibre alignment of the GF-PP produced using the same in-house wet deposition and compression moulding processes [68].

Figure 5-15 shows the tensile strength of GF-PP should in fact increase with glass fibre strength; suggesting strength regeneration alone should improve the overall GF-PP strength. The rate of GF-PP tensile strength increase with IFSS appears dependant on fibre strength. The K-T model suggests very little change in GF-PP strength when reinforced with fibres less than 1.0 GPa across all IFSS values. Improving the IFSS is more beneficial to GF-PP strength when combined with stronger reinforcing fibres. Overall, the K-T model suggests that regenerating both fibre strength and IFSS should significantly increase GF-PP tensile strength.

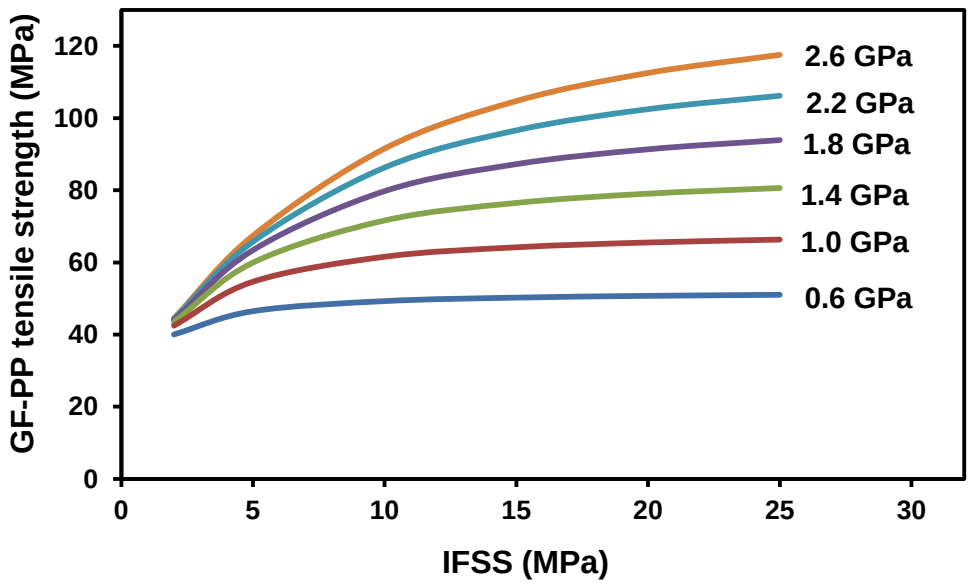

Figure 5-15 Tensile strength of GF-PP estimated using K-T model at various fibre strengths and IFSS

Estimated tensile strength of GF-PP based on RGF using K-T model

It was found that the average fibre length/fibre length distribution within GF-PP varied depending on whether the fibres had or had not been previously treated with NaOH (7 mol/L for 2 hour). This is attributed to the stronger NaOH treated fibres breaking less frequently during composite production, and was also observed in other studies [68]. Table 5-7 gives the average length of fibres within the GF-PP.

Table 5-7 Average fibre length and fibre tensile strength of fibres in GF-PP where NaOH treatment is at 7 mol/L for 2 hour

Specimen	Average fibre length (mm)	Average fibre strength (GPa)
RGF/PP	2.16 ± 0.17	0.81±0.12
RGF+NaOH/PP	2.55 ± 0.21	1.30±0.21

The actual fibre length distributions and measured fibres tensile strengths from Table 5-7 were used in the K-T model to estimate the expected strength of GF-PP produced with the RGF. Since the orientation factor is not known for the GF-PP in this work, an upper and lower limit for GF-PP tensile strength were calculated for random-in-plane (η_o=0.375) and 3D random (η_o=0.2) fibre orientation respectively. Figure 5-16 gives the expected tensile strength of GF-PP produced with fluidised bed RGF. In this chapter, GF-PP will be produced with MAPP modified PP, which is expected to increase the IFSS. Microbond tests using MAPP have not been carried out; therefore, the actual IFSS is unknown for these specimens. As such, Figure 5-16 expresses the GF-PP tensile strength across a wide range of IFSS values.

Similarly to Figure 5-15 above, Figure 5-16 suggests that a significant increase in GF-PP tensile strength should be expected by increasing the fibre strength with NaOH treatment. Under random-in plane fibre orientation and optimum IFSS, GF-PP prepared with NaOH treated fibres could reach up to 80 MPa, according to Figure 5-16. Although the IFSS is unknown when MAPP is used, Nagel reported an IFSS of over 25 MPa between sized fibres and MAPP modified PP matrix [68].

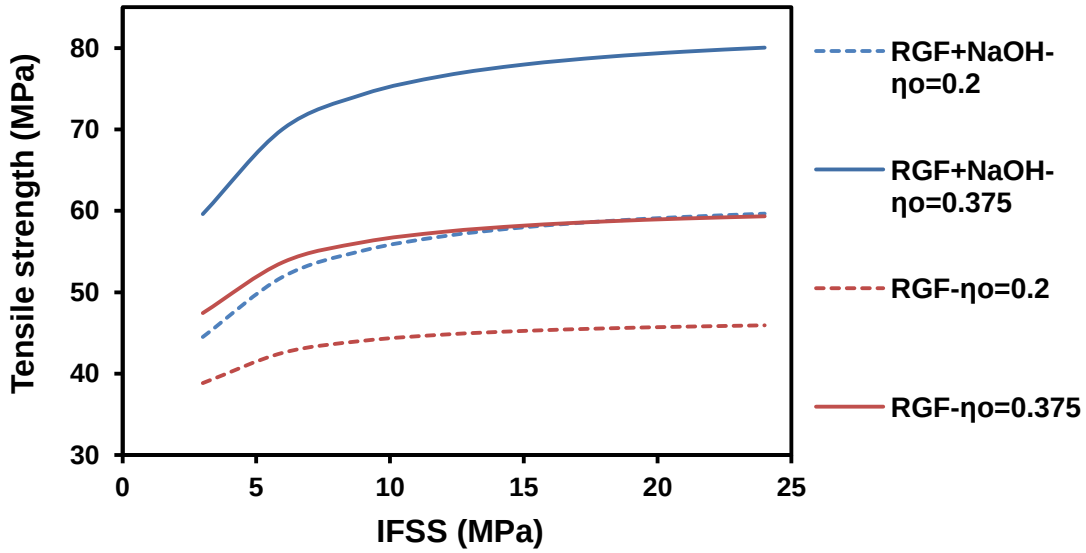

Figure 5-16 Calculated tensile of GF-PP produced with fluidised bed RGF, based on K-T model

5.3.1.2 Effect of MAPP content on GF-PP tensile strength

Prior to using MAPP in GF-PP produced with RGF, the effect of MAPP content on GF-PP prepared with new fibres (PPG 8069 chopped glass fibres) was investigated. Other authors [56, 57, 68] have also studied MAPP content on GF-PP properties, however, no examples of integrating powdered MAPP within a wet deposition process could be found in the literature. Typically, the MAPP is included during extrusion with PP, presumably yielding more uniform dispersion of the maleic anhydride throughout the PP matrix. Figure 5-17 shows the ultimate tensile strength (UTS) of GF-PP at various MAPP contents. With the integration of MAPP equal to or greater than 5%, UTS increases by approximately 40%. A similar relative maximum increase in strength was observed by Nagel when using the same fibre volume fraction [68]. Nagel's data has been added to Figure 5-17 for reference.

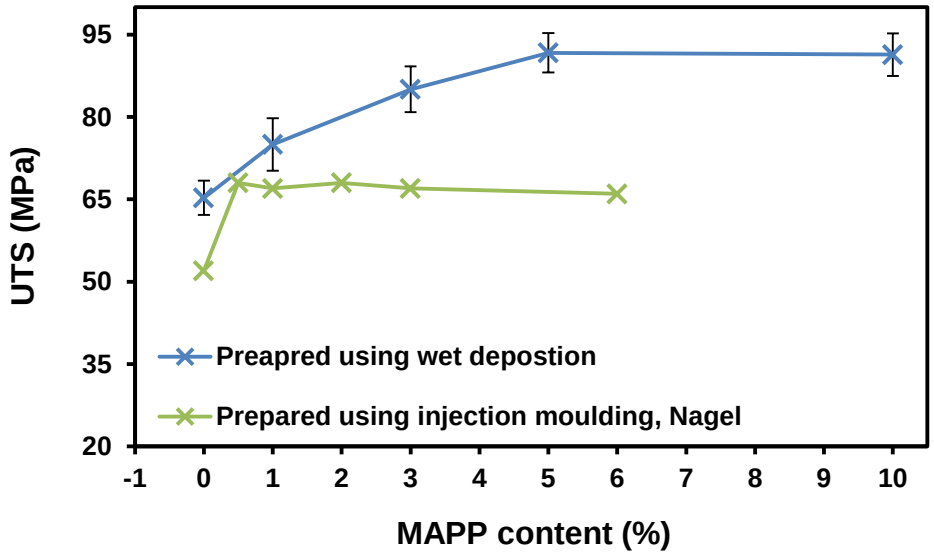

Figure 5-17 Ultimate tensile strength of GF-PP at various MAPP weight percentages, Nagel data reproduced from [68]. UTS plateaus at relatively high MAPP content, likely a result of incorporating as a powder within the wet deposition process.

Despite the significant rise in strength observed Figure 5-17, 5% MAPP content is higher than is typically required to achieve optimum GF-PP strength or IFSS with new fibres [68]. Nagel observed peak GF-PP tensile strength with an MAPP content of just 0.5% weight [68]. Nagel produced GF-PP via injection moulding with PP that was previously extruded with MAPP. It would appear that integrating the MAPP as a powder during wet deposition is not optimal for GF-PP strength increase, likely due to non-homogenous dispersion of MAPP with in PP matrix. Despite melting during the compression moulding process used to produce the GF-PP in this work, it is likely that there remain areas of the glass fibres which are not in contact with MAPP, leading to poor IFSS at these regions. Other factors such as fibre diameter, fibre length distribution, sizing present on the fibres and maleic anhydride content within the MAPP used will also likely influence the optimal MAPP content for GF-PP strength, which cannot simply be controlled between studies. It should be noted that the tensile strength of GF-PP reported by Nagel [68] (reproduced in Figure 5-17) is most likely lower than that found in this work because of shorter glass fibre length as a result of preparing using injection moulding. For the remainder of this work, an MAPP content of 5% will be used given the results from Figure 5-17.

According to the K-T model in Figure 5-16, under optimum conditions, the tensile strength of recycled and regenerated fibres could approach 90% of those produced using new glass fibres in Figure 5-17.

5.3.1.3 Effect of interface regeneration on GF-PP tensile properties

In this section, the tensile properties of various GF-PP prepared with RGF without strength regeneration is given. Table 5-8 defines the materials and treatments used in this section.

Table 5-8 Defining treatments and materials used in Figure 5-18 - Figure 5-27

	Meaning
RGF	Glass fibre recycled in fluidised bed at 500 °C
HCl	10 vol% HCl treatment for 1 hour
APS	1 vol% APS treatment for 15 min
PP	Unmodified polypropylene matrix
PP-MAPP	Polypropylene matrix modified with 5% MAPP

Figure 5-18 gives the UTS of the various GF-PP produced. For reference, the UTS for GF-PP prepared with new glass fibre (PPG 8069) was measured to be 65.3±3.9 GPa and 91.7±3.6 GPa with 0% and 5% MAPP content respectively, as shown in Figure 5-17. The UTS of GF-PP reinforced with fibres without any treatments (RGF/PP) is similar to was observed by Thomason et al. when measuring the strength of un-reinforced PP. This suggests that the RGF without any subsequent treatment have little to no reinforcement value in terms of GF-PP strength. When treating with APS and using unmodified PP matrix there is no increase in the UTS of the GF-PP. The microbond data in Figure 4-47 however did indicate a slight improvement in IFSS when using APS and RGF, therefore it may be expected that this would also be observed in the GF-PP strength. According to the K-T model shown in Figure 5-15 however, increasing the IFSS of weak fibres provides only slight improvements in GF-PP strength. The increase in IFSS when using APS on RGF in Figure 4-47 was less than 2 MPa, which may be insufficient to yield any

significant increase in GF-PP strength. It is unclear why GF-PP produced with RGF treated in HCl and APS show improvement in UTS, given that the HCl treatment did not appear to increase IFSS over APS treatment alone. Although out with the range of error, the increase in UTS is slight and the strength of the GF-PP is still far less than those produced with virgin glass fibres.

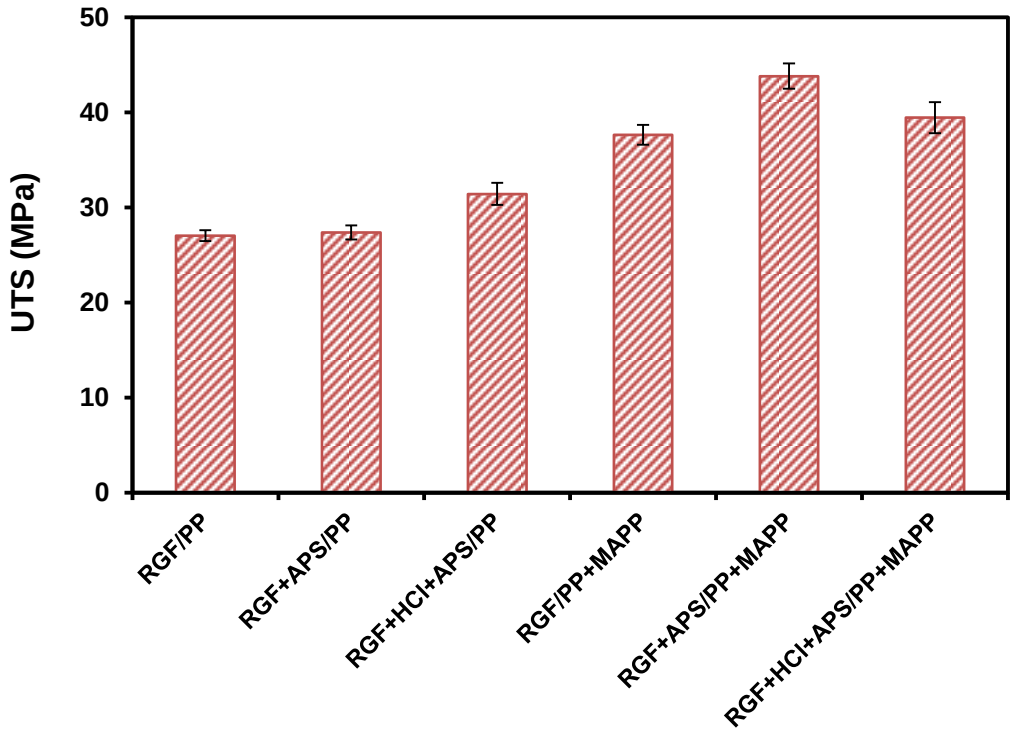

Figure 5-18 UTS of GF-PP produced using fluidised bed RGF after various treatments

Figure 5-18 shows a marked increase in GF-PP strength when prepared with MAPP modified PP matrix. Ancillary IFSS values were not measured for samples containing MAPP, however, an increase in adhesion is likely the cause for the rise in UTS. In agreement with other studies [55, 155-157], using MAPP on un-sized fibres can still increase adhesion, indicated by the improvement in GF-PP UTS in Figure 5-18. Combining APS sized RGF with a matrix containing MAPP yields composites with the highest tensile strength, exhibiting an increase of around 63%. Using HCl and APS treatments in combination with MAPP reduces the UTS compared to APS alone. Given the lack in directly measured IFSS data, it is currently unclear what effect HCl treatment will have on the adhesion when used with MAPP modified PP matrices. Given HCl did no effect the strength of RGF, the probable cause for the

drop in UTS is a change in IFSS. To fully understand this phenomenon further work must be carried out.

The strength of the GF-PP in Figure 5-18 remains significantly lower than observed in other studies. Nagel reported a GF-PP strength of around 55 MPa when prepared with thermally conditioned fibres (at 500 °C) treated in only APS with an unmodified PP matrix [68]. With similar average fibre lengths and fibre volumes fractions, the cause for this disparity is likely a function of fibre strength. The strength of the fluidised bed RGF in this work are 50% lower than was reported by Nagel after thermally conditioning within a furnace at the same temperature. The additional damage sustained during recycling within the fluidised bed clearly significantly reduces their reinforcement potential and ultimately commercial value.

Figure 5-19 gives the failure strain for the various GF-PP produced with RGF. Given the large error bars it is difficult to reach any conclusions regarding the GF-PP prepared with un-modified PP. GF-PP produced with MAPP display significantly lower failure strains. It is the consensus that fibre ends act as failure initiation sites in discontinuous fibre composites [204-207]. Stress concentration at the fibre ends causes the growth of micro-voids and the formation of cracks along the fibre matrix interfaces. Several authors have observed a significant reduction in failure strain of GF-PP with increase IFSS [164], specifically with the addition of MAPP [205]. This suggests that the increase in UTS observed in Figure 5-18 may indeed be a result of increased IFSS when MAPP is used. Nagel also observed a reduction in unreinforced PP failure stain with MAPP loading, therefore a change in matrix properties should not be overlooked as a contributing factor to the observations in Figure 5-19 [68]. It is known that the other factors such as fibre length [206, 208, 209], fibre orientation [208, 210] and fibre content [163, 204, 206-208, 210] influence stain at failure of GF-PP however these are all presumed constant for composites tested in Figure 5-19.

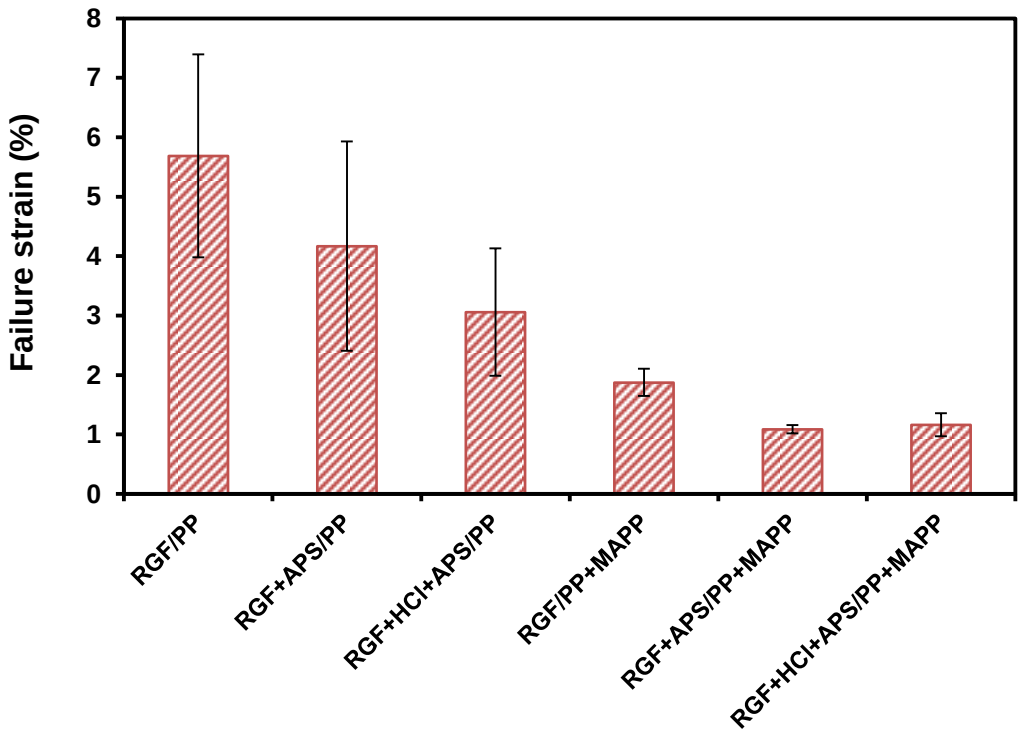

Figure 5-19 Failure strain of GF-PP produced using fluidised bed RGF after various treatments. Matrix modification with MAPP significantly reduces the failure strain of the GF-PP.

Figure 5-20 gives the yield strain of the various GF-PP, which was automatically calculated by the Instron analysis software at 0.2% plastic deformation. For reference, the yield strain for GF-PP prepared with new glass fibre (PPG 8069) was measured to be 2.79±0.18% and 2.92±0.20% with 0% and 5% MAPP content respectively. The trend in yield strain closely maps to that of UTS in Figure 5-18, with an increase in yield strain for the stronger GF-PP prepared with the MAPP modified PP matrix. A similar relation was observed by Nagel, however the yield strains found in this work are significantly lower [68]. This is presumably due to the considerably higher strength of GF-PP measured in [68].

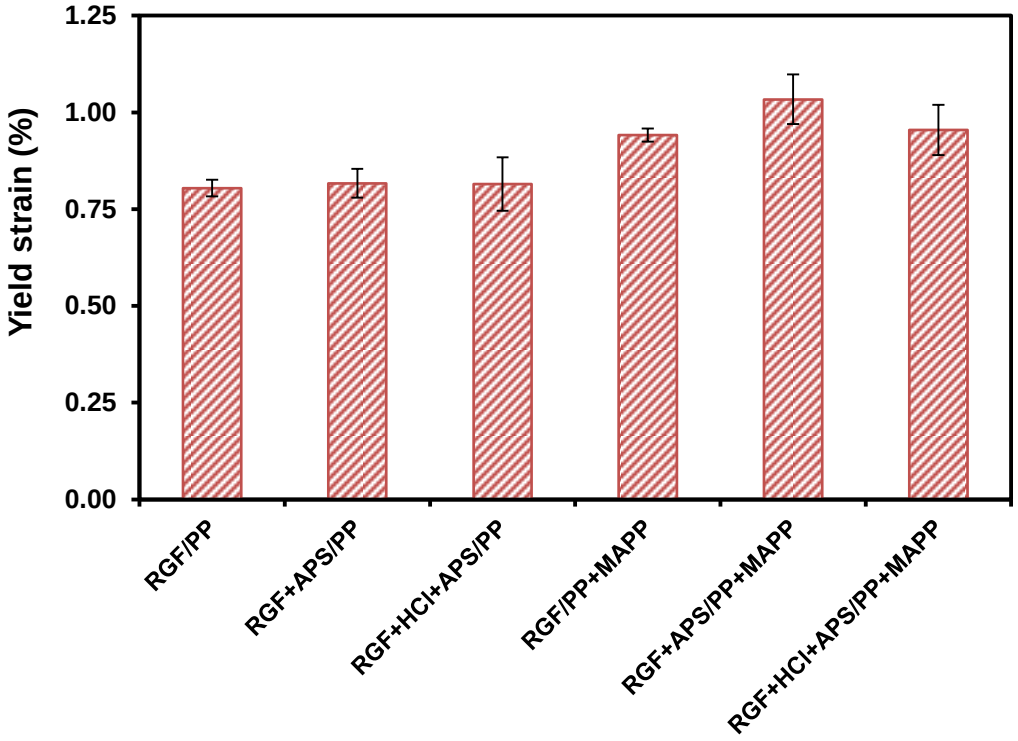

Figure 5-20 Yield strain of GF-PP produced using fluidised bed RGF after various treatments

Figure 5-21 gives the modulus of the various GF-PP, which was automatically calculated using the Instron analysis software. For reference, the modulus for GF-PP prepared with new glass fibre (PPG 8069) was measured to be 4.19±0.24 GPa and 4.67±0.17 GPa with 0% and 5% MAPP content respectively. The modulus of discontinuous GF-PP depends mainly on the fibre content [163, 207, 211, 212] and fibre orientation [208, 213, 214]. The fibre length also influences the modulus, however Thomason and Vlug observed the modulus of GF-PP is practically inependent of fibre length when longer than 0.5 mm [211]. Given the measured average fibre length in Table 5-7 is significant higher than 0.5 mm, it may be expected that (for the given fibre content and orientation) the maximum GF-PP stiffness is attained. There is of course a distribution of fibre lengths within the composites in Figure 5-21 and a portion of the fibre content will indeed be below 0.5 mm. It therefore appears plausible that in this case, fibre length may indeed influence GF-PP modulus.

Figure 5-21 shows that GF-PP prepared with MAPP modified PP exhibit a significantly higher modulus than those with PP only. This was also observed with GF-PP prepared with new glass fibres. A constant fibre volume fraction was used

throughout this work so is not the cause for the variation in modulus. All GF-PP specimens were prepared using the same procedure therefore; it is unclear how the modulus could vary due to inconsistent fibre orientation. There does not appear to be an evident mechanism for MAPP powder to influence the fibre orientation during the wet deposition method used to prepare the GF-PP; however, one should not be discounted.

The literature is presently lacking studies into the effect of MAPP on the modulus of discontinuous glass fibre composites. Lichao et al. observed an increase in modulus of PP–glass fibre/basalt fibre hybrid composites when MAPP was presented in the PP matrix [215]. Hong et al. also observed an increase in modulus of jute fibre-PP composites when MAPP was introduced [216], which was accredited to increased IFSS. The increased UTS observed in Figure 5-18 when using MAPP is attributed to increased IFSS, which may also be the cause for the increase in modulus.

It is not entirely clear how the MAPP or the method for introducing the MAPP will affect the modulus of the PP matrix as a whole. According to the rule of mixtures the matrix modulus will influence the overall composite stiffness [204]. This may be another cause for the variation in modulus when MAPP is used, which requires further work to fully explain.

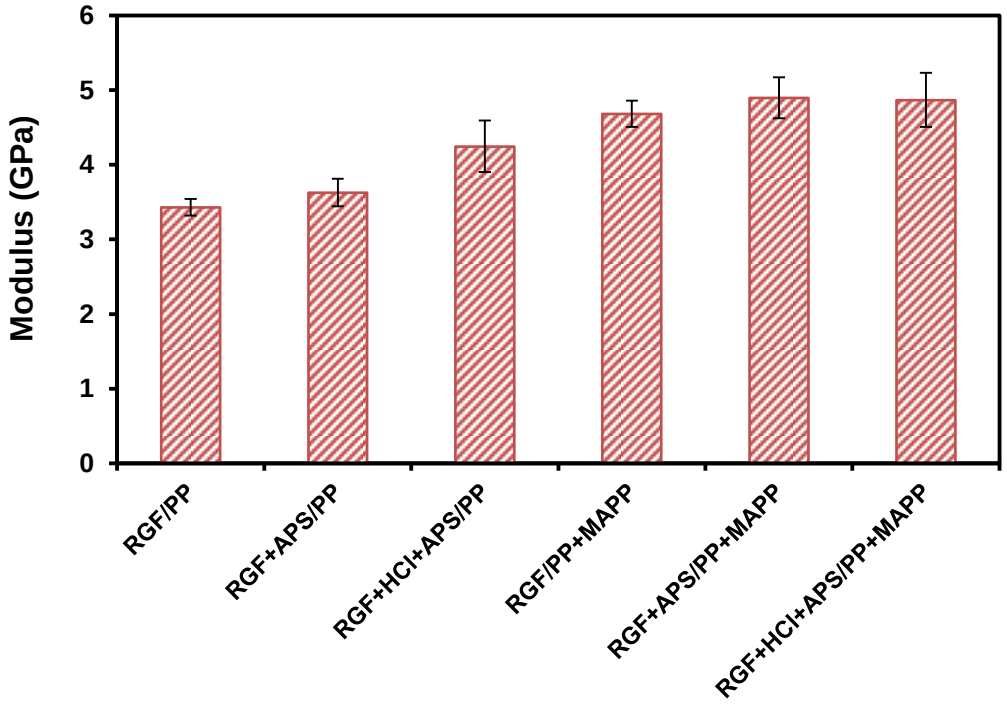

Figure 5-21 Modulus of GF-PP produced using fluidised bed RGF after various treatments. GF-PP containing MAPP universally show a rise in the modulus which may be a higher of greater IFSS.

5.3.1.4 Effect of fibre strength and interface regeneration on GF-PP mechanical properties

In this section the tensile, flexural and impact properties of various GF-PP prepared with RGF with and without strength regeneration is given. All fibres were recycled in the fluidised bed at 500 °C. All NaOH treatments were carried out at 7 mol/L for 2 hour, given that this was found to be optimal for strength regeneration in Chapter 4. As before, Table 5-8 defines the materials and treatments used.

Tensile properties of GF-PP

Figure 5-22 gives the UTS of GF-PP prepared with RGF treated in NaOH with various treatments used in an attempt to regenerate IFSS. As a comparison, the data from Figure 5-18 is included, showing the UTS of GF-PP prepared with RGF not treated in NaOH.

The UTS of GF-PP reinforced with fibres without any IFSS regeneration treatments (RGF/PP) is significantly increased with the use of the NaOH treatment. This is most

likely a result of an increase in reinforcement potential of the strengthened fibres. Furthermore, the reduction in diameter observed in Figure 4-26 after the NaOH treatment, would, according the K-T model, increase the UTS of the GF-PP. In discontinuous fibre composites, reducing the fibre diameter (for a given fibre strength and IFSS) will reduce the critical fibre length. This leads to a greater proportion of fibres longer than the critical fibre length being present, therefore, producing composite with higher tensile strength.

Despite the improvement, the UTS of GF-PP produced with NaOH treated fibres remains lower than is observed in other studies [15, 68]. Thomason et al. reported GF-PP strength of around 52 MPa when prepared with thermally conditioned and NaOH strengthened fibres [15]. Similar composite preparation techniques, average fibre length, fibre diameter and fibre volume fraction were used in both this work and by Thomason et al. [15]. The strength of NaOH treated fibres used in [15] was around 1.6 GPa, which is slightly stronger than those used in this work found in Figure 4-44. In both this work (Figure 4-47) and in [15], it was found that IFSS is low (<9 MPa) when fibres were thermally conditioned/recycled and treated with just NaOH. Under such conditions, the K-T models suggests that increase in fibre strength of around 0.2-0.3 GPa provides little improvement to overall GF-PP strength. It is therefore unlikely that the difference in fibre strength is the sole cause for the disparity in composite strength. Despite having comparable average fibre lengths, the proportion of fibres greater than the critical fibre length was not given in [15]. Since many of the strength determining parameters used in [15] are similar to this work, the fibre length distribution (opposed to average fibre length) may be the cause for the disparity in GF-PP strength.

Fibres treated with NaOH then APS or HCl+APS provide no additional improvement to GF-PP UTS. For APS only treated fibres this is not surprising, given that no additional improvement to IFSS was observed in Figure 4-47 for these specimens. HCl+APS treatment on the NaOH treated fibres were however shown to considerably improve IFSS in Figure 4-47. The cause for this not translating to GF-PP strength is ambiguous. Using the fibre length distributions and fibre strengths from the specimens treated with NaOH, the K-T model suggest that increasing the IFSS from 7.2 MPa to 12.1 MPa (as was found in Figure 4-47) provides an 8.5% increase in GF-PP tensile strength. It was found in Figure 4-56 however that HCl reduces the strength of NaOH treated fibres. When taking this reduction in strength into account, the overall strength increase in GF-PP after HCl+APS treatments is

estimated to be just 4.2%. Although an increase is still expected according to the K-T model, it is likely too small to fall out with the margin of error at 95% confidence limit.

Figure 5-22 shows that introducing MAPP into the PP matrix significantly increases the strength of the GF-PP prepared using NaOH treated fibres. As before, this suggests the MAPP can increase the IFSS between the glass fibre and PP matrix. It still appears however that the strength of the GF-PP is lower than would be expected according to other studies [15, 68]. The addition of APS or HCl+APS treatments do not appear to significantly alter the strength of GF-PP when MAPP is used. Although it is understood that MAPP can increase the IFSS without the presence of a sizing (most likely through polar interactions), MAPP in combination with a coupling agent (such as APS) provide a further increase in IFSS through acid-base interactions [155-157]. The lack of improvement when APS is used in combination with MAPP suggests that; 1) the APS remains (to some degree) un-bonded to the surface of the glass fibres, or 2) the MAPP is not interacting with APS that is bonded to the fibre surface. Further work needs to be carried in terms of identifying the cause for the apparent lack in IFSS when using these fluidised bed RGF with PP matrices. Some methods for exploring this issue are proposed in the Future Work section.

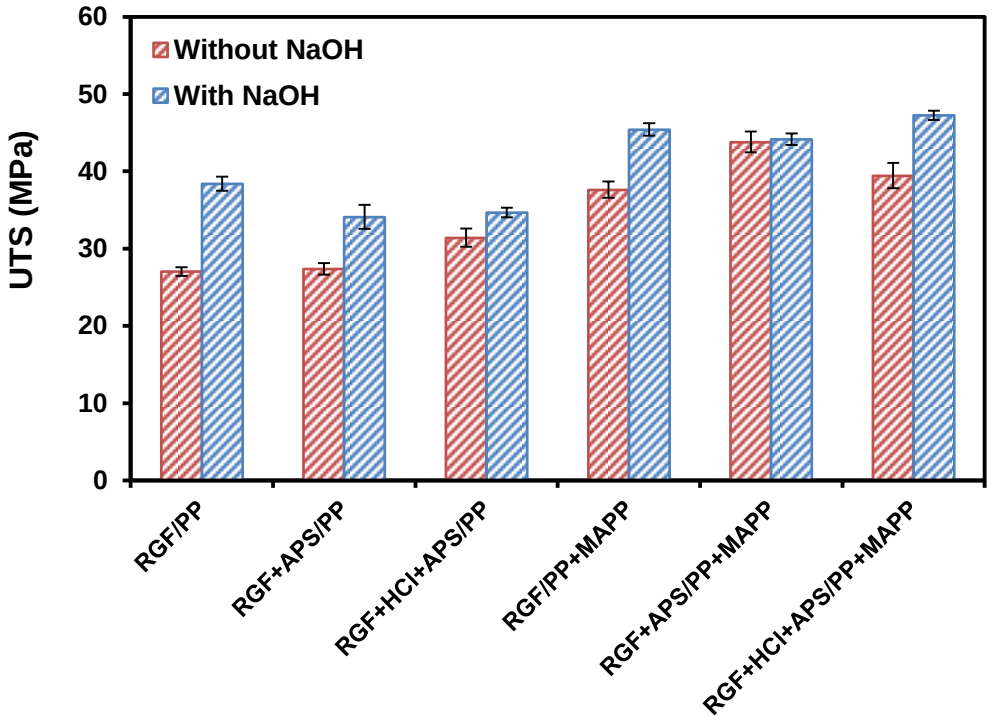

Figure 5-22 UTS of GF-PP produced using fluidised bed RGF after various treatments. Under most circumstances, using RGF treated in NaOH improves the UTS of GF-PP.

The trend in failure strain of GF-PP prepared with NaOH treated fibres, shown in Figure 5-23, closely follows that found when using RGF not treated with NaOH. It appears that the tensile strength of the glass fibres (within the range 0.6-1.4 GPa) does not significantly affect the failure strain of GF-PP. To the best of the author's knowledge, there is no other work in the literature relating fibre strength to the failure strain of GF-PP.

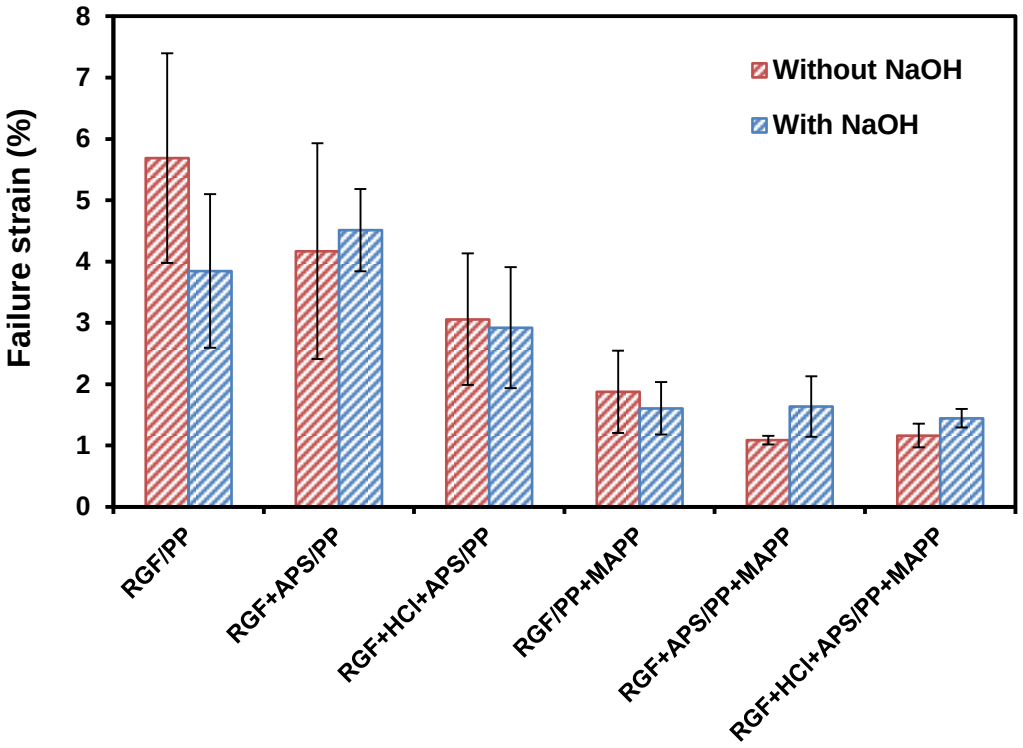

Figure 5-23 Failure strain of GF-PP produced using fluidised bed RGF after various treatments

Figure 5-24 gives examples of stress-strain plots obtained during tensile testing of GF-PP prepared with RGF after various regeneration treatments and matrix modification. The stress strain curves in Figure 5-24 show that all specimens, except those prepared with a modified PP matrix, show significant plastic deformation prior to failing. In contrast, the composites prepared with the MAPP modified PP matrix failed almost immediately beyond the yield strain. This would be expected given the dramatic reduction in failure strain observed in Figure 5-23 when MAPP was used.

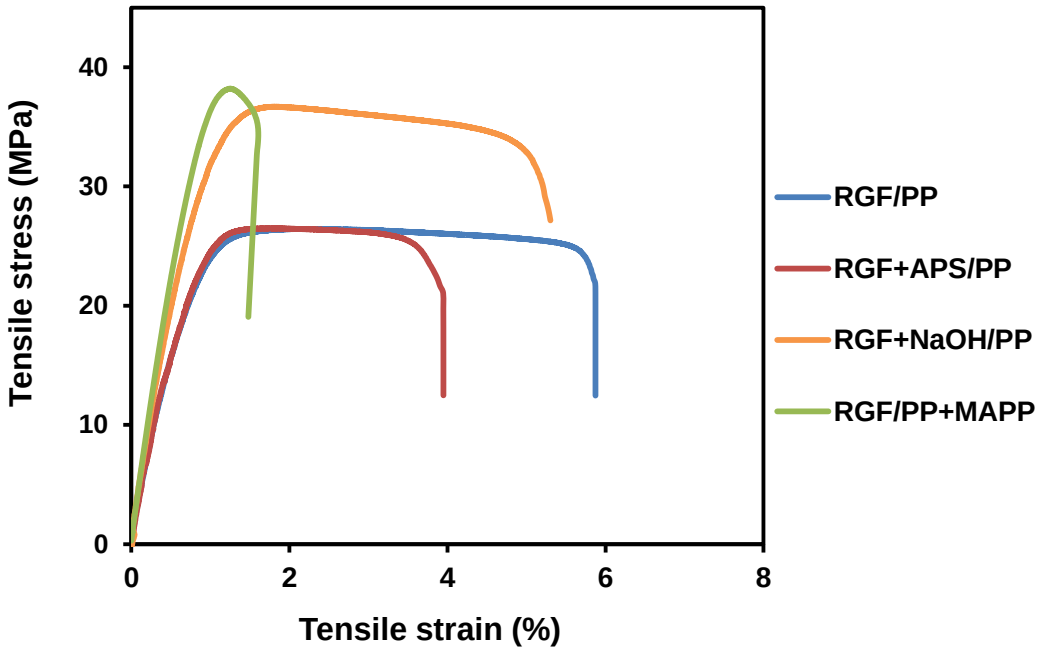

Figure 5-24 Stress-strain plots obtained during tensile testing of GF-PP prepared with RGF after various regeneration treatments and matrix modification

The modulus of the GF-PP produced with NaOH treated fibres is given in Figure 5-25. There appears to be no significant variation between GF-PP prepared with or without NaOH treated fibres. Again, GF-PP with MAPP modified matrices appear to have a slightly higher modulus which may be attributed to increased IFSS in those specimens [215, 216].

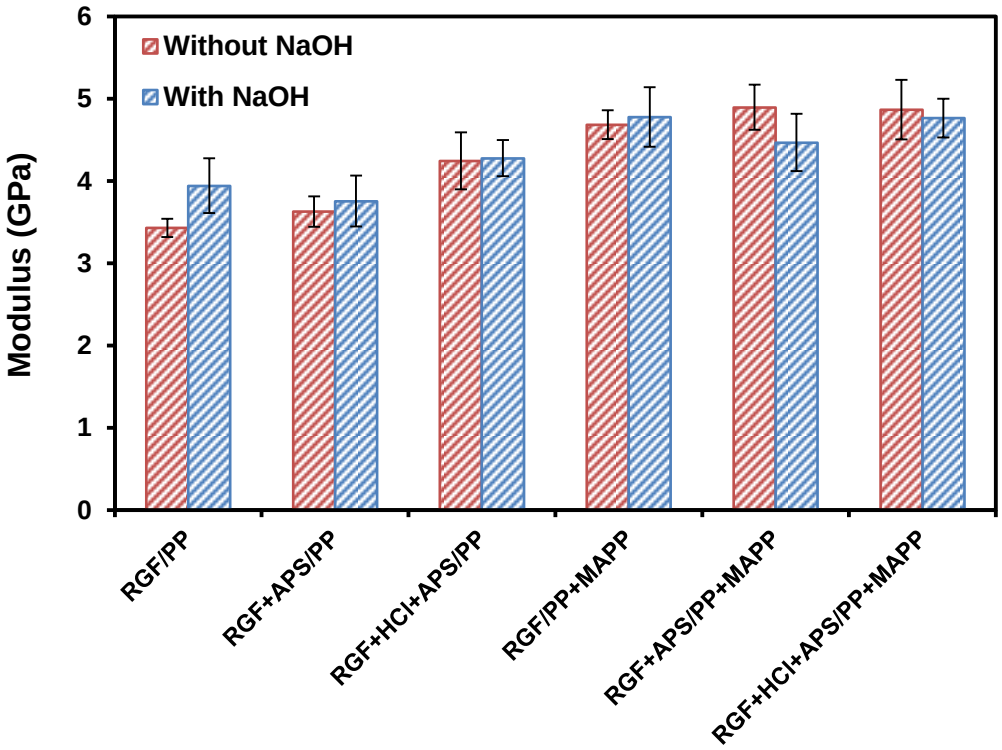

Figure 5-25 Modulus of GF-PP produced using fluidised bed RGF after various treatments. Preparing GF-PP with NaOH treated RGF does not appear to effect the composite modulus.

Flexural strength of GF-PP

Figure 5-26 gives the flexural strength of GF-PP prepared with fluidised bed RGF. As before, NaOH treatment was carried out at 7 mol/L for 2 hour. The notation used in Figure 5-26 is outlined in Table 5-8. The flexural strength of GF-PP has previously been shown to be dependent on fibre content [206, 207, 212], fibre length [206] and IFSS [217]. Within the literature, the flexural strength of GF-PP produced with new fibres has been found to be 60-230 MPa depending on the properties listed [217, 218].

Figure 5-26 shows that for each specimen the flexural strength is higher than that observed under tension, which is typical for such materials and suggests the surface of the GF-PP has less flaws/defects relative to the bulk material. The flexural strength of GF-PP is increased by treating fibres in NaOH. This is likely due to the increased fibre strength in these specimens. Figure 5-26 shows the addition of APS treatment slightly increases the flexural strength of GF-PP prepared with fibres not treated in NaOH. This may be a result of slightly higher IFSS, which was observed in Figure 4-47. Similarly, no significant increase in flexural strength was observed for

specimens prepared with NaOH treated fibres, where no increase in IFSS was observed in Figure 4-47. Specimens containing MAPP show further improvement in flexural strength. This is expected with increased IFSS and in agreement with Bowland et al., who found that flexural strength of GF-PP increased with MAPP content [217]. GF-PP containing NaOH treated fibres have the highest flexural strength and exhibit around a 70% increase in strength compared un-modified PP reinforced with untreated RGF. Despite this increase in flexural strength in Figure 5-26, the specimens are still lower than is found in the literature using new glass fibres.

Bowland et al. prepared “long” glass fibre polypropylene (using direct long fibre thermoplastic moulding) and observed a GF-PP flexural strength of approximately 130 MPa [217]. Lin et al. prepared GF-PP with “short” glass fibres and reported a flexural strength of around 120 MPa [219]. In both studies [217, 219], PP matrix was modified with maleic anhydride and a similar fibre loading of 30% by weight was used. No values for average fibre length, or length distribution, was divulged in [217, 219] making direct comparison to the flexural strength of GF-PP in Figure 5-26 difficult. It is clear however that further work must be carried out to determine how the strength of the GF-PP can be additionally improved. As was found from the tensile data, it would appear a lack in IFSS could be the source for the poor GF-PP strength. The cause for this needs identification in order to maximise the reinforcement potential of the fluidised bed RGF.

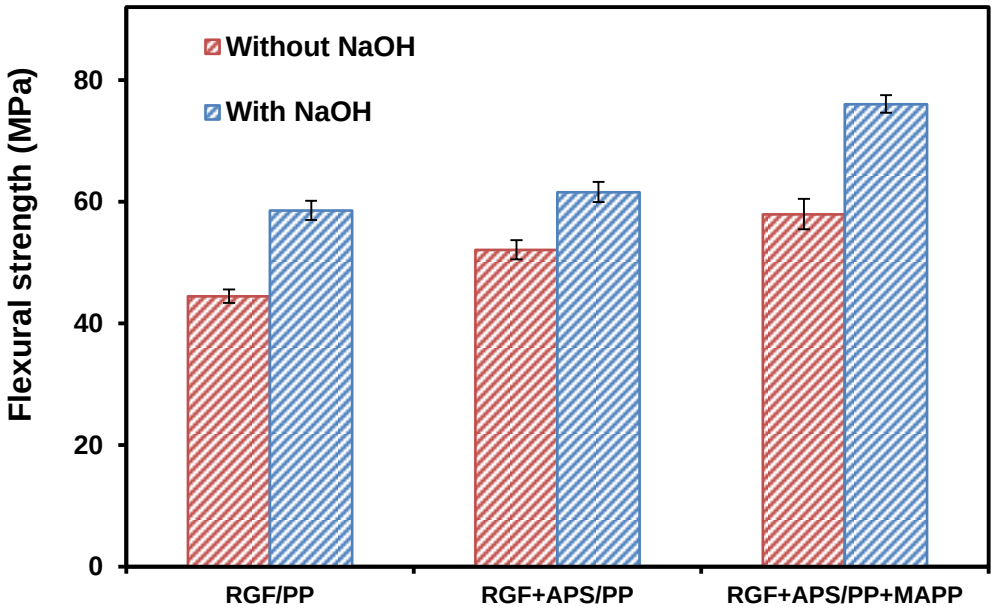

Figure 5-26 UFS of GF-PP produced using fluidised bed RGF after various treatments. In all cases, NaOH treatment increases the GF-PP UFS, with MAPP modification providing additional improvement to the strength.

Unnotched charpy impact strength of GF-PP

Figure 5-27 gives the unnotched charpy impact energy of GF-PP prepared with fluidised bed RGF. As before, NaOH treatment was carried out at 7 mol/L for 2 hour. The notation used in Figure 5-27 is outlined in Table 5-8. From the literature, it is understood that unnotched impact strength of GF-PP is dependent on the fibre length [212, 220], fibre content [163, 212, 220-222] and the IFSS [155, 164, 222]. Williams et al. propose models for the unnotched impact failure of fibre composites, suggesting the impact strength increases with fibre strength [223]. No studies directly measuring the influence of fibre strength on GF-PP unnotched impact strength could be found.

Figure 5-27 shows there is no change in impact energy of GF-PP prepared with RGF not treated with NaOH solution. From the tensile strength data in Figure 5-18, it is believed that the IFSS increases when the PP matrix is modified with MAPP. This suggests that (for these GF-PP composites) the impact energy is not influenced by fibre-matrix adhesion. From Figure 5-27 it can be seen that the impact energy of GF-PP prepared with NaOH treated fibres is considerably higher in all cases. In agreement with [223], it appears (under these circumstances) that increasing the

strength of reinforcement fibre improves the unnotched impact energy of GF-PP. The addition of MAPP in the matrix reduces the impact energy of the GF-PP when prepared with NaOH treated fibres probably due to less fibre pull-out.

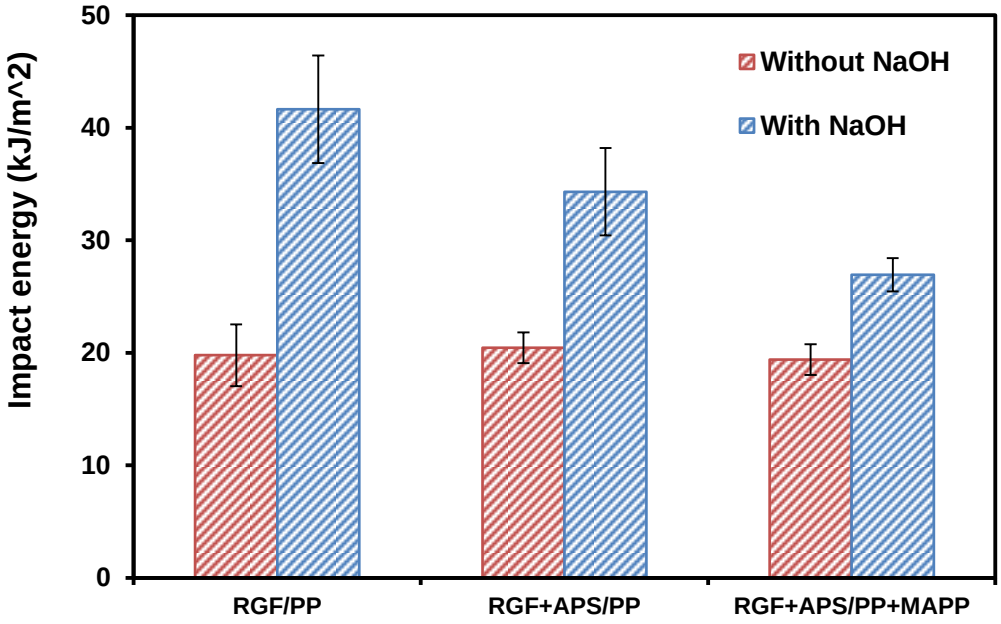

Figure 5-27 Unnotched charpy impact energy of GF-PP prepared with fluidised bed RGF

There is not a firm consensus on the effect of IFSS on GF-PP impact energy in the literature. Mader et al. [164] observed an increase in impact energy when the IFSS was optimised with a suitable film former. Another study by Mader and Pisabova [155], however, could not determine a trend between IFSS and impact energy of GF-PP when investigating various film formers and matrix modification with MAPP. Nagel and Bowland observed an increase in impact energy of GF-PP with the addition of MAPP, however, this decreased when an optimum MAPP content was exceeded.

Unlike traditional materials such as metal or plastics, the impact failure mode of composite materials is often complex and difficult to determine [224]. Several energy dissipation mechanisms during impact testing have been identified for fibres reinforced composites, including matrix fracture, matrix deformation, fibre pull-out and fibre fracture [212, 220, 225]. No decisive conclusion can be made on the failure mechanisms of the specimens in Figure 5-27 however; the contributions of the

energy mechanisms were affected by fibre strength and the addition of MAPP. Since the IFSS does not appear to influence the impact energy of GF-PP prepared with fibres not treated in NaOH, it would appear that energy is predominantly absorb though fibre fracture, matrix deformation and fracture. The impact energy of GF-PP increases when prepared with NaOH treated fibres, suggesting that, for these specimens, fibre fracture also governs the energy absorption. The addition of MAPP into these specimens reduces the impact energy; indicating that fibre debond and pull out are also mechanisms which significantly influence the energy adsorption. The cause for the disparity in adhesion dependence between GF-PP produced with and without NaOH treated fibres may be related to the different fibre strengths. Strengthened glass fibres could potential enable debonding and subsequent fibre pull-out to significantly improve energy absorption. This is simply an assertion and further work is required to fully understand the impact failure mechanisms.

5.3.1.5 Effect of NaOH concentration on GF-PP tensile strength

The effect of varying the NaOH concentration used to regenerate the RGF strength was also investigated in terms of GF-PP tensile strength. Fibres were recycled in the fluidised bed at 500 °C then treated in NaOH for 2 hour in each case. As shown in Figure 5-22, APS does not improve the strength of GF-PP reinforced with fibres treated in NaOH and was therefore not applied to fibres used in Figure 5-28 and Figure 5-29. All samples were prepared with PP modified with 5% MAPP. Figure 5-28 shows the UTS of GF-PP produced with RGF treated with 5, 7 and 10 mol/L NaOH solutions. As would be expected, there is an increase in strength of GF-PP for each of the NaOH concentrations used, with a second order polynomial accurately describing the relation. Given the error bars, there is no significant variation in GF-PP strength with NaOH concentration. Under these circumstances such an aggressive NaOH treatment may therefore not be required to achieve similar GF-PP tensile strengths.

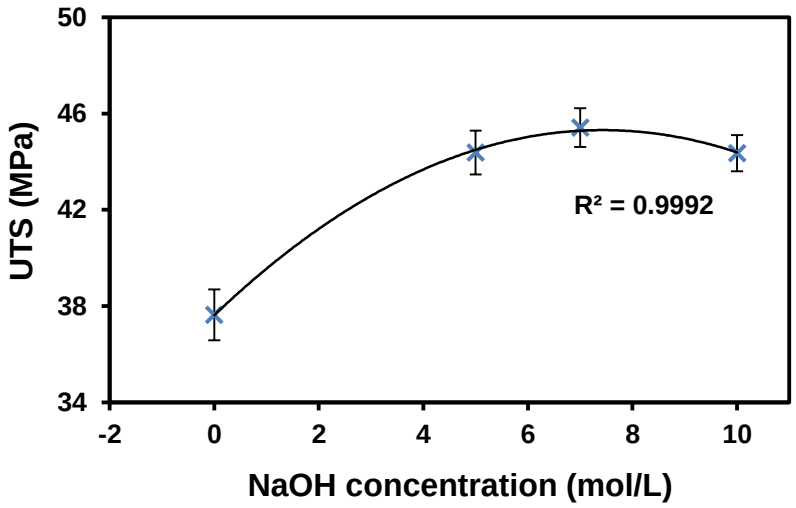

Figure 5-28 Effect of NaOH concentration on GF-PP strength

Figure 5-29 gives the UTS of GF-PP prepared with NaOH treated fibres as a function of fibre tensile strength. As with NaOH concentration, there is clearly an overall trend of increase UTS of GF-PP with fibre strength, as would be expected from the K-T model in Figure 5-15. However, given the relatively large error bars, there is no clear trend between the GF-PP reinforced with NaOH treated fibres. If IFSS could be further improved the influence of fibre strength may become clearer, since, according to Kelly-Tyson model in Figure 5-15, the strength of GF-PP prepared with higher strength fibres increase more rapidly with an increase in IFSS.

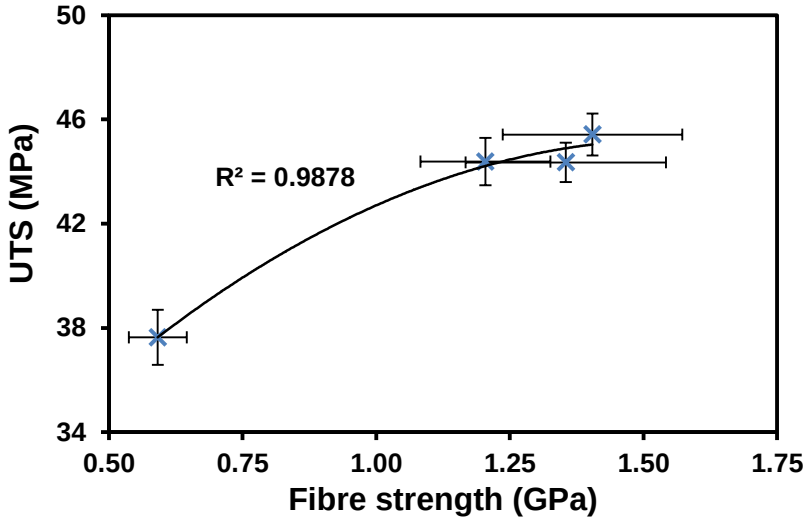

Figure 5-29 UTS of GF-PP prepared with NaOH treated fibres as a function of fibre tensile strength

5.3.1.6 Effect of hot water treatment on GF-PP tensile strength

In Figure 4-44 it was observed that the strength of fluidised bed RGF could be improved by the action of hot water treatment for 4 days. To investigate how this translated to composite strength, GF-PP were produced with hot water treated RGF and compared to GF-PP prepared with untreated RGF. In each case, APS was applied to the fibres and PP matrix modified with 5% MAPP was used since this was the optimum condition for GF-PP based on recycled only fibres, as seen in Figure 5-18.

Table 5-9 gives the UTS of the GF-PP prepared with hot water treated fibres. The hot water treatment actually reduces the GF-PP average UTS; however, given the error, this is not significant. It is not entirely clear why the increase in fibres strength attained with the hot water treatment did not translate to GF-PP strength improvement. At 5 mm gauge length the difference in fibre strength (in Figure 4-44) was not significant given the relatively large errors in the data. Overall, the four day hot water treatment does not appear to improve the strength of GF-PP, most likely because the fibre strength regeneration (if any) was relatively low at 5 mm gauge length.

Table 5-9 Tensile strength of GF-PP produced with 4 day water treatment at 90 °C

Sample	Fibre treatment	Matrix	UTS (MPa)
RGF+APS/PP-MAPP	1 vol% APS	PP matrix modified with 5% MAPP	43.8±1.34
RGF+hot water+APS/PP-MAPP	Water treatment at 90 °C for 4 days followed by 1 vol% APS	PP matrix modified with 5% MAPP	40.9±1.06

5.3.1.7 Effect of integrating new glass fibres on GF-PP tensile strength

The effect of preparing GF-PP with a mixture of fluidised bed recycled and new (PPG 8069) chopped glass fibres was investigated. The influence of treating RGF in APS and using modified PP matrix was also investigated when used in combination

with new glass fibres. No HCl treatment was used as it was found in Figure 5-18 that APS treatment in conjunction with a MAPP modified matrix is optimum for RGF without any strength regeneration treatments. The total glass fibre content remained constant throughout, only the ratio between new and RGF was altered. The new glass fibres were not treated in APS as they are already commercially sized and presumed to have a silane based coupling agent present. Table 5-10 gives a description of the samples tested in Figure 5-30.

Table 5-10 Description of samples in Figure 5-30

Sample	Fibre	Matrix
RGF/PP	Fluidised bed recycled at 500 °C	Unmodified PP
RGF+APS/PP-MAPP	Fluidised bed recycled at 500 °C treated with APS	PP modified with 5% MAPP

Figure 5-30 gives the UTS of the GF-PP prepared with both recycled and new glass fibres. Whether the interfacial adhesion is improved (with APS and MAPP) or not, there appears to be a near linear relation between UTS and ratio of new fibre content. Replacing 50% of new fibres with fluidised bed RGF reduces the strength of GF-PP by approximately 33% and 28% when interface is and is not improved respectively. This is in contrast to Kennerley et al. who reported the strength of polyester based DMC was unchanged when replacing 50% of the glass fibres with fluidised bed RGF [14]. Moreover, Kennerley did not apply an additional sizing to the RGF to improve adhesion with polyester matrix. Åkesson et al. also reported a reduction in composite properties when replacing new glass fibres with RGF at a ratio of 50%. A 45% reduction in flexural strength was reported when replacing with microwave pyrolysis RGF in GF-polyester composites. No studies reporting the effect of combining new and RGF in GF-PP (or any thermoplastic) could be found in the literature.

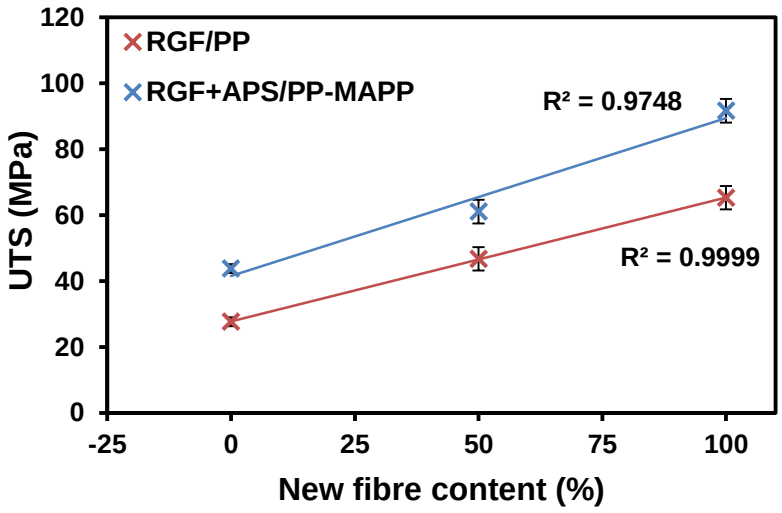

Figure 5-30 UTS of GF-PP prepared with both recycled and new glass fibres. There appears to be a near linear relation between UTS and ratio of new fibre content.

5.3.2 Tensile properties of GF-EP prepared with recycled and regenerated glass fibres

Given the appeal of superior mechanical properties, much research has focused on the tensile properties of GF-EP containing continuous fibre reinforcement; be that unidirectional [226-229] or woven [230-232]. Reported tensile strength of unidirectional and woven reinforced GF-EP range from 710-1000 MPa [227, 229] and 110-470 MPa [230, 232-234] respectively. The fibre volume fraction remains relatively consistent between studies (typically 50-55%), however specimen geometry and preparation techniques vary significantly, making direct comparison problematic.

Prior downsizing of recyclate and loss of alignment during the recycling process meant that GF-EP prepared with RGF was reinforced discontinuously with random fibre orientation. Fewer studies in the literature report the tensile properties of discontinuous-randomly oriented GF-EP. Heckadka et al. report the tensile strength of GF-EP prepared with chopped strand mats (CSM) to be 170-220 MPa depending on fibre content [233]. The length of fibres in the CSM were not disclosed however are likely significantly longer than those in this work, given that CSM typically use a fibre length of around 50 mm. Matei et al. prepared GF-EP with 5 mm long fibres, and measured a tensile strength of 79 MPa [235]. No fibre content was reported, however, the strength of GF-EP found in [235] is slightly higher than was measured for unreinforced epoxy in Chapter 3.

In this thesis, GF-EP were prepared with glass fibres recycled from the wind turbine blade. As in Chapter 4, NaOH and APS regeneration treatments were applied to these RGF, where NaOH treatment was 7 mol/L for 2 hour. Ashing of the tensile specimens after tensile testing revealed that the glass fibre content of the GF-EP were relatively low, at just 19.9±0.6% by weight. Other than hand layup, vacuum infusion was the only in house method available to prepare the GF-EP from RGF, and was believed that this process would yield superior composites in terms of void and fibre content. Unlike new glass fibre textiles (continuous or discontinuous), the mats prepared with RGF were “fluffy” in architecture and highly porous, as can be seen in Figure 5-7. Despite the air being removed when under vacuum, it was observed that the volume of the composite increased significantly as the resin was introduced (more so than when using new glass fibre textiles). The vacuum pump was ran for 10 min after epoxy resin had infused the mats in this work, however, running for longer would likely help draw out excess resin and increase fibre content.

Figure 5-31 gives the UTS of GF-EP produced using fluidised bed RGF, the strength of epoxy only specimens (from Figure 3-12) is included for reference. Introduction of the RGF provide a slight increase in UTS, however, when considering the error, it is unclear how significant this improvement is. GF-EP strength increases by approximately 14 MPa when reinforced with RGF treated in NaOH, which is apparently a consequence of the significant increase in both RGF strength (Figure 4-44) and IFSS (Figure 4-52) after NaOH treatment. The strength of GF-EP prepared with RGF and RGF+NaOH slightly increase when APS is applied; again, given the uncertainty, the increase is not significant. Due to fibre breakage during microbond testing, no valve for IFSS with APS treated RGF could be found, although it was concluded that APS does indeed increase adhesion when used with RGF. Figure 5-31 suggests that the rise in adhesion, provided by APS alone, is not sufficient to translate to a substantial increase in the reinforcement potential of RGF. It is understood that the optimal fibre loading for maximising FRT strength is significantly higher than that of the GF-EP prepared with RGF in this work [197]. The true reinforcement potential of the RGF may therefore not be realised in terms of the measured UTS of the GF-EP in Figure 5-31.

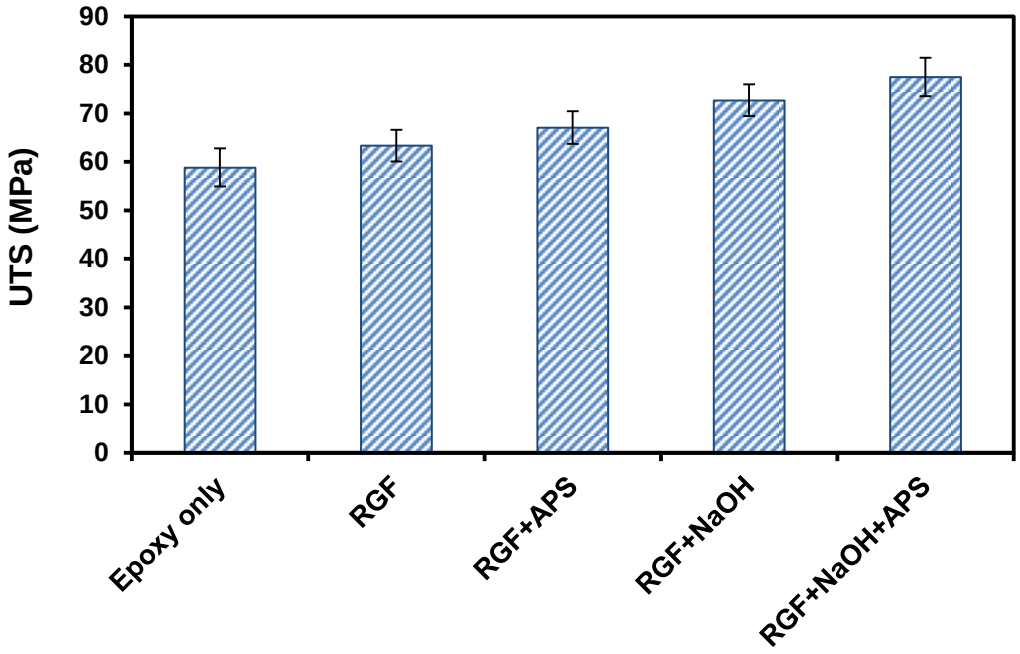

Figure 5-31 UTS of GF-EP produced using fluidised bed RGF after various treatments. Reinforcing with RGF provides only a slight strength gain compared to epoxy only, most likely due to low fibre content.

Figure 5-32 gives the modulus of the GF-EP prepared with fluidised bed recycled glass fibres. For all specimens, the introduction of the RGF provides a significant increase in modulus. The modulus of discontinuous GF-EP does not appear to be affected by the fibre strength or IFSS, represented by the NaOH treated fibres. It is understood that the modulus of GF-EP is influenced by the fibre content [236], therefore a further increase in GF-EP stiffness may be achieved by increasing the fibre loading.

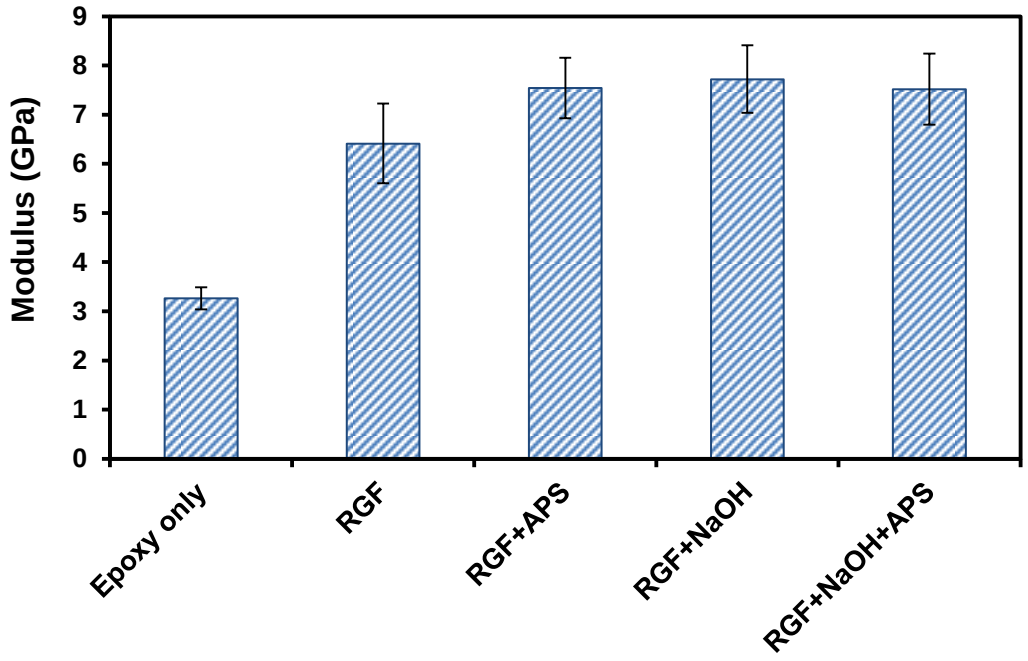

Figure 5-32 Modulus of GF-EP produced using fluidised bed RGF after various treatments. In all cases, the modulus of the GF-EP is greatly increased with the addition of the RGF.

Figure 5-33 gives the failure strain of the GF-EP prepared with the fluidised bed recycled glass fibres. As would be expected, reinforcing with glass fibres decreases the failure strain of the GF-EP [237]. Increasing fibre strength and IFSS with epoxy, using NaOH, does not significantly influence the failure strain of the GF-EP. This is in contrast to the observations made in Figure 5-23, which suggested that increasing adhesion through MAPP modification significantly reduced the failure strain of GF-PP. This disparity may be a result of epoxy being a considerably more brittle matrix material than PP [68]. For FRP reinforced with discontinuous glass fibres, failure strain does not vary with fibre loading [237], therefore no change in Figure 5-33 would be expected if RGF content of GF-EP was increased.

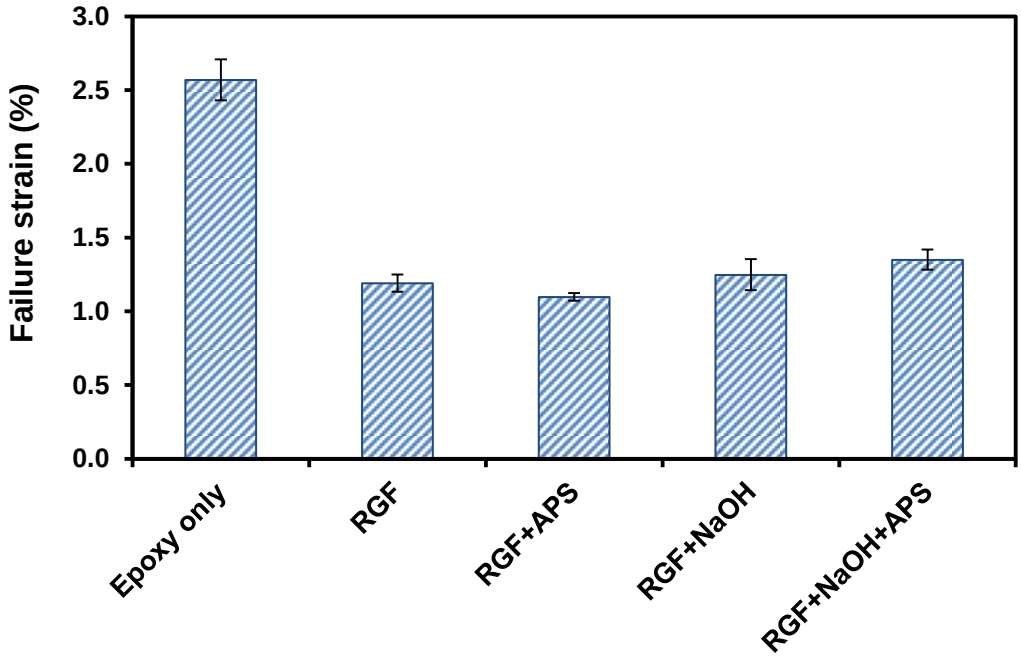

Figure 5-33 Failure strain of GF-EP produced using fluidised bed RGF after various treatments

5.4 Conclusions

In this chapter, recycled and regenerated glass fibres were used to produce GF-PP, which were subsequently mechanically characterised. Using the K-T model it was initially established that regenerating the strength and/or IFSS of fluidised bed RGF should significantly improve the strength of GF-PP. A method for integrating powdered MAPP into the wet deposition was established. It was found that the tensile strength of GF-PP prepared with new fibres could be increased by up to 40% using this technique. Loading greater than 5% MAPP by weight yielded no further improvement to GF-PP strength.

For specimens containing un-modified PP matrix, it was found that the tensile and flexural strength of GF-PP could be significantly improved by the used of NaOH treatment (7 mol/L for 2 hour). This was attributed to the increase in fibre strength after the NaOH treatment. Despite the IFSS data in Figure 4-47, the tensile strength of GF-PP prepared with NaOH treated fibres was not improved through HCl treatment. This may be explained by the impact of the relatively low increase in IFSS being diminished by a simultaneous loss in fibre strength, as a result of the HCl treatment. The addition of 5% weight MAPP improved the tensile and flexural strength of GF-PP for all specimens. This was attributed to an increase in IFSS

provided by the MAPP. It was found that MAPP could increase adhesion to fibres without an APS coating.

All the fibre strength and IFSS regeneration treatments investigated in this chapter yielded GF-PP that are significantly lower than that of GF-PP prepared with new glass fibres. The fibre strength regeneration in this work is similar to that in other studies that yielded significantly stronger GF-PP. It is therefore believed that a weak IFSS is the cause for the poor composite strength. The application of APS did not influence the tensile strength of GF-PP prepared with NaOH treated fibres. This suggests the APS is not functioning effectively as a coupling agent between the fibre and matrix (whether modified or un-modified). This could be related to APS not sufficiently bonding to the glass fibres surface. It is unclear how recycling GF-EP in the fluidised bed affects the surface functionality of the recovered fibres. Other studies have simply investigated the IFSS after thermal conditioning fibres within a furnace, opposed to after thermal recycling from a polymer matrix. In the case of NaOH treated fibres, significant material is etched exposing a new external surface. The composition and structure of this new surface is not understood; it is therefore unknown how this may affect compatibility with APS. Further work must be carried out to fully understand the cause of poor GF-PP strength in order to maximise the reinforcement potential of RGF.

Other tensile properties such as strain at failure and modulus were also discussed. Treatment in NaOH did not appear to influence the failure strain. This suggests that fibre strength does not affect the failure strain of the GF-PP investigated in this work. It was found that the tensile strain at failure is significantly reduced when the PP matrix is modified with 5% MAPP. A similar phenomenon was overserved in other studies and is most likely attributed to an increase in IFSS. The modulus of GF-PP increased with the addition of 5% MAPP, whether the reinforcing fibres were or were not treated in NaOH. Like other others studies, this is attributed to an increase in IFSS provided by the MAPP.

The impact energy of the GF-PP was found to increase when prepared with NaOH treated fibres. It is believed that increasing the fibre strength also improves the impact energy. The addition of MAPP only affected the impact energy of GF-PP containing NaOH treated fibres, which was significantly reduced as a result. The cause for this may be differences in impact failure mechanism caused by the variation in fibre strength.

Other studies focusing on GF-PP in this chapter included investigating the effect of NaOH concentration, as well as mixing recycled and new fibres, on the tensile strength of GF-PP. Varying the NaOH concentration between 5 and 10 mol/L has little effect on the strength of GF-PP. This suggests that a less aggressive NaOH treatment may be used without significantly compromising the strength of GF-PP. A linear relation between new fibre content and GF-PP tensile strength was also found within the ratios tested.

GF-EP was prepared with fibres recycled from a scrap wind turbine blade using the fluidised bed rig. It was found that the resulting GF-EP had sub-optimal fibre loading, likely limiting their mechanical properties and the observable influence of the RGF. It was found that GF-EP prepared with NaOH treated RGF yielded approximately 14 MPa increase in UTS compared to unreinforced epoxy. APS treatment was not shown to significantly influence the UTS of GF-EP. It was found that GF-EP modulus increased while failure strain decreased when reinforced with RGF. Treating fibres in NaOH and/or APS provided no significant change to either modulus or failure strain, suggesting that (under these circumstances) neither is affected by variation in fibre strength of IFSS.

6. Conclusions and Future work

In this chapter, the aims of the thesis are reiterated and an overview of the conclusions that were drawn is given. Future research that can be performed based on the results and outcomes of this work are proposed.

6.1 Conclusions of the thesis

Fibre strength loss and sizing decomposition during recycling significantly reduces the reinforcing capability of thermally RGF, which is a key impediment in the commercialisation of recycling GRT. The main aim of this thesis was to investigate the potential for retaining and/or regenerating the strength and interface properties of thermally RGF; in order to produce composites reinforced with RGF that could complete with those prepared with new glass fibres. To achieve this, four objectives were outlined:

1. Develop an in-house process for thermally recycling GRT
2. Investigate the use of a catalyst to aid epoxy thermal decomposition
3. Investigate methods for regenerating the strength and interface properties of RGF
4. Investigate the performance of composites reinforced with thermally recycled and regenerated glass fibres

6.1.1 Thermal recycling glass fibres in fluidised bed

The effects of fluidisation velocity and bed temperature were investigated in terms of fibre recovery efficiency and cleanliness. It was found that the bed temperature is critical for increasing the yield efficiency of RGF from GF-EP recyclate. Increasing bed temperature up to 550 °C significantly reduces the degree of non-decomposed contamination on the RGF. The fluidisation velocity did not appear to influence the yield efficiency of the rig; however, additional sand contaminants did appear to increase when fluidising at ≥ 1.7 m/s.

The influence of fluidisation velocity and bed temperature on the tensile strength of RGF was established. It was found that neither fluidisation velocity nor bed temperature affects the strength of RGF. The lack of temperature-fibre strength

dependence suggests the fibres sustain addition mechanical damage elsewhere during the recycling process, which surpasses the thermal weakening.

6.1.2 Catalysed thermal recycling of glass fibres

The effect of CuO, Co_3O_4 and CeO_2 on reducing temperature and time required for GF-EP thermal recycling was investigated. It was found that all metal oxides had negligible effect on the Tg and normalised ΔH of the epoxy cure, and was concluded that the addition of metal oxide does not negatively affect the epoxy cure. The tensile strength of epoxy specimens was found to be unaffected when integrating metal oxide nanopowders at a weight loading of 5%. TGA was used to study the thermal decomposition of epoxy in the presence of the metal oxides. It was found that CuO is superior at reducing epoxy thermal stability, enabling full decomposition at just 375 °C under isothermal conditions in air. Using the K-A-S method, the apparent Ea at various conversions during epoxy decompositions was calculated. It was found that the metal oxides reduced the apparent Ea at conversion values associated with char decomposition.

An investigation into thermal weakening of glass fibre suggested that reducing the thermal recycling temperature and/or time could significantly increase the potential strength retention of thermally conditioned fibres. When applied to GF-EP thermal recycling in a furnace, CuO, CeO_2, and Co_3O_4 could reduce the epoxy matrix decompostion temperture required for glass fibre liberation by 120, 50 and 50 °C respectively. This yielded at least a 40% reduction in furnace energy consumption when recylcing with the aid of the metal oxides. The strength retention of fibres recycled using the metal oxides was increased by around 20%, depending on sample arrangement and recycling conditions. This was significantly lower than the strength of glass fibres thermally conditions under similar heating schedules, therefore, additional causes for the strength loss were investigated.

It was found that the thermal loading on fibres during GF-EP recycling increased significantly above the furnace set point temperature, which was attributed to exothermic epoxy decompostion. It was demonstrated that similar transitory high temperature exposure could considerably degrade fibre strength. Fibre strength loss was promoted when thermally conditioned in contact with the metal oxides. It was also confirmed that the metal oxides increased sizing decompostion during heating.

Consequently, sizing removal faciliated by the metal oxides as well as exposure to temperatures greater than the target recycling temperature likely contribute to the lack in strength retention of furnace RGF.

GF-EP with integrated CuO was recycled in the fluidised bed rig. Fibres could be recycled at just 400 °C with 60% yield, which was comparable to uncatalysed GF-EP at 500 °C. The tensile strength of RGF was not affected when using the catalyst during recycling. Despite this, it is postulated that such a decrease in bed temperature would reduce the energy required to recycle GF-EP. Finally, it was demonstrated that using CuO up to three times did not reduce its ability to facilitate an increase in thermal decomposition of epoxy.

6.1.3 Regenerating recycled glass fibres

It was found that soaking in hot NaOH solutions could significantly increase the tensile strength of glass fibres recycled from in-house prepared GF-EP recyclate. The treatment time required for strength regeneration were significantly higher for fibres recycled in the fluidised bed, compared to thermally conditioned fibres. It was concluded that increased damage sustained during the recycling processes required more etching to remove/sufficiently modify the surface flaws. It was determined that the rate of strength regeneration increases with NaOH concentration, with 7 and 10 mol/L yielding fibres with the highest measured strength of approximately 1.4 GPa. It appears this is a consequence of higher concentrated solutions providing accelerated etching of the fibre surface. Despite this, the tensile strength of NaOH treated fibres could not be characterised as a function of diameter reduction. Even when sufficient material was etched from the fibre surface to remove the largest flaws, according to fracture mechanics, the strength does not approach that of pristine fibres. This is likely due to NaOH creating features/artefacts on the newly exposed surface, which limits the potential for strength regeneration.

Hot water treatment also provided an increase in fibre strength, which plateaued at approximately 1 GPa after 96 hour. While still lower than as received fibres, the relative increase in fibre strength exceeds observations reported in studies on hot water treated bulk glass. Hot APS and water vapour treatments yielded no increase in the strength of RGF despite their reported effectiveness when used on thermally conditioned and abraded bulk glass respectively.

NaOH and hot water treatments were also applied to glass fibres recycled from a section of scrap (GF-EP based) wind turbine blade. It was found the NaOH treatment (7 mol/L for 2 hour) increased RGF strength from 0.7 to 1.7 GPa. Hot water soaking for 96 hour yield similar strength regeneration when applied to these RGF, demonstrating that the treatments can also increase the strength of “real world” end-of-life GRT.

The IFSS between RGF and PP was measured using the microbond technique. An IFSS with RGF/RGF+NaOH was found to be approximately 8 MPa, which was similar to that given by Nagel for thermally conditioned glass fibres [68]. No significant improvement in IFSS was observed with the addition of a coupling agent APS. This most likely due to 1) the APS is not bonded to the RGF surface, or 2) the APS is bonded to the glass surface however, the amine functional group of APS has only weak interaction with the PP.

Other studies suggest that exposing glass fibres to elevated temperatures can condense silanol groups on the fibre surface and in turn reduce chemical interaction with APS [62]. RGF and RGF+NaOH were also soaked in HCl as a means of improving IFSS with PP by increasing silanol concentration and therefore APS bonding with RGF surface. RGF treated in NaOH exhibited an increase in IFSS after HCl treatment. Given that untreated RGF IFSS did not increase with HCl along with correlating FTIR data; the increase exhibited in IFSS by RGF+NaOH after HCl is not likely due to increased silanol concentration.

Recycling the scrap wind turbine blade in the fluidised bed reduced the IFSS of RGF with epoxy by approximately 40%. APS appears to increase adhesion when applied to RGF, however, it proved difficult (using the microbond test) to quantify the IFSS with epoxy due to fibre weakness. Treating the RGF in NaOH (7 mol/L for 2 hour) significantly increased IFSS with epoxy to around 50 MPa, which approximates that observed with new, APS coated glass fibres. It is suggested that surface pitting/roughening, observed under SEM, and caused by NaOH etching may contribute to this rise in IFSS by facilitating matrix mechanical anchoring.

6.1.4 Reusing recycled and regenerated glass fibres

In this chapter, recycled and regenerated glass fibres were used to produce GF-PP, which were subsequently mechanically characterised. For specimens containing un-

modified PP matrix, it was found that the tensile and flexural strength of GF-PP could be significantly improved by pre-treating fibres in NaOH (7 mol/L for 2 hour), which was attributed to the increase in fibre strength. The tensile strength of GF-PP prepared with NaOH treated fibres was not improved by treating in HCl, despite the measured increase in IFSS in Chapter 4. Additional fibre strength loss may explain the ineffectiveness of HCl treatment failing to improve GF-PP strength. Adding 5% weight MAPP to the PP matrix increased the tensile and flexural strength of GF-PP for all specimens. It was concluded that an increase in IFSS was provided by the MAPP. It was also found that MAPP could increase adhesion to fibres without an APS coating. It was found that reducing NaOH concentration to 5 mol/L did not affect the tensile strength of GF-PP, suggesting that a less aggressive NaOH treatment may be used without significantly compromising the properties of GF-PP.

Despite similar fibre strength regeneration, the strength of GF-PP in this work is significantly lower than was reported in other studies. It was concluded that a weak IFSS is the cause for the lack in GF-PP strength increase. Applying APS to fibres did not alter the strength of GF-PP prepared with NaOH treated fibres, whether the PP matrix was or was not modified with MAPP. APS may not be functioning effectively as a coupling agent through insufficient bonding with the recycled glass fibre surface. It is still unclear whether this is an effect of thermal recycling from GF-EP in the fluidised bed or a result of the aggressive NaOH treatment.

Treating fibres in NaOH did not appear to influence the tensile failure strain, suggesting that fibre strength does not influence the failure strain of the GF-PP. It was observed that the tensile strain at failure is significantly reduced with the additional of MAPP, which was attributed to increased IFSS. The modulus of GF-PP increased with the addition of MAPP. As in other others studies, this is attributed to an increase in IFSS provided by the MAPP.

GF-PP prepared with NaOH treated fibres exhibited significantly higher impact energies. The addition of MAPP however significantly reduced the improvement provided by the increase in fibre strength of NaOH treated fibres. It was found that MAPP did not affect the impact energy of GF-PP prepared with un-treated RGF. The cause for the disparity in trends may be differences in impact failure mechanism caused by the variation in fibre strength.

It was observed that GF-EP prepared with NaOH treated RGF increased UTS by 14 MPa compared to unreinforced epoxy. No significant change to GF-EP UTS was

found as a result of treating fibres in APS prior to GF-EP preparation. It was found that GF-EP failure strain decreased and modulus increased when reinforced with fluidised bed recycled fibres. Treating RGF in APS and/or NaOH provided no significant change to either modulus or failure strain. This suggests that neither is affected by variation in fibre strength or IFSS. It is thought that the relatively low RGF loading limited the mechanical properties of GF-EP, which may be further improved by preparing GF-EP with higher RGF content.

6.2 Future work

The most significant challenges that have been identifies through this work that should direct future research are as follows:

1) A technique to facilitate the integration of metal oxide catalyst within the fluidised bed recycling process should be developed.
2) Given a commercial fluidised bed recycling process may have scrap from a variety of waste streams, the functionality of metal oxides at catalysing thermal decomposition of other thermosetting polymers should be assessed.
3) During the design of a commercial scale fluidised bed recycling process, it is essential to understand the composition of the decomposition emissions. The effect of the metal oxide catalysts on these emissions should therefore be investigated.
4) The underlying mechanism of adhesion between glass fibre and PP matrix interface must be better understood in order for the IFSS to be optimised when using RGF.
5) The influence of thermally recycling glass fibres on their compatibility with silane coupling agents must be better understood.
6) The strength regeneration of the recycled glass fibres must be cost effective in order to become commercialised. Further work into 1) designing a process plan and 2) optimising the regeneration treatments themselves could shed light on the commercial viability of the treatments investigated in this thesis.
7) A technique(s) for preparing GRP from RGF with sufficient fibre volume fraction must be developed to maximise the potential value of RGF.

Sections 6.2.1 - 6.2.4 examine the recommended avenues of further research listed above in greater detail (as well as other areas of research), and propose

experimentation and analytical techniques that could be utilised to shed light on the various areas of continued uncertainty.

6.2.1 Thermal recycling glass fibres in fluidised bed

The fluidised bed developed in this work is a lab scale prototype, and as such requires further design iterations to improve its performance. It was found that the liberated fibres are fluffy in architecture, leading to blocking when throughput is too high. To resolve this issue, piping cross sectional area prior to separation could be increased. Since it was observed that the recycling temperature does not appear to influence the recover fibre strength, it is believed that excessive mechanical damage to fibres may be occurring during separation. A less aggressive means of separating the fibre from the gas stream could be implemented to resolve this issue. Pickering et al*.* implemented a rotating mesh based separation system, which appears better suited to promote fibre strength retention [13]. To increase efficiency, an afterburner could also be included prior to the outlet, which would recover energy from the evolved gases.

Recyclate was uniformly cut throughout this work, whereas industrial scale size reduction (such as with hammer mill/shredder) will produce a distribution of recyclate dimensions. Composites based on other commonly used thermosets (such as polyester or vinyl ester) should also be recycled in the fluidised bed. It is import that an industrial scale fluidised bed recycling system can process glass fibre composites with varying matrices; this could be shown feasible with the lab scale prototype.

A cost analysis of the fluidised bed recycling process for recycling GFT should be carried out to determine its commercial feasibility. This was carried out by Pickering et al*.* some time ago; however, may require updating to take current costs (such as energy, landfill and material costs) into account [13].

6.2.2 Catalysed thermal recycling of glass fibres

In order to develop a commercial catalysed fluidised bed for composite recycling, the catalyst should be integrated into the process itself, not within the polymer. This would allow the continuous reuse of the catalyst and not require composite

manufacturers to integrate it in their products. Using the catalyst as the particulate medium or as a constituent of the particulate medium would appear the most suitable method of integration. Fluidising nanopowders is notoriously difficult; therefore, the catalyst cannot simply be added to the process in the form used in this work. Lewis et al. integrate CuO as a catalyst into a gas-solid fluidised bed [99]. This was achieved by grafting CuO to silica gel particles that was then used as the fluidised medium. If successful, such a technique could provide continuous contact with the recyclate and catalyst. Further work is require to determine whether this method (or a similar method) of integration would be suitable.

A catalysed fluidised bed (as with uncatalysed) should be capable of simultaneously processing a range of thermoset-based composites. The effect of the metal oxides on other thermosets thermal decomposition should therefore be investigated. As well as alternative thermosets, the catalytic activity of other metal oxides could be investigated. Shinbara et al. reported the effectiveness of a wide range of metal oxides (ZnO, Y_2O_3, Cr_2O_3, ZrO_2, WO_3, MoO_3, Ta_2O_5, Cu_2O, V_2O_5, SnO_2, NiO, Sb_2O_3 and MgO) which could be further investigated for use in the fluidised bed [115]. Both of these studies could be carried out by simply replicating the work in Chapter 3 using alternative thermosets and metal oxides.

A cost analysis of using metal oxides within a fluidised bed recycling process should also be performed. The significant reduction in recycling temperature provided when using metal oxides should be translated into energy and cost saving for an industrial scale process. This must be balances with the additional material cost of the catalyst itself. If the catalyst can be reused in the process, even if relatively high quantities are initially required, the cost benefit of long-term reduction in operating conditions could be realised.

The effect of using a catalyst on the epoxy oxidative decomposition products, and quantity of volatile organic compounds (VOC) in the emission should be investigated. This is essential for the design of an industrial scale system in order to control potentially harmful emissions. Shinbara et al. [115] and Shima et al. [117] report the use of metal oxides (TiO_2 and Cr_2O_3) can fully decompose polymeric materials to H_2O and CO_2, without the presence VOC. This could be further investigated by decomposing epoxy in the presence of the metal oxides using TGA and analysing the evolved gas using mass spectroscopy or in situ FTIR, as was performed by Jiang et al. [88] and Tranchard et al. [86] respectively.

6.2.3 Regenerating recycled glass fibres

Further work into the understanding the mechanism of adhesion between recycled glass fibre and PP matrix interface must be established in order for the IFSS to be optimised. Initially it must be determined whether APS treatment does in fact lead to APS condensing on the surface of the RGF. This could be achieved by treating a RGF in APS then using hot water extraction to remove the chemisorbed layer of polysiloxane without hydrolysing the physisorbed layer of APS oligomers [154]. Performing X-ray photoelectron spectroscopy (XPS) on RGF before and after the APS and hot water extraction will allow the relative atomic composition of the glass surface to be compared. An apparent increase in amine groups after the APS and extraction treatments would suggest the APS has bonded to the fibres, as only physisorbed APS will not be hydrolysed.

It must also be determined whether compatibility with APS is affected when recycling fibres from composites, opposed to thermally conditioning fibres as performed in other studies [5, 15]. This can again be achieved using the hot water extraction technique and XPS analysis outlined about. Rather than using RGF, new glass fibres could be thermally condition at typical recycling temperature (≥ 500 °C) to remove the sizing then the experiment can be performed as with the RGF. Comparing relative changes in surface composite between recycled and thermally conditioned fibres could indicate the degree of APS coverage on the fibre surface after re-silanisation. A comparison could also be made using the microbond technique. The IFSS with PP after re-silanisation could be characterised for thermally conditioned fibres and compare the RGF data.

Obtaining IFSS data between RGF and MAPP modified PP would allow better understanding of the GF-PP behaviour. This has been carried out in other studies with thermally conditioned fibres [68], but not fibres recycled from composites. Instead of APS, other commonly used silane coupling agents such as glycidoxypropyltrimethoxy silane or mercaptopropyltrimethoxy silane) or commercial film formers could also be applied to RGF with the goal of improving IFSS.

In terms of fibre strength regeneration, more work into strengthening through water vapour treatments could be carried out. Li and Tomozawa reported significant increase in bulk glass strength with the action of water vapour; however, in this work no such benefit was observed [52]. Given the inexpensive materials required to perform this treatment, studying other conditions in an attempt to gain strength

regeneration of recycled glass fibre would be worthwhile. Treating the fibres in vapour at temperature lower than 250 °C may be beneficial; as it is understood that exposure to such elevated temperature could adversely affect fibre strength.

From a commercial aspect, the strength regeneration of the fibres must be cost effective, be that NaOH or hot water treatment. Given the relatively long soaking times required, the treatments would have to be carried out in a batch process. The treatments could be performed within a heated vessel, which is loaded with solution and RGF, after the required quantity of glass fibres have been recovered with the fluidised bed. By using multiple vessels, simultaneously treating batches of RGF, this process could effectively become continuous. In the case of the NaOH treatment, NaOH solution will require (after a certain number of uses) processing to remove reaction products prior to recirculating and reusing to treat another batch of RGF. Further work must therefore focus on optimisation of the NaOH treatment in terms of 1) reusability of NaOH solution, 2) ratio of NaOH solution to fibre mass required and 3) treatment temperature, prior to analysing the cost of scaling up. Parameters such as the quantity of NaOH consumed during treatment and the potential resale value of reaction products (such as RGF and sodium silicate) will greatly affect the commercial viability of the treatment.

Highly concentrated NaOH solutions were required to obtain strength regeneration of the RGF in this work. This may be a result of limiting the fibre treatment time. It is feasible that less aggressive NaOH treatment could provide comparable improvements in fibre strength by simply extending the treatment time. A program of work to investigate this could be carried out by soaking RGF in NaOH solution of various pH levels for a multitude of treatment durations. The NaOH regeneration treatment parameters could then be optimised in terms of NaOH concentration, treatment time and resulting strength of the RGF.

6.2.4 Reusing recycled and regenerated glass fibres

It is plausible that the fibres are weakened during GF-PP preparation; it would therefore be insightful to measure the strength of fibres in the GF-PP after processing. This could be achieved by dissolving the PP matrix with boiling xylene as outlined in [238]. This allows the fibres to be extracted without ashing, which

would otherwise damage them. A technique outline by Thomason and Kalinka could then be used to measure sub-millimetre fibres [182].

An alternative GF-PP preparation technique could be used which would provide a more homogeneous dispersion of maleic anhydride though out the PP matrix. This could lead to GF-PP with superior mechanical properties than those in this work. Producing GF-PP via injection moulding with pre-compounded MAPP modified PP would likely solve the dispersion problem, however such a technique would significantly reduce the length of the glass fibres, and may limit their reinforcement potential.

The failure behaviour of the GF-PP in this work is not fully understood. Failure of composites containing MAPP failed in a far more brittle manner than GF-PP with unmodified PP. This was attributed to IFSS however, that was not confirmed. SEM with in situ tensile testing could be used to understand the failure behaviour of the GF-PP [239]. SEM of fracture surfaces could also indicate the level of adhesion between fibre and matrix in GF-PP.

In this work, it was found that infusing randomly orientated mats of RGF with epoxy yielded GF-EP with relatively low fibre volume fractions and poor mechanical properties. In addition, it was reported by Pickering that increasing pressure (up to 10 bar) during infusion can only produce FRP with fibre volume fraction of 15% when using discontinuous recycled carbon fibre reinforcement [240]. Improved mechanical properties can be achieved when fibres are aligned in GRP. The optimal mechanical properties of FRP are typically attained with fibre volume fractions of around 60%, which can only be achieved using aligned fibres [196]. Kacir et al. demonstrated that wet alignment techniques could successfully align 90% of new glass fibres within a tolerance of ±15° [202]. Further work is required; however, it may be feasible to use such methods to produce aligned glass fibre composites with improved mechanical properties.

7. References

[1] Composites Market by Fiber Type (Glass, Carbon), Resin Type (Thermoset, Thermoplastic), Manufacturing Process (Layup, Filament Winding, Pultrusion), Application (Transportation, Aerospace & Defense, Wind Energy), Region - Global Forecast to 2022. marketsandmarkets.com; 2017.

[2] M. H. Advanced Composites – The Engine for Growth. 2013.

[3] Advanced Composites Market by Type (Carbon, S-Glass, Aramid), by Manufacturing Process, by Resin Type (Thermoplastics and Thermosetting), by Application (Aerospace & Defense, Automotive, Wind, Sporting Goods, Pipe & Tanks, Construction, Marine), and by Region Global Forecast to 2020. marketsandmarkets.com; 2015.

[4] Fiber Market & Specialty Synthetic Fibers Market, by Type (Para & Meta Aramid, UHMW Polyethylene, Carbon Fiber, POA, Glass Fiber & Others), by Application (Aerospace & Defense, Automotive, Wind Energy, Safety, Friction Materials, etc.), and by Geography - Forecasts and Trends to 2020. marketsandmarkets.com; 2015.

[5] Yang L, Sáez ER, Nagel U, Thomason JL. Can thermally degraded glass fibre be regenerated for closed-loop recycling of thermosetting composites? Composites Part A: Applied Science and Manufacturing. 2015;72:167-74.

[6] Yang Y, Boom R, Irion B, van Heerden D-J, Kuiper P, de Wit H. Recycling of composite materials. Chemical Engineering and Processing: Process Intensification. 2012;51:53-68.

[7] Pickering SJ. Recycling technologies for thermoset composite materials—current status. Composites Part A: Applied Science and Manufacturing. 2006;37(8):1206-15.

[8] Job S. Recycling glass fibre reinforced composites – history and progress. Reinforced Plastics. 2013;57(5):19-23.

[9] Job S. Recycling composites commercially. Reinforced Plastics. 2014;58(5):32-8.

[10] Stewart R. 2 - Legislation for recycling waste composites A2 - Goodship, Vannessa. Management, Recycling and Reuse of Waste Composites: Woodhead Publishing; 2010. p. 20-38.

[11] Directive 2000/53/EC on end-of life vehicles. Official Journal of the European Union 2000:L269/34.

[12] Oliveux G, Dandy LO, Leeke GA. Current status of recycling of fibre reinforced polymers: Review of technologies, reuse and resulting properties. Progress in Materials Science. 2015;72:61-99.

[13] Pickering SJ, Kelly RM, Kennerley JR, Rudd CD, Fenwick NJ. A fluidised-bed process for the recovery of glass fibres from scrap thermoset composites. Composites Science and Technology. 2000;60(4):509-23.

[14] Kennerley JR, Kelly RM, Fenwick NJ, Pickering SJ, Rudd CD. The characterisation and reuse of glass fibres recycled from scrap composites by the action of a fluidised bed process. Composites Part A: Applied Science and Manufacturing. 1998;29(7):839-45.

[15] Thomason JL, Nagel U, Yang L, Sáez E. Regenerating the strength of thermally recycled glass fibres using hot sodium hydroxide. Composites Part A: Applied Science and Manufacturing. 2016;87:220-7.

[16] Shuaib SJGLPTMGONA. Composite Recycling: Where are we now? : Composites UK; 2016.

[17] Oliveux G, Bailleul J-L, Salle ELGL. Chemical recycling of glass fibre reinforced composites using subcritical water. Composites Part A: Applied Science and Manufacturing. 2012;43(11):1809-18.

[18] Kao CC, Ghita OR, Hallam KR, Heard PJ, Evans KE. Mechanical studies of single glass fibres recycled from hydrolysis process using sub-critical water. Composites Part A: Applied Science and Manufacturing. 2012;43(3):398-406.

[19] Derosa R, Telfeyan E, Mayes JS. Current State of Recycling Sheet Molding Compounds and Related Materials. Journal of Thermoplastic Composite Materials. 2005;18(3):219-40.

[20] Piñero-Hernanz R, García-Serna J, Dodds C, Hyde J, Poliakoff M, Cocero MJ, et al. Chemical recycling of carbon fibre composites using alcohols under subcritical and supercritical conditions. The Journal of Supercritical Fluids. 2008;46(1):83-92.

[21] Torres A, de Marco I, Caballero BM, Laresgoiti MF, Legarreta JA, Cabrero MA, et al. Recycling by pyrolysis of thermoset composites: characteristics of the liquid and gaseous fuels obtained. Fuel. 2000;79(8):897-902.

[22] Williams PT, Cunliffe AM, Jones N. Recovery of value-added products from the pyrolytic recycling of glass-fibre-reinforced composite plastic waste. Journal of the Energy Institute. 2005;78(2):51-61.

[23] Cunliffe AM, Williams PT. Characterisation of products from the recycling of glass fibre reinforced polyester waste by pyrolysis. Fuel. 2003;82(18):2223-30.

[24] Larsen K. Recycling wind turbine blades. Renewable Energy Focus. 2009;9(7):70-3.

[25] Jacob A. Composites can be recycled. Reinforced Plastics. 2011;55(3):45-6.

[26] Pimenta S, Pinho ST. Recycling carbon fibre reinforced polymers for structural applications: Technology review and market outlook. Waste Management. 2011;31(2):378-92.

[27] Pickering SJ. 4 - Thermal methods for recycling waste composites A2 - Goodship, Vannessa. Management, Recycling and Reuse of Waste Composites: Woodhead Publishing; 2010. p. 65-101.

[28] Melendi-Espina S, Morris CN, Turner TA, Pickering SJ. Recycling of carbon fibre composites. Carbon 2016. Pennsylvania2016.

[29] Genis A, Sandri M. Owens Corning Investor Presentation 2015 - Composite solutions. 2015.

[30] Kennerley JR, Fenwick NJ, Pickering SJ, Rudd CD. The properties of glass fibers recycled from the thermal processing of scrap thermoset composites. Journal of Vinyl and Additive Technology. 1997;3(1):58-63.

[31] Feih S, Boiocchi E, Mathys G, Mathys Z, Gibson AG, Mouritz AP. Mechanical properties of thermally-treated and recycled glass fibres. Composites Part B: Engineering. 2011;42(3):350-8.

[32] Jenkins PG, Yang L, Liggat JJ, Thomason JL. Investigation of the strength loss of glass fibre after thermal conditioning. Journal of Materials Science. 2014;50(3):1050-7.

[33] Thomason JL, Kao CC, Ure J, Yang L. The strength of glass fibre reinforcement after exposure to elevated composite processing temperatures. Journal of Materials Science. 2013;49(1):153-62.

[34] Bashir ST, Yang L, Anderson R, Tang PL, Liggat JJ, Thomason JL. A simple chemical approach to regenerating the strength of thermally damaged glass fibre. Composites Part A: Applied Science and Manufacturing. 2017;102:76-87.

[35] Thomason JL, Yang L, Meier R. The properties of glass fibres after conditioning at composite recycling temperatures. Composites Part A: Applied Science and Manufacturing. 2014;61:201-8.

[36] Fenwick N. Recycling of composite materials using fluidised bed processes [PhD]: University of Nottingham; 1996.

[37] Åkesson D, Foltynowicz Z, Christéen J, Skrifvars M. Microwave pyrolysis as a method of recycling glass fibre from used blades of wind turbines. Journal of Reinforced Plastics and Composites. 2012;31(17):1136-42.

[38] Cunliffe AM, Jones N, Williams PT. Pyrolysis of composite plastic waste. Environmental Technology. 2003;24:653-63.

[39] Thomas WF. An investigation of the factors likely to affect the strength and properties of glass fibres. Physics and Chemistry of Glasses. 1960;1(1):4–18.

[40] James Thomason PJ, Liu Yang. Glass Fibre Strength-A Review with Relation to Composite Recycling. Fibers. 2016;4(18).

[41] Otto WH. Compaction Effects in Glass Fibers. Journal of the American Ceramic Society. 1961;44(2):68-72.

[42] Yang L, Thomason JL. The thermal behaviour of glass fibre investigated by thermomechanical analysis. Journal of Materials Science. 2013;48(17):5768-75.

[43] Aslanova MS, Ivanov NV, Balashov YS. Effect of chemical composition on the relaxation properties of thin glass fibers. Glass and Ceramics. 1970;27(8):468-71.

[44] Ya M, Deubener J, Yue Y. Enthalpy and Anisotropy Relaxation of Glass Fibers. Journal of the American Ceramic Society. 2008;91(3):745-52.

[45] Yue Y. Features of the relaxation in hyperquenched inorganic glasses during annealing. Physics and Chemistry of Glasses. 2005;46(4):354-8.

[46] Lund MD, Yue Y. Impact of Drawing Stress on the Tensile Strength of Oxide Glass Fibers. Journal of the American Ceramic Society. 2010;93(10):3236-43.

[47] Feih S, Mouritz AP, Case SW. Determining the mechanism controlling glass fibre strength loss during thermal recycling of waste composites. Composites Part A: Applied Science and Manufacturing. 2015;76:255-61.

[48] Gupta PK. Strength of glass fibers. In: Elices M, Llorca J, editors. Fiber Fracture. Oxford: Elsevier Science Ltd; 2002. p. 127-53.

[49] Sakka S. Effects of reheating on strength of glass fibres. Bulletin of the Institute for Chemical Research, Kyoto University. 1957;34(6):316-20.

[50] Mould RE. Strength and Static Fatigue of Abraded Glass Under Controlled Ambient Conditions: III, Aging of Fresh Abrasions. Journal of the American Ceramic Society. 1960;43:160-7.

[51] Ito S, Tomozawa M. Crack Blunting of High ‐ Silica Glass. Journal of the American Ceramic Society. 1982;65(8):368-71.

[52] Li H, Tomozawa M. Mechanical strength increase of abraded silica glass by high pressure water vapor treatment. Journal of Non-Crystalline Solids. 1994;168:287-92.

[53] Li S, Sun S, Liang H, Zhong S, Yang F. Production and characterization of polypropylene composites filled with glass fibre recycled from pyrolysed waste printed circuit boards. Environmental Technology. 2014;35(21):2743-51.

[54] Shi J, Bao L, Kobayashi R, Kato J, Kemmochi K. Reusing recycled fibers in high-value fiber-reinforced polymer composites: Improving bending strength by surface cleaning. Composites Science and Technology. 2012;72(11):1298-303.

[55] Nagel U, Yang L, Kao CC, Thomason JL. Effects of Thermal Recycling Temperatures on the Reinforcement Potential of Glass Fibers. Polymer Composites. 2016.

[56] Roux C, Denault J, Champagne MF. Parameters regulating interfacial and mechanical properties of short glass fiber reinforced polypropylene. Journal of Applied Polymer Science. 2000;78(12):2047-60.

[57] Bikiaris D, Matzinos P, Larena A, Flaris V, Panayiotou C. Use of silane agents and poly(propylene-g-maleic anhydride) copolymer as adhesion promoters in glass fiber/polypropylene composites. Journal of Applied Polymer Science. 2001;81(3):701-9.

[58] Thomason JL, Adzima LJ. Sizing up the interphase: an insider's guide to the science of sizing. Composites Part A: Applied Science and Manufacturing. 2001;32(3–4):313-21.

[59] Rudzinski S, Häussler L, Harnisch C, Mäder E, Heinrich G. Glass fibre reinforced polyamide composites: Thermal behaviour of sizings. Composites Part A: Applied Science and Manufacturing. 2011;42(2):157-64.

[60] Gao P, Ward Y, Su KB, Weng LT. Effects of chemical composition and thermal stability of finishes on the compatibility between glass fiber and high melting temperature thermoplastics. Polymer Composites. 2000;21(2):312-21.

[61] Pham Q-T, Chern C-S. Thermal stability of organofunctional polysiloxanes. Thermochimica Acta. 2013;565:114-23.

[62] Liu XM, Thomason JL, Jones FR. The Concentration of Hydroxyl Groups on Glass Surfaces and Their Effect on the Structure of Silane Deposits. Silanes and Other Coupling Agents, Volume 5: CRC Press; 2009. p. 25-38.

[63] González-Benito J, Baselga J, Aznar AJ. Microstructural and wettability study of surface pretreated glass fibres. Journal of Materials Processing Technology. 1999;92:129-34.

[64] Zhuravlev LT. Surface characterization of amorphous silica—a review of work from the former USSR. Colloids and Surfaces A: Physicochemical and Engineering Aspects. 1993;74(1):71-90.

[65] Zhuravlev LT. Concentration of hydroxyl groups on the surface of amorphous silicas. Langmuir. 1987;3(3):316-8.

[66] Young GJ. Interaction of water vapor with silica surfaces. Journal of Colloid Science. 1958;13(1):67-85.

[67] Carré A, Lacarrière V, Birch W. Molecular interactions between DNA and an aminated glass substrate. Journal of Colloid and Interface Science. 2003;260(1):49-55.

[68] Nagel U. The processing and characterisation of recycled glass fibre composites. UK: University of Strathclyde; 2016.

[69] Holdich RG. Fluidisation. Fundamentals of Particle Technology: Midland Information Technology & Publishing; 2002. p. 67-76.

[70] Kennerley J. Recycling fibres recovered from composite materials using a fluidised bed process [PhD]: University of Nottingham; 1998.

[71] Standard Terminology of Fire Standards.

[72] Gervasoni BD, Khairallah GN, O'Hair RAJ, Wille U. The role of peroxyl radicals in polyester degradation – a mass spectrometric product and kinetic study using the distonic radical ion approach. Phys Chem Chem Phys. 2015;17:9212-21.

[73] Beyler CL, Hirschler MM. Thermal Decompostion of Polymers. In: DiNenno PJ, editor. SFPE Handbook of Fire Protection Engineering. Boston: Quincy, Mass. : National Fire Protection Association; Boston, Mass. : Society of Fire Protection Engineers; 1995. p. 110-31.

[74] Vu DQ, Gigliotti M, Lafarie-Frenot MC. Experimental characterization of thermo-oxidation-induced shrinkage and damage in polymer–matrix composites. Composites Part A: Applied Science and Manufacturing. 2012;43(4):577-86.

[75] Decelle J, Huet N, Bellenger V. Oxidation induced shrinkage for thermally aged epoxy networks. Polymer Degradation and Stability. 2003;81(2):239-48.

[76] Zahra Y, Djouani F, Fayolle B, Kuntz M, Verdu J. Thermo-oxidative aging of epoxy coating systems. Progress in Organic Coatings. 2014;77(2):380-7.

[77] Celina MC, Dayile AR, Quintana A. A perspective on the inherent oxidation sensitivity of epoxy materials. Polymer. 2013;54(13):3290-6.

[78] Colin X, Marais C, Verdu J. Kinetic modelling and simulation of gravimetric curves: application to the oxidation of bismaleimide and epoxy resins. Polymer Degradation and Stability. 2002;78(3):545-53.

[79] Ernault E, Richaud E, Fayolle B. Thermal oxidation of epoxies: Influence of diamine hardener. Polymer Degradation and Stability. 2016;134(Supplement C):76-86.

[80] Bishop DP, Smith DA. Combined pyrolysis and radiochemical gas chromatography for studying the thermal degradation of epoxy resins and polyimides. I. The degradation of epoxy resins in nitrogen between 400°C and 700°C. Journal of Applied Polymer Science. 1970;14(1):205-23.

[81] Lee L-H. Mechanisms of thermal degradation of phenolic condensation polymers. II. Thermal stability and degradation schemes of epoxy resins. Journal of Polymer Science Part A: General Papers. 1965;3(3):859-82.

[82] Chen KS, Yeh RZ. Pyrolysis kinetics of epoxy resin in a nitrogen atmosphere. Journal of Hazardous Materials. 1996;49(2–3):105-13.

[83] Rwei S-P, Kao S-C, Liou G-S, Cheng K-C, Guo W. Curing and pyrolysis of epoxy resins containing 2-(6-oxido-6H -dibenz(c,e)(1,2)oxaphosphorin-6-yl)-1,4-naphthalenediol or bisphenol S. Colloid Polym Sci. 2003;281:407-15.

[84] Chen KS, Yeh RZ, Wu CH. Kinetics of Thermal Decomposition of Epoxy Resin in Nitrogen-Oxygen Atmosphere. Journal of Environmental Engineering. 1997;123:1041-6.

[85] Wang Q, Shi W. Kinetics study of thermal decomposition of epoxy resins containing flame retardant components. Polymer Degradation and Stability. 2006;91(8):1747-54.

[86] Tranchard P, Duquesne S, Samyn F, Estèbe B, Bourbigot S. Kinetic analysis of the thermal decomposition of a carbon fibre-reinforced epoxy resin laminate. Journal of Analytical and Applied Pyrolysis. 2017;126(Supplement C):14-21.

[87] Régnier N, Fontaine S. Determination of the Thermal Degradation Kinetic Parameters of Carbon Fibre Reinforced Epoxy Using TG. Journal of Thermal Analysis and Calorimetry. 2001;64(2):789-99.

[88] Jiang G, Pickering SJ, Walker GS, Bowering N, Wong KH, Rudd CD. Soft ionisation analysis of evolved gas for oxidative decomposition of an epoxy resin/carbon fibre composite. Thermochimica Acta. 2007;454(2):109-15.

[89] Wang J, Li Y, Jin Y, Wang Z. Kinetics and Mechanism of Thermal Decomposition of Polyepoxyphenylsilsesquioxane/Epoxy Resin Systems from Isothermal Measurement. Journal of Macromolecular Science, Part A. 2014;51(3):249-53.

[90] Chen KS, Yeh RZ. Pyrolysis kinetics of epoxy resin in a nitrogen atmosphere. Journal of Hazardous Materials. 1996;49(2):105-13.

[91] Vyazovkin S, Burnham AK, Criado JM, Pérez-Maqueda LA, Popescu C, Sbirrazzuoli N. ICTAC Kinetics Committee recommendations for performing kinetic computations on thermal analysis data. Thermochimica Acta. 2011;520(1–2):1-19.

[92] Murzin DY, Salmi T. Chapter 1 - Setting the Scene. Catalytic Kinetics (Second Edition). Amsterdam: Elsevier; 2016. p. 1-34.

[93] Murzin DY, Salmi T. Chapter 2 - Catalysis. Catalytic Kinetics (Second Edition). Amsterdam: Elsevier; 2016. p. 35-100.

[94] Spivey JJ. Complete catalytic oxidation of volatile organics. Industrial & Engineering Chemistry Research. 1987;26(11):2165-80.

[95] Franz G, Sheldon RA. Oxidation. Ullmann's Encyclopedia of Industrial Chemistry: Wiley-VCH Verlag GmbH & Co. KGaA; 2000.

[96] Hong SG, Wang TC. Effect of copper oxides on the thermal oxidative degradation of the epoxy resin. Journal of Applied Polymer Science. 1994;52(9):1339-51.

[97] Chan MG, Allara DL. Infrared reflection studies of the mechanism of oxidation at a copper—polyethylene interface. Journal of Colloid and Interface Science. 1974;47(3):697-704.

[98] Geldart D, Wong ACY. Fluidization of powders showing degrees of cohesiveness—I. Bed expansion. Chemical Engineering Science. 1984;39(10):1481-8.

[99] Lewis WK, Gilliland ER, Reed WA. Reaction of Methane with Copper Oxide in a Fluidized Bed. Industrial & Engineering Chemistry. 1949;41(6):1227-37.

[100] Poreddy R, Engelbrekt C, Riisager A. Copper oxide as efficient catalyst for oxidative dehydrogenation of alcohols with air. Catalysis Science & Technology. 2015;5(4):2467-77.

[101] Stanmore BR, Brilhac JF, Gilot P. The oxidation of soot: a review of experiments, mechanisms and models. Carbon. 2001;39(15):2247-68.

[102] Trovarelli A. Catalysis by Ceria and Related Materials2002.

[103] Ganduglia-Pirovano MV, Hofmann A, Sauer J. Oxygen vacancies in transition metal and rare earth oxides: Current state of understanding and remaining challenges. Surface Science Reports. 2007;62(6):219-70.

[104] Conesa JC, Martínez-Arias A, Fernández-García M, Soria J. Surface structure and redox chemistry of ceria-containing automotive catalytic systems. Research on Chemical Intermediates. 2000;26(1):103-11.

[105] Machida M, Murata Y, Kishikawa K, Zhang D, Ikeue K. On the Reasons for High Activity of CeO2 Catalyst for Soot Oxidation. Chemistry of Materials. 2008;20(13):4489-94.

[106] Liu S, Wu X, Liu W, Chen W, Ran R, Li M, et al. Soot oxidation over CeO2 and Ag/CeO2: Factors determining the catalyst activity and stability during reaction. Journal of Catalysis. 2016;337:188-98.

[107] Krishna K, Bueno-López A, Makkee M, Moulijn JA. Potential rare earth modified CeO2 catalysts for soot oxidation: I. Characterisation and catalytic activity with O2. Applied Catalysis B: Environmental. 2007;75(3):189-200.

[108] Heponiemi A, Azalim S, Hu T, Lassi U. Cerium Oxide Based Catalysts for Wet Air Oxidation of Bisphenol A. Topics in Catalysis. 2015;58(14):1043-52.

[109] Tschope A, Liu W, Flytzanistephanopoulos M, Ying JY. Redox Activity of Nonstoichiometric Cerium Oxide-Based Nanocrystalline Catalysts. Journal of Catalysis. 1995;157(1):42-50.

[110] Pacchioni G. Oxygen Vacancy: The Invisible Agent on Oxide Surfaces. ChemPhysChem. 2003;4(10):1041-7.

[111] Nolan M, Parker SC, Watson GW. The electronic structure of oxygen vacancy defects at the low index surfaces of ceria. Surface Science. 2005;595(1):223-32.

[112] Ranji-Burachaloo H, Masoomi-Godarzi S, Khodadadi AA, Mortazavi Y. Synergetic effects of plasma and metal oxide catalysts on diesel soot oxidation. Applied Catalysis B: Environmental. 2016;182:74-84.

[113] Ma L, Seo CY, Chen X, Sun K, Schwank JW. Indium-doped Co3O4 nanorods for catalytic oxidation of CO and C3H6 towards diesel exhaust. Applied Catalysis B: Environmental. 2018;222(Supplement C):44-58.

[114] Duan H, Xu D, Li W, Xu H. Study of the Redox Properties of Noble Metal/Co3O4 by Electrical Conductivity Measurements. Catalysis Letters. 2008;124(3):318-23.

[115] Shinbara T, Makino T, Matsumoto K, Mizuguchi J. Complete decomposition of polymers by means of thermally generated holes at high temperatures in titanium dioxide and its decomposition mechanism. Journal of Applied Physics. 2005;98(4):044909.

[116] Mizuguchi J, Tsukada Y, Takahashi H. Recovery and Characterization of Reinforcing Fibers from Fiber Reinforced Plastics by Thermal Activation of Oxide Semiconductors. Materials Transactions - The Japan Institute of Metal. 2013;54(3):384-91.

[117] Shima H, Takahashi H, Mizuguchi J. Recovery of Glass Fibers from Fiber Reinforced Plastics. Materials Transactions - The Japan Institute of Metal. 2011;52(6):1327-9.

[118] Zabihi O, Ghasemlou S. Nano-CuO/Epoxy Composites: Thermal Characterization and Thermo-Oxidative Degradation. International Journal of Polymer Analysis and Characterization. 2012;17(2):108-21.

[119] Domun N, Hadavinia H, Zhang T, Sainsbury T, Liaghat GH, Vahid S. Improving the fracture toughness and the strength of epoxy using nanomaterials - a review of the current status. Nanoscale. 2015;7(23):10294-329.

[120] Wu Z, Zhuo Q, Sun T, Wang Z. Mechanical properties of epoxy resins reinforced with synthetic boehmite (AlOOH) nanosheets. Journal of Applied Polymer Science. 2015;132(5):n/a-n/a.

[121] Gao J, Li J, Benicewicz BC, Zhao S, Hillborg H, Schadler LS. The Mechanical Properties of Epoxy Composites Filled with Rubbery Copolymer Grafted SiO2. Polymers. 2012;4:187-210.

[122] Chin-Lung Chiang C-CMM, Feng-Yin Wang, Hsu-Chiang Kuan. Thermo-oxidative degradation of novel epoxy containing silicon and phosphorous nanocomposites. European Polymer Journal. 2003;39:825-30.

[123] Galwey AK. What is meant by the term ‘variable activation energy’ when applied in the kinetic analyses of solid state decompositions (crystolysis reactions)? Thermochimica Acta. 2003;397(1):249-68.

[124] Vyazovkin S. Reply to “What is meant by the term ‘variable activation energy’ when applied in the kinetics analyses of solid state decompositions (crystolysis reactions)?”. Thermochimica Acta. 2003;397(1):269-71.

[125] Vyazovkin S. Kinetic concepts of thermally stimulated reactions in solids: A view from a historical perspective. International Reviews in Physical Chemistry. 2000;19(1):45-60.

[126] Karimian M, Schaffie M, Fazaelipoor MH. Determination of activation energy as a function of conversion for the oxidation of heavy and light crude oils in relation to in situ combustion. Journal of Thermal Analysis and Calorimetry. 2016;125(1):301-11.

[127] Walters RN, Hackett SM, Lyon RE. Heats of combustion of high temperature polymers. Fire and Materials. 2000;24(5):245-52.

[128] Thomason JL. The interface region in glass fibre-reinforced epoxy resin composites: 3. Characterization of fibre surface coatings and the interphase. Composites. 1995;26(7):487-98.

[129] Wu HF, Dwight DW, Huff NT. Effects of silane coupling agents on the interphase and performance of glass-fiber-reinforced polymer composites. Composites Science and Technology. 1997;57(8):975-83.

[130] Zinck P, Pay MF, Rezakhanlou R, Gerard JF. Mechanical characterisation of glass fibres as an indirect analysis of the effect of surface treatment. Journal of Materials Science. 1999;34(9):2121-33.

[131] Zinck P, Mäder E, Gerard JF. Role of silane coupling agent and polymeric film former for tailoring glass fiber sizings from tensile strength measurements. Journal of Materials Science. 2001;36(21):5245-52.

[132] Thomason ES-RLYJL. Investigation of strength recovery of recycled heat treated glass fibres through chemical treatments. The 19th International Conference on Composite Materials2013.

[133] Thomason JL, Rodriguez ES, Yang L. Glass fibre recovery. 2015.

[134] E SR. Regenerating the strength of thermally recycled glass fibres using chemical treatments: University of Strathclyde; 2016.

[135] Aslanova MS. The effect of different factors on the mechanical properties of glass fibers. Glass and Ceramics. 1960;17(11):563-9.

[136] Sakka S. Effects of Reheating on Strength of Glass Fibers. Bulletin of the Institute for Chemical Research, Kyoto University. 1957;34(6):316-20.

[137] Tso ST, Pask JA. Reaction of Glasses with Hydrofluoric Acid Solution. Journal of the American Ceramic Society. 1982;65(7):360-2.

[138] Liu J, Jiang M, Wang Y, Wu G, Wu Z. Tensile behaviors of ECR-glass and high strength glass fibers after NaOH treatment. Ceramics International. 2013;39(8):9173-8.

[139] Wei B, Cao H, Song S. Tensile behavior contrast of basalt and glass fibers after chemical treatment. Materials & Design. 2010;31(9):4244-50.

[140] Wallenberger FT, Watson JC, Li H. Glass Fibers. ASM Handbook, Vol 21: Composites. 2001.

[141] Bashir ST, Yang L, Liggat JJ, Thomason JL. Kinetics of dissolution of glass fibre in hot alkaline solution. Journal of Materials Science. 2017.

[142] Saez-Rodriguez E. Regenerating the strength of thermally recycled glass fibres using chemical treatments: University of Strathclyde; 2017.

[143] Wiederhorn SM, Fett T, Rizzi G, Funfschilling S, Hoffmann MJ, Guin J-P. Effect of Water Penetration on the Strength and Toughness of Silica Glass. Journal of the American Ceramic Society. 2011;94:196-203.

[144] Fett T, Rizzi G, Hoffmann MJ, Wagner S, Wiederhorn SM. Effect of water on the inert strength of silica glass: Role of water penetration. Journal of the American Ceramic Society. 2012;95:3847-53.

[145] Wiederhorn SM, Yi F, LaVan D, Richter LJ, Fett T, Hoffmann MJ. Volume Expansion Caused by Water Penetration into Silica Glass. Journal of the American Ceramic Society. 2015;98:78-87.

[146] Kim J-K, Mai Y-W, Mai Y-W. Chapter 2 - Characterization of interfaces. Engineered Interfaces in Fiber Reinforced Composites. Oxford: Elsevier Science Ltd; 1998. p. 5-41.

[147] Thomason JL. The interface region in glass fibre-reinforced epoxy resin composites: 1. Sample preparation, void content and interfacial strength. Composites. 1995;26(7):467-75.

[148] Hull D, Clyne TW. An Introduction to Composite Materials. 2 ed. Cambridge: Cambridge University Press; 1996.

[149] Thomason J. Glass Fibre Sizings2012.

[150] Plueddemann EP. Silane Coupling Agents. 2nd ed: Springer; 1991.

[151] Kim J-K, Mai Y-W, Mai Y-W. Chapter 5 - Surface treatments of fibers and effects on composite properties. Engineered Interfaces in Fiber Reinforced Composites. Oxford: Elsevier Science Ltd; 1998. p. 171-237.

[152] Khayankarn O. Stability of epoxy/glass interfaces. Lehigh County, Pennsylvania: Lehigh University; 2002.

[153] Wang D, Jones FR. TOF SIMS and XPS study of the interaction of aminosilanised E-glass fibres with epoxy resins. Part I: Diglycidyl ether of bisphenol S. Composites Science and Technology. 1994;50(2):215-28.

[154] Liu X, Thomason JL, Jones FR. XPS and AFM Study of Interaction of Organosilane and Sizing with E-glass Fibre Surface. Journal of Adhesion. 2008;84(4):322-38.

[155] Mäder E, Pisanova E. Characterization and design of interphases in glass fiber reinforced polyproplyene. Polymer Composites. 2000;21(3):361-8.

[156] Mäder E, Freitag KH. Interface properties and their influence on short fibre composites. Composites. 1990;21(5):397-402.

[157] Mäder E, Jacobasch HJ, Grundke K, Gietzelt T. Influence of an optimized interphase on the properties of polypropylene/glass fibre composites. Composites Part A: Applied Science and Manufacturing. 1996;27(9):907-12.

[158] Nygård P, Redford K, Gustafson C-G. Interfacial strength in glass fibre-polypropylene composites: influence of chemical bonding and physical entanglement. Composite Interfaces. 2002;9(4):365-88.

[159] Jannerfeldt G, Törnqvist R, Rambert N, Boogh L, Månson J-AE. Matrix Modification for Improved Reinforcement Effectiveness in Polypropylene/Glass Fibre Composites. Applied Composite Materials. 2001;8(5):327-41.

[160] Zheng A, Wang H, Zhu X, Masuda S. Studies on the interface of glass fiber-reinforced polypropylene composite. Composite Interfaces. 2002;9(4):319-33.

[161] Cantwell WJ TW, Kausch HH, Jacquemet R. The Influence of a Fiber-Matrix Coupling Agent on the Properties of a Glass Fiber / Polypropylene GMT. J Thermoplast Compos Mater. 1992;5:304–17.

[162] Thomason JL. Micromechanical parameters from macromechanical measurements on glass reinforced polypropylene. Composites Science and Technology. 2002;62(10–11):1455-68.

[163] Thomason JL. The influence of fibre length and concentration on the properties of glass fibre reinforced polypropylene. 6. The properties of injection moulded long fibre PP at high fibre content. Composites Part A: Applied Science and Manufacturing. 2005;36(7):995-1003.

[164] Mäder E, Moos E, Karger-Kocsis J. Role of film formers in glass fibre reinforced polypropylene — new insights and relation to mechanical properties. Composites Part A: Applied Science and Manufacturing. 2001;32(5):631-9.

[165] Thomason JL, Van Rooyen AA. Transcrystallized interphase in thermoplastic composites: Part II Influence of interfacial stress, cooling rate, fibre properties and polymer molecular weight. Journal of Materials Science. 1992;27(4):897-907.

[166] Thomason JL, Van Rooyen AA. Transcrystallized interphase in thermoplastic composites: Part I Influence of fibre type and crystallization temperature. Journal of Materials Science. 1992;27(4):889-96.

[167] Wagner HD, Lustiger A, Marzinsky CN, Mueller RR. Interlamellar failure at transcrystalline interfaces in glass/polypropylene composites. Composites Science and Technology. 1993;48(1):181-4.

[168] NAGAE S, OTSUKA Y, NISHIDA M, SHIMIZU T, TAKEDA T, YUMITORI S. Transcrystallization at glass fibre/polypropylene interface and its effect on the improvement of mechanical properties of the composites. Journal of Materials Science Letters. 1995;14:1234-6.

[169] Misra A, Deopura BL, Xavier SF, Hartley FD, Peters RH. Transcrystallinity in injection molded polypropylene glass fibre composites. Die Angewandte Makromolekulare Chemie. 1983;113(1):113-20.

[170] Avalos F, Lopez-Manchado MA, Arroyo M. Crystallization kinetics of polypropylene III. Ternary composites based on polypropylene/low density polyethylene blend matrices and short glass fibres. Polymer. 1998;39(24):6173-8.

[171] M A, MA L-M, F. A. Crystallization kinetics of polypropylene: II. Effect of the addition of short glass fibres. Polymer (Guildf). 1997;38:5587–93.

[172] Thomason JL, Yang L. Temperature dependence of the interfacial shear strength in glass–fibre polypropylene composites. Composites Science and Technology. 2011;71(13):1600-5.

[173] Langroudi AE, Yousefi AA, Kabiri K. Effect of silane coupling agent on interfacial adhesion of copper/glass fabric/epoxy composites. Iranian Polymer Journal. 2003;13(45):201-10.

[174] Gao X, Jensen RE, Li W, Deitzel J, McKnight SH, J.W. Gillespie J. Effect of Fiber Surface Texture Created from Silane Blends on the Strength and Energy Absorption of the Glass Fiber/Epoxy Interphase. Journal of Composite Materials. 2008;42(5):513-34.

[175] Ramezanzadeh B, Raeisi E, Mahdavian M. Studying various mixtures of 3-aminopropyltriethoxysilane (APS) and tetraethylorthosilicate (TEOS) silanes on the corrosion resistance of mild steel and adhesion properties of epoxy coating. International Journal of Adhesion and Adhesives. 2015;63:166-76.

[176] Berg J, Jones FR. The role of sizing resins, coupling agents and their blends on the formation of the interphase in glass fibre composites. Composites Part A: Applied Science and Manufacturing. 1998;29(9):1261-72.

[177] Walker P. J Coatings Techno. 1980;52:49.

[178] Khoun L, Hubert P. Cure shrinkage characterization of an epoxy resin system by two in situ measurement methods. Polymer Composites. 2010;31(9):1603-10.

[179] Yang L, Thomason J. The role of residual thermal stress in interfacial strength of polymer composites by a novel single fibre technique 15th European Conference on Composite Materials. Venice, Italy2012.

[180] Lee N-J, Jang J. The use of a mixed coupling agent system to improve the performance of polypropylene-based composites reinforced with short-glass-fibre mat. Composites Science and Technology. 1998;57(12):1559-69.

[181] Yang L, Thomason JL. Development and application of micromechanical techniques for characterising interfacial shear strength in fibre-thermoplastic composites. Polymer Testing. 2012;31(7):895-903.

[182] Thomason JL, Kalinka G. A technique for the measurement of reinforcement fibre tensile strength at sub-millimetre gauge lengths. Composites Part A: Applied Science and Manufacturing. 2001;32(1):85-90.

[183] Scheffler C, Förster T, Mäder E, Heinrich G, Hempel S, Mechtcherine V. Aging of alkali-resistant glass and basalt fibers in alkaline solutions: Evaluation of the

failure stress by Weibull distribution function. Journal of Non-Crystalline Solids. 2009;355(52–54):2588-95.

[184] Friedrich M, Schulze A, Prösch G, Walter C, Weikert D, Binh NM, et al. Investigation of Chemically Treated Basalt and Glass Fibres. Microchimica Acta. 2000;133(1):171-4.

[185] Spierings GACM. Wet chemical etching of silicate glasses in hydrofluoric acid based solutions. Journal of Materials Science. 1993;28(23):6261-73.

[186] Ito S, Tomozawa M. Crack Blunting of High-Silica Glass. Journal of the American Ceramic Society. 1982;65(8):368-71.

[187] Culler SR, Ishida H, Koenig JL. The Silane lnterphase of Composites: Effects of Process Conditions on 3-Aminopropyltriethoxysilane. Polymer Composites. 1986;7(4):231-8.

[188] Yue CY, Quek MY. The interfacial properties of fibrous composites. Journal of Materials Science. 1994;29(9):2487-90.

[189] Resins NFa. Composition Ranges for Glass Fibres.

[190] Jr. LM, Branner K, Petersen HN, Beauso J, McGugan M, Sørensen BF. Materials for Wind Turbine Blades: An Overview. Materials. 2017;10:1285.

[191] Thomason JL. Interfaces and interfacial effects in glass reinforced thermoplastics. 28th Risø International Conference on Materials Science. Roskilde, Denmark2007. p. 75-92.

[192] Min CY, Q. Chen, Yuan XH, Xu ZW. Preparation and Interfacial Properties of Glass Fiber/Polypropylene Microcomposites. Journal of Thermoplastic Composite Materials. 2011;24:173-83.

[193] Ricci C, Miliani C, Brunetti BG, Sgamellotti A. Non-invasive identification of surface materials on marble artifacts with fiber optic mid-FTIR reflectance spectroscopy. Talanta. 2006;69(5):1221-6.

[194] Minty RF, Thomason JL, Yang L. The role of the epoxy resin : curing agent ratio on composite interfacial strength and thermal performance. European Conference on Composite Materials 17. Munich2016.

[195] Iglesias JG, González-Benito J, Aznar AJ, Bravo J, Baselga J. Effect of Glass Fiber Surface Treatments on Mechanical Strength of Epoxy Based Composite Materials. Journal of Colloid and Interface Science. 2002;250(1):251-60.

[196] de Marco I, Legarreta JA, Laresgoiti MF, Torres A, Cambra JF, Chomón MJ, et al. Recycling of the Products Obtained in the Pyrolysis of Fibre-Glass Polyester SMC. Journal of Chemical Technology & Biotechnology. 1997;69(2):187-92.

[197] Pickering S, Liu Z, Turner T, Wong K. Applications for carbon fibre recovered from composites. 37th Risø International Symposium on Materials Science2016.

[198] Harper LT, Turner TA, Martin JRB, Warrior NA. Fiber Alignment in Directed Carbon Fiber Preforms — A Feasibility Study. Journal of Composite Materials. 2008;43(1):57-74.

[199] Yu H, Potter KD, Wisnom MR. A novel manufacturing method for aligned discontinuous fibre composites (High Performance-Discontinuous Fibre method). Composites Part A: Applied Science and Manufacturing. 2014;65(Supplement C):175-85.

[200] Longana ML, Ong N, Yu H, Potter KD. Multiple closed loop recycling of carbon fibre composites with the HiPerDiF (High Performance Discontinuous Fibre) method. Composite Structures. 2016;153(Supplement C):271-7.

[201] Job S. Composite Recycling: Summary of recent research and development. Materials KTN Report; 2010.

[202] Kacir L, Narkis M, Ishai O. Oriented short glass-fiber composites. I. Preparation and statistical analysis of aligned fiber mats. Polymer Engineering & Science. 1975;15(7):525-31.

[203] Bowyer WH, Bader MG. On the re-inforcement of thermoplastics by imperfectly aligned discontinuous fibres. Journal of Materials Science. 1972;7(11):1315-21.

[204] Fu SY, Lauke B, Mäder E, Yue CY, Hu X. Tensile properties of short-glass-fiber- and short-carbon-fiber-reinforced polypropylene composites. Composites Part A: Applied Science and Manufacturing. 2000;31(10):1117-25.

[205] Hassan A, Rahman NA, Yahya R. Extrusion and injection-molding of glass fiber/MAPP/polypropylene: effect of coupling agent on DSC, DMA, and mechanical properties. Journal of Reinforced Plastics and Composites. 2011;30(14):1223-32.

[206] Thomason JL, Vlug MA, Schipper G, Krikor HGLT. Influence of fibre length and concentration on the properties of glass fibre-reinforced polypropylene: Part 3. Strength and strain at failure. Composites Part A: Applied Science and Manufacturing. 1996;27(11):1075-84.

[207] Lee N-J, Jang J. The effect of fibre content on the mechanical properties of glass fibre mat/polypropylene composites. Composites Part A: Applied Science and Manufacturing. 1999;30(6):815-22.

[208] Spahr DE, Friedrich K, Schultz JM, Bailey RS. Microstructure and fracture behaviour of short and long fibre-reinforced polypropylene composites. Journal of Materials Science. 1990;25(10):4427-39.

[209] Curtis PT, Bader MG, Bailey JE. The stiffness and strength of a polyamide thermoplastic reinforced with glass and carbon fibres. Journal of Materials Science. 1978;13(2):377-90.

[210] Ericson ML, Berglund LA. Processing and mechanical properties of orientated preformed glass-mat-reinforced thermoplastics. Composites Science and Technology. 1993;49(2):121-30.

[211] Thomason JL, Vlug MA. Influence of fibre length and concentration on the properties of glass fibre-reinforced polypropylene: 1. Tensile and flexural modulus. Composites Part A: Applied Science and Manufacturing. 1996;27(6):477-84.

[212] Thomason JL. The influence of fibre length and concentration on the properties of glass fibre reinforced polypropylene: 5. Injection moulded long and short fibre PP. Composites Part A: Applied Science and Manufacturing. 2002;33(12):1641-52.

[213] Mittal RK, Gupta VB. The strength of the fibre-polymer interface in short glass fibre-reinforced polypropylene. Journal of Materials Science. 1982;17(11):3179-88.

[214] Tomkinson-Walles GD. Performance of Random Glass Mat Reinforced Thermoplastics. Journal of Thermoplastic Composite Materials. 1988;1(1):94-106.

[215] Lichao Y, Xiaofei Y, Zhenjin C, Mengfei C, Yuqiu Y, Hamada H. Mechanical Properties of Glass Fiber/ Basalt Fiber Reinforced Polypropylene Hybrid Composites Fabricated by the DFFIM Process. SPE ANTEC Anaheim 2017. Anaheim 2017. p. 1533-6.

[216] Hong CK, Kim N, Kang SL, Nah C, Lee YS, Cho BH, et al. Mechanical properties of maleic anhydride treated jute fibre/polypropylene composites. Plastics, Rubber and Composites. 2008;37(7):325-30.

[217] Bowland C, Busche B, Woude Jv. A formulation study of long fiber thermoplastic polypropylene (part 3): mechanical properties of pp dlft composites. Automot Compos Conf Expo2011.

[218] Jang J, Lee C. Fabrication and mechanical properties of glass fibre–carbon fibre polypropylene functionally gradient materials. Journal of Materials Science. 1998;33(22):5445-50.

[219] Lin J-H, Huang C-L, Liu C-F, Chen C-K, Lin Z-I, Lou C-W. Polypropylene/Short Glass Fibers Composites: Effects of Coupling Agents on Mechanical Properties, Thermal Behaviors, and Morphology. Materials. 2015;8:8279–91.

[220] Thomason JL, Vlug MA. Influence of fibre length and concentration on the properties of glass fibre-reinforced polypropylene: 4. Impact properties. Composites Part A: Applied Science and Manufacturing. 1997;28(3):277-88.

[221] Xavier SF, Misra A. Influence of glass fiber content on the morphology and mechanical properties in injection molded polypropylene composites. Polymer Composites. 1985;6(2):93-9.

[222] C B. formulation study of long fiber thermoplastic polypropylene (Part 2): The effects of coupling agent type and properties. Automot Compos Conf Expo2009.

[223] Williams T, Allen G, Kaufman MS. The impact strength of fibre composites. Journal of Materials Science. 1973;8(12):1765-87.

[224] Adams DF. Impact testing of composite materials. CompositesWorl2012.

[225] AH. C. Strong solids. Proceedings of the Royal Society of London Series A Mathematical and Physical Sciences. 1964;282(1388):2.

[226] Shokrieh MM, Omidi MJ. Tension behavior of unidirectional glass/epoxy composites under different strain rates. Composite Structures. 2009;88(4):595-601.

[227] Torabizadeh MA. Tensile, compressive and shear properties of unidirectional glass/epoxy composites subjected to mechanical loading and low temperature services. Indian Journal of Engineering and Materials Sciences. 2013;20:299-309.

[228] Wisnom MR, Atkinson JW. Reduction in tensile and flexural strength of unidirectional glass fibre-epoxy with increasing specimen size. Composite Structures. 1997;38(1):405-11.

[229] Zhao FM, Takeda N. Effect of interfacial adhesion and statistical fiber strength on tensile strength of unidirectional glass fiber/epoxy composites. Part I: experiment results. Composites Part A: Applied Science and Manufacturing. 2000;31(11):1203-14.

[230] Gurusideswar S, Srinivasan N, Velmurugan R, Gupta NK. Tensile Response of Epoxy and Glass/Epoxy Composites at Low and Medium Strain Rate Regimes. Procedia Engineering. 2017;173:686-93.

[231] Naik NK, Yernamma P, Thoram NM, Gadipatri R, Kavala VR. High strain rate tensile behavior of woven fabric E-glass/epoxy composite. Polymer Testing. 2010;29(1):14-22.

[232] Mahato KK, Biswal M, Rathore DK, Prusty RK, Dutta K, Ray BC. Effect of loading rate on tensile properties and failure behavior of glass fibre/epoxy composite. IOP Conf Ser: Mater Sci Eng. 2016;115.

[233] Heckadka SS, Nayak SY, Narang K, Pant KV. Chopped Strand/Plain Weave E-Glass as Reinforcement in Vacuum Bagged Epoxy Composites. Journal of Materials Processing Technology. 2015;2015:1-7.

[234] Jagannatha TD, GHarish G. Mechanical properites of carbon/glass fibre reinforced epoxy hybrid polymer composites. Int J Mech Eng. 2015;4(2):131-7.

[235] Matei S, Stoicanescu M, Crisan A. Composites with Short Fibers Reinforced Epoxy Resin Matrix. Procedia Technology. 2016;22:174-81.

[236] Sudheer M, R. PK, Somayaji S. Analytical and Numerical Validation of Epoxy/Glass Structural Composites for Elastic Models. American Journal of Materials Science. 2015;5(3C):162-8.

[237] Goh KL. Physical Properties of Fibres and Matrix. Discontinuous-Fibre Reinforced Composites: Fundamentals of Stress Transfer and Fracture Mechanics: Springer London 2017. p. 22.

[238] Lee N-J, Jang J. The effect of fibre-content gradient on the mechanical properties of glass-fibre-mat/polypropylene composites. Composites Science and Technology. 2000;60(2):209-17.

[239] Sato N, Kurauchi T, Sato S, Kamigaito O. Microfailure behaviour of randomly dispersed short fibre reinforced thermoplastic composites obtained by direct SEM observation. Journal of Materials Science. 1991;26(14):3891-8.

[240] Pickering S. Recycling and Disposal of Thermoset Composites. Workshop on Life Cycle Assessment (LCA) for Composites, Composites Gateway. Totnes 2013.

[241] Gas fluidization technology. Chichester ; New York: Chichester ; New York : Wiley; 1986.

[242] Thermopedia. Thermopedia - Fluidized bed. 2010.

[243] Cahyadi A, Neumayer AH, Hrenya CM, Cocco RA, Chew JW. Comparative study of Transport Disengaging Height (TDH) correlations in gas–solid fluidization. Powder Technology. 2015;275:220-38.

[244] Gibilaro LG. 2 - Single particle suspension. In: Gibilaro LG, editor. Fluidization Dynamics. Oxford: Butterworth-Heinemann; 2001. p. 8-13.

[245] Hoffmann AC, Stein LE. Gas Cyclones and Swirl Tubes: Principles, Design, and Operation: Springer Berlin Heidelberg; 2002.

[246] Rhodes MJ. Introduction to Particle Technology: John Wiley & Sons; 2008.

[247] Feih S, Boiocchi E, Kandare E, Mathys Z, Gibson AG, Mouritz AP. Strength degradation of glass and carbon fibres at high temperature. ICCM-17 17th International Conference on Composite Materials. Edinburgh, UK2009.

[248] Jenkins P. Investigation of the strength loss of heat treated glass fibre: University of Strtahclyde; 2016.

[249] Yin Y, Binner JGP, Cross TE, Marshall SJ. The oxidation behaviour of carbon fibres. Journal of Materials Science. 1994;29(8):2250-4.

[250] Iacocca RG, Duquette DJ. The catalytic effect of platinum on the oxidation of carbon fibres. Journal of Materials Science. 1993;28(4):1113-9.

Appendix A. Fluidised bed recycling rig design

This section details the process of designing the main components of the fluidised bed recycling system. The system can intuitively be separated into two discrete units; thermal decomposition of composite matrix with glass fibre liberation followed by fibre recovery from combustion gases. Features of the fluidised bed reactor such as geometry and distributor plate design are determined. A fibre separation and recovery unit, utilising a cyclone separator is also designed.

In order to begin the design process, serval operating conditions/design aspects of the system must be estimated. Table A-1 gives these parameters and the estimated values. The fluidised bed temperature operating range was estimated based on the typical thermal decomposition temperature of a range of thermoset plastics such as epoxy and polyester [7]. The range of fluidisation velocities, estimated reactor size, sand particle size and settled bed height were selected based on similar systems [36].

Table A-1 Fluidised bed recycling system initial design parameters

Parameter	Value
Fluidisation velocity	1.2-1.7 m/s
Fluidising sand particle size	500-1500 μm
Bed temperature	450-550 °C
Reactor size	~0.2 m
Settled bed height	0.1-0.15 m

A.1 Reactor

A.1.1 Distributor plate

The distributor plate consists of two perforated plates, essentially a circular plate with evenly distributed holes, with a fine mesh sandwiched in between. The mesh

contains the sand bed while the perforated plates serve to distribute the airflow in a manner suitable to encourage the fluidisation of the sand.

The total porosity of the distributor plate (Φ_{Dist}) is give as the multiple of the perforated plate porosity (Φ_{Plate}) and mesh porosity (Φ_{mesh}) is given in Equation A-1.

Equation A-1 Total porosity of fluidisation plate

$$\Phi_{Dist} = \Phi_{Plate}\Phi_{mesh}$$

The porosity of the distributor plate is an important design aspect of the system, which influences the pressure drop across the distributor plate, jet velocity and ultimately the fluidisation of the sand. A suitable plate porosity for the test rig was selected by assessing its effect on the pressure drop across a range of expected fluidisation velocities and bed heights. An excessive pressure drop across the plate was considered negatively as this presents additional resistance to the air supply to the reactor, causing unnecessary losses in the flow. The operating temperature of the bed was assumed 500 °C throughout the distributor plate design.

The pressure drop across the distributor plate (ΔP_{dist}) is given in Equation A-2.

Equation A-2 Pressure drop across the distributor plate [241]

$$\Delta P_{dist} = \frac{\rho_g U_{or}^2}{2Cd_{or}^2}$$

The jet velocity (U_{or}) and distributor orifice coefficient (Cd_{or}) are given in Equation A-3 and Equation A-4 respectively.

Equation A-3 Jet velocity [241]

$$U_{or} = \frac{V_f}{\Phi_{Dist}}$$

Equation A-4 Distributor orifice coefficient [241]

$$Cd_{or} = 0.7 + (Re_{dist} - 300)\left(\frac{0.68 - 0.7}{200}\right)$$

The distributor Reynolds number (Re_{dist}) is given in Equation A-5.

Equation A-5 Distributor Reynolds number [241]

$$Re_{dist} = \frac{1.3DV_f\rho_g}{\mu}$$

In addition to the pressure drop across the distributor plate, there is also the pressure drop across the sand bed (ΔP_{bed}), given in Equation A-6.

Equation A-6 Pressure drop across the sand bed [241]

$$\Delta P_{bed} = H_s(1-\varepsilon)(\rho_s - \rho_g)g$$

The distributor plate and bed pressure drops are summed to give the total pressure drop. Using the method outlined above, the pressure drops given as a function of total porosity for a range of the bed depths and fluidisation velocities in Figure A-1. Based on this assessment a total plate porosity of 9% was selected giving a maximum total pressure drop of 6.95 kPa (at fluidisation velocity and bed height of 1.5 m/s and 0.15 m respectively). The mesh used has a porosity of 39.9% therefore, the perforated plates have a porosity of 22.6%.

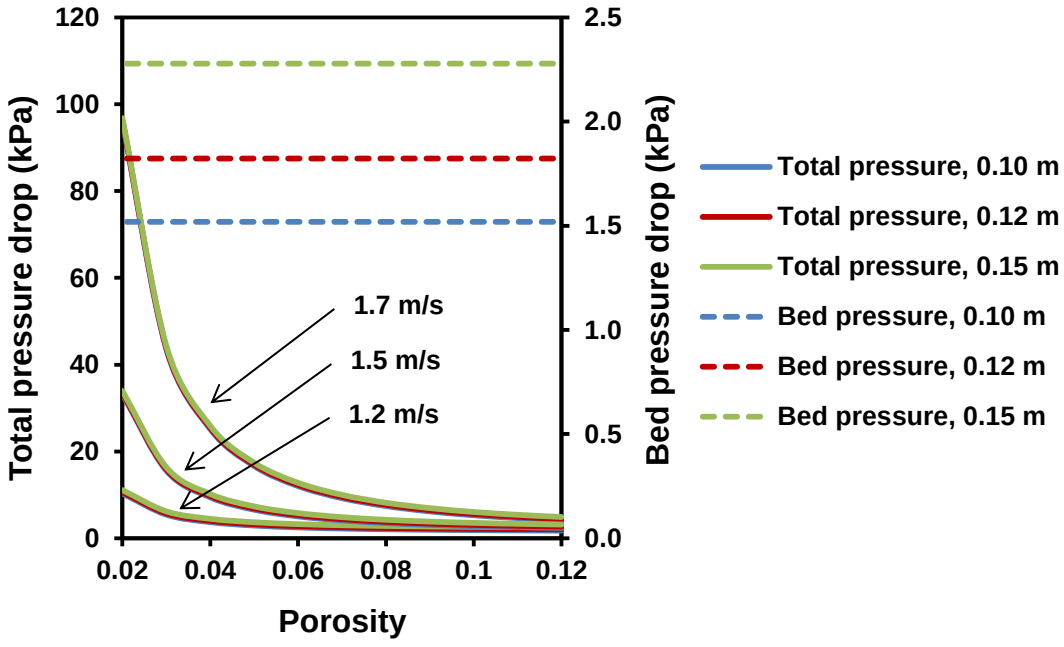

Figure A-1 Pressure drops given as a function of porosity for a range of the bed depths and fluidisation velocities

Finally, the maximum distance between orifices in the perforated plate (c), for various orifice diameters, was found based on the geometry shown in Figure A-2 using Equation A-7. It was thought that diminishing this distance could reduce the likelihood of recyclate becoming settled in stagnant regions between orifices. This area of un-fluidisation can have very little mass transfer leading to the possibility of fibres/scrap composite becoming trapped.

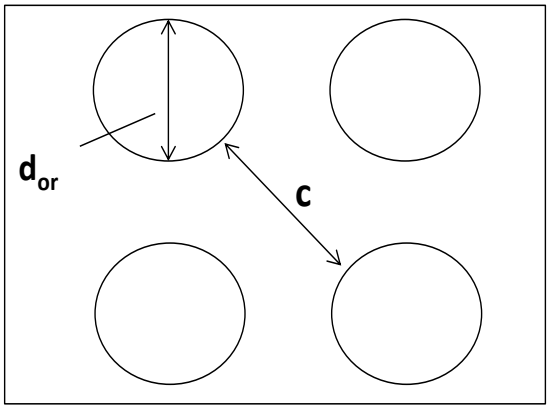

Figure A-2 Geometric pattern of orifices in perforated plat

Equation A-7 Maximum distance between holes in the perforated plate

$$c = \sqrt{2\left(d_{or}\frac{0.886}{\sqrt{\Phi_{Dist.}}}\right)^2} - d_{or}$$

The maximum distance between orifices is given in Figure A-3. An orifice diameter of 2 mm was select in order to reduce the distance between orifices to around 2.6 mm at a total plate porosity of 9%.

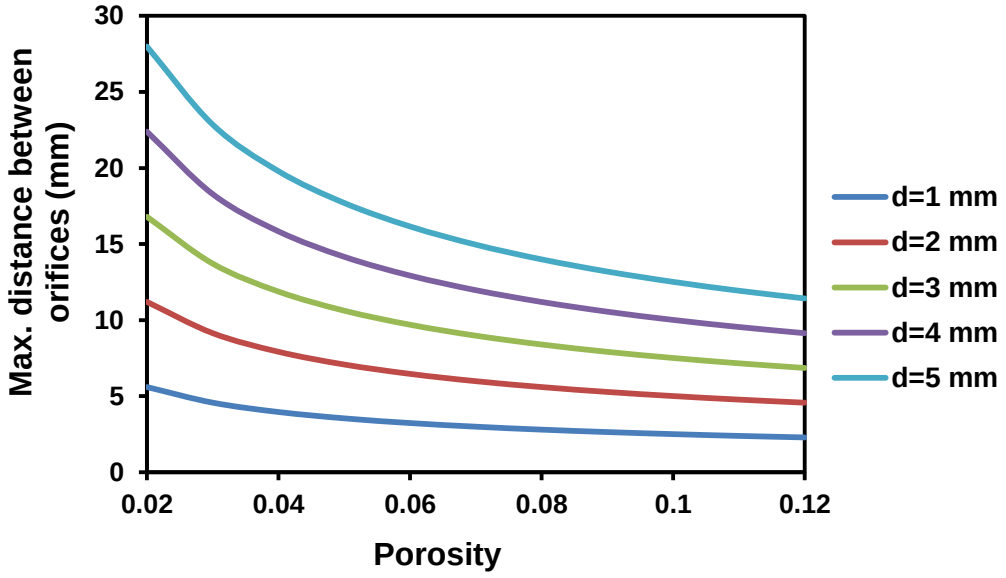

Figure A-3 Maximum distance between orifices as a function of porosity for various orifice diameters

The perforated plate was water jet cut from 316 stainless steel, a CAD model of which can be seen in Figure A-4.

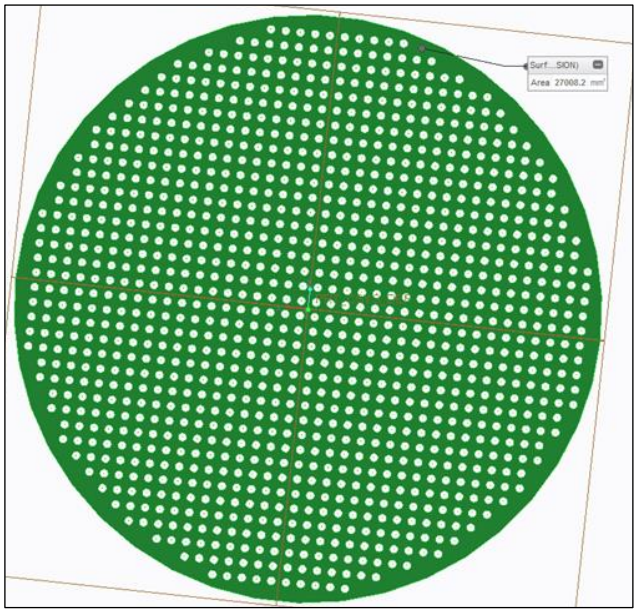

Figure A-4 CAD model of final perforated plate design

A.1.2 Reactor height

The required height of the reactor was established by assessing the transport disengagement height (TDH) of the fluidised sand particles. The TDH is the maximum height, above which only particles whose free fall velocity is less than the gas velocity can occur [242]. For a monodisperse material, above this height the particle concentration is zero. Designing the reactor to be higher than the TDH for a given fluidised particle should therefore minimise the entrainment of particles and reduce contamination of RGF. Despite the development of many TDH correlations, poor agreement between predicted and experimental values is prominent [243]. Equation A-8 gives a correlation for finding TDH as described in [243], where Ar and Re_p are given in Equation A-9 and Equation A-10 respectively.

Equation A-8 TDH correlation for particles size 750-2500 µm [243]

$$TDH = 1200 H_s Re_p^{1.55} Ar^{-1.1}$$

Equation A-9 Archimedes number [244]

$$Ar = \frac{d_p^3 \rho_g (\rho_s - \rho_g) g}{\mu^2}$$

Equation A-10 Reynolds number of particle [244]

$$Re_p = \frac{\rho_g V_f d_p}{\mu}$$

The TDH was found for silica sand with an average particle size of 750 µm and a reactor diameter of 0.211 m. The range of fluidisation velocities, settled bed depths and operating temperatures where investigated, which the fluidised bed is expected to operate at. The results are shown in Figure A-5. Based on the study, a reactor height of 1.3 m was chosen which is higher than the TDH across the majority of the range of expected operating conditions.

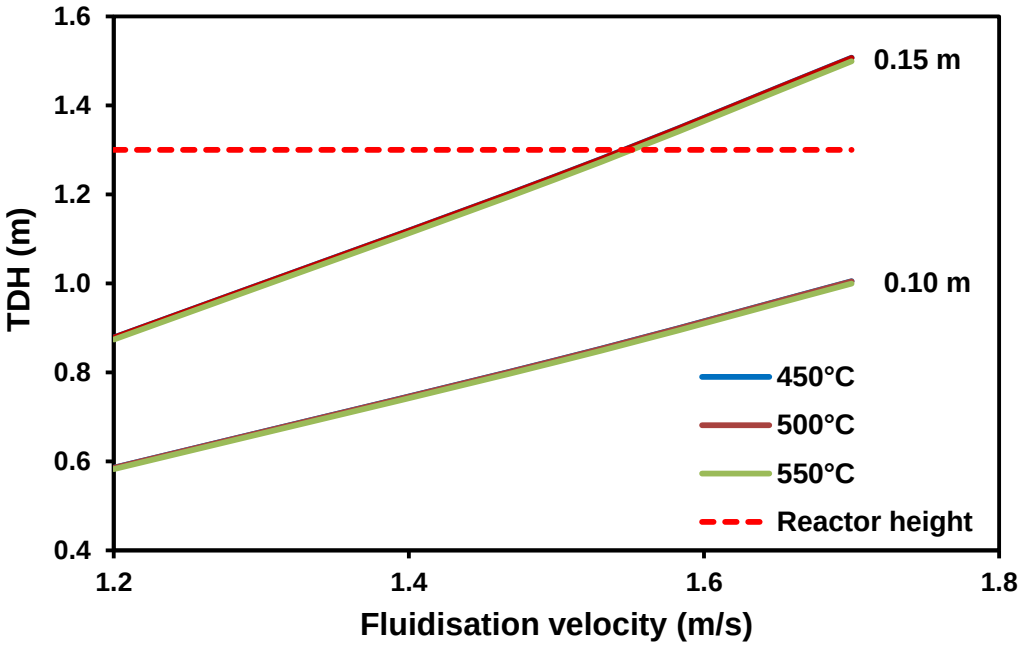

Figure A-5 Investigation into the effect of fluidisation velocity, bed height and operating temperature on TDH

A.2 Cyclone separator

Standard methods for designing cyclone separators, as given in textbooks, begin with the assumption that the particulate material to be separated from the air stream approximates a spherical geometry. An approach capable of approximating the efficiency of a cyclone for separating alternative geometries, similar to those of the RGF, could not be sourced by the author. In order to proceed with the cyclone separator design an assumption was therefore made that the particulate material was spherical. The design methodology followed that outline in [245] using various models, the geometry of the cyclone can be seen in Figure A-6. The cyclone diameter, inlet velocity and mass fraction of particulates in the gas stream were varied; in each case, the resulting fractional separating efficiency was plotted as a function of particle size and the pressure drop across the cyclone was found.

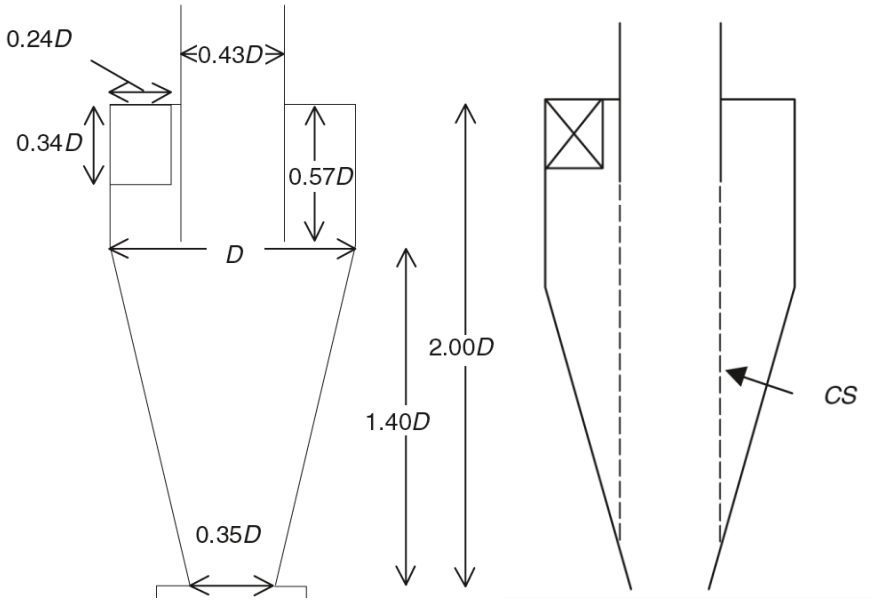

Figure A-6 LHS) Geometry of cyclone separator as given in [245], RHS) Schematic of control surface CS given in [245]

A.2.1 Barth model for calculating fractional efficiency

Beginning with the Barth model for calculating the overall efficiency of the cyclone, the radial gas velocity at control surface, CS (v_{rCS}) is found using Equation A-11.

Equation A-11 Radial gas velocity at CS

$$v_{rCS} = \frac{Q}{\pi D_x H_{CS}}$$

The fibre outlet is smaller than the gas outlet therefore CS intersects the cone near its lower end, the height of the surface CS (H_{CS}) is shorter than the physical height and is given in Equation A-12.

Equation A-12 Height of surface HC

$$H_{CS} = (H - S) - H_c(R_x - R_d)/(R - R_d)$$

The tangential velocity at CS ($v_{\theta CS}$) is found using Equation A-13

Equation A-13 Tangential velocity at CS

$$v_{\theta CS} = \frac{v_{\theta\omega}\left(\frac{R}{R_x}\right)}{\left(1 + \frac{H_{CS}R\pi f v_{\theta\omega}}{Q}\right)}$$

To find $v_{\theta CS}$ the wall velocity ($v_{\theta\omega}$) is found using Equation A-14, derived from the ratio of the moment-of-momenta of the gas in the inlet and the gas flowing along the wall.

Equation A-14 Wall velocity

$$\alpha \equiv \frac{v_{in}R_{in}}{v_{\theta\omega}R} = 1 - 0.4\left(\frac{b}{R}\right)^{0.5}$$

The cut-diameter of the cyclone (x_{50}) can then be found using Equation A-15.

Equation A-15 Cut diameter of the cyclone

$$x_{50} = \sqrt{\frac{v_{rCS}9\mu D_x}{\rho_P v_{\theta CS}^2}}$$

Finally, the overall fractional separation efficiency is determined from Equation A-16.

Equation A-16 Overall fractional separation efficiency of cyclone

$$\eta(x) = \frac{1}{1 + \left(\frac{x_{50}}{x}\right)^{6.4}}$$

A.2.1.1 Barth model for calculating pressure drop

Continuing with the Barth model, the pressure drop across the cyclone can be established. The mean gas velocity in the inlet and vortex finder (v_x) is found using Equation A-17.

Equation A-17 Mean gas velocity in the inlet and vortex finder

$$v_x = \frac{v_{in}ab}{(\pi D_x^2/4)}$$

The friction factor (f) for a given particle loading (c_O) is found using Equation A-18.

Equation A-18 Friction factor

$$f = f_{air} + f_{dust} = 0.005\left(1 + 3\sqrt{c_O}\right)$$

Finally, the pressure drop in the body (Δp_{body}) and vortex finder (Δp_x) are found using Equation A-19 and Equation A-20 respectively and summed to give the overall pressure drop across the cyclone (Δp).

Equation A-19 Pressure drop in the body

$$\frac{\Delta p_{body}}{\frac{1}{2}\rho_c v_x^2} = \frac{D_x}{D}\left(\frac{1}{\left(\frac{v_x}{v_{\theta CS}} - \frac{(H-S)}{0.5D_x}f\right)^2} - \left(\frac{v_{\theta CS}}{v_x}\right)^2\right)$$

Equation A-20 Pressure drop in the vortex finder

$$\frac{\Delta p_x}{\frac{1}{2}\rho_c v_x^2} = \left(\frac{v_{\theta CS}}{v_x}\right)^2 + K\left(\frac{v_{\theta CS}}{v_x}\right)^{\frac{4}{3}}$$

Equation A-21 Overall pressure drop across the cyclone

$$\Delta p = \Delta p_{body} + \Delta p_x$$

A.2.1.2 Particle size

The fibres under investigation have an average diameter of around 15 μm and length dependent on feedstock processing prior to recycling in the fluidised bed. An equivalent particle diameter (relative to fibre geometry) can be found by equating the volumes of a sphere and cylinder, Equation A-22 and Equation A-23 respectively.

Equation A-22 Volume of a sphere

$$V_p = \frac{4}{3}\pi\left(\frac{D_p}{2}\right)^3$$

Equation A-23 Volume of a cylinder

$$V_f = \pi\left(\frac{D_f}{2}\right)^2 L_f$$

The equivalent particle diameter can therefore be found as a function of fibre length, Equation A-24 and plotted as shown in Figure A-7.

Equation A-24 Equivalent particle diameter

$$D_p = \frac{3}{2} D_f^2 L_f$$

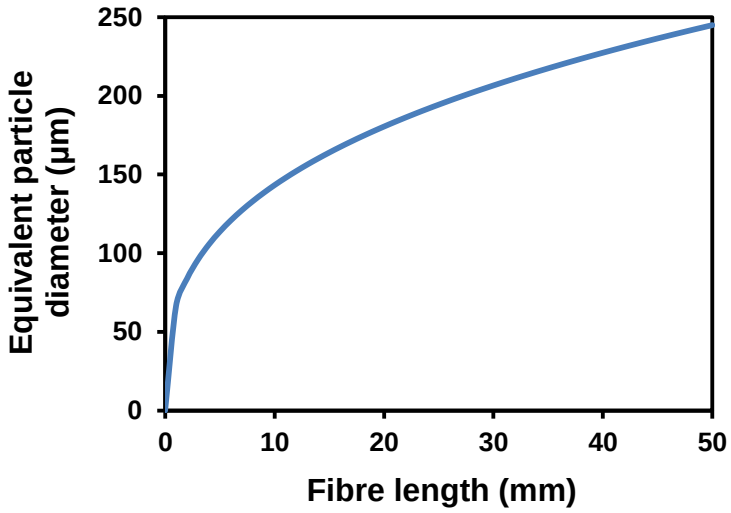

Figure A-7 Equivalent particle diameter as a function of fibre length, where D_f=15 µm

The dimensions of material being separated are much larger than that of typical dust loaded gas streams and the calculated efficiency would be 100%. Throughout the analysis, smaller particle sizes (up to 10 µm) were investigated; since the separation efficiency increases with particle size the efficiency should only improve for larger particles/fibres.

A.2.1.3 Cyclone separator design assessment

A recommended pressure drop of 5-15 mbar is given by [246]; stating “at pressure drops below the bottom limit, the cyclone represents little more than a settling chamber, giving low efficiency due to low velocities within it which may not be capable of generating a stable vortex”. This range was used as a guide throughout the design process and only cyclone geometries and operating conditions yielding a pressure drop within this range were considered. The temperature within the

cyclone was estimated to be 300 °C therefore the properties of the gas stream used throughout the analysis were air at said temperature.

Initially the cyclone diameter was varied from 0.1-0.3 m with a constant mass flow rate of 0.03 kg/s. Figure A-8 gives the pressure drop across the cyclone as a function of the cyclone diameter. At around 13 mbar, only a diameter of 0.15 m yields a pressure drop within the recommender range outlined in [246]. According to the model, the mass flow within the system is so low that a cyclone any larger than 0.15 m would have a low inlet velocity and insufficient pressure drop.

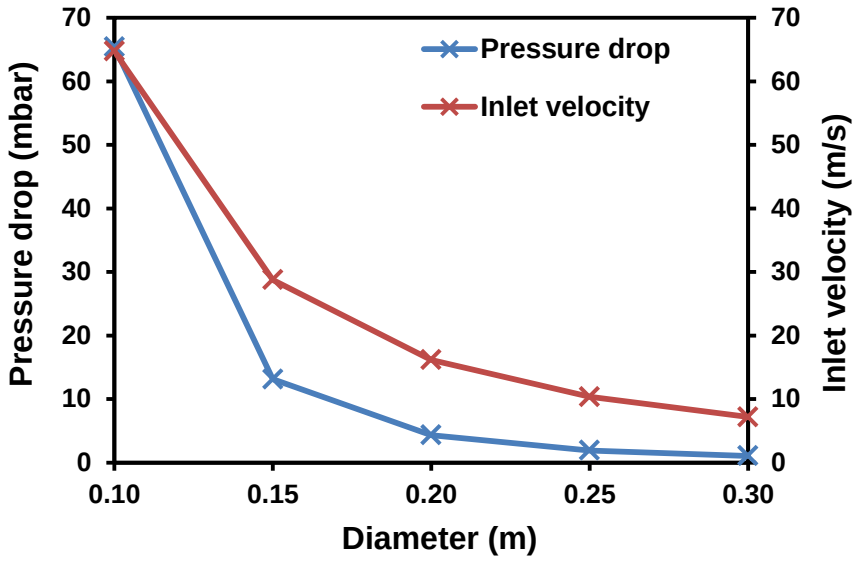

Figure A-8 Pressure drop and inlet velocity for various cyclone diameters with a mass flow rate of 0.03 kg/s

The fractional separation efficiency as a function of particle size is given in Figure A-9. In agreement with [246], the efficiency is improved with a higher pressure drop provided by reducing the cyclone diameter.

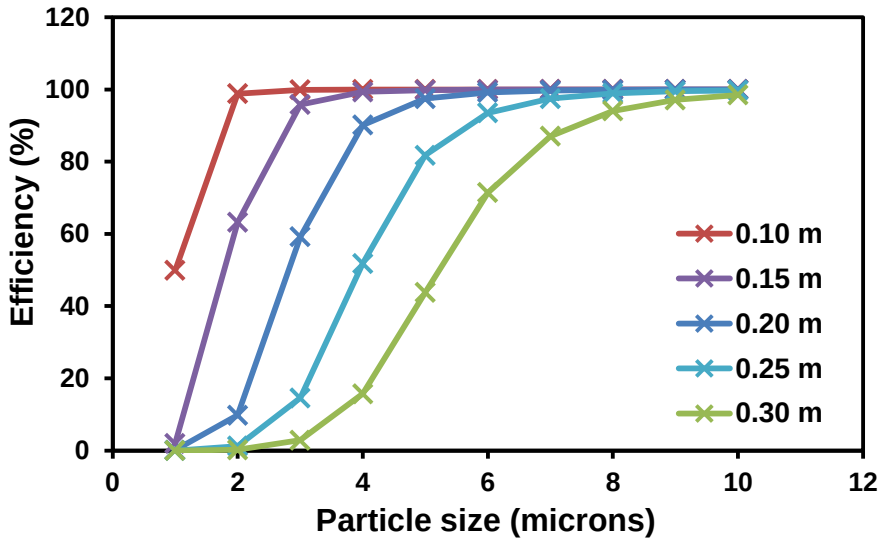

Figure A-9 Fractional separation efficiency as a function of particle size with a mass flow rate of 0.03 kg/s

A cyclone diameter of 0.15 m was used based on this analysis and the effect of varying the mass flow rate on pressure drop and efficiency further explored in Figure A-10 and Figure A-11 respectively. An estimated range of suitable inlet velocities of 18-31 m/s (0.02-0.035 kg/s) was found, while still operating within the recommended pressure drop range (5-15 mbar). Again, the determined efficiency is very high and approaches 100% for all inlet velocities investigated.

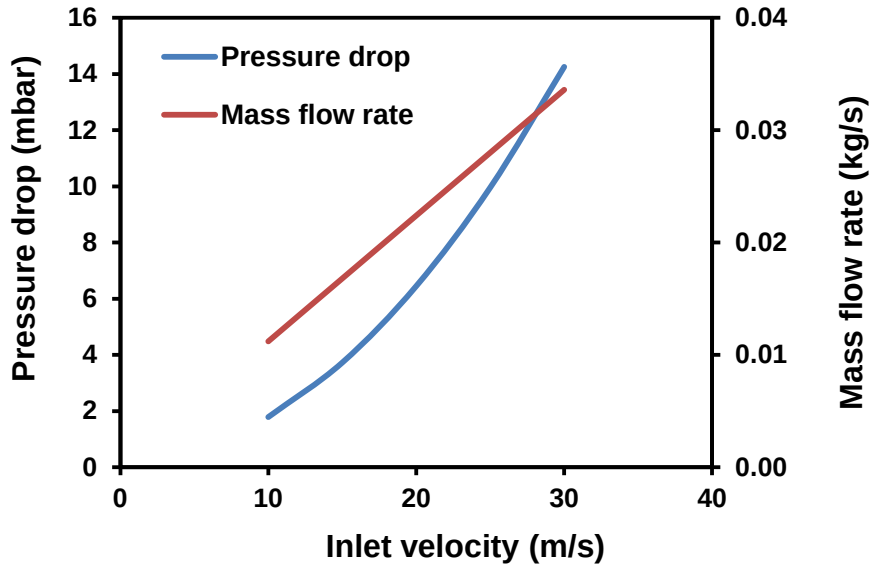

Figure A-10 The effect of varying the mass flow rate on pressure drop for a 0.15 m diameter cyclone

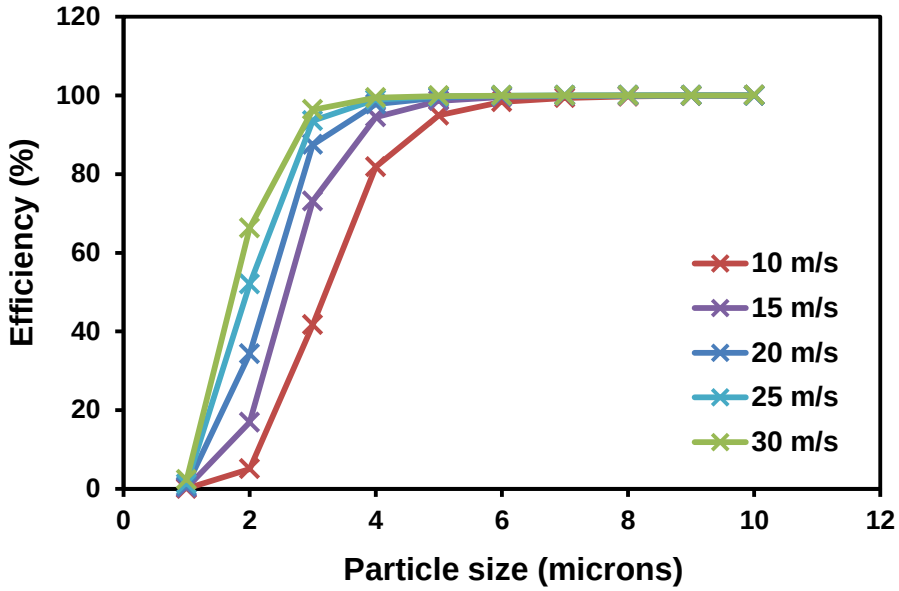

Figure A-11 The effect of varying the mass flow rate on fractional efficiency for a 0.15 m diameter cyclone

Finally, the impact of feed rate, and as a result particulate loading, was investigated in terms of pressure drop and efficiency in Figure A-12 and Figure A-13 respectively. The glass fibre content of feedstock was assumed to be 60% by weight. The pressure drop is relatively stable with feed rate and remains within the recommended range, furthermore, the efficiency is also relatively unaffected by the feed rate and quickly approaches 100%.

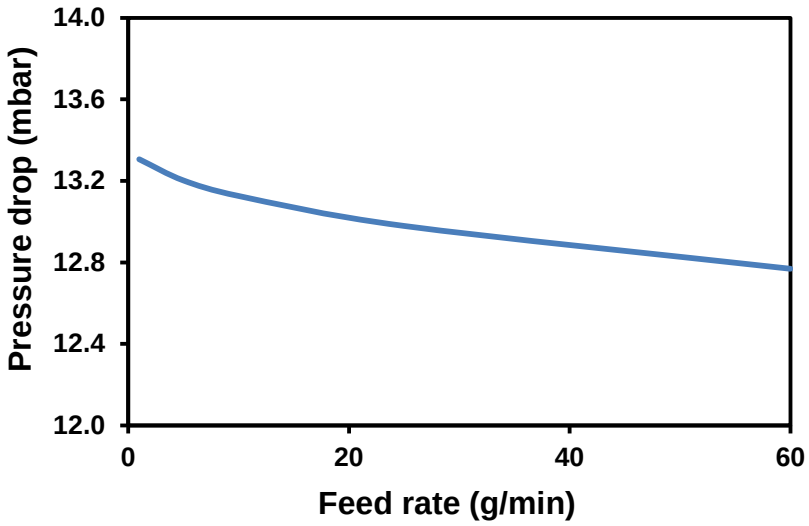

Figure A-12 The effect of varying the feed rate on pressure drop for a 0.15 m diameter cyclone with a mass flow rate of 0.03 kg/s

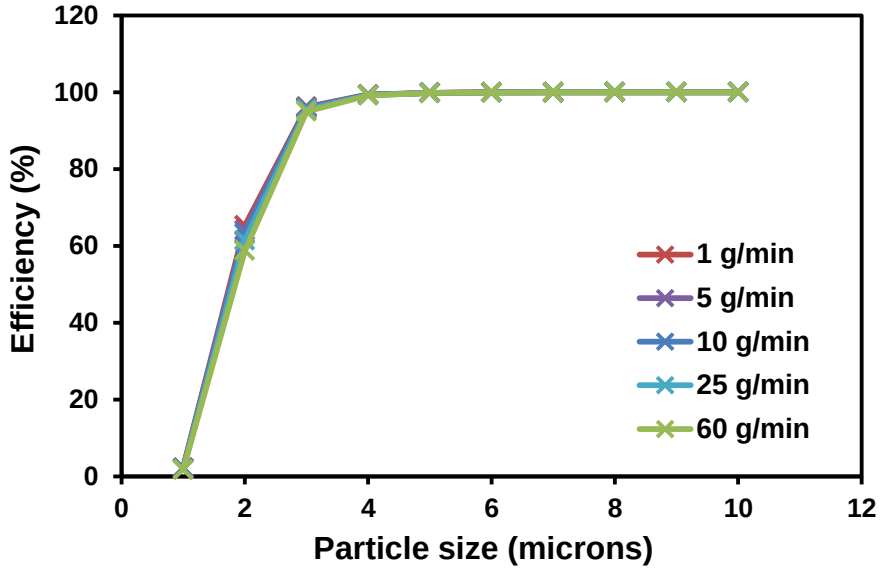

Figure A-13 The effect of varying the feed rate on fractional efficiency for a 0.15 m diameter cyclone with a mass flow rate of 0.03 kg/s

A.2.2 Final design

Based on the above analysis, a cyclone with a diameter of 0.15 m and geometry given in Figure A-14 was selected for separating the fibres from the gas stream.

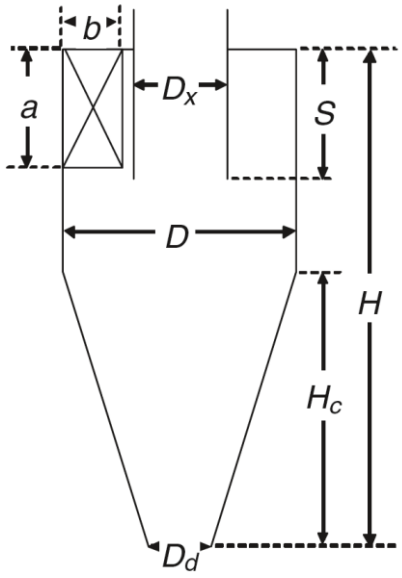

Figure A-14 Nomenclature for geometry of final cyclone design

Table A-2 gives the dimensions of the cyclone separator.

Table A-2 Dimensions of the cyclone separator

Dimension	Ratio	Length (m)
D	1D	0.150
D_x	0.43D	0.0645
D_d	0.35D	0.0525
a	0.34D	0.0510
b	0.24D	0.0360
S	0.57D	0.0855
H	2D	0.300
H_C	1.4D	0.210

Appendix B. Bundle vs. single fibre thermal conditioning

In this section, the influence of both thermal and mechanical handling damage on thermally conditioned fibres is investigated.

B.1 Introduction

Jenkins et al. proposed that the strength of thermally conditioned glass fibre was still being considerably underestimated, and that it was possible to reduce the degree of mechanical damage that glass fibres are subjected to using current methods of thermal conditioning and testing [32]. To assess the impact of both thermal and mechanical damage on thermally conditioned fibres Jenkins et al. developed two protocols: bundle thermal conditioning and single fibre thermal conditioning [32]. The difference between these two methods was the point of fibre separation from the bundle as shown in Figure B-1. Single fibre treatments are performed in order to minimise the handling of thermally conditioned fibres as well as prevent fibre-fibre abrasion.

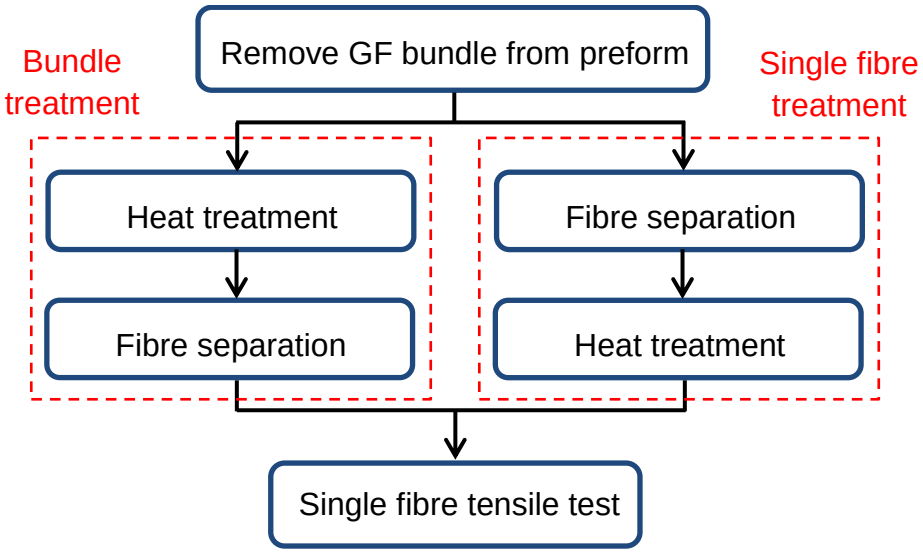

Figure B-1 Different procedures for single and bundle thermal conditioning

Jenkins et al. showed that thermally conditioned fibres are more susceptible to damage caused by mechanical handling [32] (as shown in Figure B-2) and suggested this is due to the removal of the protective sizing. It has been demonstrated previously that the removal of glass fibre sizing after heating can contribute to fibre strength loss above purely thermal weakening [42].

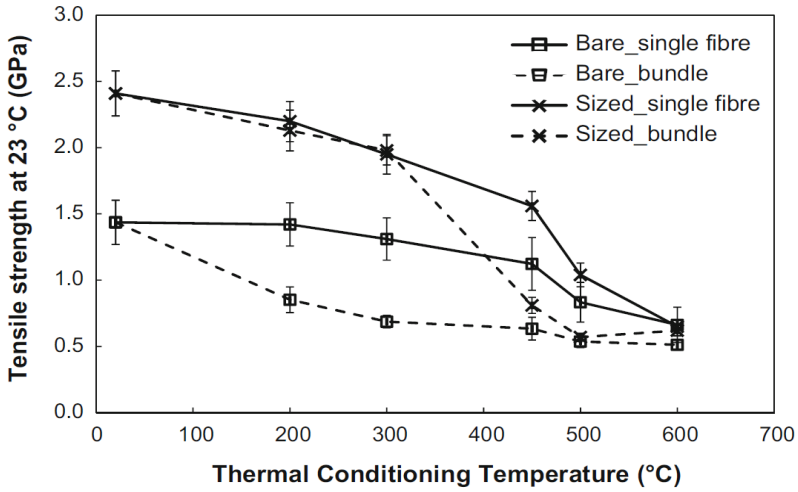

Figure B-2 Tensile strengths of bare and APS-sized fibres after thermal condition, taken from [32]

Although a wide variety of conditioning temperatures were investigated in [32], treatment times were limited to 25 min. In this work, the effect of thermal and mechanical weakening is further investigated. As in [32], the strength of fibres heated as a bundle and single fibre are compared at different conditioning temperatures, however a wide variety of conditioning times are also explored. A phenomenological model for fibre strength as a function of conditioning temperature and time, similar to that present by Feih et al. [31], is developed based on the experimental data.

B.2 Experiment

B.2.1 Materials

E-glass fibres used in this work were from a tri-axial (0 °/ -45 °/+45 °) 3-ply mat supplied by Hexcel Reinforcements UK Ltd.

B.2.2 Single fibre thermal conditioning

In the single fibre thermal conditioning process, single fibres were extracted from a bundle prior to thermal conditioning. These were then attached to wire frames using Glassbond cement. The design of the frames was different for brief (≤ 10 min) and extended (> 10 min) single fibre thermal conditioning. Figure B-3 shows the wire frame used for extended single fibre thermal conditioning. Multiple frames could be placed in the furnace at once to attain enough thermally conditioned fibres for each test condition.

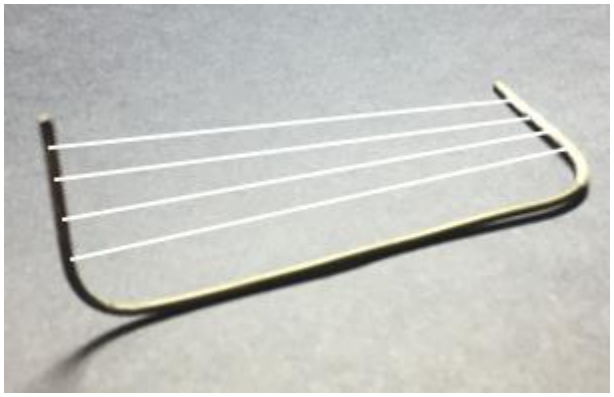

Figure B-3 Wire frame used for extended single fibre thermal conditioning with position of attached fibre drawn on

Figure B-4 shows the wire frame used for brief single fibre thermal conditioning. The wire frames were narrow enough so they could be lowered into the furnace through the chimney. In both cases, the fibres were mounted with some slack along the length to ensure thermal expansion of the frame would not induce longitudinal tensile stress. Brief and extended bundle thermal conditioning were performed as described in Chapter 3.

Figure B-4 Wire frame used for brief single fibre thermal conditioning with position of attached fibre drawn on

Both bundles and single fibres were subject to 16 different conditioning schedules, the temperatures and times used are shown in Table B-1.

Table B-1 Conditioning temperatures and durations used in the investigation

Conditioning time (min)	1	10	25	60
Conditioning temperature (°C)	300	400	500	600

B.3 Results and discussion

Figure B-5 and Figure B-6 show the single fibre tensile strength of fibres thermally conditioned as bundles and single fibres respectively. The strength is given relative to the as received strength, which is 2.55 GPa. In agreement with Chapter 3, there is a trend in increased rate of strength loss with treatment temperature, regardless of the conditioning protocol. Furthermore, this rate of strength loss is higher initially then generally decreases with conditioning time, again in agreement with Chapter 3. These relationships are also well established in the literature [31-33, 35, 247].

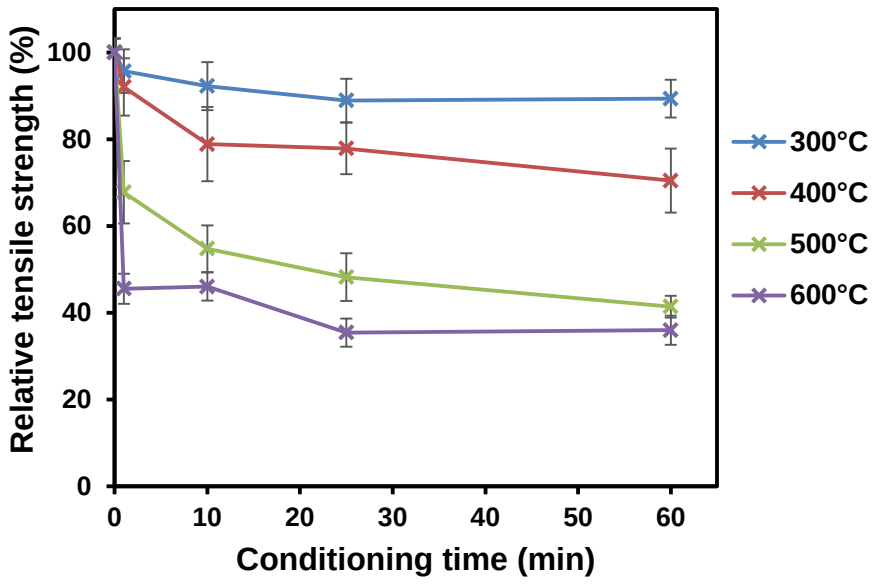

Figure B-5 Tensile strength of glass fibres thermally conditioned as fibre bundles

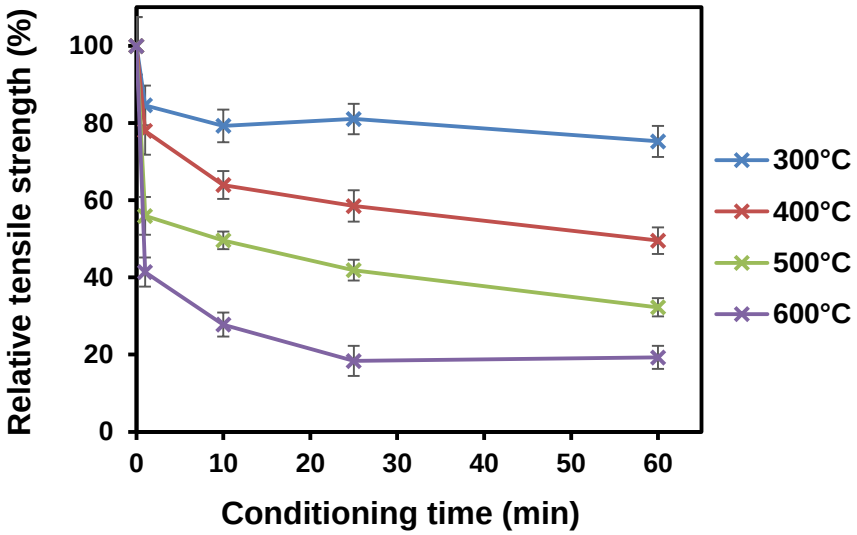

Figure B-6 Tensile strength of glass fibres thermally conditioned as single fibres

The strength loss is higher for glass fibres conditioned as single fibres, as shown in Figure B-7 for fibres conditioned for 60 min. This trend was consistent for all the treatment schedules investigated. This is contrary to the observations made by Jenkins et al. [32], which reported that extracting individual fibres from the bundle before thermal conditioning reduced the degree of mechanical damage and therefore overall strength loss.

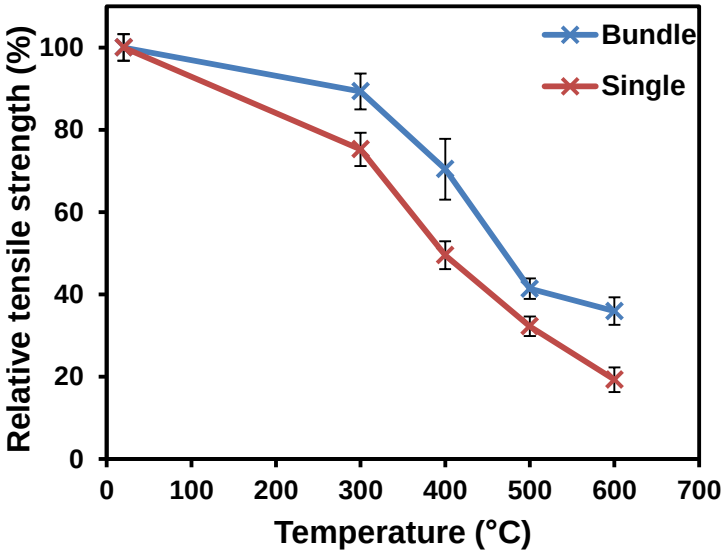

Figure B-7 Tensile strength of fibres heated as bundles and single fibres for 60 min

The reason for this discrepancy may be explained by the difference in sizings on the fibres under investigation. Jenkin et al. used E-glass fibres sized with only APS [32], whereas the fibres taken from the mat in this work are fully commercially sized. The exact sizing composition is proprietary and cannot be made readily available however likely contains an epoxy based film former, since the mat in question was intended for use with epoxy systems. During sample preparation, it was observed that removing single fibres from the bundle prior to thermal conditioning was considerably more difficult than after thermal conditioning. This is possibly due to the presences of binding agent/film former on the commercially sized fibres causing the fibres to stick together. After thermal conditioning the bundles, the fibres were loose and no longer bound together in a bundle. This is likely due to the sizing decomposing which allowed fibres to be easily removed from the thermally conditioned bundle, reducing the handling required to extract single fibres.

In contrast, it was observed that extracting single fibres from bundles sized with APS alone (as used in [32]) was significantly more difficult after thermal conditioning as they appeared to be bonded together [142, 248]. The reason for the high strength loss of bundle heated fibres may be a result of the additional mechanical damage sustained during fibre extraction. It should also be noted that the strength loss of fibres heated as bundles reported in [32] is significantly higher than observed in this work. After conditioning at 500 °C for 25 min, the residual strength is report to be just 20-25% in [32]; compared to approximately 50% in this work. This further suggests that the additional strength loss when thermally conditioning bundles sized with APS alone in [32] is a result of difficulty in extracting already weakened fibres.

The reason for the fibres in APS sized bundles bonding together after thermal conditioning is not yet fully understood. Through thermochemical analysis and TGA of APS decomposition, Jenkin et al. showed the region of maximum mass loss commences at 300 °C with the maximum rate of mass loss occurring around 440 °C. This corresponded to the decomposition of the organic fraction of the polymer chain with a peak in the volatilisation of C_2H_4 occurring around 400 °C [32]. The maximum strength loss of fibres conditioned as bundles in [32] occurs between 300–450 °C which coincides with the APS decomposition. Given this correlation, it was suggested that the loss in protection from sizing is the reason for the sudden strength loss of fibres treated as bundles [32].

It is postulated here that the decomposition of APS during thermal conditioning could result in a silane network forming and bonding adjacent fibres in the bundle. This makes extracting single fibres more difficult and causes additional mechanical damage. The increase in strength loss in [32] when using bundles would therefore solely be a result of testing APS only sized glass fibres. Figure B-8 gives a comparison of the two proposed strength loss mechanisms. The reason why this does not occur when thermally conditioning commercially sized fibre bundles is yet unclear. It may be due to an increased distance between adjacent fibres in the bundle preventing crosslinking between the fibres as a result of the additional sizing components.

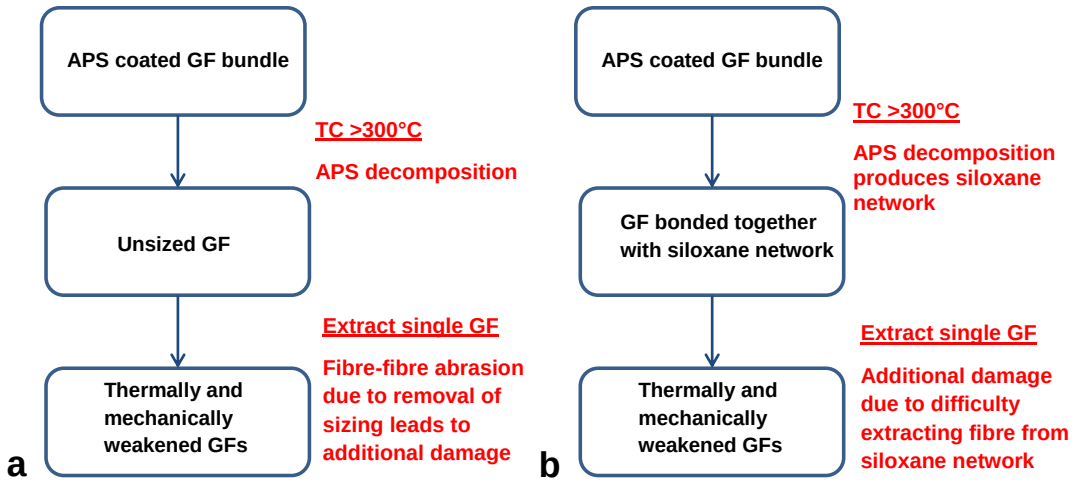

Figure B-8 Comparison between strength loss mechanism of thermally conditioned APS coated bundles (a) outline in [32] (b) outlined in this work

B.3.1 Phenomenological model of strength loss

A phenomenological model was developed based on the experimental data in Figure B-5 and Figure B-6. The tensile strength can be represented by an exponential decay function similar to that developed by Feih et al. [31], relating fibre tensile strength to temperature and conditioning time. Strength loss can be represented mathematically as a function of conditioning temperature in Equation B-1.

Equation B-1 Strength loss of glass fibre as a function of conditioning temperature [31]

$$\sigma_{loss}(T) = \left(\frac{\sigma_{f(0)} - \sigma_{f(a)}}{2}\right)\left(1 + tanh\left(p_f(T - T_{50\%})\right)\right)$$

Where $\sigma_{f(0)}$ and $\sigma_{f(a)}$ are original fibre strength and strength following thermal conditioning at the glass transition temperature respectively. $T_{50\%}$ is the temperature at 50% strength loss and p_f is curve fitting constant. Equation B-2 gives the fibre strength as a function of temperature and time.

Equation B-2 Fibre strength as a function of temperature and time [31]

$$\sigma_{f(t,T)} = \sigma_{f(0)} - \sigma_{loss}(T)tanh\left(k_f(T)t\right)$$

Where $k_f(T)$ represents the rate of strength loss and is give in Equation B-3.

Equation B-3 Rate of fibre strength loss [31]

$$k_f(T) = k_1 e^{k_2 T}$$

k_1 and k_2 are constants for a given temperature.

Figure B-9 and Figure B-10 give the phenomenological models for fibres thermally conditioned as bundles and single fibres respectively. In the tested range, the models give reasonable approximations of the strength loss as a function of temperature and time. Allowing for the error, 75% and 70% of the measured data fits the model for bundle and single fibre thermal conditioning respectively.

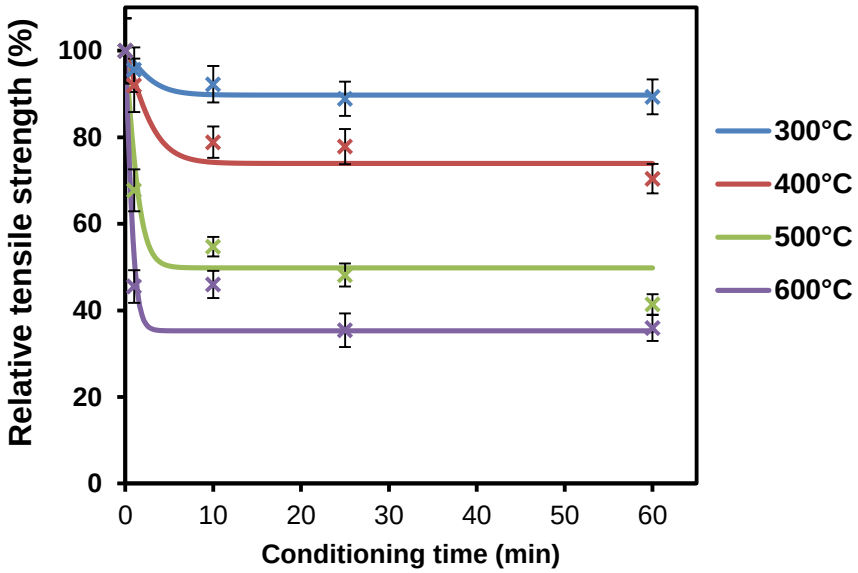

Figure B-9 Phenomenological model based on measured strengths of glass fibres thermally conditioned as fibre bundles

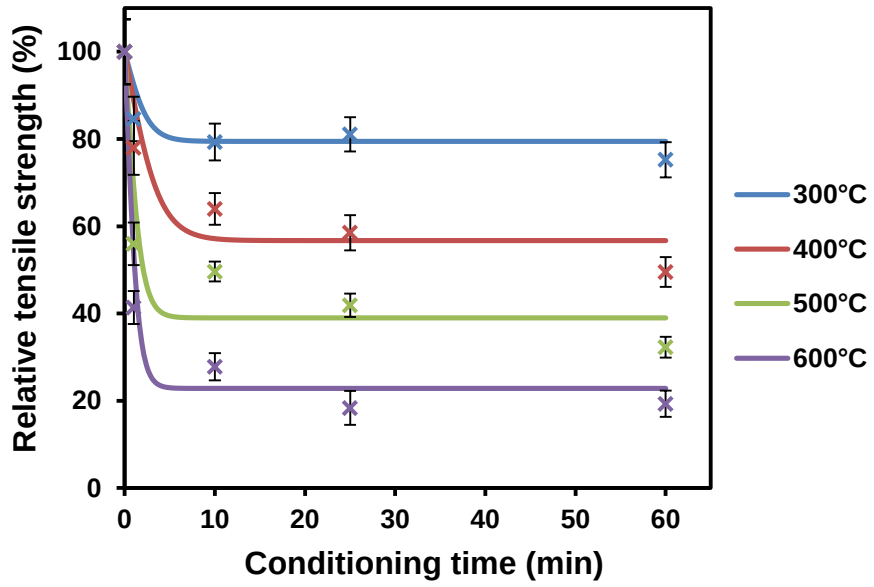

Figure B-10 Phenomenological model based on measured strengths of glass fibres thermally conditioned as single fibres

Table B-2 gives an example of fitting parameters used for the phenomenological model when thermally conditioning at 300 °C.

Table B-2 Fitting parameters for phenomenological model at 300 °C

Parameter	Single fibre heat-treatment	Bundle fibre heat-treatment
$\sigma_{f(a)}\ (MPa)$	400	900
$T_{50\%}\ (K)$	706	763
$p_f\ (K^{-1})$	5.0E-3	4.4E-3
$k_1\ (s^{-1})$	4.6E-3	3.8E-3
$k_2\ (K^{-1})$	5.7E-4	3.0E-4

B.4 Conclusions

This section has detailed an investigation into the effects of thermal conditioning on the tensile strength of commercial glass fibres. The strength of fibres after single fibre and bundle thermal conditioning were compared as a means of investigating the effect of thermal and mechanical damage during the sample preparation process. It was found that fibres thermally conditioned as single fibres were weaker than when treated in a bundle. It was observed that fibres were more difficult to remove prior to thermal conditioning and it is suggested that attempting to extract fibres from as received bundles results in additional mechanical damage. This is contrary to the literature [32], where strength retention is higher for single fibre thermal conditioning. The difference in sizing between studies is thought to be the cause for this discrepancy and an alternative mechanism for strength loss in APS only sized fibre bundles is proposed. Finally, a phenomenological model giving fibre strength as a function of conditioning temperature and time was developed for both bundle and single fibre treatments.

Appendix C. Metal oxides as a catalyst for carbon fibre recycling

The focus of this thesis is thermal recycling of GRT. However, both glass and carbon fibres are typically used with analogous thermoset matrix material and similar thermal recycling processes have been proposed for both. This section investigates whether it is feasible to use metal oxides during recycling of carbon fibre reinforced thermosets (CRT), and if the same benefits seen for GRT can be translated to recycling carbon fibre based composites.

C.1 Experimental

C.1.1 Materials

The carbon fibre used throughout this study was HexTow IM7 supplied by Hexcel. The fibres were unsized and supplied on a roving with 12K filament tow. The prepreg used to produce laminates was IM7 carbon fibres infused with CYCOM 977-3 epoxy resin. The carbon fibre reinforced epoxy (CF-EP) laminates were manufactured by curing eight layers the prepreg in a Polystat 400S heated press following the suppliers heating and pressure schedule. The metal oxides used were the same as described in Chapter 3.

C.1.2 Thermal analysis

C.1.2.1 Carbon fibre thermal decomposition

TGA was performed on the carbon fibres in the presence of each metal oxide. A carbon fibre bundle was chopped into 5 mm lengths. 5 mg of the chopped carbon fibre was thoroughly mixed with 20 mg of metal oxide. The mixture was placed in an alumina pan and TGA was performed using a TA Instruments Q50. The specimens were heated at 10 °C/min from RT to 900 °C in air.

C.1.2.2 CF-EP thermal decomposition

TGA was also performed on the CF-EP laminates. TGA samples were prepared by cutting disks with a diameter of 5 mm from the cured laminate using a water jet cutter. The resulting CF-EP samples had a mass of 25 mg. The CF-EP disks were placed on a 20 mg bed of metal oxide and heated at 3 °C/min in air.

C.1.3 Thermally conditioning carbon fibres

The dependence of heating temperature on the carbon fibre tensile strength was investigated. Thermal conditioning was performed using a Carbolite CWF 12/13 furnace. Carbon fibre bundles were heated in an air atmosphere at 400, 500 and 550 °C for 60 min. Single fibre tensile specimens were then prepared and tested as outline in Chapter 3.

The effect of physical contact with each of the metal oxides during heating on carbon fibre strength was also investigated. As outlined in Chapter 3, metal oxide powder was applied to the carbon fibre bundles and thermally conditioned in the furnace for 25 min at 400 °C. Single fibre tensile testing was then performed on the thermally conditioned fibres.

C.2 Results and discussion

C.2.1 Thermal analysis

C.2.1.1 Carbon fibre decomposition

Figure C-1 shows the decomposition thermograms of chopped carbon fibre with each metal oxide applied. All metal oxides reduce the thermal stability of the carbon fibre, with CuO having the largest impact. As shown in Table C-1, CeO_2 and Co_3O_4 reduce the onset decomposition temperature of carbon fibre by around 50 °C, whereas CuO has a much larger effect, reducing by around 130 °C.

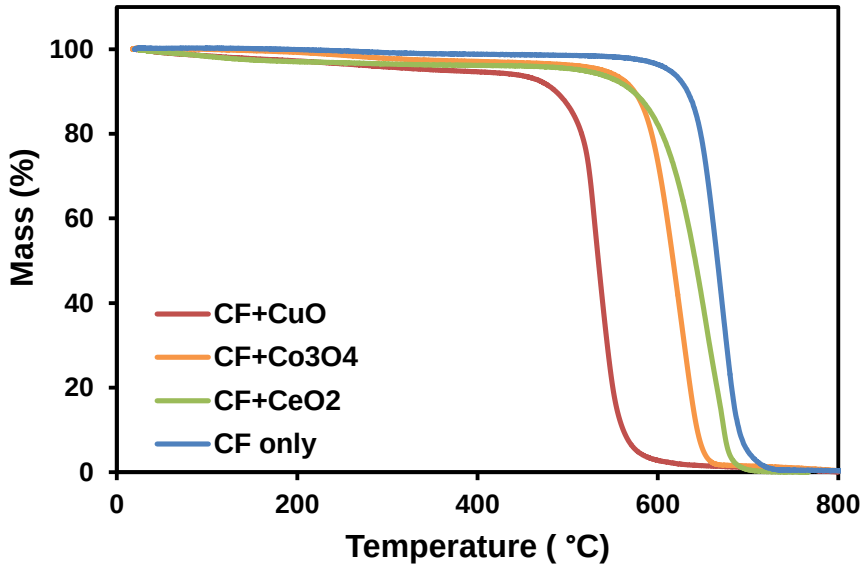

Figure C-1 Carbon fibre thermal decomposition with the application of each of the metal oxides using TGA at 10 °C/min in air

It appears that the ability of the metal oxides tested to aid thermal decomposition of epoxy is intrinsically related to the decomposition of carbon fibre. It is known that the residual material present after the first stage of epoxy thermal decomposition, referred to as char, has high carbon content. The beneficial ability of the oxides to catalyse the decomposition of such material appears to also increase the rate of carbon fibre oxidation. As the driving force behind carbon fibre weakening during heating is mass loss due to surface oxidation [247, 249], the metal oxides may in fact have an adverse effect if applied to CRT recycling.

Table C-1 Thermal decomposition onset temperature of carbon fibre with the application of the metal oxides

Sample	Onset temperature (°C)
CF only	630
CF+CuO	499
CF+Co_3O_4	576
CF+CeO_2	585

C.2.1.2 CF-EP decomposition

TGA was used to examine the thermal stability of CF-EP in the presence of the metal oxides. Figure C-2 shows the thermograms obtained when heating the CF-EP applied with each of the metal oxides at 3 °C/min in air. A three-stage decomposition process with similar decomposition temperatures can be seen for each sample except that containing CuO. The initial two stages are likely representative of the epoxy matrix decomposing and the latter the residual carbon fibres decomposition. This three-stage decomposition is in line with what is observed in the literature [86-88]. Unlike CeO_2 and Co_3O_4, CuO significantly decreases the thermal stability of the CF-EP above 450 °C. There is no clear distinction between the second stage of epoxy and the carbon fibre decomposition with CuO applied, resulting in the GF-EP fully decomposition 60 °C lower than the un-catalysed sample.

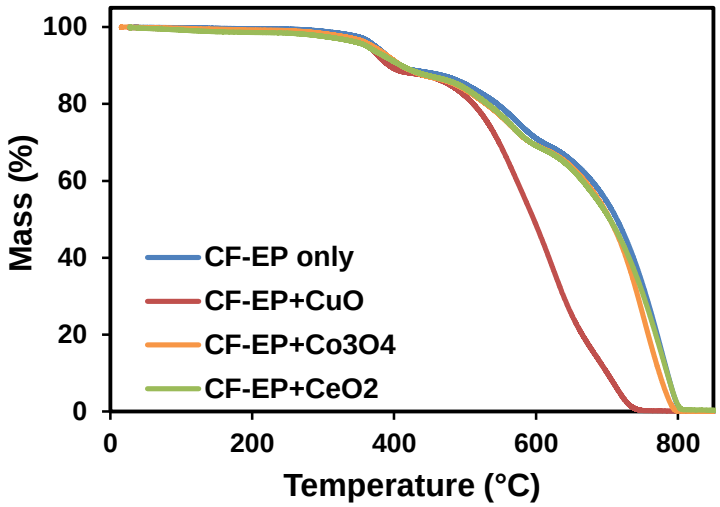

Figure C-2 CF-EP thermal decomposition with the application of each of the metal oxides using TGA at 3 °C/min in air

C.2.2 Strength of thermally conditioned carbon fibre

C.2.2.1 Effect of thermal conditioning temperature

Figure C-3 shows the average fibre strength after the various conditioning temperatures. The strength of the un-conditioned carbon fibres are low compared to that typically found in the literature. The reason for this is somewhat unclear; however, it may be a result of using unsized carbon fibres. This phenomenon is

observed when testing unsized glass fibres and is attributed to additional damage to the unprotected fibre, caused by handling during sample preparation [32]. Figure C-3 shows the carbon fibres sustain significant damage after thermally conditioning at 500 and 550 °C. Like thermal weakening of glass fibres, the strength loss is clearly temperature dependent [247]. Although using a metal oxide during thermal recycling would appear beneficial to retaining carbon fibre strength from Figure C-3, the thermal analysis in Figure C-1 suggests the metal oxides would promote oxidation of the fibres themselves.

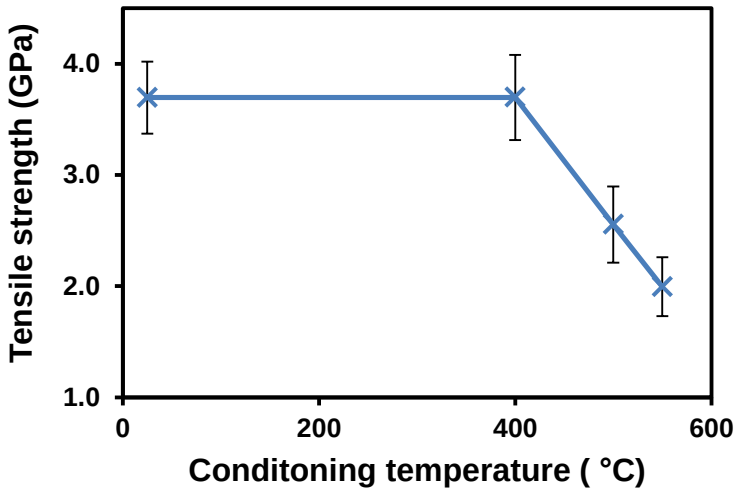

Figure C-3 Tensile strength of carbon fibre thermally conditioned at 400, 500 and 550 °C for 60 min in air

C.2.2.2 Effect of contact with metal oxides

Figure C-4 shows the tensile strength of the carbon fibres after thermally conditioning in the presence of the metal oxides. As established previously in Figure C-3, fibres thermally conditioned at 400 °C in the absence of any metal oxide experienced no strength loss. As suggested by the TGA results in Figure C-1, all carbon fibres applied with the metal oxide powder experience a significant tensile strength loss. CuO has the most detrimental effect on fibre strength, reducing it by 46% relative to thermally conditioned fibres alone. CeO_2 and Co_3O_4 have a similar impact by reducing strength by 20 and 24% respectively.

There was an apparent lack of correlation between carbon fibre tensile strength and diameter. This may be a result of non-uniform oxidation of the fibre surface.

Localised accelerated oxidation, called pitting, has been shown by Iacocca et al. to occur as a result of impurities on the fibre surface such as platinum [250]. This may be taking place at the interface of the carbon fibres and metal oxide and was unable be observed through the optical microscope. In any respect, all three metal oxides tested reduce thermal stability of the carbon fibres tested and in doing so promote considerable fibre tensile strength loss. This is in stark contrast to the aim of reducing the temperature required for CRT thermal recycling.

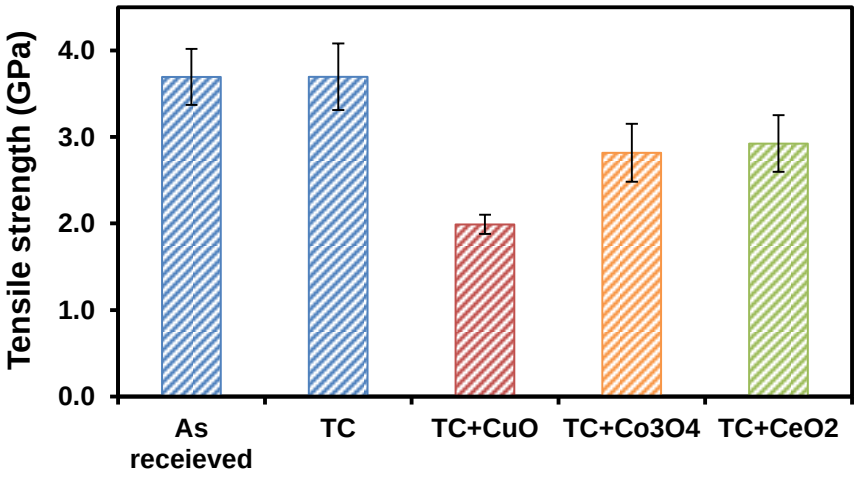

Figure C-4 Tensile strength of carbon fibres thermally conditioned in the presence of the metal oxides at 400 °C for 25 min

C.3 Conclusions

It is clear that all metal oxides tested reduce the thermal stability of the carbon fibres tested and in turn decreases fibre tensile strength. In accordance with the strength loss mechanism outlined in the literature, it is thought that the metal oxides increase oxidation of the carbon fibre surface resulting in weakening of the fibres. As a result, it is recommended that these metal oxides should not be utilised within a CRT thermal recycling system to aid matrix decomposition.

Appendix D. Fibre length degradation during GF-PP processing

It was observed that the average fibre length in GF-PP prepared with RGF were considerably shorter than was within the (in-house prepared) GF-EP recyclate prior to recycling in the fluidised bed. Three main processes were identified as potential causes for this degradation in fibre length 1) recycling in fluidised bed, 2) wet deposition and 3) hot pressing. To determine how the average fibre length degraded during recycling and processing into GF-PP, the length of fibres before and after each process were measured. Figure D-1 shows the degradation of average fibre length throughout processing of the fibres. Hot pressing causes the largest reduction in fibre length followed by thermal recycling within the fluidised bed. The hot pressing actually involves two presses, preconsolidation and compression moulding. It is unclear how the fibre length degrades during each; however, compression moulding is performed at double the pressure used for preconsolidating so is likely more damaging. In order to retain the length of recycled fibre in the GF-PP, further work could be done to investigate the effect of reducing the pressure during compression moulding. Figure D-2 shows the fibre length distribution after the various processes produced by the FASEP software used to calculate the average fibre lengths in Figure D-1.

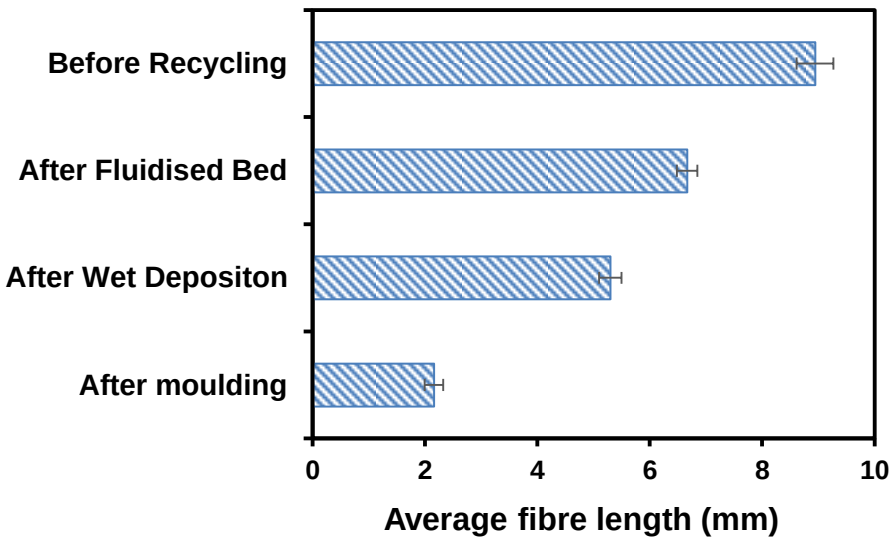

Figure D-1 Average length of fluidised bed RGF during recycling and processing into GF-PP

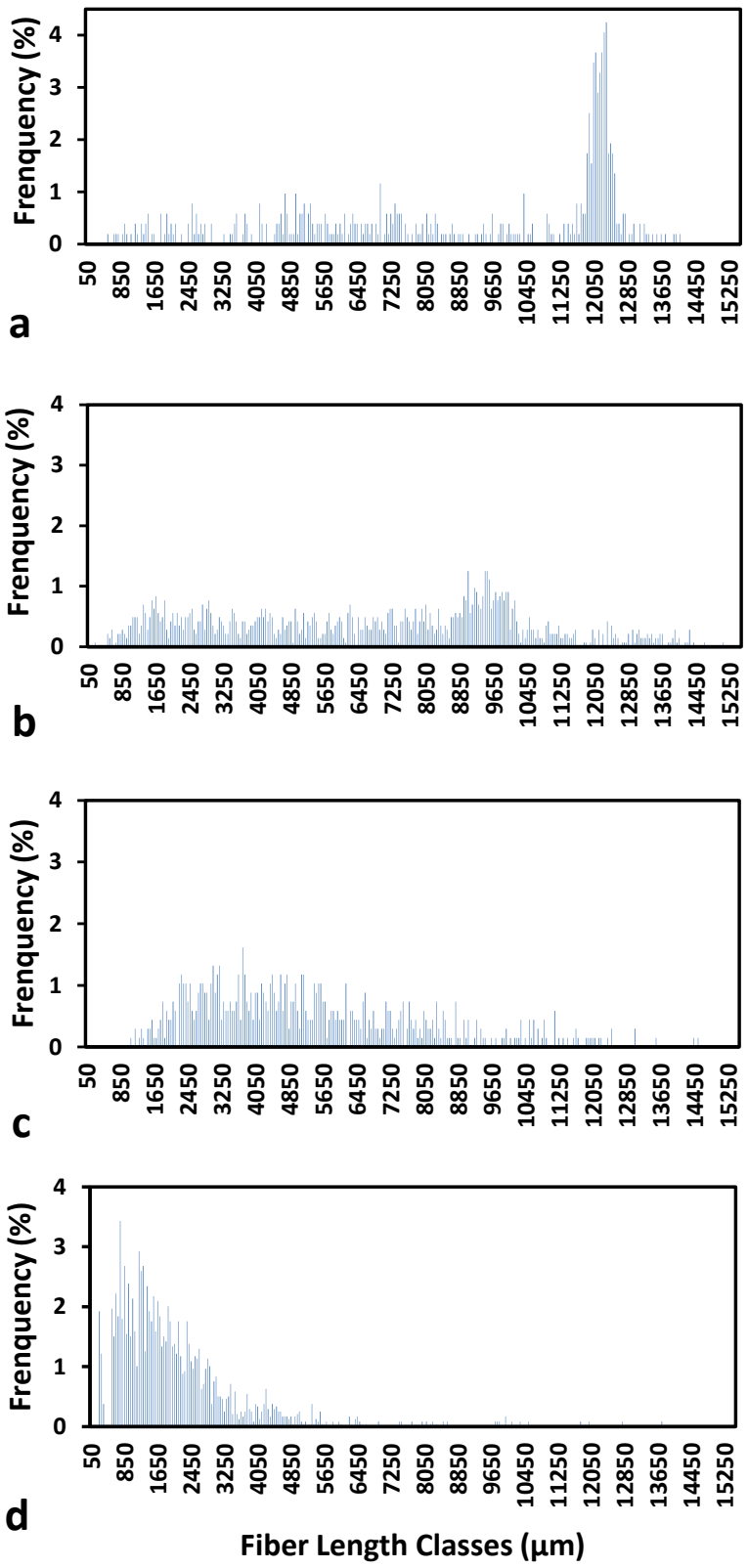

Figure D-2 Fibre length distribution produced by the FASEP software a) before recycling, b) after the fluidised bed, c) after wet deposition, d) after moulding

Appendix E. Extended Kelly-Tyson model derivation

The extended Kelly-Tyson model developed by Bowyer and Bader [203] is a model that describes the tensile strength of discontinuous fibre composites and is based on the assumption that the critical fibre length changes with the stress in the composite.

E.1 Critical fibre length

Tensile stress in fibre σ_f with diameter D_f under load P_f can be given as:

$$\sigma_f = \frac{4P_f}{\pi D_f^2}$$

Shear stress τ in fibre with length L_f can be expressed as:

$$\tau = \frac{2P_f}{\pi D_f L_f}$$

Balancing loads gives:

$$\sigma_f = \frac{2\tau L_f}{D_f}$$

When tensile stress on fibre equals the fibre tensile strength σ_{fu}, fibre length is the critical fibre length L_c, i.e:

$$\sigma_f = \sigma_{fu}, L_f = L_c$$

Therefore critical fibre length is given as:

$$L_c = \frac{\sigma_{fu} D_f}{2\tau}$$

E.2 Extended Kelly-Tyson model

A fibre with length shorter than the critical length L_i is called a subcritical fibre and is experience a stress $(\sigma_f)_i$

$$(\sigma_f)_i = \frac{\tau L_i}{D_f}$$

A fibre with length longer than the critical length $(\sigma_f)_j$ is called a supercritical fibre and experience a stress $(\sigma_f)_j$

$$(\sigma_f)_j = E_f \varepsilon_c \left(1 - \frac{E_f \varepsilon_c D_f}{\tau L_j}\right)$$

Where ε_c is composite strain and E_f is the fibre modulus. The contribution of all subcritical fibres with the volume fraction v_i can be described as:

$$X = \sum_{L_i < L_c} \left(\frac{\tau L_i}{D_f}\right) v_i$$

The contribution of all supercritical fibres with the volume fraction v_j can be described as:

$$Y = \sum_{L_j > L_c} E_f \varepsilon_c \left(1 - \frac{E_f \varepsilon_c D_f}{\tau L_j}\right) v_j$$

The stress σ_m in the matrix with a modulus E_m can be calculated from:

$$\sigma_m = E_m \varepsilon_c (1 - v_f)$$

The terms above can be combined to calculate the composite tensile stress σ_c where η_o describes the fibre orientation:

$$\sigma_c = \eta_o (X + Y) + \sigma_m$$

To solve for composite strength, σ_{cu}

$$E_m \varepsilon_c = \sigma_{mu}$$

$$E_f \varepsilon_c = \sigma_{fu}$$

$$L_c = \frac{\sigma_{fu} D_f}{2\tau}$$

Where σ_{mu} is the strength of the matrix. Therefore, the composite strength can be expressed as:

$$\sigma_{cu} = \eta_o \left(\sum_{L_i < L_c} \left(\frac{\tau L_i}{D_f}\right) v_i + \sum_{L_i > L_c} \left(\frac{2\tau L_c}{D_f}\right) \left(1 - \left(\frac{L_c}{2L_j}\right)\right) v_j \right) + \sigma_m (1 - v_f)$$